High-Dimensional Response-Excitation PDF Methods for Uncertainty Quantification and Stochastic Modeling

by

Heyrim Cho

B.Sc., Korea Advanced Institute of Science and Technology; Daejeon, Korea, 2007

M.Sc., Korea Advanced Institute of Science and Technology; Daejeon, Korea, 2009

A dissertation submitted in partial fulfillment of the

requirements for the degree of Doctor of Philosophy

in The Division of Applied Mathematics at Brown University

PROVIDENCE, RHODE ISLAND

May 2015

Abstract of "High-Dimensional Response-Excitation PDF Methods for Uncertainty Quantification and Stochastic Modeling", by Heyrim Cho, Ph.D., Brown University, May 2015

The probability density approach based on the response-excitation theory is developed for stochastic simulations of non-Markovian systems. This approach provides the complete probabilistic configuration of the solution that enables a comprehensive study of stochastic systems. By using functional integral methods we determine a computable evolution equation for the joint response-excitation probability density function (REPDF) of stochastic dynamical systems and stochastic partial differential equations driven by colored noise. We establish its connection to the classical response approach and its agreement to the Dostupov-Pugachev equations (Dostupov, 1957) and the Malakhov-Saichev equations (Gurbatov et al, 1991). An efficient algorithm has been proposed by using adaptive discontinuous Galerkin method and probabilistic collocation method combined with sparse grid. For high-dimensional REPDF systems, we develop the algorithms concerning high-dimensional numerical approximations, namely, separated series expansion and the ANOVA approximation. These methods reduce the computational cost in high-dimensions to several low-dimensional operations. Alternatively, reduced order PDF equations are obtained by using the Mori-Zwanzig framework and conditional moment closures, which establish a preliminary work of goal-oriented PDF equations. Finally, we demonstrate the effectiveness of the proposed numerical methods to various stochastic systems including the tumor cell growth model, chaotic nonlinear oscillators, advection reaction equation, and Burgers equation. The second part of the thesis focuses on simulations of multi-scale stochastic systems. The Karhunen-Loève expansion is extended to characterize multiple correlated random processes and local decomposed random fields. We then propose interface conditions based on conditional moments and PDE-constrained optimization that preserve the global statistics while propagating uncertainty. Finally, the decomposition algorithm is recast to couple distinct

PDF models including the REPDF system.

Contents

List of Tables

List of Figures

Chapter 1

Introduction

The relevance of uncertainty in science and engineering has been recognized in many different applications including stochastic resonance in sensory neurons [137], chemical excitable systems [7, 228], structural dynamics [18, 111, 171], tumoral cell growth [58, 205, 223], spin relaxation in magnetic phenomena [4], and optical instabilities [93, 229]. Accordingly, stochastic differential equations modeling such systems and simulations of corresponding probabilistic solutions have received considerable interest. Moreover, advances in computing power and algorithm have increased the impact of computer simulations for our society, which makes uncertainty quantification more essential. Without a valid quantification of the variation between the simulated prediction and the true value, benefit from the computational model will remain limited.

The overall framework of uncertainty quantification entails quantifying the source of uncertainty and propagating uncertainty through the computational model. The source of uncertainty can arise from insufficient information about the true value, such as rough estimates of the parameters, unknown boundary and initial conditions, or imprecise geometry. The random nature of the physical system or approximative constitutive laws can induce uncertainty as well. Various methods have been de-

veloped to characterize randomness through random variables and random fields, for instance, Karhunen-Loève (KL) expansion [88, 141], kriging [32, 151], polynomial chaos [71, 213], and kernel density estimation [22]. Once the probabilistic configurations of random inputs and excitations are prescribed, the propagation of uncertainty associated with the computational system can be computed according to different stochastic methods.

1.1 Review of computational probabilistic methods

Computational methods for stochastic simulations can be roughly classified as statistical methods and non-statistical methods. Well-known methods for the former include Monte-Carlo simulations, Bayesian methods, and importance sampling. The later includes stochastic spectral methods [71, 213, 214], high-dimensional model representations [110, 155], stochastic biorthogonal expansions [190, 191, 198] and proper generalized decompositions [33, 133]. Here, we briefly review some of the methods, focusing on the stochastic spectral method and probability density approach.

1.1.1 Stochastic spectral methods

Stochastic spectral methods [6, 208, 212] employ spectral elements for the solution with respect to the random inputs by using Askey-type orthogonal polynomial functions. They include generalized polynomial chaos method (gPC) [71, 213], probabilistic collocation method (PCM) [130, 212], multi-element probabilistic collocation method (MEPCM) [60], and many other variants. Based on the input and solution that are in the form of finite order spectral expansion, the method employs standard projection approach based on the Galerkin or collocation basis, denoted as gPC or PCM, respectively. As a result, the problem is reconstructed as a deter-

ministic system regarding the expansion coefficients and the dimensionality depends on the order of the approximating polynomials as well as the number of random parameters. The gPC and PCM have been extended to overcome several computational limits including low regularity and the curse of dimensionality. By using hp adaptive approach, multi-element gPC (megPC) [199, 203] and multi-element PCM (mePCM) [60] resolve the issue of low stochastic regularity and demonstrate their effectiveness on solutions that have discontinuous dependency on random parameters. However when high-dimensionality occurs, the usual tensor product often makes the computational cost intractable, due to its exponential growth with respect to the dimensions. Thus, various methods have been developed adopting sparse grid (PCM-sparse) [130, 212] and ANOVA approximation (PCM-ANOVA) [11, 61] to the spectral methods. Moreover, anisotropic adaptive approaches [70, 204, 220] that seeks effective dimensions generalize the PCM-sparse and PCM-ANOVA methods available to even higher dimensions.

Compared to the Monte-Carlo approach, the stochastic spectral methods can efficiently calculate the moment statistics up to the order of truncation for solutions to stochastic ODE and PDE systems with comparatively less computational cost. However, we notice that there exists an infinite number of probability density associated with a fixed set of moments truncated at certain level. Thus, in the following section, we review stochastic models that directly compute the probability density functions (PDFs).

1.1.2 Probability density approach

The main advantage of probability density approach is that it contains the full statistics of the solution. Considering a stochastic system that reveals complicated dynamics such as bifurcation, metastability, heavy-tail distribution, or rare events, methods based on sampling or moment statistics often require extremely expensive compu-
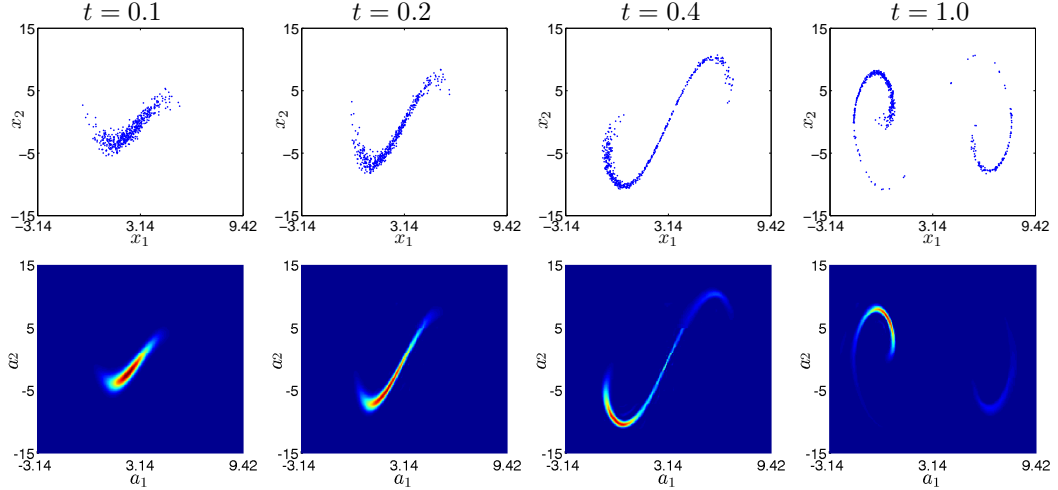
Figure 1.1: Comparison between the sample phase space (first row) and the joint PDF of the position and the momentum of a randomly forced nonlinear pendulum (second row) [for a detailed description of this problem see section 3.2.1]. The PDF solution is obtained by using the proposed adaptive discontinuous Galerkin method. It is seen that the position of the sample particles are in very good agreement with the computed PDF at different times.

tational cost or result in misleading conclusions due to their finite order truncation. However, the PDF provides the complete probabilistic description of the phenomena, which enables an accurate and thorough investigation for such complex systems.

In addition, partial differential equations involving PDFs arise naturally in many different areas of mathematical physics, so called kinetic equations. For example, they play an important role in modeling rarefied gas dynamics [26, 27], semiconductors [119], stochastic dynamical systems [117, 127, 128, 174], structural dynamics [18, 111, 171], stochastic partial differential equations (PDEs) [36, 103, 118, 194, 195], turbulence [64, 124, 125, 147], system biology [58, 137, 223], etc. Perhaps the most well-known kinetic equation is the Fokker-Planck equation [127, 161, 179], which describes the evolution of the probability density function of Langevin-type dynamical systems subject to Gaussian white noise. Another well-known example of kinetic equation is the Boltzmann equation [201] describing a thermodynamic system involving a large number of interacting particles [27]. Other examples that may not be widely known are the Dostupov-Pugachev equations [49, 111, 174, 196], the reduced-

Fokker-Planck [127, 161]	$\dfrac{\partial p}{\partial t} + \displaystyle\sum_{i=1}^{n} \dfrac{\partial}{\partial z_i}\left(G_i p\right) = \dfrac{1}{2}\sum_{i,j=1}^{n}\dfrac{\partial^2}{\partial z_i \partial z_j}\left(b_{ij} p\right)$
Boltzmann [26, 45]	$\dfrac{\partial p}{\partial t} + \displaystyle\sum_{k=1}^{3} v_k \dfrac{\partial p}{\partial z_k} = H(p, p)$
Liouville [49, 103, 111, 174]	$\dfrac{\partial p}{\partial t} + \displaystyle\sum_{k=1}^{n}\dfrac{\partial}{\partial z_k}\left(G_k p\right) = 0$
Malakhov-Saichev [118, 194]	$\dfrac{\partial p}{\partial t} + \dfrac{\partial}{\partial z}\left(\displaystyle\sum_{k=1}^{3} G_k \int_{-\infty}^{z}\dfrac{\partial p}{\partial x_k}dz'\right) = -\dfrac{\partial(Hp)}{\partial z}$
Mori-Zwanzig [195, 230]	$\dfrac{\partial p_1}{\partial t} = PLp_1 + PLe^{tQL}p_2(0) + PL\displaystyle\int_{0}^{t}e^{(t-s)QL}QLp_1 ds$

Table 1.1: Examples of kinetic equations arising in different areas of mathematical physics.

order Nakajima-Zwanzig-Mori equations [195, 230], and the Malakhov-Saichev PDF equations [118, 194] (see Table 1.1).

An interesting new approach for the complete probabilistic description of a stochastic system driven by colored noise was recently proposed by Sapsis [168]. The key idea - inspired by the work of Beran [8] - was to perform analysis on the extended probability space consisting of the joint *response-excitation* statistics. In particular, the Hopf equation [103, 109, 164] governing the dynamics of the joint response-excitation characteristic functional of the system was reduced to a *differential constraint* involving the one-point response-excitation probability density function. This differential constraint was then supplemented with additional marginal compatibility conditions and other constitutive relations in order to obtain a closed system of equations. This led to the formulation of a new theory, which was shown to be consistent with standard stochastic approaches such as moment equations or Fokker-Planck equations. In this way, the closure problem arising in the standard response approach for non-Markovian systems [127, 178] was apparently overcome.

The response-excitation theory has been developed in [196] by using functional integral techniques that simplifies considerably the derivation of the differential constraints given in [168]. Moreover, this theory also generalizes classical PDF approaches for systems having smooth nonlinearities of non-polynomial type. In addition, this framework has been extended in the context of first-order nonlinear scalar PDEs [194] allowing efficient mathematical derivations compared to those ones based on the more rigorous Hopf characteristic functional approach [103, 109, 164].

1.1.3 Difficulties in probability density approach

In spite of their potential for the comprehensive understanding of stochastic systems, computing the numerical solution to a PDF equation is a very challenging task that involves several distinct problems:

1. *High-dimensionality:* Kinetic equations describing realistic physical systems usually involve many phase variables. For example, the Fokker-Planck equation of classical statistical mechanics yields a joint probability density function in n phase variables, where n is the dimension of the underlying stochastic dynamical system, plus time.

2. *Multiple scales:* Kinetic equations can involve multiple scales in space and time, which could be hardly accessible by conventional numerical methods. For example, the Liouville equation is a hyperbolic conservation law whose solution is purely advected (with no diffusion) by the underlying system's flow map. This can easily yield mixing, fractal attractors, and all sort of complex dynamics.

3. *Lack of regularity:* The solution to a kinetic equation is, in general, a distribution [96]. For example, it could be a multivariate Dirac delta function, a function with shock-type discontinuities [36], or even a fractal object (see Fig-

ure 1 in [195]). From a numerical viewpoint, resolving such distributions is not trivial, although in some cases it can be done by taking integral transformations or projections [221].

4. *Conservation properties:* There are several properties of the solution to a kinetic equation that must be conserved in time. The most obvious one is mass, i.e., the solution to a kinetic equation always integrates to one. Another property that must be preserved is the positivity of the joint PDF, and the fact that a partial marginalization still yields a PDF.

5. *Long-term integration:* The flow map defined by nonlinear dynamical systems can yield large deformations, stretching and folding of the phase space. As a consequence, numerical schemes for kinetic equations associated with such systems will generally loose accuracy in time. This is known as long-term integration problem and it can be eventually mitigated by using adaptive methods.

Over the years, many different techniques have been proposed to address these issues, with the most efficient ones being problem-dependent. For example, a widely used method in statistical fluid mechanics is the particle/mesh method [129, 146–148], which is based directly on stochastic Lagrangian models. Other methods make use of stochastic fields [188] or direct quadrature of moments [63]. In the case of the Boltzmann equation, there is a very rich literature. Both probabilistic approaches such as direct simulation Monte Carlo (DSMC) [12, 162], as well as deterministic methods, e.g., discontinuous Galerkin (DG) and spectral methods [31, 59], have been proposed to compute the solution. Probabilistic methods such as DSMC are extensively used because of their very low computational cost compared to finite-volumes, finite-differences or spectral methods, especially in the multi-dimensional case. However, DSMC usually yields poorly accurate and fluctuating solutions, which need to be post-processed appropriately, for example through variance reduction techniques.

We refer to Dimarco and Pareschi [45] for a recent review.

1.2   Thesis Outline

The objective of this thesis is to introduce stochastic simulation based on the probability density approach, particularly using the response-excitation probability density functions (REPDFs). The first part of the thesis focuses on numerical methods developed for the REPDF evolution equation as well as classical response PDF equations. The range of applicability of the proposed numerical approaches is sketched in Figure 1.2 as a function of the number of phase variables n and the number of parameters m appearing in the kinetic equation. The second part of the thesis is devoted to stochastic domain decomposition methods that eventually yields coupling algorithms between distinct probabilistic computational models including probability density systems.

In chapter 2, we introduce the theory underlying the REPDF that relies on functional integral approach. We determine the set of equations arising from the response-excitation theory for a simple first-order nonlinear ordinary differential equation and discuss the question of computability and well-posedness of the boundary value problem for the joint response-excitation density equation. In addition, the connection between the response-excitation approach and the classical response approach is established. Then, we derive computable response-excitation probability density evolution equations of ordinary differential equations involving random parameters as well as first order non-linear and quasi-linear partial differential equations. Finally, we close this chapter with a simple numerical application of this approach to the tumor cell growth model [223].

In chapter 3, we develop an efficient numerical method to compute the solution of the joint REPDF equation corresponding to an arbitrary nonlinear stochastic dy-

namical system. This allows us to address the question of whether the joint REPDF approach can provide an effective computational tool to simulate the effects of *colored random noise* in physical systems. The numerical challenges associated with this task are two-fold; first the dimensionality, which may be eventually handled by using closures or techniques for high-dimensional systems; and second, the solution which may be *discontinuous* and *compactly supported* over disjoint domains (see Figure 1.1). This obviously requires the development of appropriate numerical techniques, and we propose a method based on the adaptive discontinuous Galerkin method [38]. In order to improve the computational efficiency, we have also developed *non-conforming* adaptive strategies based on two different adaptive criteria: (1) a combination of local variance and boundary flux difference; and (2) a concentration of sample points in phase space. Afterwards, the adaptive discontinuous Galerkin method is combined with the probabilistic collocation method that is devised for the excitation space. We also employ the sparse grid collocation method to overcome the high-dimensionality occurring in the excitation space. The effectiveness of this algorithm is demonstrated in several nonlinear stochastic dynamical systems subject to colored noise.

In chapter 4, we address the high-dimensionality of REPDF equation by using numerical approximation for high-dimensional functions, namely, separated series expansion (SSE) methods and ANOVA approximations. The key idea of separated representations is to approximate a multi-dimensional function in terms of series involving products of one-dimensional functions [33, 108, 131, 133]. As we will see, this allows us to reduce the problem of computing the solution to high-dimensional kinetic equations to a sequence of one-dimensional problems that can be solved recursively and in parallel by using alternating direction algorithms, e.g., alternating least squares (ALS). The second approach we consider is based on ANOVA approximation methods [25, 68, 110, 227]. The basic idea is to represent multivariate PDFs
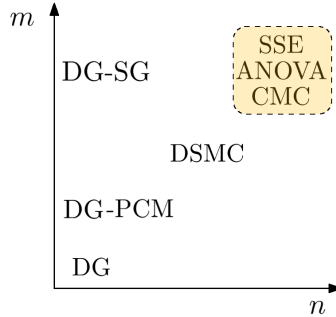
Figure 1.2: Range of applicability of different numerical methods for solving kinetic equations as a function of the number of phase variables n and the number parameters m appearing in the equation. Shown are: Separated series expansion methods (SSE - section 4.1.1), conditional moment closures (CMC - section 5.2), high-dimensional model representations (ANOVA - section 4.1.2), adaptive discontinuous Galerkin methods (DG - section 3.1.1) with sparse grids (SG) or tensor product probabilistic collocation (PCM - section 3.1.2) in the parameter space, direct simulation Monte Carlo (DSMC). The proposed new classes of algorithms are enclosed with dashed lines.

in terms of series expansions involving functions with a smaller number of variables. For example, a second-order ANOVA approximation of a multivariate PDF in N variables is a series involving functions of at most two variables. This allows us to reduce the problem of computing high-dimensional PDF solutions to a sequence of problems involving low-dimensional PDFs. These two approaches are compared in terms of accuracy and computational cost, accompanied by a numerical application to kinetic equations arising in stochastic partial differential equations (random advection problems).

In chapter 5, we propose reduced-order PDF equations to overcome high-dimensionality in kinetic systems. In other words, we employ dimension reduction techniques to model the probability density of the quantities of interest in high-dimensional stochastic systems. Those of our interest are often only a few phase variables or a low-dimensional phase space function. The first idea stems from techniques of irreversible statistical mechanics, in particular the Nakajima-Zwanzig-Mori formalism (see, e.g., [23, 28, 56, 230]). The Mori-Zwanzig (MZ) projection operator

framework is employed to derive reduced-order PDF equations based on operator cumulant resummation. In particular, the MZ formalism for the joint REPDF is applied to study the stochastic Burgers equation. We perform stochastic simulations of the Burgers problem and study random flows induced by high-dimensional random initial conditions and random forcing terms. We then discuss the statistical properties of the solution, including the shock development and clustering. The other approach addresses the high-dimensionality mainly in the *phase space* by conditional moment closure approximation. This method relies on deriving a hierarchy of coupled PDF equations for each given stochastic dynamical system. Such hierarchy resembles the Bogoliubov-Born-Green-Kirkwood-Yvon (BBGKY) hierarchy of kinetic gas theory [126]. The proposed conditional moment closures are applied to kinetic equations arising in nonlinear stochastic dynamical system such as Kraichnan-Orszag and Lorenz-96 systems. In addition, this framework provides an approximated system of the probability density evolution for higher-order PDEs exceeding second-order, that cannot be written explicitly in a standard differential equation due to its nonlocal interaction.

The second part starts from chapter 6. Here, we present extensions of the KL expansion to characterize uncertainty with nontrivial correlated statistics. At first, we present two methods that extend the classical KL expansion to multi-correlated non-stationary stochastic processes. We call the first method as multiple uncorrelated KL (muKL) expansion based on the spectral decomposition of a suitable *assembled process*, and it yields series expansions in terms an identical set of *uncorrelated* random variables. The second approach, multiple correlated (mcKL) expansion method, relies on expansions in terms of *correlated* sets of random variables. The cross-covariance structure the processes is imposed by setting the cross-correlation between such sets of random variables appropriately. Both these methods are straightforward to use and can be readily employed in stochastic simulations based on Monte-Carlo,

polynomial chaos [71, 213] or probabilistic collocation [61]. In addition, we also introduce a localized KL expansion of random processes and fields for the purpose of domain decomposition. By using an alternative overlapping decomposition corresponding to the random space, this expansion preserves second-order global statistical properties, i.e., the two-point correlation function across different domains. The convergence result of the local expansion method is provided as well. Applications of this expansion are presented in the following chapters.

In chapter 7, we propose new algorithms to propagate uncertainty across scales in nonlinear stochastic dynamical systems by using *domain decomposition methods*. This technique has been used extensively in deterministic problems [98, 173] to speed up computations, and only recently it was considered in the context of stochastic PDEs [53, 54, 169]. Such extensions, however, are based on stochastic linear algebra and do not provide new insights in the most appropriate coupling conditions for *interacting partially correlated stochastic simulations*. Most of the work that has been done so far addresses this problem by imposing artificial boundary conditions, e.g., based on physical intuition, or assumes statistical independence between the solution in different sub-domains [112] Here, we develop a new general framework for multi-scale propagation of uncertainty in heterogeneous stochastic systems based on multi-level domain decomposition methods. The key idea relies on new types of interface conditions combined with reduced-order local representations and generalized Schwarz methods. In this way, the stochastic problem can be reduced to a sequence of problems of smaller stochastic dimension, while properly propagating uncertainty with interface conditions that preserve global statistical properties. In addition, this methodology is applied to domain decomposition for PDF approach. The motivation of domain decomposition to reduce the computational cost when the characteristic of the randomness across the domain is vastly changing appeals to the PDF systems as well. According to the characteristic of the random excitation, there

exist a range of distinct PDF models that is known to be appropriate (for instance, see Fig. 7.11). Thus, we develop coupling algorithms for PDF systems based on the interface methods presented in this chapter.

Part I

Response-Excitation PDF approach

Chapter 2

Derivation of REPDF equation

In this chapter, we introduce the theory underlying the REPDF and derive the evolution equation by using the functional integral approach. In section 2.1, we determine the set of equations arising from the response-excitation theory for a simple first-order nonlinear ordinary differential equation driven by purely additive random noise. The connection between the response-excitation approach and the classical response approach is established in section 2.2, for random noise with arbitrary correlation time. Ordinary differential equations involving random parameters are treated in section 2.3, and subsequently, first order non-linear and quasi-linear partial differential equations are discussed in section 2.4 and 2.5, respectively. Finally, in section 2.6, we present a numerical application to the tumor cell growth model recently proposed by [223].

2.1 Theory of response-excitation probability density

In this section we develop a systematic methodology to determine an equation for the joint response-excitation probability density function of a stochastic dynamical

system driven by colored noise. To this end, let us first consider the following simple prototype problem

$$\dot{x}(t;\omega) = g(x(t;\omega), t) + f(t;\omega), \quad x(t_0;\omega) = x_0(\omega), \tag{2.1.1}$$

where $f(t;\omega)$ is a smooth colored random noise while $g(x,t)$ is a nonlinear function, which is assumed to be Lipschitz continuous in x and continuous in t[1]. The solution to (5.2.2) (when it exists) is a *nonlocal* functional of the forcing process f, which will be denoted as $x_t[f]$. Similarly, we use the shorthand notation f_s to identify the random variable $f(s;\omega)$, i.e. the stochastic process f at time s. We also assume that the problem (5.2.2) admits the existence of the joint response-excitation probability density function, i.e. the joint probability density function of the *response process* $x_t[f]$ at time t and the *excitation process* f_s at time s. Such a probability density has the following functional integral representation

$$
\begin{aligned}
p_{x(t)f(s)}^{(a,b)} &\overset{\text{def}}{=} \langle \delta(a - x_t[f]) \delta(b - f_s) \rangle \\
&= \int \mathcal{D}[f] Q[f] \delta(a - x_t[f]) \delta(b - f_s), \quad s, t \geq t_0 \quad a, b \in \mathbb{R}, \tag{2.1.2}
\end{aligned}
$$

where $Q[f]$ denotes the probability density functional of the random forcing ([62], p. 467) while $\mathcal{D}[f]$ is the functional integral measure [90,91,144]. The representation

---

[1]We shall assume that the process $f(t;\omega)$ is real-valued and at least continuous with probability measure $\mathcal{P}_f$ and sample space $\mathcal{Y}$, which can be taken to be a quite general separable Banach space. For example, $\mathcal{Y} = C^{(k)}(I)$, $I \subseteq \mathbb{R}$, for $k \in \mathbb{N} \cup \{0\}$. Standard existence and uniqueness theory ([174]) then ensures that there is a stochastic process $x(t;\omega)$ with sample space $\mathcal{X} = \mathcal{C}^{(k+1)}(I)$ (i.e., at least differentiable), a probability measure $\mathcal{P}_x$ and a joint probability space $(\mathcal{X} \times \mathcal{Y}, \mathcal{B}(\mathcal{X} \times \mathcal{Y}), \mathcal{P}_{xf})$ such that the joint process $\{x(t;\omega), f(t;\omega)\}$ verifies the stochastic ordinary differential equation (5.2.2).

(2.1.2) is based on the following finite dimensional result (see, e.g., Eq. (15) of [100])

$$\widehat{p}^{(a,b)}_{x(t_i)f(t_j)} \overset{\text{def}}{=} \underbrace{\int \cdots \int}_{N} Q\left(f(t_1),...,f(t_N)\right) \delta\left(a - x_{t_i}\left(f(t_1),...,f(t_N)\right)\right)$$

$$\delta\left(b - f(t_j)\right) df(t_1) \cdots df(t_N), \qquad (2.1.3)$$

where $Q\left(f(t_1),...,f(t_N)\right)$ denotes the joint probability density of the forcing process at times $t_1,...,$ t_N (i.e. a random vector), while $x_{t_i}\left(f(t_1),...,f(t_N)\right)$ is a nonlinear mapping from $\mathbb{R}^N$ into $\mathbb{R}$ representing the response process at time t_i as a function of the forcing process at times $t_1,...,$ t_N. The functional integral (2.1.2) is defined as the limit of Eq. (2.1.3) as N goes to infinity. In this sense, in Eq. (2.1.2) we recognize the standard definitions of $Q[f]$ and $\mathcal{D}[f]$ as given, e.g., by [144] and [106]

$$Q[f] \overset{\text{def}}{=} \lim_{N \to \infty} Q\left(f(t_1),...,f(t_N)\right), \qquad (2.1.4)$$

$$\mathcal{D}[f] \overset{\text{def}}{=} \lim_{N \to \infty} \prod_{j=1}^{N} df(t_j), \qquad (2.1.5)$$

$$x_t[f] \overset{\text{def}}{=} \lim_{N \to \infty} x_t\left(f(t_1),...,f(t_N)\right), \qquad (2.1.6)$$

for an arbitrary discretization of the integration period into N points.

An evolution equation for the joint response-excitation probability density of the system (5.2.2) can be determined by differentiating Eq. (2.1.2) with respect to t. This yields

$$
\begin{aligned}
\frac{\partial p^{(a,b)}_{x(t)f(s)}}{\partial t} &= -\frac{\partial}{\partial a}\langle \delta\left(a - x_t[f]\right) \dot{x}_t \delta\left(b - f_s\right)\rangle \\
&= -\frac{\partial}{\partial a}\langle \delta\left(a - x_t[f]\right) g\left(x_t[f], t\right) \delta\left(b - f_s\right)\rangle - \frac{\partial}{\partial a}\langle \delta\left(a - x_t[f]\right) f_t \delta\left(b - f_s\right)\rangle \\
&= -\frac{\partial}{\partial a}\left(g\left(a,t\right) p^{(a,b)}_{x(t)f(s)}\right) - \frac{\partial}{\partial a}\langle \delta\left(a - x_t[f]\right) f_t \delta\left(b - f_s\right)\rangle, \qquad s,t \geq t_0.
\end{aligned}
$$

$$(2.1.7)$$

Taking the limit for $s \to t$ gives the following result, first obtained by [168] using a Hopf characteristic functional approach

$$\lim_{s \to t} \frac{\partial p_{x(t)f(s)}^{(a,b)}}{\partial t} = -\frac{\partial}{\partial a}\left(g\left(a,t\right)p_{x(t)f(t)}^{(a,b)}\right) - b\frac{\partial p_{x(t)f(t)}^{(a,b)}}{\partial a}, \qquad t \geq t_0 \quad a,b \in \mathbb{R}. \quad (2.1.8)$$

This equation looks like a closed evolution equation for the joint response-excitation probability density function of the stochastic dynamical system along the direction $s = t$. In the work of [168], Eq. (2.1.8) was also accompanied with an initial condition $p_{x(t_0)f(t_0)}^{(a,b)}$ and with the *marginal compatibility condition*[2]

$$\int_{-\infty}^{\infty} p_{x(t)f(s)}^{(a,b)}da = p_{f(s)}^{(b)}, \qquad t,s \geq t_0 \quad b \in \mathbb{R} \qquad (2.1.9)$$

expressing the fact that the evolution of the joint response-excitation density has to be consistent with the evolution of the excitation density $p_{f(t)}^{(b)}$. Note that since the stochastic process $f(t;\omega)$ is given, $p_{f(t)}^{(b)}$ is a known function. In addition, the joint density $p_{x(t)f(t)}^{(a,b)}$ has to satisfy the following two obvious, yet essential, *constitutive conditions*2

$$p_{x(s)f(t)}^{(a,b)} \geq 0, \qquad \int_{-\infty}^{\infty}\int_{-\infty}^{\infty} p_{x(s)f(t)}^{(a,b)}dadb = 1, \qquad t,s \geq t_0 \quad a,b \in \mathbb{R}. \qquad (2.1.10)$$

The system (2.1.8)-(2.1.10) was proposed as a computable set of equations describing the evolution of the joint response-excitation probability density function of dynamical systems driven by colored noise. Note that in the extended probability space consisting of the joint response-excitation statistics, the standard closure problem arising, e.g., in the classical colored noise master equation [82] seems to be overcome. However, the presence of the limit partial derivative at the left hand side of Eq. (2.1.8) should warn us on the fact that we are not dealing with a standard par-

---

[2]The integral is formally written from $-\infty$ to ∞ although the probability density $p_{x(t)f(s)}^{(a,b)}$ may be *compactly supported*.

tial differential equation. Indeed Eq. (2.1.8) is rather a *differential constraint* [193] to be satisfied by the joint response-excitation probability density function of any solution to Eq. (5.2.2) along the line $s = t$. Preliminary insight into the question of well-posedness of the boundary value problem (2.1.8)-(2.1.10) can be gained by expanding Eq. (2.1.7) for s in the neighborhood of t. This gives us a first-order correction to the differential constraint (2.1.8), which ultimately leads to a standard partial differential equation for the joint density $p_{x(t)f(t)}^{(a,b)}$ on the infinitesimal strip

$$
\mathcal{S}^{(\varepsilon)} = \bigcup_{t \geq t_0} I_t^{(\varepsilon)}, \quad \text{where} \quad I_t^{(\varepsilon)} \stackrel{\text{def}}{=} \{s \geq t_0 \,, |s - t| \leq \varepsilon\}, \quad t \geq t_0\,, \quad \varepsilon \to \mathbb{R}^+\,.
$$

$$(2.1.11)$$

To this end, let us assume that the random forcing process is differentiable in time and expand it into a Taylor series around s as

$$
f_t = f_s + (t - s)\dot{f}_s + \cdots\,.
$$

$$(2.1.12)$$

A substitution of this expansion back into Eq. (2.1.7) yields, after simple mathematical manipulations,

$$
\frac{\partial p_{x(t)f(s)}^{(a,b)}}{\partial t} = -\frac{\partial}{\partial a}\left(g\left(a,t\right) p_{x(t)f(s)}^{(a,b)}\right) - b\frac{\partial p_{x(t)f(s)}^{(a,b)}}{\partial a} + (t - s)\frac{\partial}{\partial a}\int_{-\infty}^{b}\frac{\partial p_{x(t)f(s)}^{(a,b')}}{\partial s}db'\,.
$$

$$(2.1.13)$$

This equation holds for all $t \geq t_0$ and for $s \in I_t^{(\varepsilon)}$, i.e., s in the neighborhood of t (see (2.1.11)). Analysis of Eq. (2.1.13) clearly shows that the derivatives $\partial p_{x(t)f(s)}^{(a,b)}/\partial t$ and $\partial p_{x(t)f(s)}^{(a,b)}/\partial s$ are *coupled*. In other words, in order to compute the joint response-excitation probability density function in the neighborhood of $s = t$ we need an additional expression for $\partial p_{x(t)f(s)}^{(a,b)}/\partial s$. This is also the case when we take the limit

$s \to t$. In fact, by using the obvious identity

$$\frac{\partial p_{x(t)f(t)}^{(a,b)}}{\partial t} = \lim_{t \to s} \frac{\partial p_{x(t)f(s)}^{(a,b)}}{\partial s} + \lim_{s \to t} \frac{\partial p_{x(t)f(s)}^{(a,b)}}{\partial t} \qquad (2.1.14)$$

we can see that the dynamics of the joint response-excitation probability density function in the direction $s = t$ (i.e. a directional derivative) can be represented as a superimposition of two differential constraints: the first one is Eq. (2.1.8), while the second one is

$$\lim_{t \to s} \frac{\partial p_{x(t)f(s)}^{(a,b)}}{\partial s} = -\frac{\partial}{\partial b} \langle \delta \left(a - x_t[f] \right) \delta \left(b - f_t \right) \dot{f}_t \rangle . \qquad (2.1.15)$$

This yields the partial differential equation

$$\frac{\partial p_{x(t)f(t)}^{(a,b)}}{\partial t} = -\frac{\partial}{\partial a} \left(g\left(a,t\right) p_{x(t)f(t)}^{(a,b)} \right) - b \frac{\partial p_{x(t)f(t)}^{(a,b)}}{\partial a} - \frac{\partial}{\partial b} \langle \delta \left(a - x_t[f] \right) \delta \left(b - f_t \right) \dot{f}_t \rangle ,$$

$$(2.1.16)$$

which is the complete evolution equation governing the dynamics of the joint response-excitation probability density function of the system. Equation (2.1.16) can be evaluated further if one has available an expression for the average $\langle \delta \left(a - x_t[f] \right) \delta \left(b - f_t \right) \dot{f}_t \rangle$ or, equivalently, $\langle \delta \left(a - x_t[f] \right) \delta \left(b - f_s \right) \rangle$. Such expression involves nonlocal functionals of the random forcing process f and it can be found in [196]. As we shall see in the next subsection, if we do not include the limit derivative (2.1.15) - i.e. the differential constraint complementary to Eq. (2.1.8) - within the set of equations, then the system (2.1.8)-(2.1.10) turns out to be *undetermined*, in the sense that it possibly admits an infinite number of solutions[3].

---

[3]In the numerical scheme employed by [168] this multiplicity was overcome by using a representation of the solution to Eq. (2.1.8) in terms of a Gaussian kernels. This introduces implicitly a symmetry in the covariance structure of the system, which ultimately results in a closure model.

2.1.1 Ill-posedness of the boundary value problem (2.1.8)-(2.1.10)

Let us consider the following trivial first-order dynamical system driven by a smooth random force $f(t; \omega)$

$$\begin{cases} \dot{x}\,(t;\omega) + x\,(t;\omega) = f(t;\omega) \\ x\,(t_0;\omega) = x_0\,(\omega) \end{cases} \tag{2.1.17}$$

For the purposes of the present example it is enough to set $f(t;\omega) = \sin(t) + \xi(\omega)$, where $\xi(\omega)$ is a Gaussian random variable. Let us also assume that the initial state of the system $x_0\,(\omega)$ is Gaussian distributed with zero-mean, and that $x_0\,(\omega)$ is independent of $\xi(\omega)$. The analytical solution to (2.1.17) is obviously

$$
x(t;\omega) = e^{-(t-t_0)} \left[\int_{t_0}^{t} e^{(\tau-t_0)} f(\tau;\omega)d\tau + x_0(\omega) \right]
$$
$$
= e^{-(t-t_0)} \left[\xi(\omega)\left(e^{t-t_0}-1\right) + x_0(\omega) + \frac{1}{2}e^{t-t_0}\left(\sin(t)-\cos(t)\right) - \frac{1}{2}\left(\sin(t_0)-\cos(t_0)\right) \right].
$$
$$\tag{2.1.18}$$

This allows us to obtain the joint probability of $x(t;\omega)$ and $f(s;\omega)$ by using the classical mapping approach (see, e.g., [141] p. 142). Specifically, we consider the following mapping between the random variables $(\xi(\omega), x_0(\omega))$ and $(x(t;\omega), f(s;\omega))$

$$\begin{cases} x(t;\omega) = A(t)\xi(\omega) + B(t)x_0(\omega) + C(t) \\ f(s;\omega) = \sin(s) + \xi(\omega) \end{cases} \tag{2.1.19}$$

where

$$ A(t) \overset{\text{def}}{=} 1 - e^{-(t-t_0)}, \qquad\qquad B(t) \overset{\text{def}}{=} e^{-(t-t_0)}, $$
$$ C(t) \overset{\text{def}}{=} \frac{1}{2}\left[(\sin(t)-\cos(t)) - e^{-(t-t_0)}\left(\sin(t_0)-\cos(t_0)\right) \right]. $$

This yields the joint response-excitation probability density function

$$p_{x(t)f(s)}^{(a,b)} = \frac{1}{2\pi B(t)} \exp\left[-\frac{1}{2}\left(b - \sin(s)\right)^2 - \frac{(a - A(t)b + A(t)\sin(s) - C(t))^2}{2B(t)^2} \right].$$

(2.1.20)

It is straightforward to verify that (2.1.20) satisfies

$$\lim_{s \to t} \frac{\partial p_{x(t)f(s)}^{(a,b)}}{\partial t} = \frac{\partial}{\partial a}\left(a p_{x(t)f(t)}^{(a,b)} \right) - b\frac{\partial p_{x(t)f(t)}^{(a,b)}}{\partial a}, \quad t \geq t_0 \quad a, b \in \mathbb{R},$$

(2.1.21)

which is the equation arising from Eq. (2.1.8) by setting $g(a, t) = -a$. Also, the marginal compatibility condition (2.1.9) as well as the constitutive relations (2.1.10) are obviously verified. However, if we set $C(t) = \alpha(t)$ in (2.1.20), where $\alpha(t)$ is an *arbitrary function* such that $\alpha(t_0) = 0$, then we easily see that we still have a probability density function satisfying Eqs. (2.1.21), (2.1.9), (2.1.10) and the initial condition. This suggest that this boundary value problem is not well-posed, in the sense that it admits an infinite number of solutions. In addition, we remark that setting $C(t) = \alpha(t)$ in (2.1.20) is not the only degree of freedom we have, as other solutions can be constructed. These observations provide a definitive answer to the question raised by [168], p. 295, regarding the solvability theory of the system (2.1.8)-(2.1.10). The multiplicity of solutions admitted by such system arises because the correlation structure between the response process x_t and the excitation process f_s was not properly taken into account in the formulation of the theory.

2.2 An evolution equation for the response probability density

In the past few decades, many researchers attempted to determine a closed equation describing the evolution of the response probability density of a stochastic system

driven by colored random noise (see, e.g., [57, 62, 84, 127, 178]). Perhaps, the first effective approach was developed by the school surrounding [178] and co-workers. The starting point is the functional representation of the response probability density. For the system (5.2.2) we have

$$p_{x(t)}^{(a)} = \langle \delta\left(a - x_t[f]\right) \rangle, \tag{2.2.1}$$

where the average is with respect to the joint probability functional of the excitation process and the initial state. Differentiation of (2.2.1) with respect to time yields

$$\frac{\partial p_{x(t)}^{(a)}}{\partial t} = -\frac{\partial}{\partial a}\left(g(a,t)p_{x(t)}^{(a)}\right) - \frac{\partial}{\partial a}\langle f_t\delta\left(a - x_t[f]\right)\rangle. \tag{2.2.2}$$

This equation can be evaluated further if one has available an expression for the average appearing in the last term at the right hand side. Among different methods devised to represent such quantity we recall small correlation time expansions [41, 62, 113, 178], cumulant resummation methods [113, 114], functional derivative techniques [81, 82, 92], path integral methods [121, 142, 189, 210], decoupling approximations [84] and operator projection methods [57, 75].

2.2.1 Consistency of the response-excitation theory with the classical response theory

It is important at this point to prove that the response-excitation theory is consistent with classical approaches for the response probability density function. This establishes a full correspondence between the two methods. To this end, let us first consider the differential constraint (2.1.8) and integrate it with respect to the variable

b from $-\infty$ to ∞. This yields

$$\frac{\partial p_{x(t)}^{(a)}}{\partial t} = -\frac{\partial}{\partial a}\left(g\left(a,t\right)p_{x(t)}^{(a)}\right) - \frac{\partial}{\partial a}\left(\int_{-\infty}^{\infty}bp_{x(t)f(t)}^{(a,b)}db\right). \qquad (2.2.3)$$

Now, let us take a closer look at the last term at the right hand side of Eq. (2.2.3). By definition (2.1.2), we have

$$\int_{-\infty}^{\infty}bp_{x(t)f(t)}^{(a,b)}db = \int_{-\infty}^{\infty}b\langle\delta\left(a-x_t[f]\right)\delta\left(b-f_t\right)\rangle db$$

$$= \langle\delta\left(a-x_t[f]\right)\int_{-\infty}^{\infty}b\delta\left(b-f_t\right)db\rangle$$

$$= \langle\delta\left(a-x_t[f]\right)f_t\rangle. \qquad (2.2.4)$$

If we substitute this result into Eq. (2.2.3) we obtain exactly Eq. (2.2.2). Therefore, we have shown that the differential constraint (2.1.8) is consistent with the classical response approach for random noise with arbitrary correlation time. This result extends the one obtained by [168] for systems driven by white-noise.

Next, we consider the evolution equation (2.1.16). By following the same steps that led us to the consistency result just discussed, we can show that the classical response approach is also included in Eq. (2.1.16). In fact, if we perform an integration with respect to b from $-\infty$ to ∞ we see that the last term in Eq. (2.1.16) vanishes. This is due to the properties of the probability density function at $\pm\infty$. Therefore, both the differential constraint (2.1.8) and the full evolution equation (2.1.16) are consistent with the classical response theory.

2.3 REPDF evolution equation for nonlinear stochastic ODEs

Let us consider the following nonlinear stochastic dynamical system

$$\frac{dx(t;\omega)}{dt} = G(x(t;\omega), \xi(\omega), t), \qquad x(t_0;\omega) = x_0(\omega), \qquad (2.3.1)$$

where $x(t;\omega) \in \mathbb{R}^n$ is a multi-dimensional stochastic process, while $\xi(\omega) \in \mathbb{R}^m$ and $x_0(\omega) \in \mathbb{R}^n$ are random variables with known joint probability function. The stochastic system (2.3.1) can be high dimensional as it can arise, for instance, from a discretization of a stochastic PDE subject to random boundary conditions, random initial conditions or random forcing terms [4]. The existence and the uniqueness of the solution to (2.3.1) for each realization of $\xi(\omega)$ and $x_0(\omega)$ allows us to consider the stochastic flow $x(t;\omega)$ as a deterministic function of $\xi(\omega)$ and $x_0(\omega)$, i.e. $x(t;\omega) = x(t; \xi(\omega), x_0(\omega))$.

Under this hypothesis, by using the response-excitation theory [49, 111, 196] it is straightforward to obtain an exact closed equation for the joint REPDF of the random vectors $x(t;\omega)$ and $\xi(\omega)$, namely

$$p_{x(t)\xi}^{(a,b)} \stackrel{\text{def}}{=} \langle \delta(a - x(t;\omega))\, \delta(b - \xi(\omega)) \rangle, \qquad t \geq t_0 \quad a \in \mathbb{R}^n \quad b \in \mathbb{R}^m, \qquad (2.3.2)$$

where the average operator $\langle \cdot \rangle$ is with respect to the joint PDF of the random input variables $\xi(\omega)$ and $x_0(\omega)$, while δ denotes a multi-dimensional Dirac delta function,

---

[4]In this case, the phase space variables $x_j(t;\omega)$ could be the Galerkin or the collocation coefficients of an expansion of the solution relatively to suitable spatial basis function $\phi_j(x)$, i.e.

$$u(x,t;\omega) = \sum_{j=1}^{n} x_j(t;\omega)\phi_j(x).$$

i.e.,

$$\delta(a - x(t; \omega)) \stackrel{\text{def}}{=} \prod_{i=1}^{n} \delta(a_i - x_i(t; \omega)), \qquad \delta(b - \xi(\omega)) \stackrel{\text{def}}{=} \prod_{k=1}^{m} \delta(b_k - \xi_k(\omega)).$$

The evolution equation for the joint REPDF (5.2.25) can be derived by differentiating the functional integral representation (5.2.25) with respect to t. By using well known identities involving the Dirac delta function [96, 100, 196], the time differentiation yields

$$\frac{\partial p_{x(t)\xi}^{(a,b)}}{\partial t} = -\sum_{i=1}^{n} \frac{\partial}{\partial a_i} \langle \dot{x}_i(t) \prod_{i=1}^{n} \delta(a_i - x_i(t; \omega)) \prod_{k=1}^{m} \delta(b_k - \xi_k) \rangle$$

$$= -\sum_{i=1}^{n} \frac{\partial}{\partial a_i} \langle G_i(x(t), t; \xi_1, ..., \xi_M) \prod_{i=1}^{n} \delta(a_i - x_i(t; \omega)) \prod_{k=1}^{m} \delta(b_k - \xi_k) \rangle,$$

and we obtain

$$\frac{\partial p_{x(t)\xi}^{(a,b)}}{\partial t} = \mathcal{L}(t) p_{x(t)\xi}^{(a,b)}, \tag{2.3.3}$$

where

$$\mathcal{L}(t) \stackrel{\text{def}}{=} -\sum_{i=1}^{n} \frac{\partial G_i(a, b, t)}{\partial a_i} - \sum_{i=1}^{n} G_i(a, b, t) \frac{\partial}{\partial a_i}$$

is a *first-order* (time-dependent) linear partial differential operator in n variables $(a_1,...,a_n)$ and m parameters $(b_1,...,b_m)$. Time-dependence can arise, e.g., due to time-dependent random boundary conditions in SPDEs or time-dependent random forcing terms in SODEs.

The REPDF equation (2.3.3) is supplemented with appropriate boundary conditions and with the initial condition $p_{x(t_0)\xi}^{(a,b)}$, expressing the joint PDF of $x_0(t_0; \omega)$ and $\xi(\omega)$. Kinetic equations of type (2.3.3) were determined long time ago by Dostupov and Pugachev in [49]. More recently, Li and Chen [111] introduced a similar theory in the context of stochastic dynamics of structures (see [111] Ch. 7-8 and [29]) by using conservation of probability arguments.

We notice that the REPDF equation (2.3.3) is analogous to the Liouville equation of classical statistical mechanics, as it governs the evolution of the joint PDF of the phase space. This analogy can be exploited even further by noting that the ODE system (2.3.1) can be rewritten as a larger system subject only to a random initial condition. To this end, it is sufficient to define a new set of phase variables $y(t; \omega)$ evolving according to

$$\frac{dy(t; \omega)}{dt} = 0 \,, \qquad y(t_0; \omega) = \xi(\omega) \,, \qquad y(t; \omega) \in \mathbb{R}^m \,, \tag{2.3.4}$$

and replace the vector $\xi(\omega)$ in (2.3.1) with $y(t; \omega)$. This yields

$$\frac{dx(t; \omega)}{dt} = G(x(t; \omega), y(t; \omega), t) \,, \qquad x(t_0; \omega) = x_0(\omega) \,. \tag{2.3.5}$$

The system (2.3.4)-(2.3.5) is equivalent to (2.3.1), but now the random variables $\xi(\omega)$ appear as an initial condition for $y(t; \omega)$. In this form the Liouville theory applies, leading us to the joint REPDF equation (2.3.3).

Time integration schemes for (2.3.3) relying directly on formal representations, such as Magnus expansions [14], usually require the computation of exponential operators involving $\mathcal{L}(t)$. As a result of discretization of the phase space, $\mathcal{L}(t)$ typically becomes a very large matrix and, as a consequence, the exponentiation operation is exceedingly costly [165, 182].

2.4 REPDF equations for first-order nonlinear stochastic PDEs

Let us consider the nonlinear scalar evolution equation

$$\frac{\partial u}{\partial t} + \mathcal{N}(u, u_x, x, t) = 0 \,, \tag{2.4.1}$$

where $\mathcal{N}$ is a continuously differentiable function. For the moment, we restrict our attention to only one spatial dimension and assume that the field $u(x, t; \omega)$ is random as a consequence of the fact that the initial condition or the boundary condition associated with Eq. (2.4.1) are random. A more general case involving a random forcing term will be discussed later in this section. As is well known, the full statistical information of the solution to Eq. (2.4.1) can be always encoded in the Hopf characteristic functional of the system [194]. In some very special cases, however, the functional differential equation satisfied by the Hopf functional can be reduced to a standard partial differential equation for the one-point one-time characteristic function or, equivalently, for the PDF of the system. First-order nonlinear scalar stochastic PDEs of the form (2.4.1) belong to this class and, in general, they admit a reformulation in terms of the joint density of u and its first order spatial derivative u_x at the *same* space-time location, i.e.,

$$p_{uu_x}^{(a,b)} = \langle \delta(a - u(x,t))\delta(b - u_x(x,t)) \rangle. \tag{2.4.2}$$

The average operator $\langle \cdot \rangle$ here is defined as an integral with respect to the joint probability density functional of the random initial condition and the random boundary condition. A differentiation of Eq. (2.4.2) with respect to time yields

$$\frac{\partial p_{uu_x}^{(a,b)}}{\partial t} = -\frac{\partial}{\partial a}\langle \delta(a - u)u_t\delta(b - u_x) \rangle - \frac{\partial}{\partial b}\langle \delta(a - u)\delta(b - u_x)u_{xt} \rangle. \tag{2.4.3}$$

If we substitute Eq. (2.4.1) and its derivative with respect to x into Eq. (2.4.3) we obtain

$$\frac{\partial p_{uu_x}^{(a,b)}}{\partial t} = \frac{\partial}{\partial a}\left(\mathcal{N}p_{uu_x}^{(a,b)}\right) + \frac{\partial}{\partial b}\langle\left(\frac{\partial \mathcal{N}}{\partial u}u_x + \frac{\partial \mathcal{N}}{\partial u_x}u_{xx} + \frac{\partial \mathcal{N}}{\partial x}\right)\delta(a - u)\delta(b - u_x)\rangle. \tag{2.4.4}$$

Next, let us recall that $\mathcal{N}$ and its derivatives are at least continuous functions (by assumption) and therefore by using [194] they can be taken out of the averages. Thus, the only item that is missing in order to close Eq. (2.4.4) is an expression for the average of u_{xx} in terms of the probability density function. Such an expression can be easily obtained by integrating the identity

$$\frac{\partial p_{uu_x}^{(a,b)}}{\partial x} = -b\frac{\partial p_{uu_x}^{(a,b)}}{\partial a} - \frac{\partial}{\partial b}\langle \delta(a-u)\delta(b-u_x)u_{xx}\rangle \qquad (2.4.5)$$

with respect to b from $-\infty$ to b and taking into account the fact that the average of any field vanishes when $b \to \pm\infty$ due to the properties of the underlying probability density functional. Therefore, Eq. (2.4.5) can be equivalently written as

$$\langle \delta(a-u)\delta(b-u_x)u_{xx}\rangle = -\int_{-\infty}^{b}\frac{\partial p_{uu_x}^{(a,b')}}{\partial x}db' - \int_{-\infty}^{b}b'\frac{\partial p_{uu_x}^{(a,b')}}{\partial a}db' . \qquad (2.4.6)$$

A substitution of this relation into Eq. (2.4.4) yields the final result

$$\begin{aligned}\frac{\partial p_{uu_x}^{(a,b)}}{\partial t} &= \frac{\partial}{\partial a}\left(\mathcal{N}p_{uu_x}^{(a,b)}\right) + \frac{\partial}{\partial b}\left[\left(b\frac{\partial \mathcal{N}}{\partial a} + \frac{\partial \mathcal{N}}{\partial x}\right)p_{uu_x}^{(a,b)}\right.\\ &\quad \left.-\frac{\partial \mathcal{N}}{\partial b}\left(\int_{-\infty}^{b}\frac{\partial p_{uu_x}^{(a,b')}}{\partial x}db' + \int_{-\infty}^{b}b'\frac{\partial p_{uu_x}^{(a,b')}}{\partial a}db'\right)\right],\end{aligned} \qquad (2.4.7)$$

where $\mathcal{N}$ here is a function of a, b, x and t, respectively. Equation (2.4.7) is the correct evolution equation for the joint PDF associated with the solution to an arbitrary nonlinear evolution problem in the form (2.4.1). This equation made its first appearance in [118], although the original published version has many typos and a rather doubtful derivation[5]. A generalization of Eq. (2.4.1) includes an external

---

[5]The equation numbering in this footnote corresponds to the one in Ref. [118]. First of all, we notice a typo in Eq. (1.5), i.e. two brackets are missing. Secondly, according to Eq. (1.1) f is a multivariable function that includes also x and therefore one term is missing in Eq. (1.6). Also, the final result (1.8) seems to have three typos, i.e., the variable v is missing in the last integral within the brackets (this typo was corrected in the subsequent Eq. (1.9)) and there are two signs that are wrong. We remark that these sign errors are still present in Eq. (1.9).

random force in the form

$$\frac{\partial u}{\partial t} + \mathcal{N}(u, u_x, x, t) = f(x, t; \omega) \,. \tag{2.4.8}$$

Depending on the type of the random field f and on its correlation structure, different stochastic methods can be employed. For instance, if the characteristic variation of f is much shorter than the characteristic variation of the solution u then we can use small correlation space-time expansions. In particular, if the field f is Gaussian then we can use the Furutsu-Novikov-Donsker [46, 65, 136] formula (see also [16, 17, 103]). Alternatively, if we have available a Karhunen-Loève expansion

$$f(x, t; \omega) = \sum_{k=1}^{m} \lambda_k \xi_k(\omega) \psi_k(x, t) \,, \tag{2.4.9}$$

then we can obtain a closed and exact equation for the joint probability of u, u_x and all the (uncorrelated) random variables $\{\xi_k(\omega)\}$ appearing in the series (2.4.9), i.e.,

$$p_{u(x,t)u_x(x,t)\{\xi_k\}}^{(a,b,\{c_k\})} = \langle \delta(a - u(x,t))\delta(b - u_x(x,t)) \prod_{k=1}^{m} \delta(c_k - \xi_k) \rangle \,. \tag{2.4.10}$$

For the specific case of Eq. (2.4.8) we obtain the PDF equation

$$
\begin{aligned}
\frac{\partial P}{\partial t} &= \frac{\partial}{\partial a}(\mathcal{N}P) + \frac{\partial}{\partial b}\left[\left(b\frac{\partial \mathcal{N}}{\partial a} + \frac{\partial \mathcal{N}}{\partial x}\right)P \right. \\
&\left. - \frac{\partial \mathcal{N}}{\partial b}\left(\int_{-\infty}^{b}\frac{\partial P}{\partial x}db' + \int_{-\infty}^{b}b'\frac{\partial P}{\partial a}db'\right)\right] - \left[\sum_{k=1}^{m}\lambda_k c_k \psi_k\right]\frac{\partial P}{\partial a} \,,
\end{aligned}
\tag{2.4.11}
$$

where we have used the shorthand notation

$$P \overset{\text{def}}{=} p_{u(x,t)u_x(x,t)\{\xi_k\}}^{(a,b,\{c_k\})} \,. \tag{2.4.12}$$

Note that Eq. (2.4.11) is linear and exact but it involves 4 variables (t, x, a and b) and m parameters ($\{c_1, ..., c_m\}$). In any case, once the solution is available[6] we can integrate out the variables ($b, \{c_k\}$) and obtain the *response probability of the system*, i.e. the probability density of the solution u at every space-time point as

$$p_{u(x,t)}^{(a)} = \int_{-\infty}^{\infty} \cdots \int_{-\infty}^{\infty} p_{u(x,t)u_x(x,t)\{\xi_k\}}^{(a,b,\{c_k\})} \, db \, dc_1 \cdots dc_m \,. \qquad (2.4.13)$$

The integrals above are formally written from $-\infty$ to ∞ although the probability density we are integrating out may be compactly supported. We conclude this section by observing that the knowledge of the probability density function of the solution to a stochastic PDE at a specific location does *not* provide all the statistical information of the system. For instance, the calculation of the two-point correlation function $\langle u(x,t)u(x',t') \rangle$ requires the knowledge of the joint probability density of the solution u at two different locations, i.e. $p_{u(x,t)u(x',t')}^{(a,b)}$. We will go back to this point in section 2.5.

2.4.1 Nonlinear advection problem with an additional quadratic nonlinearity

Let us consider the following quadratic prototype problem (see, e.g., [145], p. 358)

$$\begin{cases} \dfrac{\partial u}{\partial t} + u \dfrac{\partial u}{\partial x} + \nu \left(\dfrac{\partial u}{\partial x} \right)^2 = 0 \,, \quad \nu \geq 0 \,, \quad x \in [0, 2\pi] \,, \quad t \geq t_0 \\[2mm] u(x, t_0; \omega) = A \sin(x) + \eta(\omega) \,, \quad A > 0 \\[2mm] \text{Periodic B.C.} \end{cases} \qquad (2.4.14)$$

where $\eta(\omega)$ is a random variable with known probability density function. If we substitute Eq. (2.4.14) and its derivative with respect to x into Eq. (2.4.3) we

---

[6]Later on we will discuss in more detail numerical algorithms and techniques that can be employed to compute the numerical solution to a multidimensional linear PDE like (2.4.11).

obtain

$$\frac{\partial p_{uu_x}^{(a,b)}}{\partial t} = \left(ab + \nu b^2\right) \frac{\partial p_{uu_x}^{(a,b)}}{\partial a} + b p_{uu_x}^{(a,b)} + \frac{\partial}{\partial b} \langle \delta(a-u)\delta(b-u_x) \left(u_x^2 + u u_{xx} + 2\nu u_x u_{xx}\right) \rangle.$$

$$(2.4.15)$$

At this point we need an explicit expression for the last average at the right hand side of Eq. (2.4.15) in terms of the probability density function (2.4.2). Such an expression can be easily determined by using the averaging rule [194] and identity (2.4.6). We finally get

$$\frac{\partial p_{uu_x}^{(a,b)}}{\partial t} = - a \frac{\partial p_{uu_x}^{(a,b)}}{\partial x} + b p_{uu_x}^{(a,b)} + \frac{\partial}{\partial b} \left(b^2 p_{uu_x}^{(a,b)}\right) - $$
$$\nu b^2 \frac{\partial p_{uu_x}^{(a,b)}}{\partial a} - 2\nu \left(b \frac{\partial p_{uu_x}^{(a,b)}}{\partial x} + \int_{-\infty}^{b} b' \frac{\partial p_{uu_x}^{(a,b')}}{\partial a} db' + \int_{-\infty}^{b} \frac{\partial p_{uu_x}^{(a,b')}}{\partial x} db'\right). \quad (2.4.16)$$

This equation is consistent with the general law (2.4.7) with $\mathcal{N}(a, b, x, t) = ab + \nu b^2$. An alternative derivation of Eq. (2.4.16) is also provided in [194] by employing the Hopf characteristic functional approach. Note that Eq. (2.4.16) is a linear partial differential equation in 4 variables (a, b, x, t) that can be integrated for $t \geq t_0$ once the joint probability of u and u_x is provided at some initial time t_0. In the present example, such an initial condition can be obtained by observing that the spatial derivative of the random initial state $u(x, t_0; \omega) = A \sin(x) + \eta(\omega)$ is the *deterministic* function

$$u_x(x, t_0; \omega) = A \cos(x). \quad (2.4.17)$$

Therefore, by applying the Dirac delta formalism, we see that the initial condition for the joint probability density of u and u_x is

$$
\begin{aligned}
p_{u(x,t_0)u_x(x,t_0)}^{(a,b)} &= \langle \delta(a - A\sin(x) - \eta)\delta(b - A\cos(x))\rangle \\
&= \delta(b - A\cos(x))\langle\delta(a - A\sin(x) - \eta)\rangle \\
&= \delta(b - A\cos(x))\frac{1}{\sqrt{2\pi}}e^{-(a-A\sin(x))^2/2}, \quad (2.4.18)
\end{aligned}
$$

provided $\eta(\omega)$ is a Gaussian random variable. At this point it is clear that Eq. (2.4.16) has to be interpreted in a weak sense in order for the initial condition (2.4.18) to be meaningful. From a numerical viewpoint the presence of the Dirac delta function within the initial condition introduces significant difficulties. In fact, if we adopt a Fourier-Galerkin framework then we need a very high (theoretically infinite) resolution in the b direction in order to resolve such initial condition and, consequently, the proper temporal dynamics of the probability function. In addition, the Fourier-Galerkin system associated with Eq. (2.4.16) is fully coupled and therefore inaccurate representations of the Dirac delta appearing in the initial condition rapidly propagate within the Galerkin system, leading to numerical errors. However, we can always apply a Fourier transformation with respect to a and b to Eqs. (2.4.16) and (2.4.18), before performing the numerical discretization. This is actually equivalent to look for a solution in terms of the joint characteristic function instead of the joint probability density function. The corresponding evolution equation is obtained in [194] and it is rewritten hereafter for convenience ($\phi_{uu_x}^{(a,b)}$ denotes the joint characteristic function of u and u_x, while i is the imaginary unit)

$$
\begin{aligned}
\frac{\partial \phi_{uu_x}^{(a,b)}}{\partial t} &= ib\frac{\partial^2 \phi_{uu_x}^{(a,b)}}{\partial b^2} - i\frac{\partial \phi_{uu_x}^{(a,b)}}{\partial b} + i\frac{\partial^2 \phi_{uu_x}^{(a,b)}}{\partial a\partial x} - i\nu a\frac{\partial^2 \phi_{uu_x}^{(a,b)}}{\partial b^2} \\
&\quad - 2\frac{i\nu}{b}\left(\frac{\partial \phi_{uu_x}^{(a,b)}}{\partial x} - a\frac{\partial \phi_{uu_x}^{(a,b)}}{\partial b} - b\frac{\partial^2 \phi_{uu_x}^{(a,b)}}{\partial b\partial x}\right). \quad (2.4.19)
\end{aligned}
$$

The initial condition for this equation is obtained by Fourier transformation of Eq. (2.4.18), i.e.

$$\phi_{u(x,t_0)u_x(x,t_0)}^{(a,b)} = \frac{1}{\sqrt{2\pi}} e^{ibA\cos(x)} \int_{-\infty}^{\infty} e^{ia\alpha-(\alpha-A\sin(x))^2/2} d\alpha \,. \tag{2.4.20}$$

We do not address here the computation of the numerical solution to the problem defined by Eqs. (2.4.16) and (2.4.18).

2.5 REPDF equations for first-order quasilinear stochastic PDEs

In this section we obtain a kinetic equation for the probability density function associated with the stochastic solutions to multidimensional quasilinear stochastic PDE in the form

$$\frac{\partial u}{\partial t} + \boldsymbol{\mathcal{P}}(u,t,\boldsymbol{x};\boldsymbol{\xi}) \cdot \nabla_x u = \mathcal{Q}(u,t,\boldsymbol{x};\boldsymbol{\eta}) \,. \tag{2.5.1}$$

In this equation $\boldsymbol{\mathcal{P}}$ and $\mathcal{Q}$ are assumed to be continuously differentiable functions, $\boldsymbol{x}$ denotes a set of independent variables[7] while $\boldsymbol{\xi} = [\xi_1, ..., \xi_m]$ and $\boldsymbol{\eta} = [\eta_1, ..., \eta_n]$ are two vectors of random variables with known joint probability density function. We remark that Eq. (2.5.1) models many physically interesting phenomena such as ocean waves [20], linear and nonlinear advection problems, advection-reaction equations [180, 186] and, more generally, scalar conservation laws. We first consider the case where the stochastic solution $u(\boldsymbol{x}, t; \omega)$ is random as consequence of the fact that the initial condition or the boundary conditions are random. In other words,

---

[7]In many applications $\boldsymbol{x}$ is a vector of spatial coordinates, e.g., $\boldsymbol{x} = (x, y, z)$. In a more general framework $\boldsymbol{x}$ is a vector of independent variables including, e.g., spatial coordinates and parameters. For example, the two-dimensional action balance equation for ocean waves in the Eulerian framework [20, 207] is defined in terms of the following variables $\boldsymbol{x} = (x, y, \theta, \sigma)$ where θ and σ denote wave direction and wavelength, respectively.

we temporarily remove the dependence on $\{\xi_k\}$ and $\{\eta_k\}$ in $\boldsymbol{\mathcal{P}}$ and $\mathcal{Q}$, respectively. In this case we can determine an exact evolution equation for the one point one time PDF

$$p^{(a)}_{u(\boldsymbol{x},t)} = \langle \delta(a - u(\boldsymbol{x},t)) \rangle. \tag{2.5.2}$$

The average here is with respect to the joint probability density functional of the random initial condition and the random boundary conditions. Differentiation of (2.5.2) with respect to t yields

$$\frac{\partial p^{(a)}_{u(\boldsymbol{x},t)}}{\partial t} = -\frac{\partial}{\partial a} \langle \delta(a - u(\boldsymbol{x},t)) \left[-\boldsymbol{\mathcal{P}}(u,t,\boldsymbol{x}) \cdot \nabla_x u + \mathcal{Q}(u,t,\boldsymbol{x}) \right] \rangle. \tag{2.5.3}$$

By using the results of the previous sections it is easy to show that this equation can be equivalently written as

$$\frac{\partial p^{(a)}_{u(\boldsymbol{x},t)}}{\partial t} + \frac{\partial}{\partial a} \left(\boldsymbol{\mathcal{P}}(a,t,\boldsymbol{x}) \cdot \int_{-\infty}^{a} \nabla_x p^{(a')}_{u(\boldsymbol{x},t)} da' \right) = -\frac{\partial}{\partial a} \left(\mathcal{Q}(a,t,\boldsymbol{x}) \, p^{(a)}_{u(\boldsymbol{x},t)} \right). \tag{2.5.4}$$

Note that this is a linear partial differential equation in $(D+2)$ variables, where D denotes the number of independent variables appearing in the vector $\boldsymbol{x}$. Such dimensionality is completely independent of the number of random variables describing the boundary conditions or the initial conditions.

As we have previously pointed out, the knowledge of the one-point one-time probability density function of the solution to a stochastic PDE does not provide all the statistical information about the stochastic system. For instance, the computation of the two-point correlation function requires the knowledge of the joint probability of the solution field at two different locations. In order to determine such equation let us consider the joint density

$$p^{(a,b)}_{u(\boldsymbol{x},t)u(\boldsymbol{x}',t)} = \langle \delta(a - u(\boldsymbol{x},t)) \delta(b - u(\boldsymbol{x}',t)) \rangle. \tag{2.5.5}$$

Differentiation of Eq. (2.5.2) with respect to time yields

$$\frac{\partial}{\partial t}p^{(a,b)}_{u(\boldsymbol{x},t)u(\boldsymbol{x}',t)} = -\frac{\partial}{\partial a}\langle \delta(a - u(\boldsymbol{x},t))\delta(b - u(\boldsymbol{x}',t))\left[-\boldsymbol{P}(u,t,\boldsymbol{x})\cdot \nabla)xu + \mathcal{Q}(u,t,\boldsymbol{x})\right]\rangle$$
$$-\frac{\partial}{\partial b}\langle \delta(a - u(\boldsymbol{x},t))\delta(b - u(\boldsymbol{x}',t))\left[-\boldsymbol{P}(u,t,\boldsymbol{x}')\cdot \nabla_{x'}u + \mathcal{Q}(u,t,\boldsymbol{x}')\right]\rangle,$$

$$(2.5.6)$$

and therefore

$$\frac{\partial}{\partial t}p^{(a,b)}_{u(\boldsymbol{x},t)u(\boldsymbol{x}',t)} = -\frac{\partial}{\partial a}\left(\boldsymbol{P}(a,t,\boldsymbol{x})\cdot \int^a \nabla_x p^{(a',b)}_{u(\boldsymbol{x},t)u(\boldsymbol{x}',t)}da'\right) - \frac{\partial}{\partial a}\left(\mathcal{Q}(a,t,\boldsymbol{x})\,p^{(a,b)}_{u(\boldsymbol{x},t)u(\boldsymbol{x}',t)}\right)$$
$$-\frac{\partial}{\partial b}\left(\boldsymbol{P}(b,t,\boldsymbol{x})\cdot \int^b \nabla_{x'}p^{(a,b')}_{u(\boldsymbol{x},t)u(\boldsymbol{x}',t)}db'\right) - \frac{\partial}{\partial b}\left(\mathcal{Q}(b,t,\boldsymbol{x}')\,p^{(a,b)}_{u(\boldsymbol{x},t)u(\boldsymbol{x}',t)}\right). \quad (2.5.7)$$

Next, we consider the full Eq. (2.5.1) and we look for a kinetic equation involving the joint probability density of u and all the random variables $\{\xi_i\}$ and $\{\eta_j\}$

$$p^{(a,\boldsymbol{b},\boldsymbol{c})}_{u(\boldsymbol{x},t)\boldsymbol{\xi}\boldsymbol{\eta}} \overset{\text{def}}{=} \langle \delta(a - u(\boldsymbol{x},t)) \prod_{k=1}^{m}\delta(b_k - \xi_k)\prod_{j=1}^{n}\delta(c_k - \eta_k)\rangle. \quad (2.5.8)$$

The average here is with respect to the joint probability density functional of the random initial condition, the random boundary conditions and all the random variables $\{\xi_i\}$ and $\{\eta_j\}$. By following exactly the same steps that led us to Eq. (2.5.4) we obtain

$$\frac{\partial}{\partial t}p^{(a,\boldsymbol{b},\boldsymbol{c})}_{u(\boldsymbol{x},t)\boldsymbol{\xi}\boldsymbol{\eta}} + \frac{\partial}{\partial a}\left(\boldsymbol{P}(a,t,\boldsymbol{x},\boldsymbol{b})\cdot \int_{-\infty}^{a}\nabla p^{(a',\boldsymbol{b},\boldsymbol{c})}_{u(\boldsymbol{x},t)\boldsymbol{\xi}\boldsymbol{\eta}}da'\right) = -\frac{\partial}{\partial a}\left(\mathcal{Q}(a,t,\boldsymbol{x},\boldsymbol{c})\,p^{(a,\boldsymbol{b},\boldsymbol{c})}_{u(\boldsymbol{x},t)\boldsymbol{\xi}\boldsymbol{\eta}}\right).$$

$$(2.5.9)$$

Thus, if $\boldsymbol{x}$ is a vector of D variables then Eq. (2.5.9) involves $(D + 2)$ variables and $(n + m)$ parameters, i.e. $\boldsymbol{b} = (b_1, ..., b_m)$, $\boldsymbol{c} = (c_1, ..., c_n)$. Therefore, the numerical solution to Eq. (2.5.9) necessarily involves the use of computational schemes specifically designed for high-dimensional problems such as sparse grid or separated

representations [33, 108, 140]. However, let us remark that if $\mathcal{P}$ and $\mathcal{Q}$ are easily integrable then we can apply the method of characteristics directly to Eq. (2.5.1) and obtain an analytical solution to the problem. Unfortunately, this is not always possible and therefore the use of numerical approaches is often unavoidable.

2.5.1   Linear advection

Let us consider the simple linear advection problem

$$
\begin{cases}
\dfrac{\partial u}{\partial t} + \dfrac{\partial u}{\partial x} = \sigma \xi(\omega)\psi(x,t)\,, & \sigma \geq 0\,, \quad x \in [0, 2\pi]\,, \quad t \geq t_0 \\[2mm]
u(x, t_0; \omega) = u_0(x; \omega) \\[2mm]
\text{Periodic B.C.}
\end{cases}
\tag{2.5.10}
$$

where $u_0(x; \omega)$ is a random initial condition of arbitrary dimensionality, $\xi(\omega)$ is a random variable and ψ is a prescribed deterministic function. We look for an equation involving the joint response-excitation probability density function

$$
p_{u(x,t)\xi}^{(a,b)} = \langle \delta(a - u(x,t))\delta(b - \xi) \rangle\,.
\tag{2.5.11}
$$

The average here is with respect to the joint probability measure of $u_0(x; \omega)$ and $\xi(\omega)$. Differentiation of (2.5.11) with respect to t and x yields, respectively

$$
\frac{\partial p_{u(x,t)\xi}^{(a,b)}}{\partial t} = -\tfrac{\partial}{\partial a}\langle \delta(a - u)u_t\delta(b - \xi)\rangle\,,
\tag{2.5.12}
$$

$$
\frac{\partial p_{u(x,t)\xi}^{(a,b)}}{\partial x} = -\tfrac{\partial}{\partial a}\langle \delta(a - u)u_x\delta(b - \xi)\rangle\,.
\tag{2.5.13}
$$

A summation of Eqs. (2.5.12) and (2.5.13) gives the final result

$$
\begin{aligned}
\frac{\partial p^{(a,b)}_{u(x,t)\xi}}{\partial t} + \frac{\partial p^{(a,b)}_{u(x,t)\xi}}{\partial x} &= -\frac{\partial}{\partial a}\langle \delta(a-u)\left[u_t + u_x\right]\delta(b-\xi)\rangle \\
&= -\frac{\partial}{\partial a}\langle \delta(a-u)\sigma\xi\psi\delta(b-\xi)\rangle \\
&= -\sigma b\psi(x,t)\frac{\partial p^{(a,b)}_{u(x,t)\xi}}{\partial a}\,.
\end{aligned}
\tag{2.5.14}
$$

Thus, the problem corresponding to Eq. (2.5.10) can be formulated in probability space as

$$
\begin{cases}
\dfrac{\partial p^{(a,b)}_{u(x,t)\xi}}{\partial t} + \dfrac{\partial p^{(a,b)}_{u(x,t)\xi}}{\partial x} = -\sigma\dfrac{\partial p^{(a,b)}_{u(x,t)\xi}}{\partial a}b\psi(x,y)\,, \quad \sigma\geq 0\,,\quad x\in[0,2\pi]\,,\quad t\geq t_0 \\[2ex]
p^{(a,b)}_{u(x,t_0)\xi} = p^{(a)}_{u_0(x)}p^{(b)}_{\xi} \\[1ex]
\text{Periodic B.C.}
\end{cases}
\tag{2.5.15}
$$

where we have assumed that the process $u_0(x;\omega)$ is independent of ξ and we have denoted by $p^{(a)}_{u_0(x)}$ and $p^{(b)}_{\xi}$ the probability densities of the initial condition and $\xi(\omega)$, respectively. Equation (2.5.15) is derived in [194] by employing a Hopf characteristic functional approach. Once the solution to Eq. (2.5.15) is available, we can compute the *response probability* of the system as

$$
p^{(a)}_{u(x,t)} = \int_{-\infty}^{\infty} p^{(a,b)}_{u(x,t)\xi}\,db
\tag{2.5.16}
$$

and then extract all the statistical moments we are interested in, e.g.,

$$
\langle u^m(x,t;\omega)\rangle = \int_{-\infty}^{\infty} a^m p^{(a)}_{u(x,t)}\,da\,.
\tag{2.5.17}
$$

2.5.2   Nonlinear advection

A more interesting problem concerns the computation of the statistical properties of the solution to the randomly forced inviscid Burgers equation

$$
\begin{cases}
\dfrac{\partial u}{\partial t} + u\dfrac{\partial u}{\partial x} = \sigma\xi(\omega)\psi(x,t)\,, \quad \sigma \geq 0\,, \quad x \in [0, 2\pi]\,, \quad t \geq t_0 \\[2mm]
u(x, t_0; \omega) = A\sin(x) + \eta(\omega) \quad A \in \mathbb{R} \\[2mm]
\text{Periodic B.C.}
\end{cases}
\tag{2.5.18}
$$

where, as before, ξ and η are assumed as independent Gaussian random variables and ψ is a prescribed deterministic function. Note that the amplitude of the initial condition controls the initial speed of the wave. We look for an equation involving the probability density (2.5.11). To this end, we differentiate it with respect to t and x

$$
\frac{\partial p^{(a,b)}_{u(x,t)\xi}}{\partial t} = -\frac{\partial}{\partial a}\langle \delta(a-u)u_t\delta(b-\xi)\rangle\,,
\tag{2.5.19}
$$

$$
\frac{\partial p^{(a,b)}_{u(x,t)\xi}}{\partial x} = -\frac{\partial}{\partial a}\langle \delta(a-u)u_x\delta(b-\xi)\rangle\,,
\tag{2.5.20}
$$

$$
a\frac{\partial p^{(a,b)}_{u(x,t)\xi}}{\partial x} = -\frac{\partial}{\partial a}\langle \delta(a-u)uu_x\delta(b-\xi)\rangle + \langle \delta(a-u)u_x\delta(b-\xi)\rangle\,.
\tag{2.5.21}
$$

By using Eq. (2.5.19) we obtain

$$
\langle \delta(a-u)u_x\delta(b-\xi)\rangle = -\int_{-\infty}^{a}\frac{\partial p^{(a',b)}_{u(x,t)\xi}}{\partial x}da'\,.
\tag{2.5.22}
$$

Finally, a summation of Eq. (2.5.19) and Eq. (2.5.21) (with the last term given by Eq. (2.5.22)) gives

$$
\begin{cases}
\dfrac{\partial p_{u(x,t)\xi}^{(a,b)}}{\partial t} + a\dfrac{\partial p_{u(x,t)\xi}^{(a,b)}}{\partial x} + \displaystyle\int_{-\infty}^{a} \dfrac{\partial p_{u(x,t)\xi}^{(a',b)}}{\partial x}da' = -\sigma b\psi(x,t)\dfrac{\partial p_{u(x,t)\xi}^{(a,b)}}{\partial a}\,, & x \in [0,2\pi]\,, \quad t \geq t_0 \\[4mm]
p_{u(x,t_0)\xi}^{(a,b)} = p_\eta(a,x)p_\xi(b) \\[3mm]
\text{Periodic B.C.}
\end{cases}
$$

$$(2.5.23)$$

where, as before

$$
p_\xi(b) = \frac{1}{\sqrt{2\pi}}e^{-b^2/2}\,, \qquad p_\eta(a,x) = \frac{1}{\sqrt{2\pi}}e^{-(a-A\sin(x))^2/2}\,. \tag{2.5.24}
$$

Equation (2.5.23) can be derived also by employing a Hopf characteristic functional approach.

2.5.3 Advection-reaction equation

Let us consider a multidimensional advection-reaction system governed by the stochastic PDE

$$
\frac{\partial u}{\partial t} + \boldsymbol{U}(\boldsymbol{x},t;\omega) \cdot \nabla u = \mathcal{H}(u)\,, \tag{2.5.25}
$$

where $\boldsymbol{x} = (x,y,z)$ are spatial coordinates, $\boldsymbol{U}(\boldsymbol{x},t;\omega)$ is a vectorial random field with known statistics and $\mathcal{H}$ is a nonlinear function of u. Equation (2.5.25) has been recently investigated by Tartakovsky and Broyda [180] in the context of transport phenomena in heterogeneous porous media with uncertain properties[8]. In the sequel, we shall assume that we have available a representation of the random field $\boldsymbol{U}(\boldsymbol{x},t;\omega)$,

---

[8]In [180] it is assumed that $\mathcal{H}$ is random as a consequence of an uncertain reaction rate constant $\kappa(\boldsymbol{x};\omega)$.

e.g., a Karhunen-Loève series of each component in the form

$$U^{(x)}(\boldsymbol{x}, t; \omega) = \sum_{i=1}^{m_x} \lambda_i^{(x)} \xi_i(\omega) \Psi_i^{(x)}(\boldsymbol{x}, t), \qquad (2.5.26)$$

$$U^{(y)}(\boldsymbol{x}, t; \omega) = \sum_{j=1}^{m_y} \lambda_j^{(y)} \eta_j(\omega) \Psi_j^{(y)}(\boldsymbol{x}, t), \qquad (2.5.27)$$

$$U^{(z)}(\boldsymbol{x}, t; \omega) = \sum_{k=1}^{m_z} \lambda_k^{(z)} \zeta_k(\omega) \Psi_k^{(z)}(\boldsymbol{x}, t). \qquad (2.5.28)$$

Note that each set of random variables $\{\xi_i\}$, $\{\eta_j\}$ and $\{\zeta_k\}$ is uncorrelated, but we can have a correlation between different sets. This gives us the possibility to prescribe a correlation structure between different velocity components at the same space-time location. Given this, let us look for an equation satisfied by the joint probability density function

$$p_{u(\boldsymbol{x},t)\boldsymbol{\xi}\boldsymbol{\eta}\boldsymbol{\zeta}}^{(a,\boldsymbol{b},\boldsymbol{c},\boldsymbol{d})} = \left\langle \delta(a - u(\boldsymbol{x},t)) \prod_{i=1}^{m_x} \delta(b_i - \xi_i) \prod_{j=1}^{m_y} \delta(b_j - \eta_j) \prod_{k=1}^{m_z} \delta(d_k - \zeta_k) \right\rangle, \qquad (2.5.29)$$

where the average is with respect to the joint probability density functional of the initial conditions, boundary conditions and random variables $\{\boldsymbol{\xi}, \boldsymbol{\eta}, \boldsymbol{\zeta}\}$. By following the same steps that led us to Eq. (2.5.4), we obtain

$$\frac{\partial P}{\partial t} + \left(\sum_{i=1}^{m_x} \lambda_i^{(x)} b_i \Psi_i^{(x)}\right) \frac{\partial P}{\partial x} + \left(\sum_{i=1}^{m_y} \lambda_i^{(y)} c_i \Psi_i^{(y)}\right) \frac{\partial P}{\partial y} + \left(\sum_{i=1}^{m_z} \lambda_i^{(z)} d_i \Psi_i^{(z)}\right) \frac{\partial P}{\partial z} = -\frac{\partial}{\partial a}(\mathcal{H}P),$$
$$(2.5.30)$$

where P is a shorthand notation for Eq. (2.5.29). Equation (2.5.30) involves 5 variables (a, x, y, z, t) and ($m_x + m_y + m_z$) parameters. Thus, the exact stochastic dynamics of this advection-reaction system develops over a high-dimensional manifold. In order to overcome such a dimensionality issue, Tartakovsky & Broyda [180] obtained a *closure approximation* of the response probability associated with the solution to Eq. (2.5.25) based on a Large Eddy Diffusivity (LED) scheme. Note that

a marginalization of Eq. (2.5.30) with respect to the parameters $\{\boldsymbol{b}, \boldsymbol{c}, \boldsymbol{d}\}$ yields an unclosed equation for $p_{u(x,t)}^{(a)}$.

2.6 A numerical application to a tumor cell growth model

In order to verify the correctness of the aforementioned Eq. (2.3.3) we present here a numerical example. In particular, we consider the transient properties of the tumor cell growth model under immune response recently proposed by [223]. This model includes additive as well as multiplicative colored noises (see also [58]) and it is described by the equations

$$\dot{x}(t;\omega) = g\left(x(t;\omega)\right) + h\left(x(t;\omega)\right) f(t;\omega) + \eta(t;\omega), \qquad x(0;\omega) = x_0(\omega), \quad (2.6.1)$$

where $x(t;\omega)$ denotes the population of tumor cells at time t while

$$g(x) \overset{\text{def}}{=} x(1 - \theta x) - \beta \frac{x}{x+1}, \quad h(x) \overset{\text{def}}{=} -\frac{x}{x+1}. \tag{2.6.2}$$

In Eqs. (2.6.2), β is the immune rate and θ is related to the rate of growth of cytotoxic cells. These parameters are typically set to $\theta = 0.1$, $\beta = 2.26$. Also, the random process $f(t;\omega)$ represents the strength of the treatment (i.e., the dosage of the medicine in chemotherapy or the intensity of the ray in radiotherapy) while $\eta(t;\omega)$ is related to other factors, such as drugs and radiotherapy, that restrain the number of tumor cells. We shall assume that $f(t;\omega)$ and $\eta(t;\omega)$ are two independent Gaussians random processes with zero mean and correlation functions given by

$$\langle f(t;\omega)f(s;\omega)\rangle = \frac{D_1}{\ell_1}e^{-6(t-s)^2/\ell_1^2}, \qquad \langle \eta(t;\omega)\eta(s;\omega)\rangle = \frac{D_2}{\ell_2}e^{-6(t-s)^2/\ell_2^2}, \tag{2.6.3}$$

ℓ_i	∞	2	1	0.5	0.2	0.1	0.05	0.02	0.01	0.005	0.002
M_i	1	1	2	3	5	9	18	43	85	170	423

Table 2.1: Number or terms M_i appearing in the series expansions (2.6.4) as a function of the correlation times ℓ_i (see Eqs. (2.6.3)). The truncation is performed in order to retain 97% of the total energy in the time interval $[0,1]$.

where ℓ_i and D_i ($i = 1, 2$) denote, respectively, the correlation times and the correlation amplitudes[9] of the processes $f(t; \omega)$ and $\eta(t; \omega)$. The factor 6 at the exponents has been introduced in order to make the correlation functions approximately zero when $|t - s| \simeq \ell_i$ (see [198]). Also, the initial condition $x_0(\omega)$ for the tumor density is set to be a standard Gaussian variable with mean $\langle x_0(\omega) \rangle = 7.266$. This mean value corresponds to the state of stable tumor ([223]) in the absence of random noises. We expand both processes $f(t; \omega)$ and $\eta(t; \omega)$ in a finite-dimensional Karhunen-Loève series

$$f(t; \omega) = \sum_{k=1}^{M_1} \phi_k(t) \xi_k(\omega), \qquad \eta(t; \omega) = \sum_{k=1}^{M_2} \psi_k(t) \zeta_k(\omega), \qquad (2.6.4)$$

where $\{\xi_1(\omega), ..., \xi_{M_1}(\omega)\}$ and $\{\zeta_1(\omega), ..., \zeta_{M_2}(\omega)\}$ are two sets of zero-mean i.i.d Gaussian random variables, while $\phi_k(t)$ and $\psi_k(t)$ are non-normalized eigenfunctions arising from the spectral decomposition of covariance kernels (2.6.3). The truncation of the series (2.6.4) is performed in order to retain 97% of the total energy in the time interval $[0, 1]$. The corresponding number of terms M_1 and M_2 is shown in table 2.1, as a function of the correlation time. In Figure 2.1 we plot several realizations of the response process $x(t; \omega)$ for different (randomly sampled) realizations of the forcing processes $f(t; \omega)$ and $\eta(t; \omega)$. The case with very small correlation times falls within the range of validity of the small correlation time approximation considered by [223]. The effective Fokker-Plank equation overcomes the curse of dimensionality, and it can be solved by standard numerical methods. However, for *large correlation*

---

[9]The correlation amplitude ultimately controls the amplitude of the process, namely, when D_1 is increased, then the amplitude of $f(t; \omega)$ increases.
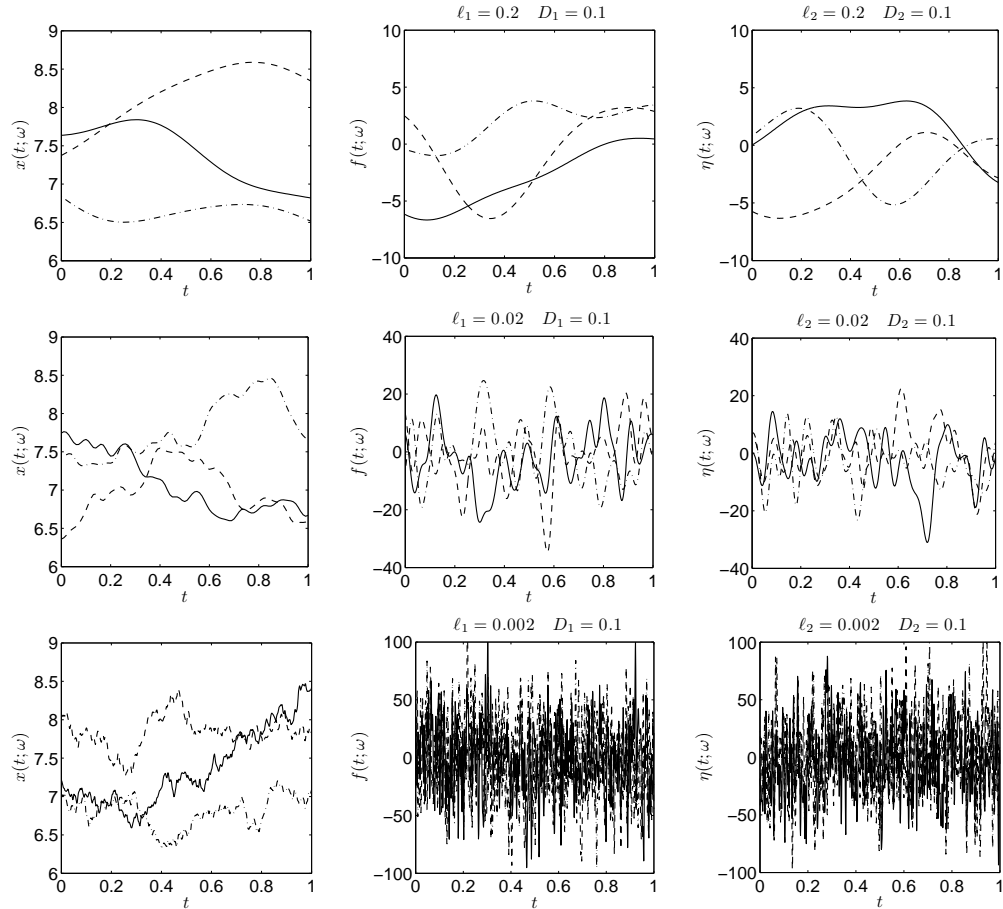
Figure 2.1: Tumor dynamics $x(t;\omega)$ corresponding to different (randomly sampled) realizations of the excitation processes $f(t;\omega)$ and $\eta(t;\omega)$. Shown are three different scenarios having random noises with different correlation times: $\ell_i = 0.2$ (first row), $\ell_i = 0.02$ (second row) and $\ell_i = 0.002$ (third row). For each case we sample three realizations of $f(t;\omega)$ and $\eta(t;\omega)$ and, correspondingly, we compute three responses of $x(t;\omega)$. The samples of $f(t;\omega)$, $\eta(t;\omega)$ and $x(t;\omega)$ are plotted by using the same linestyle along each row.

times such approach cannot be employed for obvious reasons. In these cases we need to resort to other methods, e.g., methods based directly on random variables as discussed in section 2.3. To this end, we consider the following joint response-excitation probability density associated with the system (6.2.1)-(2.6.4)

$$p_{x(t)\boldsymbol{\xi}\boldsymbol{\zeta}}^{(a,\boldsymbol{b},\boldsymbol{c})} \overset{\text{def}}{=} \langle \delta\left(a - x_t[\boldsymbol{\xi}, \boldsymbol{\zeta}]\right) \prod_{k=1}^{M_1} \delta\left(b_k - \xi_k\right) \prod_{k=1}^{M_2} \delta\left(c_k - \zeta_k\right) \rangle, \qquad (2.6.5)$$

where the average is with respect to the joint probability density of the variables $\boldsymbol{\xi}(\omega) \overset{\text{def}}{=} \{\xi_1(\omega), ..., \xi_{M_1}(\omega)\}$, $\boldsymbol{\zeta}(\omega) \overset{\text{def}}{=} \{\zeta_1(\omega), ..., \zeta_{M_2}(\omega)\}$ and the initial condition $x_0(\omega)$. By differentiating Eq. (2.6.5) with respect to time and taking into account Eq. (6.2.1), we obtain

$$\frac{\partial p_{x(t)\boldsymbol{\xi}\boldsymbol{\zeta}}^{(a,\boldsymbol{b},\boldsymbol{c})}}{\partial t} = -\frac{\partial}{\partial a}\left[\left(g(a) + h(a)\sum_{k=1}^{M_1} b_k \phi_k(t) + \sum_{k=1}^{M_2} c_k \psi_k(t)\right) p_{x(t)\boldsymbol{\xi}\boldsymbol{\zeta}}^{(a,\boldsymbol{b},\boldsymbol{c})}\right]. \qquad (2.6.6)$$

This is a linear transport equation in two variables, t and a, and M_1+M_2 parameters. Under the assumption that the initial state of the system $x_0(\omega)$ is independent of $\boldsymbol{\xi}(\omega)$ and $\boldsymbol{\zeta}(\omega)$, the initial condition for the joint density (2.6.5) is explicitly given by

$$p_{x_0\boldsymbol{\xi}\boldsymbol{\zeta}}^{(a,\boldsymbol{b},\boldsymbol{c})} = \left(\frac{1}{2\pi}\right)^{(M_1+M_2+1)/2} \exp\left[-\frac{1}{2}\left(a^2 + \sum_{k=1}^{M_1} b_k^2 + \sum_{j=1}^{M_2} c_j^2\right)\right]. \qquad (2.6.7)$$

Once the solution to Eq. (2.6.6) is available, we obtain the response probability of the system by marginalizing (2.6.5) with respect to $\{b_k\}$ and $\{c_j\}$, i.e.,

$$p_{x(t)}^{(a)} = \underbrace{\int_{-\infty}^{\infty} \cdots \int_{-\infty}^{\infty}}_{M_1+M_2} p_{x(t)\boldsymbol{\xi}\boldsymbol{\zeta}}^{(a,\boldsymbol{b},\boldsymbol{c})} db_1 \cdots db_{M_1} dc_1 \cdots dc_{M_2}. \qquad (2.6.8)$$

The numerical solution to Eqs. (6.2.1) and (2.6.6) is computed by using different approaches. Specifically, for the stochastic ODE problem (6.2.1) we have employed

(a) (b)
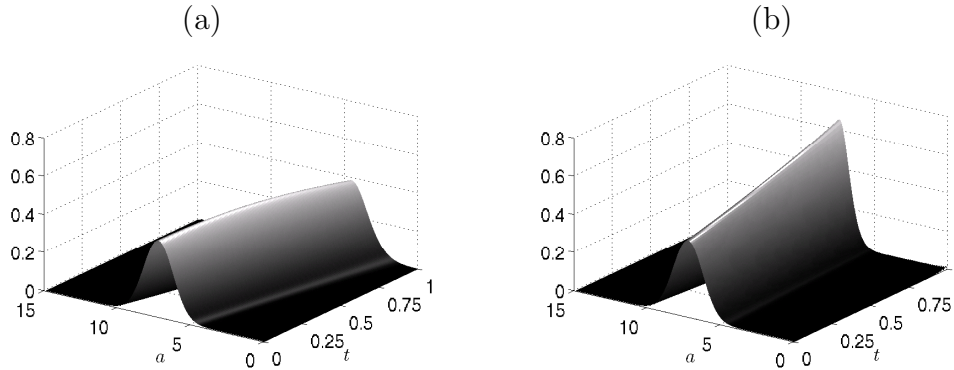
Figure 2.2: Temporal evolution of the response probability density (2.6.8) of the tumor model (6.2.1). The correlation time of both processes (2.6.4) is set at $\ell_i = 10$ (i.e. we have $M_1 = M_2 = 1$) while the amplitudes D_i appearing in the correlations (2.6.3) are set to $(D_1, D_2) = (0.1, 5)$ (a) and $(D_1, D_2) = (0.1, 0.001)$ (b).

both Monte Carlo (5×10^6 samples) and probabilistic collocation methods (PCM) [60]. In the latter case, depending on the number of random variables, we have used either Gauss-Hermite quadrature points or sparse grid (level 2) points for ξ_k and ζ_j. On the other hand, the partial differential equation (2.6.6) is first discretized in the a variable by using a Fourier-Galerkin spectral method of order 50, and then collocated at either Gauss-Hermite points or sparse grid points in the variables b_k and c_j. A second-order Runge-Kutta scheme is used to advance in time both Eqs. (6.2.1) and (2.6.6).

In Figure 2.2 we plot the time evolution of the response probability density of the system, i.e. the tumor density, for excitation processes with very large correlation time ($\ell_i = 10$) compared to the period of integration which is $[0, 1]$. We also show the effects of a variation in the correlation amplitude D_2 characterizing the random process $\eta(t; \omega)$ restraining the number of tumor cells. The observed changes in the temporal evolution of the response probability density function are consistent with the results of [223]. The relevant statistics, i.e. the mean and the variance, of the tumor density are compared in Figure 2.3 against similar results obtained by using different stochastic approaches. This comparison clearly shows that the transport equation (2.6.6) for the joint probability density function is indeed correct
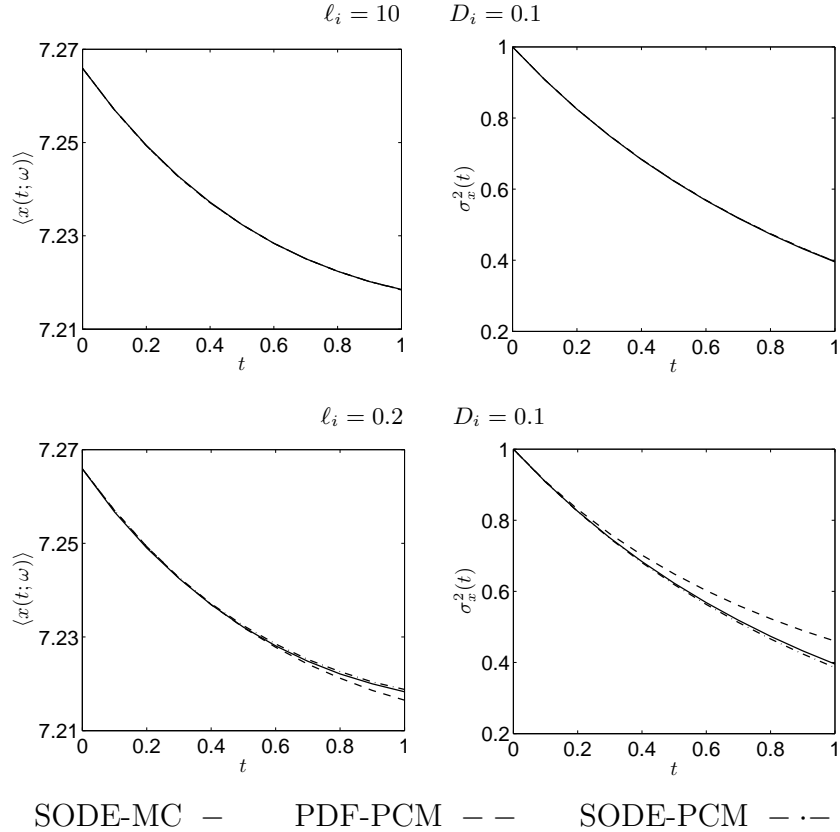
Figure 2.3: Time evolution of the mean and the variance of the tumor population for random forcing processes $f(t; \omega)$ and $\eta(t; \omega)$ with different correlation times. Shown are results obtained by using different stochastic methods: probabilistic collocation (PCM) (Gauss-Hermite for $\ell_i = 10$ (3 dimensions), and sparse grid level 2 for $\ell_i = 0.2$ (11 dimensions) applied to the stochastic ODE (6.2.1) (dashed-doted line) and the PDF equation (2.6.6) (dashed line); Monte Carlo simulation ($5 \cdot 10^6$ samples) applied to the stochastic ODE (2.6.6) (continuous line).

and allows for accurate predictions. The discrepancy observed in the lower right variance plot between the Monte Carlo solution (continuous line) and the sparse grid (level 2) solution of Eq. (2.6.6) (2 variables and 11 parameters) is due to an insufficient integration accuracy when evaluating the statistical moments from the response probability density function.

2.7 Summary

By using functional integral methods, we have determined an equation describing the evolution of the joint response-excitation probability density function of a first-order nonlinear stochastic dynamical system driven by colored random noise with arbitrary correlation time. This equation can be represented in terms of a superimposition of two differential constraints, i.e. two partial differential equations involving unusual limit partial derivatives. The first one of these constraints was determined by [168]. We have addressed the question of computability of the joint response-excitation probability density function as a solution to a boundary value problem involving only one differential constraint. By means of a simple analytical example, we have shown that such problem is undetermined, in the sense that it admits an infinite number of solutions. This result provides a definitive answer to the question first raised by [168], p. 295, regarding the solvability theory of the system of equations (2.1.8)-(2.1.10). In order to overcome this issue, we have included an additional differential constraint, i.e. the complementary constraint (2.1.15), which yields a complete evolution equation for the joint response-excitation density. This equation, however, involves an average requiring a closure approximation just like in the classical response approach [127]. Such approximation can be constructed based on small correlation time expansions.

We have also studied nonlinear differential equations involving random parameters. This class of problems can be reformulated in an exact way, i.e. without any closure, in terms of a possibly high-dimensional linear transport equation for the joint response-excitation probability density function of the system. Such equation can be solved numerically by exploiting recent advances in numerical methods for high-dimensional systems such as proper generalized decomposition [33, 132], sparse grid collocation [60, 61] or functional ANOVA techniques [25, 155, 220]. In order to investigate this possibility, we have applied one of these methods, i.e. sparse grid

collocation, to the evolution equation arising from the tumor cell growth model recently proposed by [223]. This allowed us to simulate the dynamics of the tumor density for Gaussian forcing processes with low to moderate correlation times, i.e. in a range where the small correlation time expansion considered by [223] does not apply.

Chapter 3

Numerical method for REPDF equation

In this chapter, we develop an efficient numerical method to compute the solution of the joint REPDF equation corresponding to a nonlinear stochastic dynamical system subject to colored noise. Section 3.1 presents the overall numerical method that consists of two schemes discretizing the response space and the excitation space. In section 3.1.1, we develop the adaptive discontinuous Galerkin method corresponding to the response space. The adaptive strategies are based on local variance, boundary flux difference, and a concentration of sample points in phase space. In section 3.1.2, we employ the probabilistic collocation method for the excitation dimensions possibly combined with sparse grid. The effectiveness of the proposed algorithms is demonstrated in the numerical applications of nonlinear oscillator problems involving colored noise that is presented in section 3.2.

3.1 Numerical method

It is convenient to group the independent variables appearing in solution to joint REPDF equation (2.3.3) into two main classes, i.e., those belonging to the *response*

space and those belonging to the *excitation space.* The response space is a subset of $\mathbb{R}^n$ that includes the phase variables a. These variables are differentiated in the PDF equation (2.3.3). On the other hand, the excitation space is a subset of $\mathbb{R}^m$ that includes the variables b, which appear simply as parameters in (2.3.3). Different numerical techniques are described hereafter for the discretization of the response and the excitation spaces.

3.1.1   Adaptive Discontinuous Galerkin method for the response space

The response space can be discretized by using an adaptive discontinuous Galerkin method [38, 39], possibly combined with functional ANOVA techniques [25]. As is well known, the DG method has many good features of both finite volume and finite element methods, such as flexibility and hp-adaptivity.

Discontinuous Galerkin (DG) formulation

In order to illustrate the application of the DG method to the joint REPDF equation (2.3.3), let us rewrite it in the form of hyperbolic conservation law, i.e.

$$\frac{\partial p^{(a,b)}_{x(t)\xi}}{\partial t} = -\nabla_a \cdot \left(G(a,b,t) p^{(a,b)}_{x(t)\xi} \right) , \qquad (3.1.1)$$

where ∇_a denotes the multi-dimensional gradient operator with respect to the variables $a \in \mathbb{R}^n$. It is convenient at this point to define the multi-dimensional flux

$$F[p] \overset{\text{def}}{=} G(a,b,t) p^{(a,b)}_{x(t)\xi} , \qquad (3.1.2)$$

where we have emphasized the functional dependence on $p^{(a,b)}_{x(t)\xi}$ by using the notation $F[p]$. Next, we consider a finite element discretization of the response space, i.e. the

phase space described by the variables $a \in \mathbb{R}^n$. Specifically, we select a bounded computational domain $\Omega \subseteq \mathbb{R}^n$, which is large enough to include the support of the joint REPDF $p_{x(t)\xi}^{(a,b)}$. This allows us to set zero homogeneous boundary condition at the boundary of Ω. Let Ω_h be a triangulation of Ω, consisting of elements K_i $(i = 1, ..., N_{el})$, i.e.

$$\Omega = \bigcup_{i=1}^{N_{el}} K_i \,, \qquad K_i \in \Omega_h \,. \tag{3.1.3}$$

We look for a solution to (3.1.1) in the finite element space

$$\mathcal{V}_h \stackrel{\text{def}}{=} \{ v \in L_2(\Omega) : v|_{K_i} \in H^p(K_i), \ \forall K_i \in \Omega_h \} \,. \tag{3.1.4}$$

Here $H^p(K_i)$ denotes the space of polynomials of degree at most p in n variables within the element K_i. Note that we are not imposing any continuity requirement for the solution between adjacent elements. The finite-element solution to (3.1.1) can be written as

$$\widehat{p}_{x(t)\xi}^{(a,b)} = \sum_{i=1}^{N_{el}} \widehat{p}_i(a, b, t) \,, \qquad \widehat{p}_i(a, b, t) \stackrel{\text{def}}{=} \sum_{j=0}^{d} \alpha_{K_i}^j(t, b) \psi_{K_i}^j(a) \,, \tag{3.1.5}$$

where d denotes the number of degrees of freedom within each element K_i, and $\psi_{K_i}^j(a) \in H^p(K_i)$ $(j = 1, .., d)$ is the set of basis functions in the element K_i. We substitute (3.1.5) into (3.1.1) and impose that the residual is orthogonal to the finite element space $\mathcal{V}_h$. By using the simplified notation $\widehat{p} = \widehat{p}_{x(t)\xi}^{(a,b)}$, this yields the following element-wise Galerkin formulation

$$\int_{K_i} q \frac{\partial \widehat{p}}{\partial t} da = \int_{K_i} \nabla_a q \cdot F[\widehat{p}] da - \int_{\partial K_i} q F[\widehat{p}] \cdot n_i dS \,, \qquad \forall q \in H^p(K_i) \,, \tag{3.1.6}$$

where n_i denotes the outward normal unit vector on the boundary ∂K_i. An important part of the solution process is the evaluation of the multidimensional flux

$F[\widehat{p}]$ through the element boundary ∂K_i, i.e. the computation of the last integral in (3.1.6). Since we allowed discontinuous solutions across adjacent elements, the value of $F[\widehat{p}]$ is not unique on ∂K_i. Therefore, we replace $F[\widehat{p}]$ with the *numerical flux* $\widetilde{F}[\widehat{p}_-, \widehat{p}_+]$, representing the information transferred through the boundary of adjacent elements. The quantities $\widehat{p}_-$ and $\widehat{p}_+$ here represent, respectively, the finite element solution within the element K_i and the solution within the adjacent ones. Among various schemes to compute the numerical flux $\widetilde{F}[\widehat{p}_-, \widehat{p}_+]$, we consider here the Roe scheme [163] (upwind flux), which is simple and is known to work well for advection dominated equations. Such scheme can be explicitly written as,

$$\widetilde{F}_j[\widehat{p}_-, \widehat{p}_+] = \begin{cases} F_j[\widehat{p}_-], & \bar{a} \geq 0 \\ F_j[\widehat{p}_+], & \bar{a} < 0 \end{cases}, \qquad \bar{a} = \frac{F_j[\widehat{p}_+] - F_j[\widehat{p}_-]}{\widehat{p}_+ - \widehat{p}_-}.$$

where $\widetilde{F}_j$ $(j = 1, ..., n)$ denotes the component of the numerical flux along the direction a_j.

Adaptivity

The solution to the joint REPDF equation (3.1.1) can be supported over a very small region of the response phase space (see, e.g., Figure 1.1). In order to save computational resources and resolve accurately such local dynamics, we propose an adaptive algorithm that refines the computational grid where it is needed. Such h-type refinement can be based both on error estimates involving local variances or on particle methods. Hereafter, we discuss these two different approaches.

Adaptivity based on local variance and boundary flux difference The error estimate presented in [102] for the DG discretization of the advection equation suggests that the error depends on the derivative of the solution as well on the am-
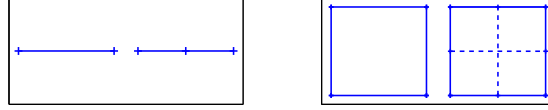
Figure 3.1: Mesh refinement in one- and two-dimensional phase spaces.

plitude of its jump at the element boundaries. This observation led us to develop a new adaptive criterion based on the boundary flux difference and the element-wise variance of the PDF.

The basic idea of the variance criterion [203] is to split the finite element K_i whenever the following inequality is satisfied

$$\sigma_{K_i}\mathcal{J}_{K_i} \geq \theta_1 \,. \tag{3.1.7}$$

Here σ_{K_i} denotes the local standard deviation of the PDF in the element K_i while $\mathcal{J}_{K_i}$ is the relative element size. The threshold θ_1 can be selected appropriately, for example with reference to the standard deviation of the PDF at the initial time. The procedure is illustrated in Figure 3.1 for finite elements in one and two dimensions, and it usually yields non-conforming grids such as those in Figure 3.8. In addition to the variance criterion, which is known to be insufficient for advection dominated equations [157], we have implemented another constraint, namely, a boundary flux difference controller

$$\int_{\partial K_i} |F[\widehat{p}_-] - F[\widehat{p}_+]| \, dS \geq \theta_2, \tag{3.1.8}$$

where we recall $\widehat{p}_-$ is the finite element solution in the element K_i while $\widehat{p}_+$ is the solution in the adjacent elements. If condition (3.1.8) is satisfied, then the element is split as in Figure 3.1.

The inverse operation, i.e., the merging of neighborhood elements, is based on the local variance criterion (3.1.7). In particular, we merge a group of elements with common boundaries if the summation of the local variances is small enough, i.e., less

or equal than a threshold θ_3.

Adaptivity based on sample paths An alternative criterion to refine the computational mesh in the phase space may be based on the analysis of a few sample trajectories of the stochastic dynamical system (2.3.1). The key idea is the following. We first sample a small ensemble of possible states of the system at time t according to the marginalized PDF

$$p_{x(t)}^{(a)} = \int_{\mathbb{R}^m} p_{x(t)\xi}^{(a,b)} db \,. \tag{3.1.9}$$

Then we evolve these states in time by integrating the system (2.3.1). Based on the analysis of the trajectories and on the concentration of samples in the phase space, we refine the computational mesh. The adaptive criterion is based on the relative number of samples within each finite element. If such number exceeds a prescribed threshold value θ_4 then the element is split as in Figure (3.1). A similar criterion is used to merge neighborhood elements. Once the adapted mesh has been identified, we interpolate the finite element solution (3.1.5) on the new mesh and solve the PDF equation (3.1.1) within the considered period of time. This procedure is illustrated in Figure 3.4, with reference to the dynamics of a stochastic nonlinear pendulum.

Validation of the variance/flux difference adaptive criterion Let us consider the one-dimensional stochastic "decay" problem

$$\frac{\partial x\,(t;\omega)}{\partial t} = -x\,(t;\omega) + \sin(t) + \xi(\omega) \qquad x\,(0;\omega) = x_0(\omega), \tag{3.1.10}$$

where $\xi(\omega)$ and $\eta(\omega)$ are zero-mean independent Gaussian random variables, both with variance 1/10. The evolution equation for the joint REPDF (3.1.1) in this case

reduces to

$$\frac{\partial p_{x(t)\xi}^{(a,b)}}{\partial t} = -\frac{\partial}{\partial a} \left[(-a + \sin(t) + b) \, p_{x(t)\xi}^{(a,b)} \right], \qquad t \geq 0, \quad a, b \in \mathbb{R}, \qquad (3.1.11)$$

with initial condition

$$p_{x(0)\xi}^{(a,b)} = p_{x_0}^{(a)} p_{\xi}^{(b)} = \frac{5}{\pi} e^{-5(a^2 + b^2)} . \qquad (3.1.12)$$

The analytical solution to (3.1.11)-(3.1.12) can be obtained by using the method of characteristics [158], as

$$p_{x(t)\xi}^{(a,b)} = \frac{5e^t}{\pi} e^{-5[\widehat{\alpha}(a,b,t)^2 + b^2]} ,$$

where

$$\widehat{\alpha}(a, b, t) \overset{\text{def}}{=} e^t(a - b) + b - \frac{1}{2} \left[1 + e^t(\sin(t) - \cos(t)) \right] . \qquad (3.1.13)$$

Next, we consider the numerical simulation of (3.1.11) by using the proposed adaptive DG numerical scheme. The computational domain for the response variable a is chosen as $\Omega = [-1, 1]$ while the excitation variable b is assumed to be in $\mathbb{R}$. Also, the finite element space (3.1.4) is defined in terms of Legendre polynomials while a Gauss-Hermite collocation method with q points is considered for the variable b[1]. The time integration follows a fourth-order Runge-Kutta scheme with time step $\Delta t = 10^{-3}$. In Figure 3.2 we show the the numerically computed response probability of the system at different times together with the corresponding adapted mesh. In order to examine the accuracy of the DG solution relatively to the analytical solution (3.1.1), we consider two different types of errors, namely, the absolute error

$$e_1(a, t) \overset{\text{def}}{=} \left| p_{x(t)}^{(a)} - \widehat{p}_{x(t)}^{(a)} \right| \qquad (3.1.14)$$

---

[1]Thus, the total number degrees of freedom of the system is $N_{el}(p+1)q$, where N_{el} denotes the number of finite elements in Ω.

Table 3.1: Number of elements at $t = 1$ by using the variance (DG-V) and the variance/flux difference (DG-VF) adaptivity criteria. Shown are results for different polynomial orders p.

p	3	4	5	6
DG-V	37	37	37	37
DG-VF	62	49	41	41

and the mean-squared error

$$e_2(t) \stackrel{\text{def}}{=} \left[\int_{-1}^{1} \left(p_{x(t)}^{(a)} - \widehat{p}_{x(t)}^{(a)} \right)^2 da \right]^{1/2} . \tag{3.1.15}$$

These errors are exhibited in Figure 3.2 at $t = 1$, for the adaptive strategies based on the local variance criterion (3.1.7) and the local variance/boundary flux difference criterion (3.1.8). The threshold parameters are set as $\theta_1 = 0.02$, $\theta_2 = 0.005/5^{\max\{p-3,0\}}$ and $\theta_3 = 0.001$ in this specific example. As it can be seen in Figure 3.2 and Table 3.1 the local variance/boundary flux difference criterion performs substantially better than the local variance criterion, without increasing significantly the number of elements.

3.1.2 Probabilistic Collocation method for the excitation space

In most applications, we are interested in the response PDF of the system, i.e. in the multi-dimensional integral

$$p_{x(t)}^{(a)} = \int_{\mathbb{R}^m} p_{x(t)\xi}^{(a,b)} db , \tag{3.1.16}$$

with respect to the parameters $(b_1, ..., b_m)$. In order to compute such integral, we use efficient cubature formulas with high polynomial exactness [60, 74, 130, 135]. In practice, we sample equation (3.1.1) with respect to the parameters b at appropriate
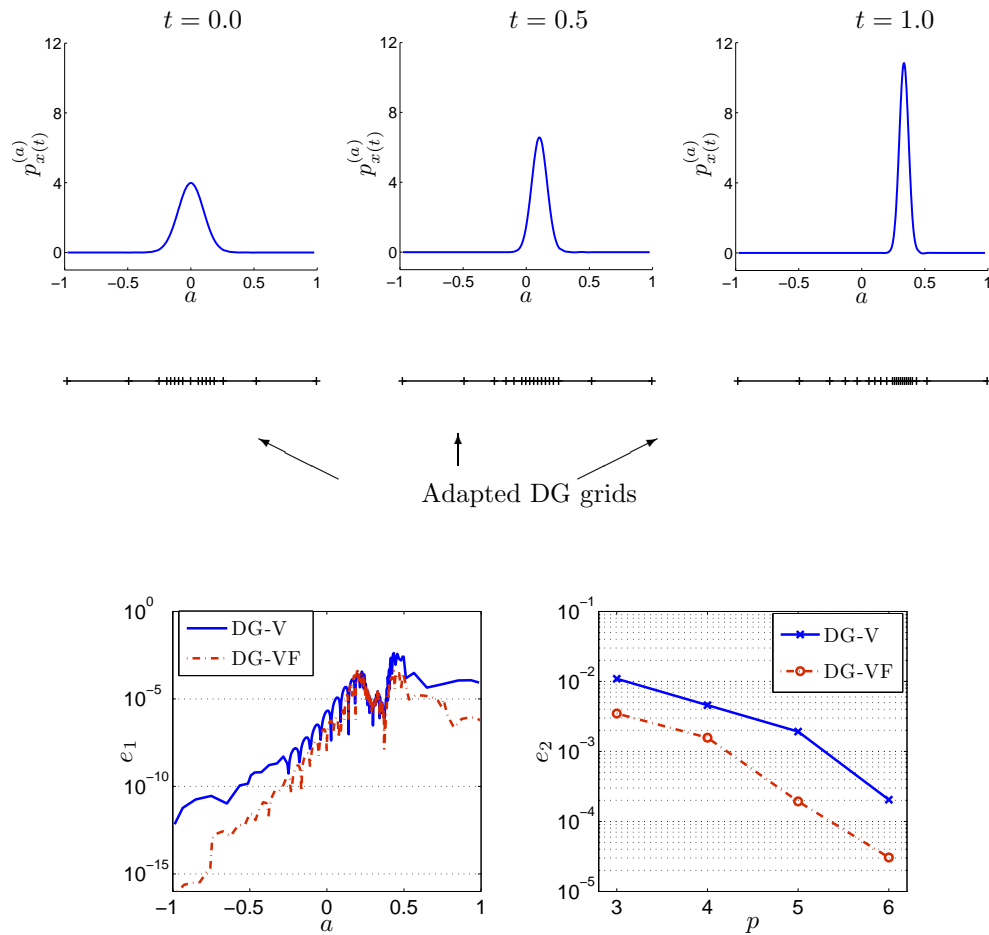
Figure 3.2: Time snapshots of the response probability of the decay problem as computed by the proposed adaptive DG method (first row). In the second row we plot the errors (3.1.14) and (3.1.15) between the DG solution and the analytical solution at the final time $t = 1$. Shown are the results of different adaptive strategies: DG-V (variance criterion), DG-VF (variance/flux difference criterion). We also show p-type convergence of e_2.

quadrature or sparse grid points and then compute an approximation to the integral (3.1.16) in the form

$$\int_{\mathbb{R}^m} p_{x(t)\xi}^{(a,b)} db \simeq \sum_{k=1}^{q} w_k p_{x(t)\xi}^{\left(a,b^k\right)}, \quad b^k = (b_1^k, ..., b_m^k),\tag{3.1.17}$$

where w_k are quadrature weights.

3.2 Numerical results

In this section we present numerical applications of the proposed adaptive discontinuous Galerkin method to different prototype stochastic problems involving randomly forced nonlinear oscillators.

3.2.1 Nonlinear Pendulum

We study the stochastic dynamics of a nonlinear pendulum subject to an external random driving torque. A deterministic version of this problem has been studied in the past as a prototype problem to understand routes to chaos (see, e.g., [13, 44, 73]). In particular, we consider the following model equation

$$\frac{d^2\theta(t;\omega)}{dt^2} + \frac{d\theta(t;\omega)}{dt} + \kappa \sin\left(\theta(t;\omega)\right) = h(t;\omega),\tag{3.2.1}$$

where θ denotes the position of the pendulum, $\kappa \sin\left(\theta\right)$ is the restoring torque, and $h(t;\omega)$ is an external random driving torque with prescribed statistical properties. Equation (3.2.1) can be written as a first-order system as

$$\begin{cases} \dfrac{dx_1(t;\omega)}{dt} = x_2(t;\omega), \\ \dfrac{dx_2(t;\omega)}{dt} = -x_2(t;\omega) - \kappa \sin\left(x_1(t;\omega)\right) + h(t;\omega), \end{cases}\tag{3.2.2}$$
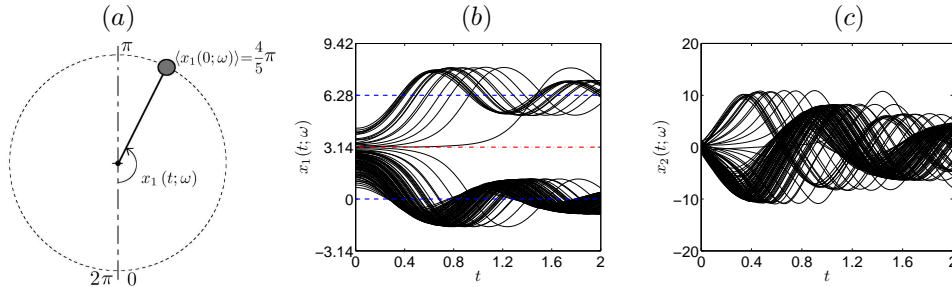
Figure 3.3: (a) Sketch of pendulum, illustrating the mean initial position. In Figure (b) and (c) we show the temporal dynamics of several sample paths of the position and the velocity, respectively.

where $x_1(t;\omega) = \theta(t;\omega)$ and $x_2(t;\omega) = d\theta(t;\omega)/dt$. We assume that we have available a Karhunen-Loève representation external random torque in the form

$$h(t;\omega) = \sum_{k=1}^{m} \xi_k(\omega) h_k(t), \qquad (3.2.3)$$

where $\{\xi_k(\omega)\}$ is a set of uncorrelated random variables with known joint probability density function, and $h_k(t)$ are unnormalized eigenfunctions of the autocorrelation of $h(t;\omega)$. By using the method discussed in section 2.4, it is straightforward to obtain the evolution equation for the joint PDF of the vector $\{x_1(t;\omega), x_2(t;\omega)), \xi_1(\omega), ..., \xi_m(\omega)\}$

$$p_{x(t)\xi}^{(a,b)} \overset{\text{def}}{=} p_{x_1(t)x_2(t)\xi_1\cdots\xi_m}^{(a_1,a_2,b_1,\cdots,b_m)} = \left\langle \delta(a_1 - x_1)\delta(a_2 - x_2) \prod_{k=1}^{m} \delta(b_k - \xi_k) \right\rangle, \qquad (3.2.4)$$

where the average is with respect to the joint PDF of $\{\xi_k(\omega)\}$ and the initial state $\{x_1(t_0;\omega), x_2(t_0;\omega)\}$. The kinetic equation has the form (2.3.3) with

$$\mathcal{L}(t) = -a_2\frac{\partial}{\partial a_1} + \mathcal{I} + \left(a_2 + \kappa\sin(a_1) - \sum_{k=1}^{m} b_k h_k(t) \right)\frac{\partial}{\partial a_2}. \qquad (3.2.5)$$

In particular, let us consider here the simple case where the random torque $h(t;\omega)$

$$\theta_4 = 0.005 \qquad \theta_4 = 0.012$$
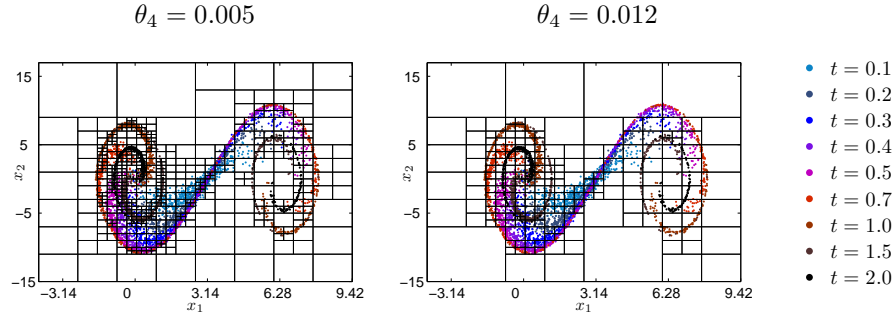
Figure 3.4: Sample phase plane of the pendulum at several time steps t and non-conforming grid based on the entire sample path $t \in [0, 2]$. Shown are results for different values of adaptive parameter θ_4

depends only on one Gaussian random variable ξ_1, i.e.,

$$h(t; \omega) = \xi_1(\omega) \sin(10t) . \tag{3.2.6}$$

We set the parameter κ in (3.2.1) as $\kappa = 40$. This leads us to the PDF equation

$$\frac{\partial p_{x(t)\xi}^{(a,b)}}{\partial t} = -\frac{\partial}{\partial a_1} \left(a_2 p_{x(t)\xi}^{(a,b)} \right) + \frac{\partial}{\partial a_2} \left([a_2 + 40 \sin(a_1) - b_1 \sin(10t)] \, p_{x(t)\xi}^{(a,b)} \right) . \tag{3.2.7}$$

The initial condition $(x_1(0; \omega), x_2(0; \omega))$ is assumed to be jointly Gaussian and independent from the variable ξ_1 in (3.2.6). Specifically, the joint PDF of x_1 (position), x_2 (momentum) and ξ_1 at the initial time $t_0 = 0$ is set as

$$p_{x(0)\xi}^{(a,b)} = \frac{4}{3(2\pi)^{3/2}} \exp \left[-\frac{8}{9} \left(a_1 - \frac{4}{5}\pi \right)^2 - 2a_2^2 - \frac{b_1^2}{2} \right] . \tag{3.2.8}$$

This system physically corresponds to a dissipative nonlinear pendulum dropped from a random initial position near the unstable vertical one, with a random velocity. Note that the mean initial position is not exactly vertical, but it is set at $\langle x_1 \rangle = 4\pi/5$, i.e. on the right semi-half of the circle (see the sketch in Figure 3.3(a)). Several realizations of the time evolution of this system are shown in Figure 3.3(b)-(c). It is seen that the pendulum never makes a complete rotation, but it simply falls to the
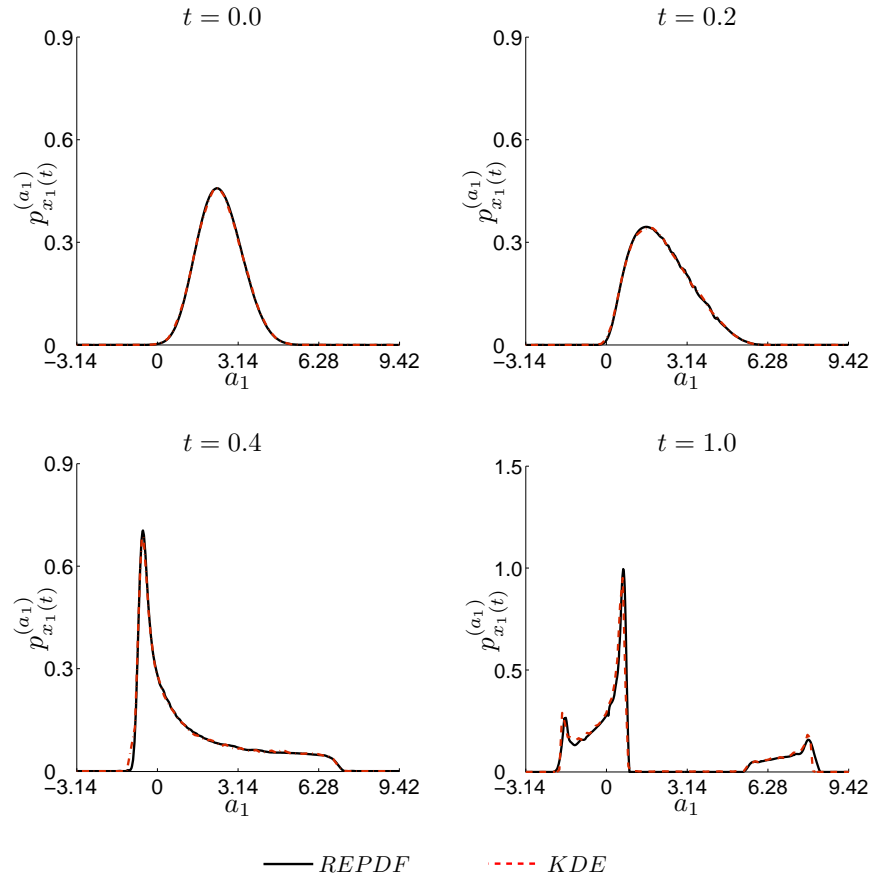
Figure 3.5: Comparison between the PDF of position of the pendulum $x_1(t;\omega)$ as computed by the proposed adaptive DG method (continuous line - REPDF) and an accurate non-parametric kernel estimation method based on 50000 samples (dashed line - KDE). Shown are results at different times.
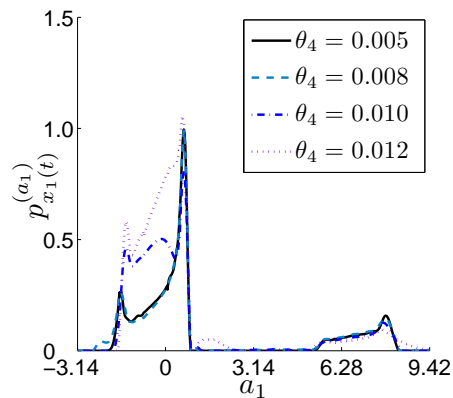
Figure 3.6: Effects of the adaptive threshold θ_4 on the response PDF of the system at time $t = 1$. The non-conforming grids corresponding to $\theta_4 = 0.005$ and $\theta_4 = 0.012$ are shown in Figure 3.4.

lower vertical position through half-rotations and then it keeps oscillating around it due to the sinusoidal driving torque. Specifically, the clockwise half-rotation leads to oscillations near $x_1 = 0$, while the counter-clockwise half-rotation leads to oscillations near $x_1 = 2\pi$. Although these two quasi-equilibrium configurations represent the same physical state, they are reached through different paths, i.e. clockwise or counter-clockwise rotations. Thus, the continuous ensemble of initial conditions is split into two disjoint ensembles in a finite time. This leads to a particular type of discontinuity in the probability space that cannot be resolved by using standard polynomial chaos (see, e.g., [199]), or global probabilistic collocation. Extensions such as ME-gPC [204] or ME-PCM [60] can resolve this discontinuity.

In Figure 1.1 we compare the DG results of the PDF equation (3.2.7) with several time snapshots of the sample phase space. We have chosen polynomial order $p = 5$ for the response space elements, $q = 9$ collocation points for the excitation space, and fourth-order Runge-Kutta scheme for the time integration, with time step $\Delta t = 5 \cdot 10^{-4}$. The adapted nonconforming mesh shown in Figure 3.4 is generated by using the adaptivity criterion based on sample paths discussed in section 3.1.1. The threshold for the relative number of particles in each element is set to $\theta_4 = 0.005$ (see Figure 3.4(a)). An analysis of Figure 1.1 shows that the symmetry of the system is broken by setting the mean initial position of the pendulum to $\langle x_1(0,\omega)\rangle = 4\pi/5$. In fact, a larger portion of the phase space evolves towards the quasi-equilibrium state through a clockwise rotation. In turn, this leads to a bi-modal probability density function, with accumulation near $x_1 = 0$, as demonstrated in Figure 3.5. The effects of the adaptive threshold θ_4 on the response PDF of the system are shown in Figure 3.6. It is seen that despite the robustness of the adaptive grid generation criterion, a proper selection of the threshold parameter is necessary for accurate results.

We emphasize that the numerical simulation of the REPDF equation (3.2.7) based on global expansion bases, such as Fourier spectral methods, would require a
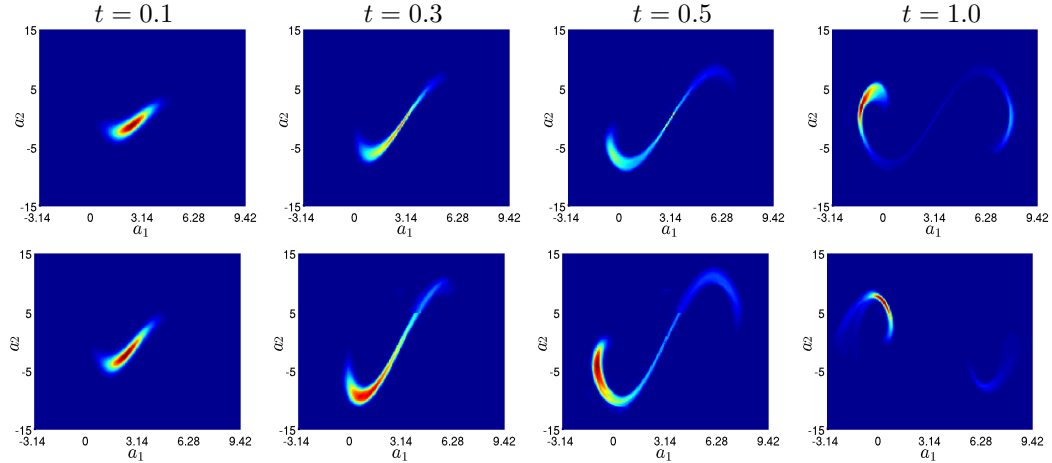
Figure 3.7: Evolution of the joint PDF of the position and the momentum of the pendulum with uniform random coefficient (top) and exponentially correlated non-Gaussian random forcing (bottom) at different times.

very high resolution to represent accurately the REPDF within the response domain $\Omega = [-4/3\pi, 3\pi] \times [-15, 17]$.

Non-Gaussian random coefficient and random forcing Non-Gaussian random fields can be easily adopted in the REPDF approach. We consider two different examples, using a non-Gaussian random coefficient and a non-Gaussian random field as the forcing term. We first take $\kappa(\omega)$ as a uniform random variable on interval $[20, 30]$. In addition, we choose $h(t; \omega)$ to be an exponentially correlated random field expanded by using Karhunen-Loève series in terms of uniform random variables. We note that the PDF of the superimposition of a finite number of independent uniform random variables is quite complicated and the references can be found in [166]. Particularly, we take $\langle h(t; \omega) \rangle = 5.0$ and the covariance function as $e^{-|t-s|}$ (see [89] for analytical expressions). In both cases, the uniform random variables are simulated with 9 Legendre collocation points in each dimension and the computed solutions are plotted in Figure 3.7 upto $t = 1.0$. Compared to the Gaussian example in Figure 1.1, the PDFs are less concentrated due to the larger variance of the uniform random variables.

3.2.2 Duffing oscillator

Many physically interesting phenomena involving nonlinear oscillations can be modeled in terms of the stochastic Duffing equation

$$\begin{cases} \dfrac{dx_1(t;\omega)}{dt} = x_2(t;\omega) \\ \dfrac{dx_2(t;\omega)}{dt} = -\gamma x_2(t;\omega) - \kappa x_1(t;\omega) - \beta x_1(t;\omega)^3 + f(t;\omega) \end{cases} \tag{3.2.9}$$

where $f(t;\omega)$ is a random forcing term. We assume that the initial condition of the system (3.2.9) is jointly Gaussian with mean (μ_1, μ_2), variance (σ_1, σ_2) and cross correlation σ_{12}. From the point of view of modern dynamical systems theory [78], the ensemble of solutions to Eq. (3.2.9) is very rich, and it has been subjected to extensive analytical and numerical investigation [19, 50, 115, 217]. The statistical properties of the random forcing term $f(t;\omega)$ also play a fundamental role in the development of the stochastic dynamics. Hereafter we consider different examples involving low dimensional as well as high-dimensional random forcing terms. In all cases, the PDF equation is solved numerically by using the proposed spectral DG method with element-wise polynomial order $p = 4$ in the response space, $q = 15$ collocation points in the excitation space, and fourth-order Runge-Kutta scheme for the time integration[2]. The grid adaptivity is based on the local variance/boundary flux difference criterion (see section 3.1.1) with parameters $\theta_1 = 0.2 \min(\sigma_1, \sigma_2)$, $\theta_2 = 0.04$, and $\theta_3 = 0.001$.

Stable oscillations and chaotic motion   The ensemble of solutions to the Duffing equation (3.2.9) includes stable oscillations and chaotic motion, depending on the

---

[2]The initial time step is set to $\Delta t = 10^{-3}$ and it is adaptively adjusted whenever it violates the CFL condition [39],

$$\frac{\Delta t}{\Delta a_1} \frac{d\mathcal{F}_1}{dp} + \frac{\Delta t}{\Delta a_2} \frac{d\mathcal{F}_2}{dp} < \frac{1}{2p+1}. \tag{3.2.10}$$
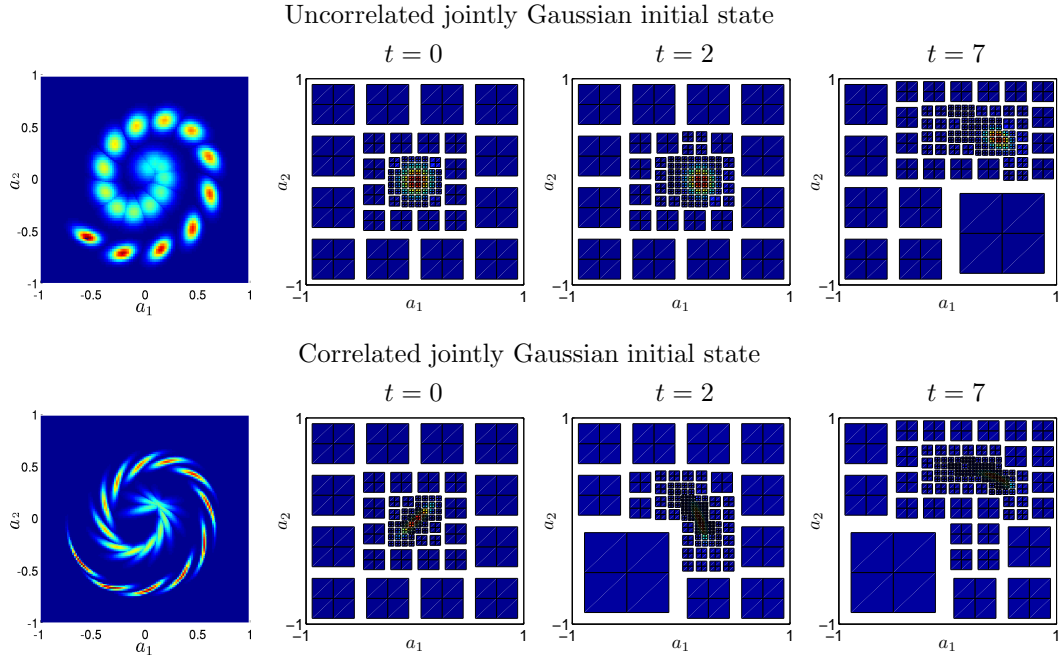
Figure 3.8: Time snapshots of the response PDF of the Duffing system and corresponding adapted grids obtained by using the local variance/flux difference criterion. Shown are also the effects of the correlation σ_{12} between the initial position x_1 and the momentum x_2 of the oscillator: First row: $\sigma_{12} = 0.0$ (uncorrelated); Second row: $\sigma_{12} = 0.09$ (correlated).

system parameters [19]. We first test our adaptive DG method on a stable manifold of periodic states. To this end, we set the damping and the stiffness coefficients in (3.2.9) and (3.2.15) to $\gamma = 0.1$, $\kappa = 1.0$ and $\beta = 1.0$ and consider a deterministic-type forcing $f(t) = D \cos(t)$. This yields the following kinetic equation governing the response PDF

$$\frac{\partial p_{x(t)}^{(a)}}{\partial t} = -\frac{\partial}{\partial a_1} \left(a_2\, p_{x(t)}^{(a)} \right) - \frac{\partial}{\partial a_2} \left(\left[-\gamma a_2 - \kappa\, a_1 - \beta a_1^3 + D \cos(t) \right] p_{x(t)}^{(a)} \right).$$

(3.2.11)

The initial condition is jointly Gaussian with parameters $\mu_{1,2} = 0.0$, $\sigma_{1,2} = 0.1$, and variable correlation σ_{12}.

The time dynamics of the response PDF of the Duffing system is shown Figure 3.8 for initial conditions with different correlation coefficient and $D = 0.2$. We notice
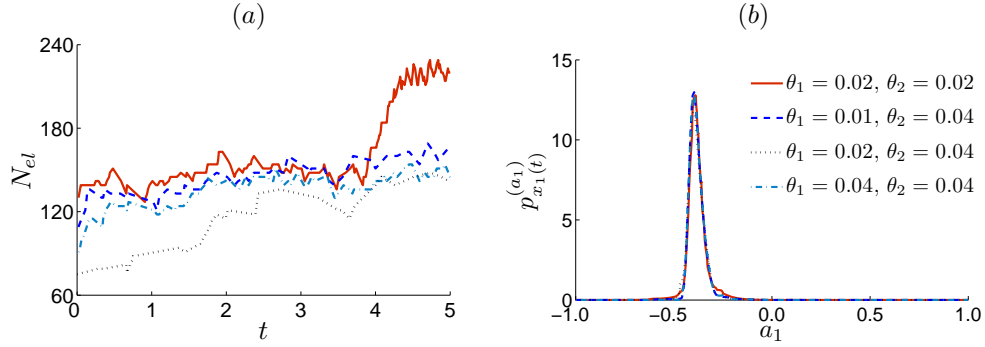
Figure 3.9: (a) Number of elements N_{el} generated by the variance/flux difference adaptive criterion versus time. Shown are results obtained by using different thresholds θ_1 and θ_2 and a jointly Gaussian initial PDF with correlation $\sigma_{12} = 0.09$ (see Figure 3.8). (b) Effects of the thresholds on the PDF of $x_1(t;\omega)$ at time $t = 5$.

that the dynamics corresponding to uncorrelated initial state remains smooth and it follows a stable oscillating motion. On the contrary, the dynamics corresponding to a correlated initial state becomes steeper and skewer as time goes on. The adapted grids generated by the variance/flux difference criterion correctly follow the peak locations of the PDF, allowing us to resolve the dynamics accurately at a reasonable computational cost. The number of non-conforming finite elements produced by the variance/flux difference adaptive procedure is shown in Figure 3.9 versus time for different choices of θ_1 and θ_2. In the same figure we also exhibit the effects of such thresholds on the PDF of $x_1(t;\omega)$ at time $t = 5$. It is seen that, differently from the sample-path based adaptive technique previously discussed, the variance/flux difference procedure is not very sensitive to the selection of the threshold parameters.

We remark that if we would have used uniform grids, the number of elements would be from *four to twenty times higher* than ours, at a comparable level of accuracy. Next, we consider more complicated stochastic dynamics, such as chaotic motions. To this end, we set $\kappa = 0.0$, $\gamma = 0.1$, $\beta = 0.1$ in (3.2.9) and (3.2.11). It is known that this system undergoes several transitions as a function of the parameter D (amplitude of the forcing). In particular, the phase diagrams obtained by Bonatto *et al.* in [19] clearly show that within the range $D \in [0, 6]$ we have solutions with
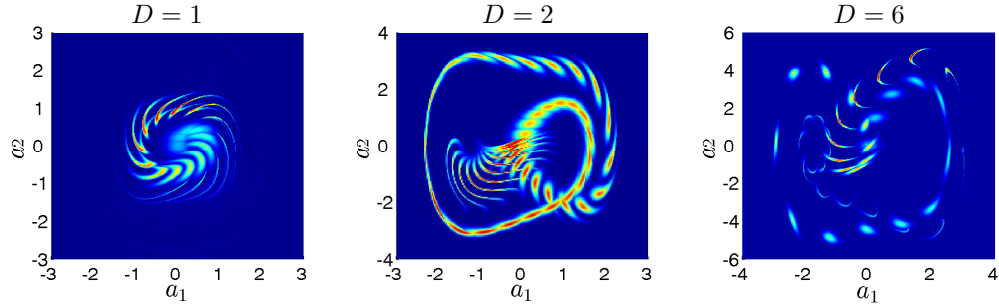
Figure 3.10: Route to chaos in the response PDF of the Duffing oscillator when the amplitude of D the forcing is increased in (3.2.15) from $D = 1$ (system with negative Lyapunov exponent) to $D = 6$ (system with positive Lyapunov exponent). Shown are time snapshots of the response PDF evolving from a jointly Gaussian and uncorrelated initial state.

negative Lyapunov exponents (regular) as well as solutions with positive Lyapunov exponents (chaotic). This is demonstrated in Figure 3.10, where we show the time snapshots of the response PDF of the system for different values of D. It is seen that the dynamics of the PDF, which is accurately captured by the proposed adaptive DG method, gradually loses its regularity when D is increased from 1 to 6.

This onset of chaos at $D \simeq 5$ can be also appreciated in Figure 3.11 where we plot the evolution the joint REPDF obtained by marginalizing the solution to the kinetic equation

$$\frac{\partial p_{x(t)\xi}^{(a,b)}}{\partial t} = -\frac{\partial}{\partial a_1}\left(a_2\, p_{x(t)\xi}^{(a,b)}\right) - \frac{\partial}{\partial a_2}\left(\left[-\gamma a_2 - \kappa\, a_1 - \beta a_1^3 + b_1 \cos(t)\right] p_{x(t)\xi}^{(a,b)}\right),$$

$$(3.2.12)$$

with respect to a_2. This equation corresponds to a random forcing in the form $f(t;\omega) = \xi(\omega)\cos(t)$ where $\xi(\omega)$ is a uniform random variable in $[0,6]$. The results of Figure 3.11 shows that at $t = 7$ the joint REPDF is scattered within the region $b_1 \in [5,6]$. This indicates a possible chaotic scenario which is consistent with the phase diagrams obtained in [19].
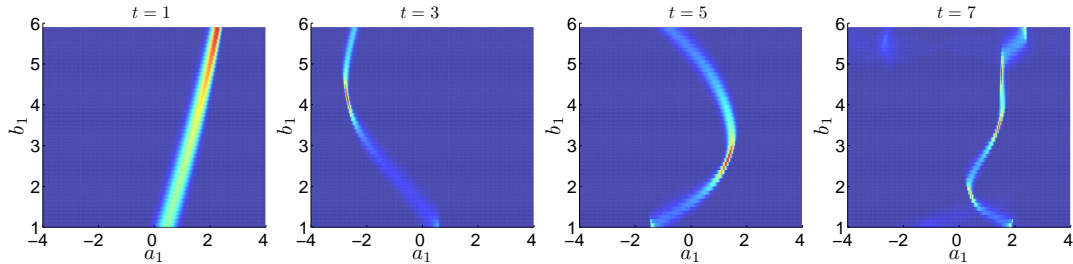
Figure 3.11: Joint REPDF of $x(t; \omega)$ and $\xi(\omega)$ (random amplitude of the forcing) at different times. The onset of chaos $\xi(\omega) \simeq 5$ and the chaotic region $\xi(\omega) \in [5, 6]$ can be appreciated at time $t = 7$, where the PDF is scattered within the region $b_1 \in [5, 6]$.

Colored random noise We address here the question of whether the joint response-excitation approach can provide an effective computational tool to simulate the effects of colored random noise in physical systems. To this end, we model the forcing term in Eq. (3.2.9) as an exponentially correlated Gaussian random process satisfying

$$\langle f(t; \omega) \rangle = 0, \qquad \langle f(t; \omega) f(s; \omega) \rangle = \frac{D}{\tau} e^{-\frac{|t-s|}{\tau}}. \tag{3.2.13}$$

where $D > 0$ denotes the amplitude of the noise. The autocorrelation of f can be made arbitrarily close to a Dirac delta function by sending the *correlation time τ* to zero[3]. We expand the process $f(t; \omega)$ in a finite-dimensional Karhunen-Loève series as

$$f(t; \omega) = \left(\frac{D}{\tau} \right)^{1/2} \sum_{k=1}^{m} \sqrt{\lambda_k} e_k(t) \xi_k(\omega), \quad t \in [0, T], \tag{3.2.14}$$

where $\xi_k(\omega)$ are uncorrelated normal random variables, while λ_k and $e_k(t)$ are, respectively, the eigenvalues and the eigenfunctions of the exponential correlation function $\exp(-|t - t'|/\tau)$ (see [89] for analytical expressions).

---

[3]In fact, $\exp(-|t - t'|\tau)/\tau$ is an element of a delta sequence [96], converging to $2\delta(t - t')$ as $\tau \to 0$.

Table 3.2: Effects of the correlation time τ on the dimensionality of the Karhunen-Loève series (3.2.14). The energy cutoff is set at the 95% of the total energy of the process.

τ	50.0	5.0	2.0	1.0	0.5	0.1	0.01
m	1	5	9	13	25	48	57

The effects of the correlation time τ on the dimensionality m of the Karhunen-Loève series (3.2.14) are reported in Table 3.2. It is seen that processes with small correlation time are high-dimensional, i.e. they depend on many random variables. As a consequence, the kinetic equation for the joint REPDF of the system can be high-dimensional as well. In fact, we obtain

$$\frac{\partial p_{x(t)\xi}^{(a,b)}}{\partial t} = -\frac{\partial}{\partial a_1}\left(a_2\, p_{x(t)\xi}^{(a,b)}\right) - \frac{\partial}{\partial a_2}\left(\left[-\gamma a_2 - \kappa\, a_1 - \beta a_1^3 + \sum_{k=1}^{m} f_k(t) b_k\right] p_{x(t)\xi}^{(a,b)}\right),$$

(3.2.15)

where we have defined

$$f_k(t) \stackrel{\text{def}}{=} \left(\frac{D\lambda_k}{\tau}\right)^{1/2} e_k(t).$$

(3.2.16)

Equation (3.2.15) is a linear transport PDE in two phase variables (a_1, a_2) and m parameters $(b_1, ..., b_m)$, i.e. its solution at time t lies in an $(m + 2)$-dimensional manifold.

White and weakly colored Gaussian random noise In the limit of zero correlation time τ, the exponentially correlated Gaussian random process (3.2.14) becomes Gaussian white noise of magnitude $\sqrt{2D}$. In this case the dynamics of the response PDF of the system is governed by the Fokker-Planck equation [161]:

$$\frac{\partial p_{x(t)}^{(a)}}{\partial t} = -\frac{\partial}{\partial a_1}\left(a_2 p_{x(t)}^{(a)}\right) - \frac{\partial}{\partial a_2}\left(g(a_1, a_2) p_{x(t)}^{(a)}\right) + D\frac{\partial^2 p_{x(t)}^{(a)}}{\partial a_2^2},$$

(3.2.17)

where $g(a_1, a_2) \stackrel{\text{def}}{=} -\gamma a_2 - \kappa a_1 - \beta a_1^3$. The second-order diffusion term is induced by the white noise forcing. A similar theory holds for weakly colored Gaussian random noise, In fact, by using the small correlation time approximation of the Furutsu-Novikov relation [62, 83, 84, 196], it is possible to obtain

$$
\begin{aligned}
\frac{\partial p_{x(t)}^{(a)}}{\partial t} &= -\frac{\partial}{\partial a_1}\left[a_2\, p_{x(t)}^{(a)}\right] - \frac{\partial}{\partial a_2}\left[g(a_1, a_2)p_{x(t)}^{(a)}\right] \\
&+ \frac{\partial^2}{\partial a_2 \partial a_1}\left[\frac{D}{\sqrt{\rho}}\left(\frac{1 - e^{(\Lambda_1 - 1/\tau)t}}{1 - \Lambda_1 \tau} - \frac{1 - e^{(\Lambda_2 - 1/\tau)t}}{1 - \Lambda_2 \tau}\right)p_{x(t)}^{(a)}\right] \\
&+ \frac{\partial^2}{\partial a_2^2}\left[\frac{D}{\sqrt{\rho}}\left(\frac{\Lambda_1(1 - e^{(\Lambda_1 - 1/\tau)t})}{1 - \Lambda_1 \tau} - \frac{\Lambda_2(1 - e^{(\Lambda_2 - 1/\tau)t})}{1 - \Lambda_2 \tau}\right)p_{x(t)}^{(a)}\right],
\end{aligned}
\tag{3.2.18}
$$

where

$$
\rho \stackrel{\text{def}}{=} \gamma^2 + 4(\kappa + 3\beta a_1^2), \quad \Lambda_1 \stackrel{\text{def}}{=} \frac{-\gamma + \sqrt{\rho}}{2}, \quad \Lambda_2 \stackrel{\text{def}}{=} \frac{-\gamma - \sqrt{\rho}}{2}.
\tag{3.2.19}
$$

The kinetic equation (3.2.18) holds for exponentially correlated Gaussian random forcing terms with very small correlation time τ, and it can be considered as a first-order correction to the Fokker-Planck equation (3.2.17), namely, the effective Fokker-Planck (EFKP) equation.

The intermediate range of correlation times is unfortunately not easily accessible by using correlation time-expansions. In fact, the numerical solution to the classical EFKP equation (3.2.18) for the case $\tau = 1$ becomes unstable after $t \geq 3$, indicating that $\tau = 1$ is beyond the convergence radius of the small correlation time approximation. This leads us to investigate the consistency of the response-excitation approach with the classical effective Fokker-Planck theory for weakly correlated random forcing. This is done in Figure 3.12 where we compare the mean and the standard deviation of the solution to the Duffing equation driven by random noise with different correlation times τ. These statistical moments are obtained by integrating the solution to the PDF equations (3.2.18) and (3.2.15). It is seen that for $\tau = 0.1$
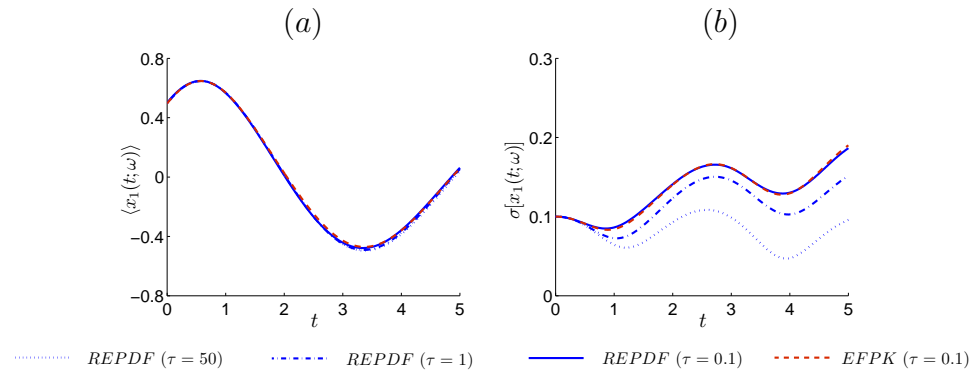
Figure 3.12: Mean (a) and standard deviation (b) of the solution to Duffing system for exponentially correlated Gaussian random forcing with different correlation times τ. The statistical properties plotted in Figure (a) and (b) are obtained by computing moments of the PDF solving the joint REPDF equation (3.2.15) and the effective Fokker-Planck (EFPK) equation (3.2.18); the moments for $\tau = 0.1$ agree to each other.
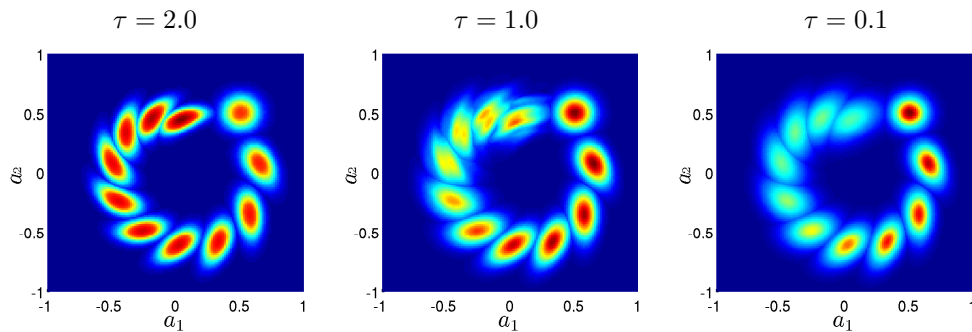
Figure 3.13: Time snapshots of the response PDF of the Duffing system for random noise with different correlation times τ. The initial condition in all cases is jointly Gaussian with mean $\mu_{1,2} = 0.5$.

the response-excitation approach[4] is consistent with the classical EFKP approach. Moreover, we propose an appropriate approach to simulate the stochastic system excited by different values of correlation time τ in Figure 3.14 and emphasize that the REPDF approach enables us to simulate the whole range of correlation time. The effects of τ on the temporal dynamics of response PDF are exhibited in Figure 3.13. It is seen that random noise with small correlation time (cases $\tau = 0.1$ and $\tau = 1.0$) induces a diffusion phenomenon in the PDF. On the other hand, for larger correlation times (case $\tau = 2$), the diffusion seems to be absent, and the maximum value of the response PDF increases in time.

3.3 Summary

In this chapter we have addressed the question of whether the joint REPDF approach can provide an effective computational tool to simulate the effects of *colored random noise in dynamical systems.* To this end, we have developed a non-conforming adaptive discontinuous Galerkin method for the joint REPDF equation governing the dynamics of an arbitrary nonlinear system with parametric-type uncertainty. Such generalized PDF equation can be high dimensional as it can arise, for example, from a discretization of stochastic PDE subject to random boundary conditions, random initial conditions or random forcing. We have proposed different techniques to deal with high-dimensionality and possible discontinuities of the PDF solution in the response-excitation space. In particular, we have combined sparse grid and multi-element collocation approaches (excitation space) with a novel adaptive discontinuous Galerkin method (response space). The effectiveness of the proposed new algorithm has been demonstrated in two prototype applications dealing with the statistical properties of the randomly forced nonlinear pendulum and the stochastic

---

[4]The dimensionality of the random forcing (3.2.14) is $m = 13$ for $\tau = 1.0$ and $m = 48$ for $\tau = 0.1$ (see Table 3.2). This means that the excitation space is 13 or 48-dimensional.
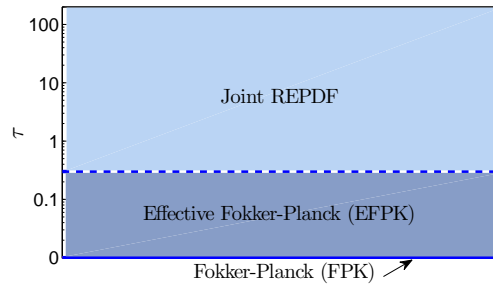
Figure 3.14: The appropriate approach for different values of τ, where we emphasize that the REPDF equation extends the classical PDF approaches and enables us to simulate the whole range of correlation time.

Duffing oscillator. The same procedure can be readily extended to the joint REPDF equations corresponding to first-order stochastic PDEs [194].

Chapter 4

High-dimensional numerical methods for PDF equation

In this chapter, we address high-dimensionality of kinetic equations summarized in Table 1.1 including the REPDF equation. We employ numerical techniques involving high-dimension functional approximations. In section 4.1, we present two different classes of new algorithms to solve high-dimensional REPDF equations, i.e., the separated series expansion method (section 4.1.1) and the ANOVA series expansion method (section 4.1.2). A brief description of finite-dimensional representation of the alternating-direction Galerkin algorithms is presented as well in section 4.1.1. In section 4.2, we discuss the computational cost of these algorithms. Finally, we apply the proposed new techniques to kinetic equations arising in stochastic partial differential equations, namely, the random advection problems, in section 4.3.

4.1 Numerical Methods

4.1.1 Separated Series Expansions (SSE)

The method of separation of variables has been widely used to approximate high-dimensional functions in terms of low-dimensional ones. In particular, let us consider the following separated expansion of an N-dimensional probability density function

$$p(z_1, \cdots, z_N) = \sum_{d=1}^{D} \alpha_d p_1^d(z_1) p_2^d(z_2) \cdots p_N^d(z_N) + \epsilon(z_1, \cdots, z_N), \qquad (4.1.1)$$

where D is the *separation rank*, p_j^d are one-dimensional functions, and ϵ is the residual. The total number of variables N in equation (4.1.1) is the sum of the phase variables n and the number of parameters m appearing in the kinetic equation. Specific examples will be given in section 4.3. The main advantage of using a representation in the form (4.1.1) to solve a high-dimensional kinetic PDE relies on the fact that the algorithms to compute $p_j^d(z_j)$ and the normalization factors α_d involve operations with one function at a time. Thus, in principle, the computational cost of such algorithms grows linearly with respect to the dimension N, potentially avoiding the curse of dimensionality.

For time-dependent PDEs, we can still look for solutions in the form (4.1.1), where we simply add additional functions of the time variable in the separated series. This approach has been considered by several authors, e.g., [2,33], and it was shown to work well for problems dominated by diffusion. However, for complex transient problems (e.g., hyperbolic dynamics), such approach is not practical as it requires a high resolution in time domain. To address this issue, a discontinuous Galerkin method in time was proposed by Nouy in [131]. The key idea is to split the integration period into small intervals (finite elements in time) and then consider a space-time separated representation of the solution within each interval. In this chapter we

follow a different approach, based on explicit or implicit time-integration schemes. In this case, the separated representation of the solution is computed at each time step. Let us formulate the method with reference to a linear kinetic equation in the form

$$\frac{\partial p(\mathbf{z},t)}{\partial t} = L(\mathbf{z})p(\mathbf{z},t), \tag{4.1.2}$$

where $\mathbf{z} = (z_1, ..., z_N)$ is the vector of phase variables and $L(\mathbf{z})$ is a linear operator. For instance, in the case of the Fokker-Planck equation (see Table 1.1) we have $m = 0$ (i.e. $N = n$) and

$$L(\mathbf{z}) = -\sum_{k=1}^{n} \left(\frac{\partial G_k(\mathbf{z})}{\partial z_k} - G_k(\mathbf{z})\frac{\partial}{\partial z_k} \right) + \frac{1}{2}\sum_{i,j=1}^{n} \left(\frac{\partial^2 b_{ij}(\mathbf{z})}{\partial z_i \partial z_j} + b_{ij}(\mathbf{z})\frac{\partial^2}{\partial z_i \partial z_j} \right).$$

The time-discrete version of (4.1.2) can be easily obtained by applying, e.g., the Crank-Nicolson scheme. This yields

$$\frac{p(\mathbf{z},t_{j+1}) - p(\mathbf{z},t_j)}{\Delta t} = \frac{1}{2}\left(L(\mathbf{z})p(\mathbf{z},t_{j+1}) + L(\mathbf{z})p(\mathbf{z},t_j) \right), \qquad \Delta t = t_{j+1} - t_j,$$

i.e.,

$$\left(I - \frac{1}{2}\Delta t L(\mathbf{z}) \right) p(\mathbf{z},t_{j+1}) = \left(I + \frac{1}{2}\Delta t L(\mathbf{z}) \right) p(\mathbf{z},t_j). \tag{4.1.3}$$

Assuming that $p(\mathbf{z},t_j)$ is known, (4.1.3) is a linear equation for $p(\mathbf{z},t_{j+1})$ which can be written concisely as[1]

$$A(\mathbf{z})\,\mathrm{p}(\mathbf{z}) = f(\mathbf{z}), \tag{4.1.4}$$

---

[1]Note that in equation (4.1.4) we have omitted the time-dependence in $p(\mathbf{z},t_{j+1})$ for notational convenience.

where

$$A(\mathbf{z}) \doteq \left(I - \frac{1}{2} \Delta t L(\mathbf{z}) \right), \qquad f(\mathbf{z}) \doteq \left(I + \frac{1}{2} \Delta t L(\mathbf{z}) \right) p(\mathbf{z}, t_j). \qquad (4.1.5)$$

The system operator $A(\mathbf{z})$ and the right-hand-side $f(\mathbf{z})$ are assumed to be separable with respect to $\mathbf{z}$, i.e.,

$$A(\mathbf{z}) = \sum_{k=1}^{n_A} A_1^k(z_1) \cdots A_N^k(z_N), \qquad f(\mathbf{z}) = \sum_{k=1}^{n_f} f_1^k(z_1) \cdots f_N^k(z_N). \qquad (4.1.6)$$

Note that $A(\mathbf{z})$ is separable if $L(\mathbf{z})$ is separable. An example is the Liouville operator associated with the Kraichnan-Orszag problem (see subsequent equations (5.2.9)-(5.2.9) and (5.2.9))

$$L(\mathbf{z}) = -z_1 z_2 \frac{\partial}{\partial z_1} - z_2 z_3 \frac{\partial}{\partial z_2} - (z_2^2 - z_1^2) \frac{\partial}{\partial z_3} - (z_2 + z_3). \qquad (4.1.7)$$

More generally, systems with polynomial-type nonlinearities always yield separable Liouvillians $L(\mathbf{z})$, and therefore separable $A(\mathbf{z})$. At this point, we look for a separated representation of the solution to (4.1.4) in the form

$$\mathrm{p}^D(\mathbf{z}) = \sum_{d=1}^{D} \alpha_d \mathrm{p}_1^d(z_1) \cdots \mathrm{p}_N^d(z_N), \qquad (4.1.8)$$

and we try to determine α_d, p_j^d and the separation rank D based on the condition

$$\left\| A(\mathbf{z}) \mathrm{p}^D(\mathbf{z}) - f(\mathbf{z}) \right\| \leq \varepsilon, \qquad (4.1.9)$$

in an appropriately chosen norm, and for a prescribed target accuracy ε. This problem does not admit a unique solution. In fact, there exist many possible choices of α_d, $p_j^d(z_j)$ and D that yield, in norm, the same target accuracy. Hence, different approaches exist to compute $p_j^d(z_j)$ and α_d. Hereafter, we focus our attention on

alternating-direction Galerkin and least squares (ALS) methods.

Alternating Direction Algorithms

The basic idea of alternating direction methods is to construct the series expansion (4.1.8) iteratively, by determining $\mathrm{p}_j^d(z_j)$ one at a time while freezing all other functions. This yields a sequence of low-dimensional problems that can be solved efficiently and in parallel [9, 10, 33, 108, 131, 133, 134]. To clarify how the method works in simple terms, suppose we have constructed an approximated solution to (4.1.4) in the form (4.1.8), i.e., suppose we have available $\mathrm{p}^D(\mathbf{z})$. Then we look for an enriched solution in the form

$$\mathrm{p}^D(\mathbf{z}) + r_1(z_1)\cdots r_N(z_N),$$

where $\{r_1(z_1),...,r_N(z_N)\}$ are N unknown functions to be determined. In the alternating direction method, such functions are determined iteratively, one at a time. Typical algorithms to perform such iterations are based on least squares,

$$\min_{r_j}\left\|\sum_{k=1}^{n_A} A_1^k\cdots A_N^k\left(\mathrm{p}^D + r_1\cdots r_N\right) - \sum_{k=1}^{n_f} f_1^k\cdots f_N^k\right\|^2, \tag{4.1.10}$$

or Galerkin methods

$$\left\langle \mathrm{q}, \sum_{k=1}^{n_A} A_1^k\cdots A_N^k\left(\mathrm{p}^D + r_1\cdots r_N\right)\right\rangle = \left\langle \mathrm{q}, \sum_{k=1}^{n_f} f_1^k\cdots f_N^k\right\rangle, \tag{4.1.11}$$

where $\langle\cdot\rangle$ is an inner product (multi-dimensional integral with respect to $\mathbf{z}$), and q is a test function, often chosen as $\mathrm{q}(\mathbf{z}) = r_1(z_1)\cdots r_N(z_N)$. In a finite-dimensional setting, the minimization problem (4.1.10) reduces to the problem of finding the minimum of a scalar function in as many variables as the number of unknowns we consider in each basis function $r_j(z_j)$, say q_z. Similarly, the alternating-direction

solution to (4.1.11) is based on the iterated solution to a sequence of low-dimensional linear system of size $q_z \times q_z$. Note that if $A(\mathbf{z})$ in Eq. (4.1.4) is a nonlinear operator, then we can still solve (4.1.10) or (4.1.11), e.g., by using Newton iterations. Once the functions $\{r_1(z_1), ..., r_N(z_N)\}$ are computed, they are normalized (yielding the normalization factor α_{D+1}) and added to $\mathrm{p}^D(\mathbf{z})$ to obtain $\mathrm{p}^{D+1}(\mathbf{z})$. The separation rank is increased until (4.1.9) is satisfied for a desired target accuracy ε.

The enrichment procedure just described has been criticized in the literature due to its slow convergence, in particular for equations dominated by advection [131]. Depending on the criterion used to construct the separated expansion, the enrichment procedure might not even converge. Recent work, indeed, aimed at finding optimal bases with granted convergence properties, i.e., bases that minimize the separation rank and simultaneously keep the overall error (4.1.9) bounded by ε. For example, Doostan and Iaccarino [47] proposed an alternating least-square (ALS) algorithm that updates simultaneously the entire rank of the basis set in the j-th direction. In this formulation, the least square approach (4.1.10) becomes

$$\min_{\left\{\mathrm{p}_j^1, ..., \mathrm{p}_j^D\right\}} \left\| \sum_{k=1}^{n_A} A_1^k \cdots A_N^k \left(\sum_{d=1}^{D} \alpha_d \mathrm{p}_1^d \cdots \mathrm{p}_N^d \right) - \sum_{k=1}^{n_f} f_1^k \cdots f_N^k \right\|^2 .$$

The computational cost of this method clearly increases compared to (4.1.10). In fact, in a finite dimensional setting, the simultaneous determination of $\left\{\mathrm{p}_j^1, ..., \mathrm{p}_j^D\right\}$ requires the solution of a $Dq_z \times Dq_z$ linear system, where q_z is the number of degrees of freedom for each $\mathrm{p}_j^d(z_j)$. However, this algorithm usually results in a separated solution with a lower separation rank D than the regular approach.

Hereafter, we propose a new alternating direction Galerkin method that, as before, updates the entire rank of the basis set in the j-th phase variable simultaneously.

To this end, we generalize the Galerkin formulation (4.1.11) to

$$\left\langle q, \sum_{k=1}^{n_A} A_1^k \cdots A_N^k \left(\sum_{d=1}^{D} \alpha_d p_1^d \cdots p_N^d \right) \right\rangle = \left\langle q, \sum_{k=1}^{n_f} f_1^k \cdots f_N^k \right\rangle, \qquad (4.1.12)$$

where $q(\mathbf{z}) = \sum_{d=1}^{D} p_1^d(z_1) \cdots p_N^d(z_N)$. The finite-dimensional representation of (4.1.12) is discussed in the following section.

Finite-Dimensional Representation of the Alternating Direction Algorithm

In this appendix we provide additional details on the discretization of the alternating direction Galerkin algorithm we proposed in section 4.1.1. To this end, let us first represent the basis functions appearing in joint probability density (4.1.1) in terms of polynomials as

$$p_n^d(z_n) = \sum_{j=1}^{q_z} p_{n,j}^d \phi_{n,j}(z_n), \qquad (4.1.13)$$

where q_z is the number of degrees of freedom in each variable. For example, in section 4.3.1, we have considered a spectral collocation method in which $\{\phi_{1,j}\}$ and $\{\phi_{2,j}\}$ are trigonometric interpolants while $\{\phi_{n,j}\}_{n=3}^{N}$ are Lagrange interpolants through Gauss-Legendre-Lobatto points. The vector

$$\mathbf{p}_n^d = \left[p_{n,1}^d, \cdots, p_{n,q_z}^d \right]$$

collects the (normalized) values of the solution at the collocation points. In such collocation framework, we can write the expansion (4.1.1) in terms of a tensor product of degrees of freedom as

$$\mathbf{p} = \sum_{d=1}^{\infty} \alpha_d \mathbf{p}_1^d \otimes \cdots \otimes \mathbf{p}_N^d. \qquad (4.1.14)$$

Accordingly, the finite dimensional version of Eq. (4.1.4) is

$$\mathbf{Ap} = \mathbf{f},$$

where

$$\mathbf{A} = \sum_{k=1}^{n_A} \mathbf{A}_1^k \otimes \cdots \otimes \mathbf{A}_N^k, \qquad \mathbf{f} = \sum_{k=1}^{n_f} \mathbf{f}_1^k \otimes \cdots \otimes \mathbf{f}_N^k, \qquad (4.1.15)$$

$$\mathbf{A}_n^k[i,j] = \int \phi_{n,i}(z_n) \, A_n^k(z_n) \phi_{n,j}(z_n) \, dz_n, \qquad \mathbf{f}_n^k[i] = \int f_n^k(z_n) \phi_{n,i}(z_n) \, dz_n. \quad (4.1.16)$$

By using a Gauss quadrature rule to evaluate the integrals, we obtain system matrices $\mathbf{A}_n^k$ that either diagonal or coincide with the classical differentiation matrices of spectral collocation methods [85]. For example, in the case of equation (4.3.3) we have the components

$$\mathbf{A}_1^1[i,j] = \mathbf{w}_x[i]\delta_{ij}, \quad \mathbf{A}_1^k[i,j] = \frac{\Delta t}{2}\mathbf{w}_x[i]\mathcal{D}_x[i,j], \;\; k = 2, ..., n_A,$$

$$\mathbf{A}_2^1[i,j] = \mathbf{A}_2^2[i,j] = \mathbf{w}_z[i]\delta_{ij}, \quad \mathbf{A}_2^{k+2}[i,j] = \frac{\sin(kt_{n+1})}{2k}\mathbf{w}_z[i]\delta_{ij}, \;\; k = 1, ..., m,$$

$$\mathbf{A}_3^k[i,j] = \mathbf{w}_b[i]\delta_{ij}, \;\; k \neq 3, \quad \mathbf{A}_3^3[i,j] = \mathbf{w}_b[i]\mathbf{q}_b[i]\delta_{ij}, \quad \cdots$$

where $\mathbf{q}_b$ denotes the vector of collocation points, $\mathbf{w}_x$, $\mathbf{w}_z$, and $\mathbf{w}_b$ are collocation weights, $\mathcal{D}_x$ is the differentiation matrix, and δ_{ij} is the Kronecker delta function. A substitution of the finite-dimensional representations (4.1.14), (4.1.15) and (4.1.16) into the Galerkin orthogonality conditions (4.1.12) yields a sequence of linear system

$$\mathbf{B}_n\widehat{\mathbf{p}}_n = \mathbf{b}_n, \qquad (4.1.17)$$

where $\mathbf{B}_n$ is a block matrix with $D \times D$ blocks of size $q_z \times q_z$, and $\mathbf{b}_n$ is multi-component vector. Specifically, the hv-th block of $\mathbf{B}_n$ and the h-th component of $\mathbf{b}_n$

are obtained as

$$\mathbf{B}_n^{hv} = \sum_{k=1}^{n_A} \left(\prod_{i \neq n}^{N} \left[\mathbf{p}_i^h \right]^T \mathbf{A}_i^k \mathbf{p}_i^v \right) \mathbf{A}_n^k, \qquad \mathbf{b}_n^h = \sum_{k=1}^{n_f} \left(\prod_{i \neq n}^{N} \left[\mathbf{p}_i^h \right]^T \mathbf{f}_i^k \right) \mathbf{f}_n^k.$$

The solution vector

$$\widehat{\mathbf{p}}_n = \left[\mathbf{p}_n^1, ..., \mathbf{p}_n^D \right]^T$$

is normalized as $\mathbf{p}_n^d / \left\| \mathbf{p}_n^d \right\|$ for all $d = 1, .., D$ and $n = 1, ..., N$. This operation yields

the coefficients $\boldsymbol{\alpha} = (\alpha_1, ..., \alpha_D)$ in (4.1.14) as a solution to the linear systems

$$\mathbf{D}\boldsymbol{\alpha} = \mathbf{d}, \qquad\qquad (4.1.18)$$

where the entries of the matrix $\mathcal{D}$ and the vector $\mathbf{d}$ are, respectively

$$\mathbf{D}^{hv} = \sum_{k=1}^{n_A} \prod_{i=1}^{N} \left[\mathbf{p}_i^h \right]^T \mathbf{A}_i^k \mathbf{p}_n^v, \qquad \mathbf{d}^h = \sum_{k=1}^{n_f} \prod_{i=1}^{N} \left[\mathbf{p}_i^h \right]^T \mathbf{f}_i^k.$$

The main steps of the algorithm are summarized in Algrithm 1.

begin
  Compute the separated representation of the initial condition $\mathbf{p}(t_0)$;
  for $t_1 \leq t_i \leq t_{n_T}$ **do**
    Compute $\mathbf{f}$ by using $\mathbf{p}(t_{i-1})$;
    Set $D = 1$;
    while $\left\| \mathbf{A}\mathbf{p}^D(t_i) - \mathbf{f} \right\| > \varepsilon$ **do**
      Initialize $\left\{ \mathbf{p}_1^D(t_i), ..., \mathbf{p}_N^D(t_i) \right\}$ at random;
      while $\left\| \mathbf{A}\mathbf{p}^D(t_i) - \mathbf{f} \right\|$ *does not decrease* **do**
        Solve Eq. (4.1.17) for $1 \leq n \leq N$;
      end
      Normalize the basis set and compute the coefficients $\{\alpha_1, ..., \alpha_D\}$;
      Set $D = D + 1$;
    end
  end
end
Algorithm 1: Main steps of the proposed alternating-direction Galerkin algorithm.

Stopping Criterion   The stopping criterion for the alternating-direction algorithm is based on the condition $\|\mathbf{A}\mathbf{p}^D - \mathbf{f}\| < \varepsilon$, which involve the computation of an N-dimensional tensor norm. This can be quite expensive and compromise the computational efficiency of the whole method. To avoid this problem, we replace the condition $\|\mathbf{A}\mathbf{p}^D - \mathbf{f}\| < \varepsilon$ with a simpler criterion for convergence, i.e.,

$$\max\left\{\frac{\|\widetilde{\mathbf{p}}_1^D - \mathbf{p}_1^D\|}{\|\mathbf{p}_1^D\|}, ..., \frac{\|\widetilde{\mathbf{p}}_N^D - \mathbf{p}_N^D\|}{\|\mathbf{p}_N^D\|}\right\} \le \varepsilon_1, \qquad (4.1.19)$$

where $\left\{\widetilde{\mathbf{p}}_1^D, ..., \widetilde{\mathbf{p}}_N^D\right\}$ denotes the solution at the previous iteration. Note that the condition (4.1.19) involves the computation of N vector norms instead of one N-dimensional tensor norm.

4.1.2   ANOVA Series Expansions

The ANOVA series expansion [25, 220] is another typical approach to model high-dimensional functions. The series involves a superimposition of functions with an increasing number of variables, and it is usually truncated at a certain interaction order. Specifically, the ANOVA expansion of an N-dimensional PDF takes the from [74]

$$p(z_1, z_2, ..., z_N) = q_0 + \sum_{i=1}^{N} q_i(z_i) + \sum_{i<j}^{N} q_{ij}(z_i, z_j) + \sum_{i<j<k}^{N} q_{ijk}(z_i, z_j, z_k) + \cdots.$$

$$(4.1.20)$$

The function q_0 is a constant. The functions $q_i(z_i)$, which we shall call first-order interaction terms, give us the overall effects of the variables z_i in p as if they were acting independently of the other variables. The functions $q_{ij}(z_i, z_j)$ describe the interaction effects of the variables z_i and z_j, and therefore they will be called second-order interactions. Similarly, higher-order terms reflect the cooperative effects of

an increasing number of variables. The interaction terms $q_{ijk\cdots}$ can be computed in different ways [155, 226], e.g.,

$$q_0 = \int p(z_1, \cdots, z_N) dz_1, \cdots dz_N,$$

$$q_i(z_i) = \int p(z_1, \cdots, z_N) \prod_{\substack{k=1 \\ k \neq i}}^{N} dz_k - q_0,$$

$$q_{ij}(z_i, z_j) = \int p(z_1, \cdots, z_N) \prod_{\substack{k=1 \\ k \neq i,j}}^{N} dz_k - q_0 - q_i(z_i) - q_j(z_j),$$

$$\cdots.$$

By using the ANOVA expansion we can represent both the parametric dependence as well as the dependence on phase variables in the solution to a kinetic equation. In the first case, PCM-ANOVA methods with appropriate anchor points [61, 68, 192, 220, 227], can be readily applied. On the other hand, representing the dependence of the solution PDF on the phase variables through the ANOVA expansion yields a hierarchy of coupled PDF equations that resembles the Bogoliubov-Born-Green-Kirkwood hierarchy of kinetic gas theory [26, 126]. We remark that the conditional moment closures in section 5.2 features similar idea.

4.2   Computational Cost

Let us consider a kinetic partial differential equation with n phase variables and m parameters, i.e., a total number of $N = n + m$ variables. Suppose that we represent the solution by using q_z degrees of freedom[2] (DOF) in each phase variable and q_b degrees of freedom in each parameter. Hereafter we compare the computational cost of the tensor product, the separated series expansion and the ANOVA expansion

---

[2]In a spectral collocation setting, q_z is the number of collocation in each phase variable.

methods we discussed in previous sections.

Tensor Product (TP) Expansion

If we consider a tensor product (TP) representation, then the total number of DOF is $q_z^n \times C(q_b, m)$, where $C(q_b, m)$ is a function depending on the way we represent the parametric dependence of the PDF solution. For example, if we consider tensor product representation of the parameter space we have $C(q_b, m) = q_b^m$. On the other hand, if we use sparse grid or ANOVA expansions we have, respectively, a logarithmic or a factorial growth of $C(q_b, m)$ with m. In a tensor product collocation setting, at each time step we need to perform matrix-vector operations for the discretized phase variables, i.e., we have $O\left(q_z^{2n}\right)$ operations. This number has to be multiplied by $C(q_b, m)$, i.e., the number of samples we are taking in the parameter space.

Separated Series Expansion (SSE)

The total number of DOFs of the SSE method is $D(nq_z + mq_b)$, i.e., it grows *linearly* with both n and m (see Table 4.1). In particular, if the separation rank D is relatively small then the separated expansion method is much more efficient than tensor product, sparse grid or ANOVA approaches, both in terms of memory requirements as well as in terms of computational cost. The alternating-direction algorithm at the basis of the separated series expansion method can be divided into two steps, i.e., the enrichment and the projection steps (see Table 1). For a separation rank d, the number of operations to perform these steps is $O(dq_z^2 + (dq_z)^3)$. Since we begin from the first basis vector and gradually increase the separation rank, this cost has to be summed up to $d = 1, ..., D$, and finally multiplied by the average number of iterations n_{itr} required to achieve the target accuracy ε. The computational cost of the projection step can be neglected with respect to the one of the enrichment step, as it reduces to solving a linear system of rather small size ($D \times D$). Thus,

	DOF	Computational Cost
TP	$q_z^n \times C(q_b, m)$	$O\left(q_z^{2n}\right) \times C(q_b, m)$
SSE	$D \cdot (nq_z + mq_b)$	$O\left(D^4 \cdot [nq_z^3 + mq_b^3]\right) \cdot n_{itr}$
ANOVA	$q_z^s \begin{pmatrix} n \\ s \end{pmatrix} \times C(q_b, m, s')$	$O\left(q_z^{2s}\right) \begin{pmatrix} n \\ s \end{pmatrix} \times C(q_b, m, s')$

Table 4.1: Number of degrees of freedom (DOF) and computational cost of solving kinetic equations by using different methods. Shown are results for Tensor Product (TP), Separated Series Expansion (SSE) and ANOVA decomposition. In the Table, n and m denote, respectively, the number of phase variables and the number of parameters appearing in the kinetic equation. We are assuming that we are representing the PDF solution with q_z degrees of freedom (DOF) in each phase variable and q_b degrees of freedom in each parameter. The function $C(q_b, m)$ depends on the specific method we are using to represent the PDF solution, e.g., tensor product collocation of sparse grid. Also, D is the separation rank and n_{iter} is the average number of iterations required for convergence of the separated expansion. The quantities s and s' are, respectively, the interaction orders of the ANOVA expansion for the phase variables and the parameters in the PDF solution.

the overall computational cost of the separated expansion method can be estimated as $O\left(D^4 \left[nq_z^3 + mq_b^3\right] n_{itr}\right)$, and it can be reduced to $O\left(D^3 \left[nq_z^2 + mq_b^2\right] n_{itr}\right)$ by using appropriate iterative linear solvers.

ANOVA Series Expansion

The number of DOFs of the ANOVA approach is $q_z^s \begin{pmatrix} n \\ s \end{pmatrix} \times C(q_b, m, s')$, where s and s' are, respectively, the interaction orders of the ANOVA expansion for the phase variables and the parameters of the PDF solution. We remark that $C(q_b, m, s')$ has a factorial dependency on m and s'. The computational cost of ANOVA is summarized in Table 4.1.

4.3 Numerical Results

In this section we provide numerical examples to demonstrate the effectiveness of the numerical methods we proposed in the chapter. To this end, we will consider kinetic partial differential equations corresponding to stochastic PDEs as well as stochastic dynamical systems.

4.3.1 Stochastic Advection of Scalar Fields

We consider the following two stochastic advection equations

$$\frac{\partial u}{\partial t} + \left(1 + \sum_{k=1}^{m} \frac{1}{2k} \sin(kt)\xi_k(\omega)\right) \frac{\partial u}{\partial x} = 0, \tag{4.3.1}$$

$$\frac{\partial u}{\partial t} + \frac{\partial u}{\partial x} = \sin(t) \sum_{k=1}^{m} \frac{1}{5(k+1)} \sin((k+1)x)\xi_k(\omega), \tag{4.3.2}$$

where $x \in [0, 2\pi]$ and $\{\xi_1, ..., \xi_m\}$ are i.i.d. uniform random variables in $[-1, 1]$. As we have shown in [194], the kinetic equations governing the joint probability density function of $\{\xi_1, ..., \xi_m\}$ and the solution to (4.3.1) or (4.3.2) are, respectively,

$$\frac{\partial p}{\partial t} + \left(1 + \sum_{k=1}^{m} \frac{1}{2k} \sin(kt)b_k\right) \frac{\partial p}{\partial x} = 0, \tag{4.3.3}$$

$$\frac{\partial p}{\partial t} + \frac{\partial p}{\partial x} = -\left(\sin(t) \sum_{k=1}^{m} \frac{1}{5(k+1)} \sin((k+1)x)b_k\right) \frac{\partial p}{\partial z}, \tag{4.3.4}$$

where $p = p(x, t, z, \mathbf{b})$, $\mathbf{b} = \{b_1, ..., b_m\}$. Note that this PDF depends on x, t, one phase variable z (corresponding to $u(x, t)$) and m parameters $\mathbf{b}$ (corresponding to $\{\xi_1, ..., \xi_m\}$). The analytical solutions to Eqs. (4.3.3) and (4.3.4) can be obtained by using the method of characteristics [158]. They are both in the form

$$p(x, t, z, \mathbf{b}) = p_0(x - X(t, \mathbf{b}), z - Z(x, t, \mathbf{b}), \mathbf{b}), \tag{4.3.5}$$

where $p_0(x, z, \boldsymbol{b})$ is the joint PDF of $u(x, t_0)$ and $\{\xi_1, ..., \xi_m\}$, and

$$X(t, \mathbf{b}) = t - \sum_{k=1}^{m} \frac{(\cos(kt) - 1)b_k}{2k^2}, \qquad Z(x, t, \mathbf{b}) = 0$$

in the case of equation (4.3.3), and

$$X(t, \mathbf{b}) = t, \qquad Z(x, t, \mathbf{b}) = \sum_{k=2}^{m+1} \frac{b_{k-1}}{10k} \left(\frac{\sin(kx - t)}{k - 1} - \frac{\sin(kx + t)}{k + 1} - \frac{2\sin(k(x - t))}{(k - 1)(k + 1)} \right)$$

in the case of equation (4.3.4). In particular, in our simulations we set

$$p_0(x, z, \mathbf{b}) = \left(\frac{\sin^2(x)}{2\pi\sigma_1} \exp\left[-\frac{(z - \mu_1)^2}{2\sigma_1} \right] + \frac{\cos^2(x)}{2\pi\sigma_2} \exp\left[-\frac{(z - \mu_2)^2}{2\sigma_2} \right] \right) \exp\left[-\frac{|\mathbf{b}|^2}{2} \right],$$

which has separation rank $D = 2$. Non-separable initial conditions can be approximated in terms of series expansions in the form (4.1.1).

Separated Series Expansion Solution

We computed the solution to (4.3.3) and (4.3.4) by using a separated series expansion and the alternating-direction Galerkin method proposed in section 4.1.1. The series is in the form

$$p(x, t, z, \mathbf{b}) \simeq \sum_{k=1}^{D} \alpha_k(t) p_k^x(x) p_k^z(z) r_k^1(b_1) \cdots r_k^m(b_m), \qquad (4.3.6)$$

where the dependence on x and z is represented by using a Fourier spectral colloca-tion method with $q_z = 50$ degrees of freedom in each variable, while the parametric dependence on b_k $(k = 1, .., m)$ is represented with Legendre polynomials of order $q_b = 7$. The series expansion (4.3.6) is computed at each time step $(\Delta t = 10^{-2})$, up to $t = 3$ by using the Crank-Nicolson scheme (4.1.4).

In Figure 4.1, we plot the first few modes $p_k(x, z) = p_k^x(x) p_k^z(z)$ of the solution
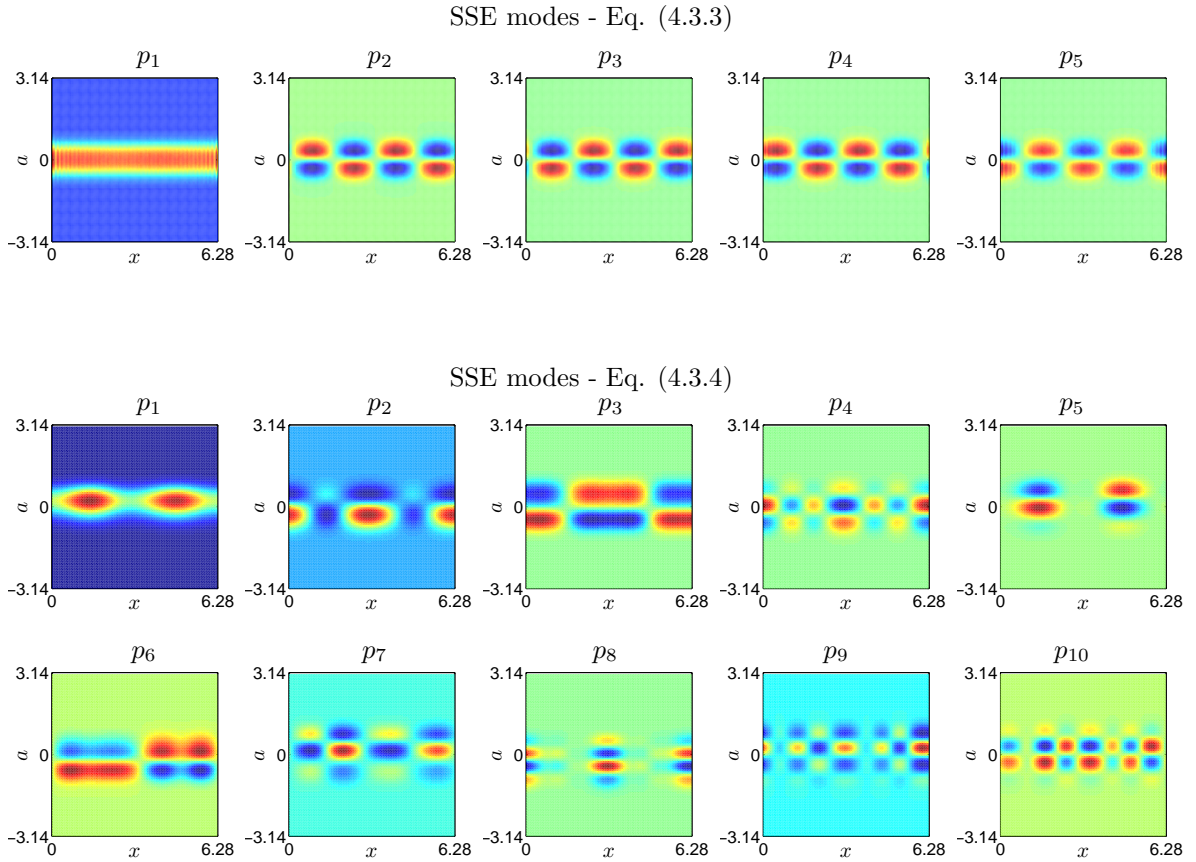
Figure 4.1: Stochastic Advection Problem: separated series expansion modes at $t = 2$.

to Eqs. (4.3.3) and (4.3.4) with $m = 54$ and $m = 3$, respectively. In the case of Eq. (4.3.3), $p_k(x, z)$ look very similar to each other for $k \geq 2$, while in the case of Eq. (4.3.4) they a are all different, suggesting the presence of modal interactions and a larger separation rank to achieve a prescribed target accuracy. This is also seen in Figure 4.2, where we plot the normalization coefficients $\{\alpha_1, ..., \alpha_D\}$. Since α_j can be interpreted as the spectrum of the separated PDF solution, we see that the stochastic advection problem (4.3.2) yields a stronger coupling between the modes, i.e., a slower spectral decay than the problem (4.3.1).

In Figure 4.3, we plot the PDF of the solution to Eq. (4.3.1). Such PDF is obtained by first solving (4.3.3) by using the separated expansion method, and then integrating (4.3.6) numerically with respect to $\{b_1, ..., b_m\}$. Convergence with respect
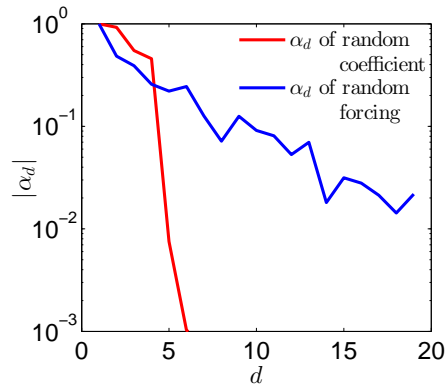
Figure 4.2: Stochastic Advection Problem: Spectra of the separated series expansion at $t = 2$.
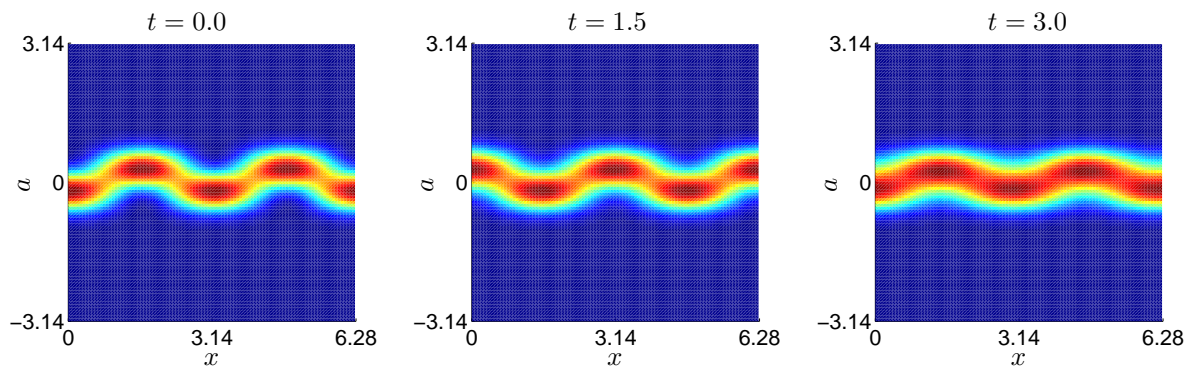
Figure 4.3: Stochastic advection problem (4.3.1): PDF of the solution at different times. The PDF dynamics is obtained by solving (4.3.3) with a separated series expansion. The separation rank is set to $D = 8$, and we consider $m = 54$ random variables in (4.3.1).
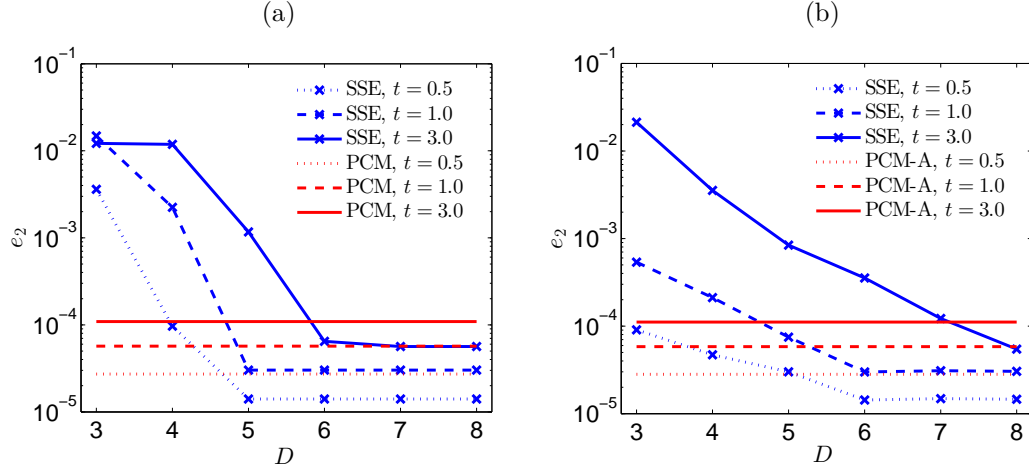
Figure 4.4: Stochastic advection problem (4.3.1): relative L_2 errors of the separated PDF solution (SSE) and the PCM-ANOVA solution (PCM-A, level 2) with respect to the analytical solution (4.3.5). Shown are results at $t = 0.5$, $t = 1$ and $t = 3$ for different separation ranks D and different number of random variables: $m = 3$ (a) and $m = 54$ (b).

to D is demonstrated in Figure 4.4. Note that the separated expansion method reaches the same error level as the PCM-ANOVA approximation with just five modes for $t \leq 1$, but it requires a larger separation rank at later times in order to keep the same accuracy. In addition, the convergence rate of the separated expansion method saturates with D due to time integration errors. In Figure 4.5, we show the PDF of the solution to the advection problem (4.3.2) at different times, where we have considered a random forcing term with $m = 24$ random variables. Such PDF is obtained by solving (4.3.4) with a separated series expansion (4.3.6) of rank $D = 8$. Convergence with respect to D is demonstrated in Figure (4.6). It is seen that the convergence rate in this case is slower than in the previous example (see Figure 4.4), and the overall relative error is larger. This is due to the presence of the time-dependent forcing term in Eq. (4.3.2), which injects additional energy in the system and yields new SSE modes (see Figure 4.1). This yields a higher separation rank for a prescribed level of accuracy. In addition, the plots suggest that the accuracy of the separated expansion method depends primarily on the separation rank D of the
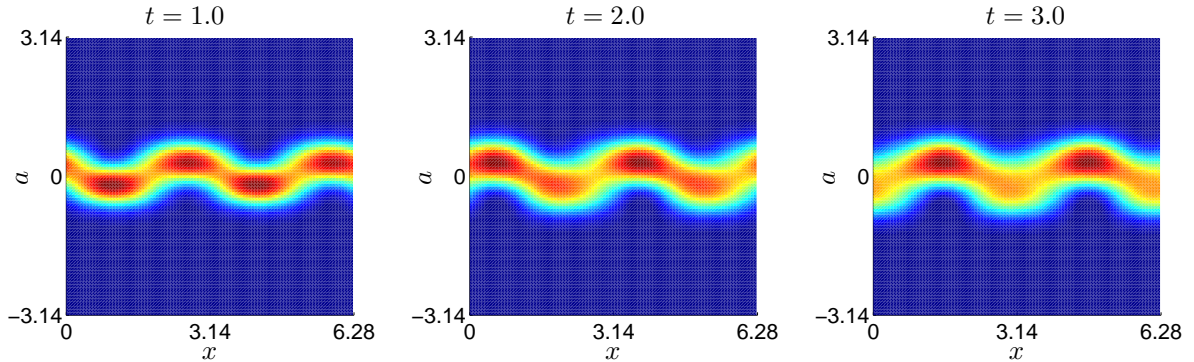
Figure 4.5: Stochastic advection problem (4.3.2): PDF of the solution at different times. The PDF dynamics is obtained by solving (4.3.4) with a separated series expansion. The separation rank is set to $D = 8$, and we consider $m = 24$ random variables in (4.3.2).

solution rather than on the dimensionality of the random forcing vector.

Adaptive Alternating Least Squares (ALS) Algorithm So far, we fixed the separation rank D throughout our simulations, to investigate convergence and accuracy of the separated series expansion method. However, in practical applications, the appropriate separation rank should be identified on-the-fly, i.e., while the simulation is running. To address this question, in this section, we propose an adaptive strategy based on the spectrum $\boldsymbol{\alpha} = \{\alpha_1, ..., \alpha_D\}$ of the separated series. The adaptive criterion is simple and effective:

- We increase the separation rank D if the ratio α_D/α_1 exceeds a threshold θ.

The corresponding adaptive algorithm initialized with a separation rank d is denoted as A_d-SSE, and it is studied hereafter with reference to Eq. (4.3.4). In Figure 4.7 we plot D versus time for different thresholds θ. It is seen that the adaptive algorithm yields a separation rank that increases in time. In particular, the case $\theta = 10^{-3}$ yields $D = 10$ at $t = 3$, which results in a slightly larger error than the one obtained for fixed $D = 10$. In Figure 4.8, we compare the accuracy of the A_6-SSE method with $\theta = 5 \cdot 10^{-4}$ and the ANOVA method (level 2). Specifically, we study the relative L_2 error of the solution to Eq. (4.3.4) for different number of random

Stochastic Advection Problem (4.3.1)   Stochastic Advection Problem (4.3.2)
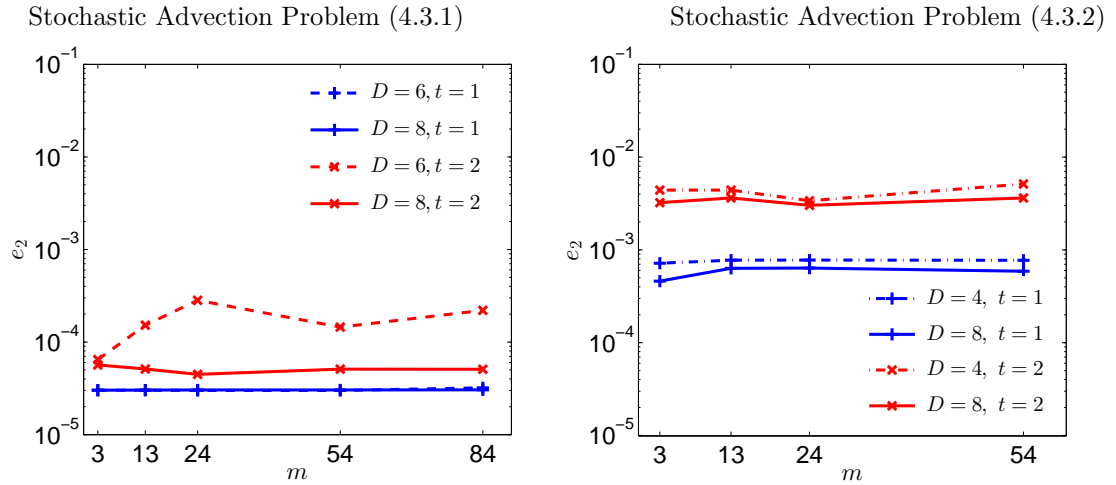
Figure 4.6: Stochastic Advection Problem: Relative L_2 errors of the separated PDF solutions with respect to the analytical solution (4.3.5). Shown are results for different number of random variables m in (4.3.1)-(4.3.2) and different separation ranks D. It is seen that the accuracy of the separated expansion method mainly depends on the separation rank rather than on the number of random variables.

(a)   (b)
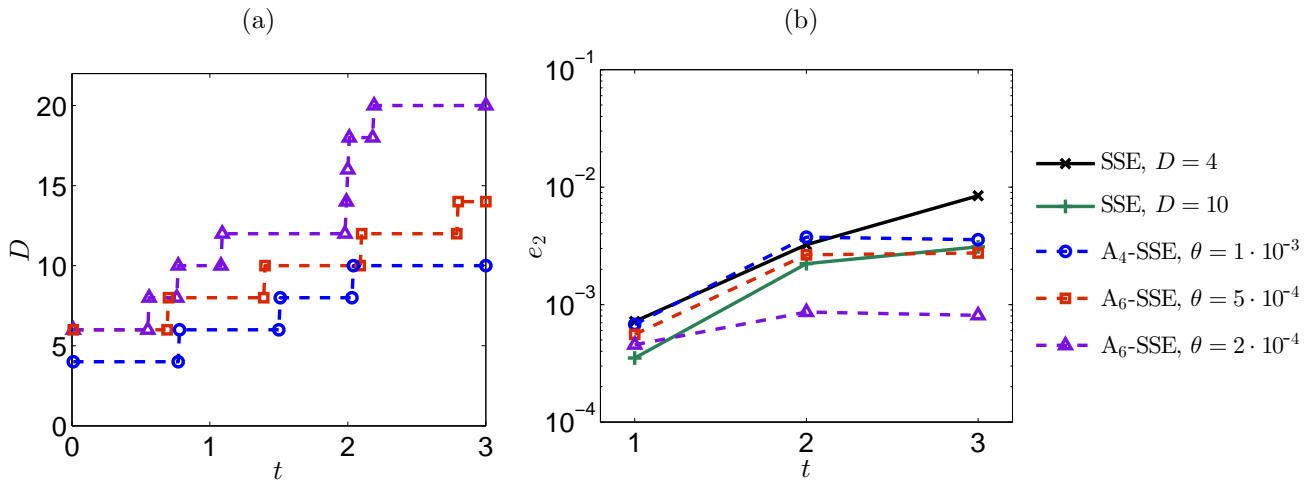
Figure 4.7: Adaptive ALS algorithm: separation rank D (a) and relative L_2 error (b) versus time for different thresholds θ. A small θ yields a large separation rank and a small relative error.
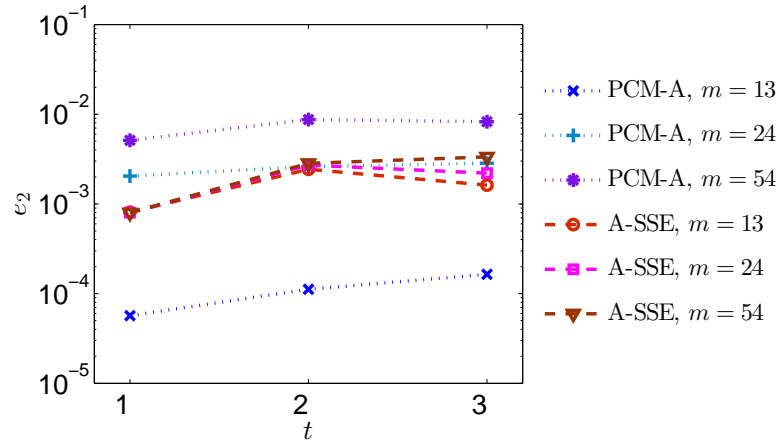
Figure 4.8: Adaptive ALS algorithm: comparison between the relative L_2 errors of the adaptive separated expansion method (A-SSE) and the PCM-ANOVA (PCM-A, level 2) method. Results are for the kinetic equation (4.3.4) with ALS threshold $\theta = 5 \cdot 10^{-4}$. It is seen that the error of the A-SSE method is slightly independent of m, while the error of PCM-ANOVA level 2 increases significantly as we increase m.

variables, i.e., $m = 13$, $m = 24$, and $m = 54$. We first notice that the error in the A_6-SSE method seems to be slightly independent of m. On the other hand, the error of PCM-ANOVA method increases significantly with m, although such error can be improved by increasing the interaction order. However, this would yield an increasing number of collocation points. For example, increasing the interaction order from two to three in this case would increase the number of collocation points from 70498 to 8578270 (see [220]). Hence, the separated series expansion method is preferable to the ANOVA approximation in this case. In Figure 4.9, we compare the computational time of the separated series expansion method with PCM-ANOVA of level two and sparse grid collocation of level three. The simulations are performed on a single CPU of Intel Xeon E5540 (2.53 GHz) and the results are normalized with respect to the computing time of the classical PCM for the case $m = 3$. It is seen that the separated expansion method method costs less than the PCM-ANOVA level 2 when $m \geq 24$ and $D \leq 8$. In the case of equation (4.3.3), the separated expansion method is more efficient than ANOVA, as it reaches the same error level with a small separation rank ($D < 8$).
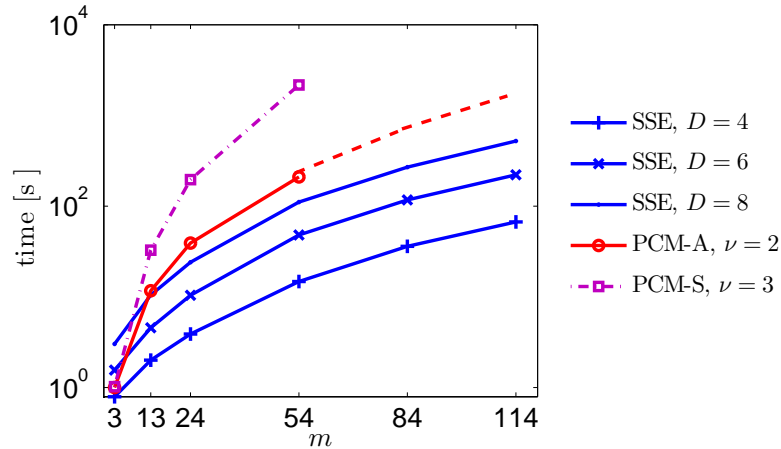
Figure 4.9: Computational time (in seconds) of the separated expansion method (SSE), PCM-ANOVA level 2 (PCM-A), and sparse grid level 3 (PCM-S) as a function of the number of random variables m and separation rank D. The results are normalized with respect to the computing time of PCM with $m = 3$. The dotted lines correspond to extrapolations based on short-runs estimates.

In summary, the separated series expansion method is effective for high-dimensional kinetic equations provided the solution has a small separation rank. If the separation rank is relatively large, then the ANOVA method is expected to be more efficient, although a rigorous quantification of this statement should be done on a case-by-case basis.

4.4 Summary

In this chapter we proposed and validated three different classes of new algorithms to compute the numerical solution of high-dimensional kinetic partial differential equations. The first class of algorithms is based on separated series expansions (SSE) and it yields a sequence of low-dimensional problems that can be solved recursively and in parallel by using alternating direction methods. In particular, we developed a new algorithm that updates the entire rank of the separated representation in each variable, minimizing separation rank and improving the convergence rate. We also proposed an adaptive version of such algorithm and we demonstrated its effectiveness

in numerical applications to random advection of passive scalar fields. The second class of algorithms relies on high-dimensional model representations (ANOVA expansions) and probabilistic (sparse) collocation methods. A common feature of all these methods is that they allow us to reduce the problem of computing the solution to high-dimensional kinetic equations to a sequence of low-dimensional problems. The range of applicability of proposed new algorithms is sketched in Figure 1.2 as a function of the number of phase variables n and the number of parameters m appearing in the kinetic equation. Both ANOVA and SSE scale linearly with the dimension of the phase space, and they yield comparable results for moderate separation ranks. For large separation ranks the ANOVA method is preferable to SSE in terms of computational cost. The choice between ANOVA and SSE does not depend on the number of variables in the kinetic equation but rather on the properties of its solution, in particular the separation rank.

Chapter 5

Dimension reduction techniques for PDF equation

In this chapter, we propose two different approaches to obtain reduced-order PDF equations. In section 5.1, we introduce the Mori-Zwanzig (MZ) projection operator framework that is based on operator cumulant resummation and perturbation methods. The reduced-order equations are derived in section 5.1.1 followed by an application to the joint REPDF of the stochastic Burgers equation in section 5.1.2. Stochastic simulations of the Burgers problem are presented in section 5.1.3 involving interesting observation of the shock development and clustering. In section 5.2, we present the conditional moment closure approach that relies on deriving a hierarchy of coupled PDF equations. Section 5.2.1 includes numerical application of the proposed closure scheme to PDF equations arising in nonlinear stochastic dynamical systems. Finally, we address the probability density approach to solve second-order stochastic PDEs in section 5.2.2.

5.1 Mori-Zwanzig Approach

5.1.1 MZ-PDF Equations by operator cumulants

Let us set $\nu = 0$ in the PDF equation (5.1.34) and rewrite it in a Liouville-type form as

$$\frac{\partial p(t)}{\partial t} = \left[\mathcal{L}_0 + \sigma \mathcal{L}_1(t)\right] p(t), \tag{5.1.1}$$

where

$$\mathcal{L}_0 \stackrel{\text{def}}{=} -\int_{-\infty}^{a} da' \frac{\partial}{\partial x} - a\frac{\partial}{\partial x}, \qquad \mathcal{L}_1(t) \stackrel{\text{def}}{=} -f(x,t;\boldsymbol{b})\frac{\partial}{\partial a}. \tag{5.1.2}$$

Since $\mathcal{L}_0$ is a time-independent linear operator, it is convenient to integrate out exactly the dynamics associated with it first, so as to circumscribe the approximation problem to $\mathcal{L}_1(t)$. This can be carried out by means of a preliminary time-dependent transformation

$$w(t) = e^{-t\mathcal{L}_0}p(t), \tag{5.1.3}$$

which is known as *interaction picture* in quantum mechanics. Substituting (5.1.3) into Eq. (5.1.1) yields

$$\frac{dw(t)}{dt} = \sigma\mathcal{N}(t)w(t), \qquad \mathcal{N}(t) \stackrel{\text{def}}{=} e^{-t\mathcal{L}_0}\mathcal{L}_1(t)e^{t\mathcal{L}_0}. \tag{5.1.4}$$

Note that $\mathcal{L}_0$ depends only on the phase variable a, representing the velocity field, but not on the phase variables $\boldsymbol{b}$ associated with the random forcing term. This implies that the PDF of $u(x,t;\omega)$ can be, in principle, obtained by inverting Eq. (5.1.3) and then integrating it with respect to $\boldsymbol{b}$. This operation can be conveniently represented in terms of an orthogonal projection operator

$$\mathcal{P}p(t) \stackrel{\text{def}}{=} q(\boldsymbol{b}) \int_{-\infty}^{\infty} \cdots \int_{-\infty}^{\infty} p(t)d\boldsymbol{b}, \tag{5.1.5}$$

where $q(\boldsymbol{b})$ denotes the joint PDF of the random vector $\boldsymbol{\xi}$ appearing in the forcing term. Note that $\mathcal{P}^2 = \mathcal{P}$ and that $\mathcal{P}\mathcal{L}_0 = \mathcal{L}_0\mathcal{P}$, i.e., $\mathcal{P}$ commutes with $\mathcal{L}_0$. In addition, integration of Eq. (5.1.5) with respect to $\boldsymbol{b}$ yields $p_u(t)$, that is the one-point one-time PDF of the velocity field that solves Eq. (5.1.27) in the inviscid limit. If we apply $\mathcal{P}$ to both sides of Eq. (5.1.3), differentiate it with respect to t, and integrate with respect to $\boldsymbol{b}$ we obtain

$$\frac{\partial p_u(t)}{\partial t} = \mathcal{L}_0 p_u(t) + e^{t\mathcal{L}_0}\int_{-\infty}^{\infty}\cdots\int_{-\infty}^{\infty}\frac{\partial \mathcal{P}w(t)}{\partial t}d\boldsymbol{b}. \tag{5.1.6}$$

The next step is to determine the law for $\partial\mathcal{P}w(t)/\partial t$. This can be done in a formally exact way by using the Mori-Zwanzig formalism, in particular the convolutionless form [23, 28, 195]. This yields

$$\frac{\partial \mathcal{P}w(t)}{\partial t} = \widehat{\mathcal{K}}(t)\mathcal{P}w(t) + \widehat{\mathcal{H}}(t)\mathcal{Q}w(0), \tag{5.1.7}$$

where $\mathcal{Q} \stackrel{\text{def}}{=} \mathcal{I} - \mathcal{P}$,

$$\widehat{\mathcal{K}}(t) \stackrel{\text{def}}{=} \sigma\mathcal{P}\mathcal{N}(t)[\mathcal{I} - \sigma\widehat{\Sigma}(t)]^{-1}, \tag{5.1.8}$$

$$\widehat{\mathcal{H}}(t) \stackrel{\text{def}}{=} \sigma\mathcal{P}\mathcal{N}(t)[\mathcal{I} - \sigma\widehat{\Sigma}(t)]^{-1}\widehat{\mathcal{G}}(t,0), \tag{5.1.9}$$

and

$$\widehat{\Sigma}(t) \stackrel{\text{def}}{=} \int_0^t \widehat{\mathcal{G}}(t,s)\mathcal{Q}\mathcal{N}(s)\mathcal{P}\widehat{\mathcal{Z}}(t,s)ds, \tag{5.1.10}$$

$$\widehat{\mathcal{G}}(t,s) \stackrel{\text{def}}{=} \overleftarrow{\mathcal{T}}\exp\left[\sigma\int_s^t \mathcal{Q}\mathcal{N}(\tau)d\tau\right], \qquad \widehat{\mathcal{Z}}(t,s) \stackrel{\text{def}}{=} \overrightarrow{\mathcal{T}}\exp\left[-\sigma\int_s^t \mathcal{N}(\tau)d\tau\right]. \tag{5.1.11}$$

In Eq. (5.1.11), $\overleftarrow{\mathcal{T}}$ and $\overrightarrow{\mathcal{T}}$ denote, respectively, the chronological and the anti-chronological time-ordering operators. If the joint PDF $p(0) = w(0)$ is separable, i.e., if the initial condition $u(x, 0; \boldsymbol{\eta})$ is independent of the random excitation vector

$\boldsymbol{\xi}$, then $w(0)$ is in the range of $\mathcal{P}$ and we have $\mathcal{Q}w(0) = 0$ in Eq. (5.1.7). In the following we will consider such case.

So far everything that has been said is exact and it led us to Eqs. (5.1.6) and (5.1.7), which are linear and of infinite order in the phase variable a. We now introduce approximations. To this end, we expand the right hand side of Eq. (5.1.7) in formal power series in the coupling parameter σ (see [195] for details). This yields

$$\frac{\partial \mathcal{P}w(t)}{\partial t} = \left(\sigma \mathcal{N}(t) + \sigma^2 \int_0^t \left[\mathcal{P}\mathcal{N}(t)\mathcal{N}(s) - \mathcal{P}\mathcal{N}(t)\mathcal{P}\mathcal{N}(s) \right] ds + \cdots \right) \mathcal{P}w(t).$$
(5.1.12)

Substituting (5.1.12) into Eq. (5.1.6) gives the reduced order kinetic equation

$$\frac{\partial p_u(t)}{\partial t} = \mathcal{L}_0 p_u(t) + e^{t\mathcal{L}_0} \left(\sigma \left\langle \mathcal{N}(t) \right\rangle_K + \sigma^2 \int_0^t \left\langle \mathcal{N}(t)\mathcal{N}(s) \right\rangle_K ds + \cdots \right) e^{-t\mathcal{L}_0} p_u(t),$$
(5.1.13)

where $\left\langle \mathcal{N}(t) \cdots \mathcal{N}(t_n) \right\rangle_K$ are Kubo-Van Kampen operator cumulants [94, 95, 195] relative to the joint PDF of the random vector $\boldsymbol{\xi}$. For instance, the first two cumulants are

$$\left\langle \mathcal{N}(t) \right\rangle_K = \int_{-\infty}^{\infty} \cdots \int_{-\infty}^{\infty} \mathcal{N}(t) q(\boldsymbol{b}) d\boldsymbol{b},$$
(5.1.14)

$$\left\langle \mathcal{N}(t)\mathcal{N}(s) \right\rangle_K = \int_{-\infty}^{\infty} \cdots \int_{-\infty}^{\infty} \left[\mathcal{N}(t)\mathcal{N}(s) q(\boldsymbol{b}) - \mathcal{N}(t) q(\boldsymbol{b}) \mathcal{N}(s) q(\boldsymbol{b}) \right] d\boldsymbol{b},$$
(5.1.15)

each one being a linear operator in the phase variables a and x. The n-th order operator cumulant $\left\langle \mathcal{N}(t_1) \cdots \mathcal{N}(t_n) \right\rangle_K$ can be calculated by using diagrammatic methods [94]. The reduced-order kinetic equation (5.1.13) is linear, formally exact, but it involves derivatives of infinite-order in both variables x and a. Such derivatives come from the operator cumulants as well as from the exponential operators appearing in Eqs. (5.1.4) and (5.1.13). In a finite-dimensional setting, these quantities can be com-

puted by using efficient numerical algorithms, e.g., based on scaling-squaring techniques, Padé approximants, or Krylov subspace projection methods [1, 52, 123, 184]. Any finite-order truncation of the series within the brackets in Eq. (5.1.13) yields an approximation whose accuracy depends on the magnitude of σ, the integration time t, as well as on the the decay rate of the Kubo-Van Kampen operator cumulants $\langle \mathcal{N}(t_1) \cdots \mathcal{N}(t_n) \rangle_K$. The latter depends on the properties of the random forcing. For example, in Langevin systems forced with Gaussian white noise it can be shown that the approximation obtained by retaining only the first two operator cumulants is exact for arbitrary σ (see [195]).

We remark that the kinetic equation (5.1.13) can be derived also by using the asymptotic perturbation theory of semigroups [55, 99]. The simplest way to do so is to consider the formal (implicit) solution to Eq. (5.1.1)

$$p(t) = e^{t\mathcal{L}_0}p(0) + \sigma \int_0^t e^{(t-s)\mathcal{L}_0} \mathcal{L}_1(s)p(s)ds, \qquad (5.1.16)$$

and generate a sequence of approximations by recursive substitution, starting from $p(0)$. This yields

$$p(t) = \left[e^{\mathcal{L}_0(t)}p(0) + \sigma \int_0^t e^{(t-s)\mathcal{L}_0} \mathcal{L}_1(s)e^{s\mathcal{L}_0}ds + \right.$$
$$\left. \sigma^2 \int_0^t \int_0^s e^{\mathcal{L}_0(t-s)} \mathcal{L}_1(s)e^{(s-z)\mathcal{L}_0} \mathcal{L}_1(z)e^{z\mathcal{L}_0}dzds \right] p(0) + O(\sigma^3). \qquad (5.1.17)$$

Assuming that $p(0)$ is separable as $p(0) = p_u(0)q(\boldsymbol{b})$, integrating Eq. (5.1.17) with respect to $\boldsymbol{b}$ yields the second-order approximation to the formal analytical solution to Eq. (5.1.13), i.e.,

$$p_u(t) = \left[e^{\mathcal{L}_0(t)}p_u(0) + \sigma \int_0^t e^{(t-s)\mathcal{L}_0} \langle \mathcal{L}_1(s) \rangle_{\boldsymbol{b}} e^{s\mathcal{L}_0}ds + \right.$$
$$\left. \sigma^2 \int_0^t \int_0^s e^{\mathcal{L}_0(t-s)} \langle \mathcal{L}_1(s)e^{(s-z)\mathcal{L}_0} \mathcal{L}_1(z) \rangle_{\boldsymbol{b}} e^{z\mathcal{L}_0}dzds \right] p_u(0) + O(\sigma^3), \quad (5.1.18)$$

where

$$\langle\cdot\rangle_{\boldsymbol{b}} \overset{\text{def}}{=} \int_{-\infty}^{\infty} \cdots \int_{-\infty}^{\infty} (\cdot)q(\boldsymbol{b})d\boldsymbol{b}. \tag{5.1.19}$$

An interesting subcase of Eqs. (5.1.6) and (5.1.18) is obtained by assuming that the random forcing does not depend on x. This yields the simplified kinetic equation

$$
\begin{aligned}
\frac{\partial p_u(t)}{\partial t} &= \mathcal{L}_0 p_u(t) + \sigma \langle f(t;\boldsymbol{b})\rangle_{\boldsymbol{b}} \frac{\partial p_u(t)}{\partial a} + \sigma^2 \int_0^t \left(e^{(t-s)\mathcal{L}_0} C(t,s) \frac{\partial^2 p_u(s)}{\partial a^2} - \right. \\
&\quad \left. (t-s)e^{(t-s)\mathcal{L}_0} \langle f(t;\boldsymbol{b})f(s;\boldsymbol{b})\rangle_{\boldsymbol{b}} \frac{\partial^2 p_u(s)}{\partial x \partial a} \right) ds + O(\sigma^3), \tag{5.1.20}
\end{aligned}
$$

where $C(t,s)$ is the temporal covariance of $f(t;\boldsymbol{\xi})$. Eq. (5.1.20) is obtained by differentiating Eq. (5.1.18) with respect to time and noting that

$$
\begin{aligned}
\mathcal{L}_1(t)e^{(s-u)\mathcal{L}_0} &= \sum_{n=0}^{\infty} \frac{1}{n!} \mathcal{L}_1(t)\mathcal{L}_0^n(s-u)^n \\
&= \sum_{n=0}^{\infty} \frac{1}{n!} \left(\mathcal{L}_0^n \mathcal{L}_1(t) - n\mathcal{L}_0^{n-1} f(t;\boldsymbol{b})\frac{\partial}{\partial x} \right)(s-u)^n \\
&= e^{(s-u)\mathcal{L}_0}\mathcal{L}_1(t) - (s-u)e^{(s-u)\mathcal{L}_0} f(t;\boldsymbol{b})\frac{\partial}{\partial x}.
\end{aligned}
$$

Let us consider the two-point joint response-excitation PDF, i.e., the joint PDF of $u(x_1, t; \omega)$, $u(x_2, t; \omega)$ and $\boldsymbol{\xi}$,

$$p_2(x_1, x_2, t; a_1, a_2, \boldsymbol{b}) = \iint \prod_{i=1}^{2} \delta(a_i - U(x_i, t; \boldsymbol{A}_0, \boldsymbol{B}))\delta(\boldsymbol{b} - \boldsymbol{B})q(\boldsymbol{A}_0, \boldsymbol{B})d\boldsymbol{A}_0 d\boldsymbol{B}. \tag{5.1.21}$$

Such PDF satisfies the obvious limiting condition

$$\lim_{x_1 \to x_2} p_2(x_1, x_2, t; a_1, a_2, \boldsymbol{b}) = \delta(a_1 - a_2)p(x_1, t; a_1, \boldsymbol{b}), \tag{5.1.22}$$

where $p(x_1, t; a_1, \boldsymbol{b})$ is the one-point PDF (5.1.30). It can be shown (see, e.g., [194, 197]) that in the inviscid limit $\nu \to 0$, the PDF (5.1.21) satisfies the exact kinetic

equation

$$\frac{\partial p_2(t)}{\partial t} = \left[\mathcal{H}_0 + \sigma \mathcal{H}_1(t)\right] p_2(t),$$ (5.1.23)

where

$$\mathcal{H}_0 \stackrel{\text{def}}{=} -\sum_{i=1}^{2} \left(\int_{-\infty}^{a_i} da_i' \frac{\partial}{\partial x_i} + a_i \frac{\partial}{\partial x_i}\right), \qquad \mathcal{H}_1(t) \stackrel{\text{def}}{=} -\sum_{i=1}^{2} f(x_i, t; \boldsymbol{b}) \frac{\partial}{\partial a_i}.$$ (5.1.24)

By following the same mathematical steps that led us to Eq. (5.1.13), we obtain the following reduced-order kinetic equation for the two-point PDF of the solution field[1]

$$\frac{\partial p_{uu'}(t)}{\partial t} \simeq \mathcal{H}_0 p_{uu'}(t) + e^{t\mathcal{H}_0} \left(\sigma \langle \mathcal{G}(t)\rangle_K + \sigma^2 \int_0^t \langle \mathcal{G}(t)\mathcal{G}(s)\rangle_K \, ds + \cdots\right) e^{-t\mathcal{H}_0} p_{uu'}(t),$$ (5.1.25)

where

$$\mathcal{G}(t) \stackrel{\text{def}}{=} e^{-t\mathcal{H}_0} \mathcal{H}_1(t) e^{t\mathcal{H}_0}.$$ (5.1.26)

The Kubo-Van Kampen operator cumulants of $\mathcal{G}$, e.g., $\langle \mathcal{G}(t)\mathcal{G}(s)\rangle_K$, are defined as in Eqs. (5.1.14)-(5.1.15). As we will see in section 5.1.3, the two-point PDF of the velocity field can be used to calculate important quantities such as the turbulent energy and indicator functions to stochastic shock clustering.

5.1.2 MZ-PDF Equations for the Burgers equation

Let us consider the following prototype initial/boundary value problem for the Burgers equation

$$\begin{cases} \dfrac{\partial u}{\partial t} + u\dfrac{\partial u}{\partial x} = \nu\dfrac{\partial^2 u}{\partial x^2} + \sigma f(x, t; \omega) & x \in [0, 2\pi] \qquad t \geq 0 \\[2mm] u(x, 0; \omega) = u_0(x; \omega) \\[2mm] u(0, t; \omega) = u(2\pi, t; \omega) \end{cases}$$ (5.1.27)

---

[1] Here we use the shorthand notation $p_{uu'}(t) = p(x, x', t; a_1, a_2)$.

where the initial condition $u_0(x;\omega)$ and the forcing term $f(x,t;\omega)$ are square integrable random fields defined on a complete probability space. For each realization of $u_0(x;\omega)$ and $f(x,t;\omega)$, the solution $u(x,t;\omega)$ takes values in the space $L_2([0,2\pi],\mathbb{R})$ on which the operator $\partial^2/\partial x^2$ is endowed with periodic boundary conditions. The problem (5.1.27) is well-posed, since we can write $u\partial u/\partial x$ as $(\partial u^2/\partial x)/2$, which is locally Lipschitz from the Sobolev space $\mathcal{W}^{1/4,2}$ [2] into $\mathcal{W}^{-1,2}$, thus, allowing us to apply general local well-posedness theorems [149,150]. The regularity of the solution to Eq. (5.1.27) depends on the regularity of the random noise $f(x,t;\omega)$. In particular, if f is space-time white noise, then u has the regularity of Brownian motion, i.e., it is not differentiable in x. In this chapter, we consider *smooth noise*, eventually yielding white-noise as a result of a suitable limiting procedure. In particular, we represent $f(x,t;\omega)$ and $u_0(x;\omega)$ in terms of series expansions involving proper sets of random variables $\boldsymbol{\xi}(\omega) = \{\xi_1(\omega),...,\xi_m(\omega)\}$ and $\boldsymbol{\eta}(\omega) = \{\eta_1(\omega),...,\eta_l(\omega)\}$

$$u_0(x;\boldsymbol{\eta}) = \sum_{k=1}^{l}\eta_k(\omega)\phi_k(x), \qquad f(x,t;\boldsymbol{\xi}) = \sum_{j=1}^{m}\xi_j(\omega)\Psi_j(x,t). \qquad (5.1.28)$$

The existence and uniqueness of the solution to Eq. (5.1.27) for each realization of $u_0(x;\boldsymbol{\eta})$ and $f(x,t;\boldsymbol{\xi})$ allows us to consider the random field $u(x,t;\omega)$ as a deterministic function of $\boldsymbol{\xi}$ and $\boldsymbol{\eta}$, i.e., we have a *flow map* U such that

$$u(x,t;\omega) = U(x,t;\boldsymbol{\eta}(\omega),\boldsymbol{\xi}(\omega)). \qquad (5.1.29)$$

Note that at initial time $U(x,0;\boldsymbol{\eta},\boldsymbol{\xi}) = u_0(x;\boldsymbol{\eta})$. The joint PDF of the solution to Eq. (5.1.27) and the random vector $\boldsymbol{\xi}(\omega)$ admits the following representation (see, e.g., [100, 194, 197])

$$p(x,t;a,\boldsymbol{b}) = \int_{-\infty}^{\infty}\cdots\int_{-\infty}^{\infty}\delta(a - U(x,t;\boldsymbol{A}_0,\boldsymbol{B}))\delta(\boldsymbol{b} - \boldsymbol{B})q(\boldsymbol{A}_0,\boldsymbol{B})d\boldsymbol{A}_0d\boldsymbol{B}, \qquad (5.1.30)$$

---

[2]The Sobolev space is defined as $\mathcal{W}^{k,p} \stackrel{\text{def}}{=} \{u \in L^p : D^\alpha u \in L^p,\ \forall|\alpha| \leq k\}$.

where $a \in \mathbb{R}$, $\boldsymbol{b} \in \mathbb{R}^m$, $\boldsymbol{A}_0 \in \mathbb{R}^l$, $\boldsymbol{B} \in \mathbb{R}^m$, $q(\boldsymbol{A}_0, \boldsymbol{B})$ denotes the (possibly compactly supported) joint PDF of the random vectors $\boldsymbol{\eta}$ and $\boldsymbol{\xi}$, and $\delta(\boldsymbol{b} - \boldsymbol{B})$ is a multi-dimensional Dirac delta function, i.e.,

$$\delta(\boldsymbol{b} - \boldsymbol{B}) \stackrel{\text{def}}{=} \prod_{k=1}^{m} \delta(b_k - B_k).$$

The one-point one-time PDF of the solution to Eq. (5.1.27) is obtained by integrating (5.1.30) with respect to $\boldsymbol{b} = \{b_1, .., b_m\}$

$$p_u(x, t; a) = \int_{-\infty}^{\infty} \cdots \int_{-\infty}^{\infty} p(x, t; a, \boldsymbol{b}) d\boldsymbol{b}. \tag{5.1.31}$$

Differentiating (5.1.30) with respect to x and t and using suitable identities involving the Dirac delta function yields the following exact joint response-excitation PDF equation[3] :

$$\frac{\partial p(t)}{\partial t} + \int_{-\infty}^{a} \frac{\partial p(t)}{\partial x} da' + a \frac{\partial p(t)}{\partial x} = -\sigma f(x, t; \boldsymbol{b}) \frac{\partial p(t)}{\partial a} - \nu \frac{\partial}{\partial a} \left\langle \frac{\partial^2 u}{\partial x^2} \delta(a - u(x, t)) \right\rangle, \tag{5.1.32}$$

where we used the shorthand notation $p(t) \equiv p(x, t; a, \boldsymbol{b})$. The last term in the right hand side is defined as

$$\left\langle \frac{\partial^2 u}{\partial x^2} \delta(a - u(x, t)) \right\rangle \stackrel{\text{def}}{=} \iint \frac{\partial^2 U}{\partial x^2} \delta(a - U(x, t; \boldsymbol{A}_0, \boldsymbol{B})) \delta(\boldsymbol{b} - \boldsymbol{B}) q(\boldsymbol{A}_0, \boldsymbol{B}) d\boldsymbol{A}_0 d\boldsymbol{B}, \tag{5.1.33}$$

and it represents an *unclosed* term that has to be treated using *closure models* having additional assumptions [51,147]. For example, we can introduce a conditional average

---

[3]Note that differentiating (5.1.32) with respect to a allows us to remove the integral term and it yields a second-order linear PDE.

$\langle u_{xx}|u\rangle^4$ and rewrite (5.1.32) as

$$\frac{\partial p(t)}{\partial t} + \int_{-\infty}^{a} \frac{\partial p(t)}{\partial x} da' + a\frac{\partial p(t)}{\partial x} = -\sigma f(x,t;\boldsymbol{b})\frac{\partial p(t)}{\partial a} - \nu\frac{\partial}{\partial a}\left[\left\langle \frac{\partial^2 u}{\partial x^2}\middle| u \right\rangle p_u(t)\right].$$
(5.1.34)

An interesting question is what happens to the solution to the PDF equations (5.1.32) or (5.1.34) in the limit of zero viscosity $\nu \to 0$. In this case, Eq. (5.1.27) becomes a hyperbolic conservation law that can generate shock discontinuities at random space-time locations (see Figure 5.1 for a few solution samples). There has been extensive theoretical investigation of the inviscid limit to the solution to the viscous Burgers equation (see, e.g., [5, 77, 172]). From the PDF standpoint, the inviscid limit influences the conditional average in Eq. (5.1.34). In particular, it contributes sharply to the PDF dynamics nearby the space-time locations where random shocks develop. This is sometimes referred to as dissipative anomalies [51]. As we shall see in section 5.1.3, the numerical dissipation associated with finite resolution in numerical simulations of Eqs. (5.1.27) and (5.1.34) dominates the regularizing diffusion terms for $\nu \to 0$. Therefore, from a numerical standpoint, we could set $\nu = 0$ in Eqs. (5.1.27) and (5.1.34) and study the inviscid limit of the Burgers equation in the sense of *vanishing numerical viscosity* for increasing levels of resolution.

5.1.3   Stochastic simulations of Burgers equation

The numerical simulation of the stochastic Burgers problem Eq. (5.1.27) has recently attracted considerable attention [15, 80]. One difficult challenge is an effective computation of the solution in the inviscid limit, in particular in the presence of random forcing terms and random initial conditions. In fact, this could generate random

---

[4]The conditional average is explicitly defined as

$$\langle u_{xx}|u\rangle \overset{\text{def}}{=} \int_{-\infty}^{\infty} \cdots \int_{-\infty}^{\infty} U_{xx}\delta(a - U(x,t;\boldsymbol{A}_0,\boldsymbol{B}))\delta(\boldsymbol{b} - \boldsymbol{B})\widetilde{q}(\boldsymbol{A}_0,\boldsymbol{B}|u = a)d\boldsymbol{A}_0 d\boldsymbol{B}.$$

No Forcing

Weak Additive Forcing
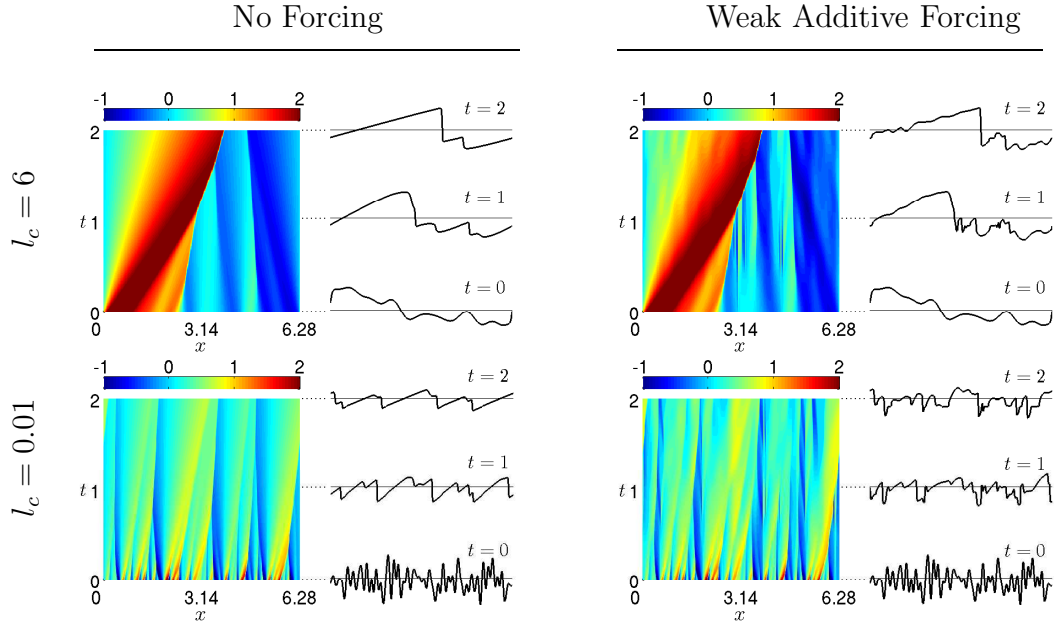
Figure 5.1: Sample solutions of the Burgers problem (5.1.27) in the inviscid limit $\nu \to 0$. Here we consider two initial conditions with different correlation length randomly sampled from (5.1.40) and a realization of the random forcing term (5.1.39). It is seen that at $t = 2$ the velocity field already developed the triangular-shaped shock structure that is characteristic of the Burgers turbulence regime. Note that even weak additive forcing ($\sigma = 0.05$) can influence the solution, especially for rough initial conditions ($l_c = 0.01$).

shock waves at random space-time locations. In this chapter we tackle this problem by using the adaptive discontinuous Galerkin method we have recently developed in [34] (see section 3.1.1).

Let us first show that the numerical viscosity of the scheme dominates the conditional average term in Eq. (5.1.34), for $\nu \to 0^5$. Such term can be accurately computed by Monte Carlo simulation, i.e., by sampling a sufficiently large number of solutions to Eq. (5.1.27), and then averaging $u_{xx} = \partial^2 u / \partial x^2$, conditioned to $u(x, t; \omega) = a$ for arbitrary a. The results are shown in Figure 5.2 for random flows

---

[5] All approaches and methodologies dealing with the numerical solution to the inviscid Burgers equation add an artificial (numerical) diffusion term which can be made arbitrarily small in some limiting process, e.g., by leveraging on hp-convergence. This means that we always have numerical non-uniqueness when computing the solution to the inviscid Burgers equation.
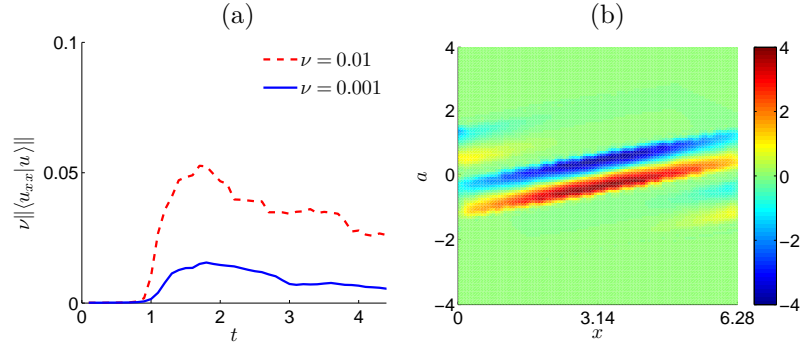
Figure 5.2: Numerical viscosity dominates the inviscid limit in the stochastic Burgers equation. In (a), we show a comparison of the L_2 norm of the conditional average $\langle u_{xx}|u \rangle$ for $\nu = 10^{-2}$ and $\nu = 10^{-3}$ versus time. At time $t = 1$, the inviscid limit of the solution to the Burgers equation subject to the random initial condition (5.1.35) generates an ensemble of shock waves. Figure (b) shows the contour values of $\langle u_{xx}|u \rangle$ for $\nu = 10^{-2}$ at time $t = 4$. Note that the minimum and the maximum values are located, respectively, near the peaks and the dips of the ensemble of shocks.

solving Eq. (5.1.27) with initial condition

$$u_0(x; \eta) = \sin(x) + \eta(\omega) \tag{5.1.35}$$

and no random forcing. Here η is a Gaussian random variable with mean π and variance $1/4$. It is seen that the norm of conditional average term in Eq. (5.1.34) becomes smaller and smaller as ν goes to 0. In other words, at *finite numerical resolution* the solution to the PDF equation corresponding to the inviscid Burgers equation provides a very good approximation to the PDF of the inviscid limit of the solution to (5.1.27) after the shock occurrence, i.e., at $t = 1$ in the present example. To this end, we verify this by comparing the solutions computed by the joint PDF equation (5.1.34) with $\nu = 0$ to an accurate[6] MC solution to Eq. (5.1.27). In particular, we consider a prototype space-independent forcing term

$$f(x, t; \omega) = \xi(\omega) \sin(t), \tag{5.1.36}$$

---

[6]Each solution sample is obtained by our adaptive DG method with a spatial discretization based on $N = 128$ finite elements of order $p = 8$ in $[0, 2\pi]$.

where $\xi(\omega)$ and $\eta(\omega)$ are independent zero-mean Gaussian random variables with standard deviation $\pi/10$ and 1, respectively. In this hypothesis, the joint PDF of u_0 and ξ is

$$p(0) = \frac{5}{\pi^2} \exp\left[-\frac{(a - \sin(x))^2}{2}\right] \exp\left[-50\frac{b^2}{\pi^2}\right].$$

We set the amplitude of the random forcing term in Eqs. (5.1.34) and (5.1.27) to $\sigma = 1$. The joint PDF equation (5.1.34) is solved by using the DG method with 50 elements of order $p = 4$ and 15-th degree Hermite polynomials for the excitation space. Time-stepping is based on 4th-order Runge-Kutta scheme with $\Delta t = 2 \times 10^{-4}$. In Figure 5.3, we plot the results of our simulations, which show that the joint PDF solution coincides with the MC approach. Thus, in what follows we set $\nu = 0$ in all kinetic equations we obtained in Section 5.1.2. Note that the shock wave at $t = 1$ arising from the system does not arise in the response PDF shown in Figure 5.3. Instead, such PDF solution looks rather smooth. As we will see in the next subsection, however, smooth multi-modal PDFs can generate flow realizations with discontinuities, i.e., shocks.

High-Dimensional Random Initial Conditions

In this section, we present numerical results for various types of spatially correlated, high-dimensional random initial conditions. First of all, we show that a smooth multi-modal PDF can generate shock realizations. This is done in Figure 5.4, where we consider the one-point PDF of the velocity field in the inviscid limit for initial conditions in the form Eq. (5.1.35). In contrast to the previous example where η was set to be zero mean, here we consider a Gaussian η with mean π and standard deviation $\pi/10$. The non-vanishing mean induces stirring of the PDF along the x direction, yielding multi-modal patterns after short time. The corresponding
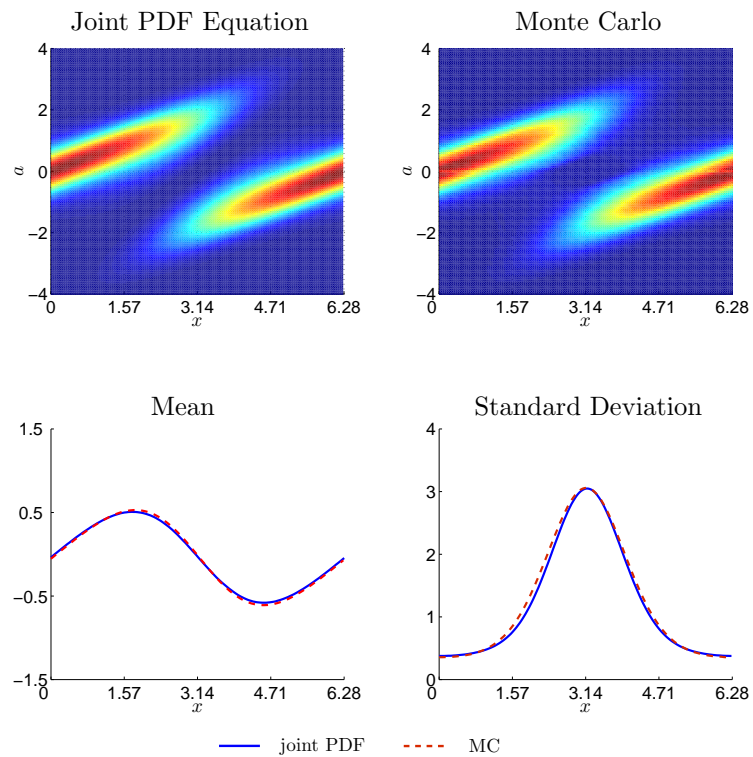
Figure 5.3: PDF of the velocity field: validation of the joint PDF equation. Shown is a comparison between the marginalized solution to Eq. (5.1.34) at $t = 1$ and a kernel density estimation [22] of the PDF of the velocity based on 50000 MC samples. We also compare the mean and the standard deviation at $t = 1$ as computed from the PDF and the MC approaches.
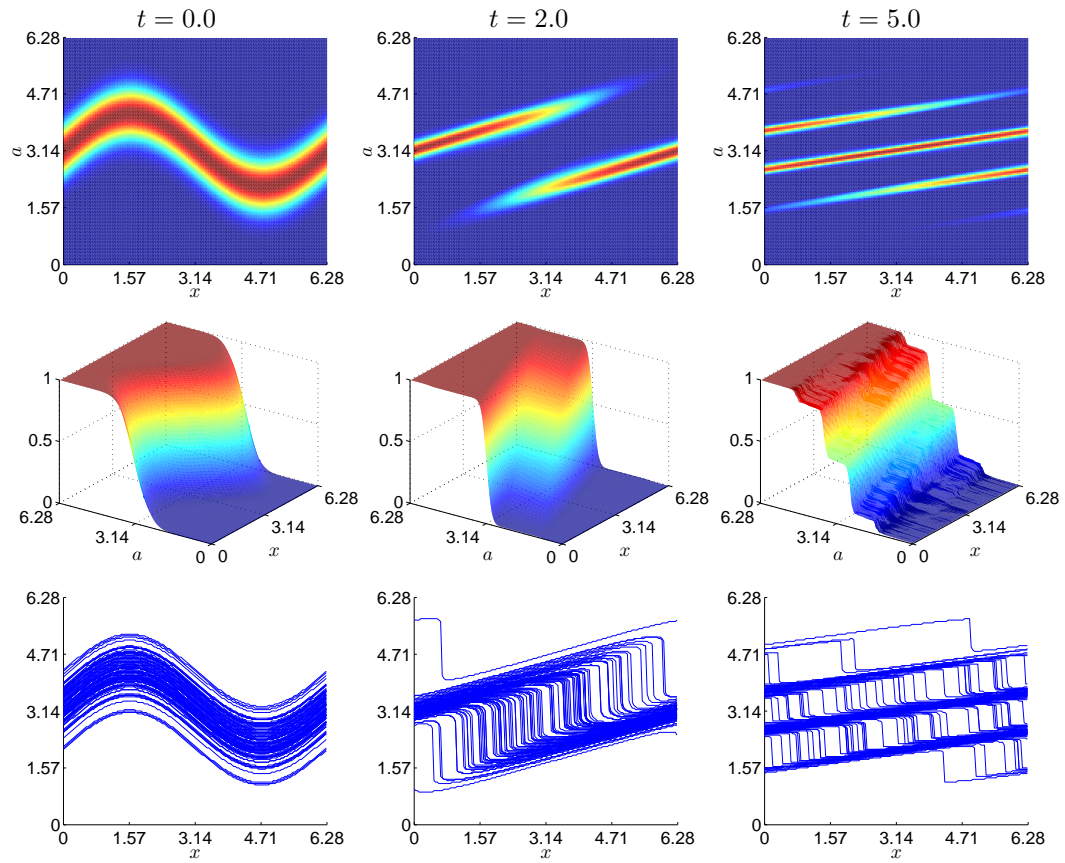
Figure 5.4: Shock realizations of the velocity field (third row) generated by smooth multi-modal PDFs (first row). The second row shows the cumulative density function of the PDFs of the first row.

cumulative distribution function (CDF) is defined as

$$C_u(t, x, a) \overset{\text{def}}{=} \int_{-\infty}^{a} p_u(t, x, a')da', \qquad (5.1.37)$$

and it is plotted in the second row of Figure 5.4. In the third row, we provide samples of the velocity field obtained from the CDF shown in the second row. It is seen that shock patterns can be generated from CDFs resembling a step function. In other words, the *location* and the *steepness* of the peaks in the one-point PDF can determine shock waves in the physical space.

However, as we point out in [36], the statistical information encoded in the one-point PDF is not sufficient to completely characterize the structure of shocks in space and time. Indeed, it is possible to manufacture a random initial condition problem for the inviscid Burgers equation having a significantly different shock structure in physical space, but exactly the same one-point PDF dynamics. To this end, simply consider a set of i.i.d. normal random variables $\{\eta_k\}$, and the Gaussian initial condition

$$u_0(x; \omega) = \frac{1}{\sqrt{m}} \sum_{k=1}^{m} \left[\eta_{2k}(\omega) \sin(kx) + \eta_{2k-1}(\omega) \cos(kx) \right], \qquad (5.1.38)$$

whose one-point PDF is Gaussian with mean 0 and variance 1 at all spatial points x, disregarding m. For large values of m we have very rough initial conditions developing shock discontinuities very early in time, while for small values of m we have smoother initial conditions developing shocks at later times. However, the one-point PDF dynamics predicted by Eq. (5.1.34) for $f = 0$ and $\nu \to 0$ is exactly the same. In other words, the one-point PDF does not encode enough statistical information to characterize shock dynamics and clustering. However, it allows us to compute all single-point statistical moments of the velocity field, as well as rare events (tails of the PDF).
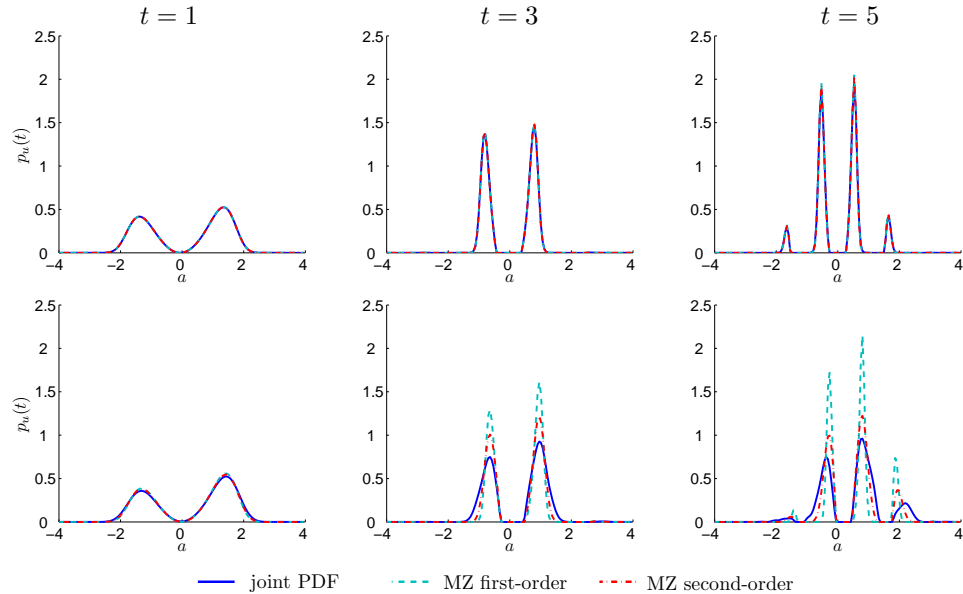
Figure 5.5: Randomly forced Burgers equation. One-point PDF of the velocity field at $x = \pi$ for exponentially correlated, homogeneous (in space) random forcing processes with correlation time $\tau = 0.01$ and amplitude $\sigma = 0.01$ (first row) and $\sigma = 0.1$ (second row). Shown are results obtained from the joint PDF equation (5.1.1), and two different truncations of the MZ-PDF equation (5.1.20).

High-Dimensional Random Forcing

The numerical simulation of the joint PDF equation (5.1.1) in the presence of a high-dimensional random forcing is a very challenging problem, as it involves the representation of a scalar field (the joint PDF) in a high-dimensional parametric space. For a moderate number of dimensions, effective approaches are multi-element and sparse adaptive probabilistic collocation [34,48,61]. On the other hand, the Mori-Zwanzig projection operator formalism we developed in previous sections allows us to formally integrate out all the phase variables associated with the random forcing (i.e., the variables $\boldsymbol{b}$), yielding *low-dimensional* PDF equations in the form Eq. (5.1.13).

Let us first consider a zero-mean homogeneous (in space) Gaussian random process with exponential covariance function

$$\langle f(t; \boldsymbol{b}) f(s; \boldsymbol{b}) \rangle_{\boldsymbol{b}} = \frac{1}{\tau} \exp\left[-\frac{|t-s|}{\tau} \right], \qquad t, s \in [0, T],$$

where τ is the correlation time. Specifically, we choose $T = 5$ and $\tau = 0.01$, i.e., a nearly white-in-time Gaussian random process. The Karhunen-Loève (KL) expansion of such weakly correlated random forcing, requires at least 57 random variables to achieve less than 5% error in the eigenspectrum. We first compute a benchmark PDF solution by solving Eq. (5.1.1) using sparse grid collocation of level 2 [130]. This entails sampling Eq. (5.1.1) at 6841 sparse grid points and then integrate the joint PDF $p(t)$ with respect to $\boldsymbol{b}$ in a 57-dimensional space by using appropriate quadrature rules. This benchmark solution is used to determine the accuracy of various truncations to the MZ-PDF equation (5.1.13), i.e. Eq. (5.1.20). This is done in in Figure 5.5, where we compare the one-point PDF of the velocity field at $x = \pi$ obtained by the first- and second-order approximations to Eq. (5.1.20). In the first-order approximation, we basically neglect all the terms of order σ^2 or higher. We see that when σ is small, e.g., $\sigma = 0.01$, both the first- and second-order approximations are in good agreement with the benchmark PDF solution up to $t = 5$. However, as σ becomes larger, the small-noise approximation based on the first- and second-order truncations slightly diverge from the MC benchmark solution. However, the computational cost of solving the second-order approximation to Eq. (5.1.20) in this case is less than 2% the cost of solving the exact equation (5.1.1). Therefore, the MZ-PDF framework provides a computationally efficient way to determine the one-point statistics of the velocity field.

Burgers Turbulence and Stochastic Shock Clustering

Let us go back to the flow example discussed in the introduction, showing a realization of shock clustering and shock displacement induced by weak space-time additive forcing (see Figure 5.1). The forcing term considered there was a sample of
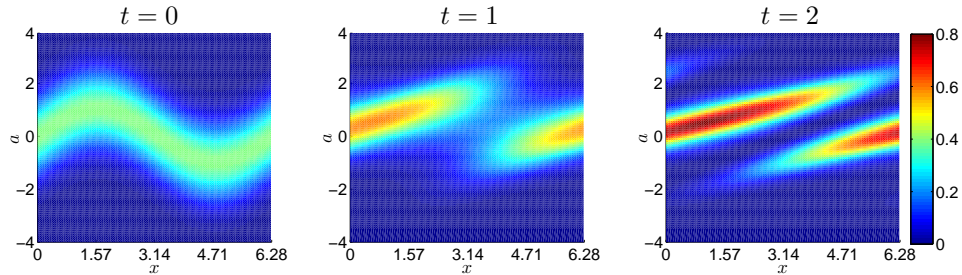
Figure 5.6: Burgers turbulence. Time snapshots of the one-point PDF obtained from the second order approximation to the MZ equation (5.1.13). We consider a rough initial condition in the form (5.1.40) with $l_c = 0.01$, and the forcing term (5.1.39) with amplitude $\sigma = 0.05$.

the space-time Gaussian random field

$$f(x, t; \boldsymbol{\xi}) = 1 + \sum_{k=1}^{5} \left[(-1)^k \left(\xi_{2k-1} \sin(2kx) + \xi_{2k} \cos(3kx) \right) e^{-\sin(2kt)} \right], \qquad (5.1.39)$$

where ξ_k are jointly normal (independent) random variables, while the initial condition is an exponentially correlated random field represented in terms of a KL series expansion [35, 89] in the form

$$u_0(x; \omega) = a_0(\eta_0 + \sin(x)) + \sum_{k=1}^{m} \sqrt{\lambda_k} \eta_k \Psi_k(x), \qquad (5.1.40)$$

where η_k are independent normal random variables, and λ_k and Ψ_k are respectively, eigenvalues and eigenfunctions of the exponential covariance function

$$C(x, y) = \frac{1}{l_c} \exp\left(-\frac{|x - y|}{l_c} \right). \qquad (5.1.41)$$

The quantity l_c denotes the spatial correlation length [192, 198] of the random initial velocity (5.1.40). In Figure 5.6, we show the time snapshots of the one-PDF of the velocity field obtained from the second-order approximation to the MZ equation (5.1.13). Specifically, we consider an initial condition in the form (5.1.40) with $l_c = 0.01$, and the forcing term (5.1.39) with amplitude $\sigma = 0.05$.

As pointed out in [36], the one-point PDF of the solution field does not tell us anything about the structure of shocks in space and time, thus about shock clustering. Therefore, if we are interested in studying this phenomenon, we should resort to other functionals of the velocity field, in particular on asymptotic properties. In Burgers turbulence, these can be grouped into two main classes: 1) *universal properties* that are independent of initial or boundary conditions, and 2) properties that depend heavily on such conditions. For instance, the k^{-2} slope in the inertial range of the energy spectrum is a universal property while the time-evolution of the kinetic energy per unit length is not [86, 101]. Many universal properties can be defined in terms of the two-point correlation function, e.g.,

$$\mathcal{J}(t) \overset{\text{def}}{=} \frac{1}{2\pi} \int_0^{2\pi} \int_{\mathbb{R}} \langle u(x,t)u(x+r,t) \rangle \, dr dx, \tag{5.1.42}$$

and the power spectral density

$$\widetilde{E}(k,t) \overset{\text{def}}{=} \frac{1}{2\pi} \int_0^{2\pi} E(x,k,t) dx, \tag{5.1.43}$$

where

$$E(x,k,t) = \frac{1}{2\pi} \int_{\mathbb{R}} \cos(kr) \left[\langle u(x,t)u(x+r,t) \rangle - \langle u(x,t) \rangle \langle u(x+r,t) \rangle \right] dr. \tag{5.1.44}$$

$\mathcal{J}(t)$ is known to be invariant in time [24]. Another interesting quantity which is ultimately related to *stochastic shock clustering* [122,177] is the turbulent energy per unit length

$$\mathcal{E}(t) \overset{\text{def}}{=} \frac{1}{2\pi} \int_0^{2\pi} \widehat{E}(x,t) dx, \qquad \text{where} \qquad \widehat{E}(x,t) \overset{\text{def}}{=} \int_0^{\infty} E(x,k,t) dk. \tag{5.1.45}$$

The two-point correlation function appearing in Eqs. (5.1.42), (5.1.44) and (5.1.45)
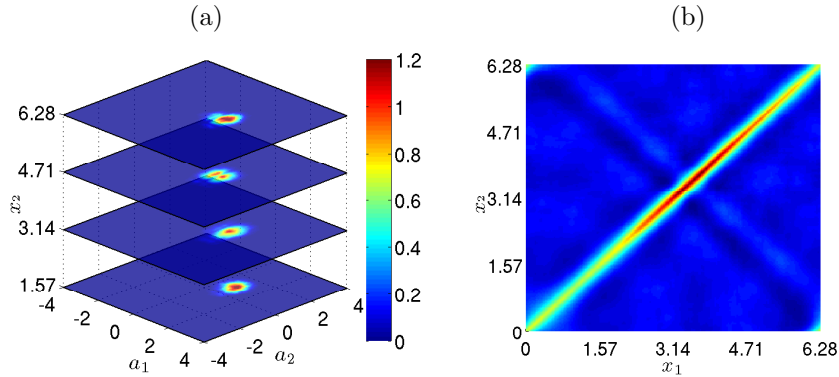
Figure 5.7: Slices of two-point PDF of the velocity field at $t = 1$ (a) and velocity correlation function (b). Specifically, in (a) we plot the two-point PDF field at $x_1 = \pi/4$ and four other points $x_2 = \{\pi/2, \pi, 3\pi/2, 2\pi\}$.

can be determined by integrating the solution to the two-point MZ-PDF equation (5.1.25) as (see Figure 5.7)

$$\langle u(x,t)u(x+r,t)\rangle = \int_{-\infty}^{\infty} \int_{-\infty}^{\infty} a_1 a_2 p(x, x+r, t; a_1, a_2) da_1 da_2. \tag{5.1.46}$$

In Figure 5.8, we plot the power spectral density (5.1.43) and the normalized turbulent energy per unit length (5.1.45) for random initial conditions (5.1.40) with different correlation lengths l_c and random forcing terms (5.1.39) of different amplitude σ. It is seen that for $\sigma = 0$ the slope of the power spectral density in the inertial range is k^{-2}, independently of l_c. This is in agreement with classical results on Burgers turbulence. We also observe a perturbation in the energy spectrum due to the energy injected in the system through the random forcing term. This slightly increases the turbulent energy per unit length, relatively to the case where there is no forcing. Note that rough random initial conditions, i.e., those with correlation length $\ell = 0.01$, are associated with an initial rapid decay of the normalized turbulent energy due to shock clustering (see also Figure 5.9). Later on, the train of triangular shocks settles down to a similarity state where the turbulent energy decays approximately as $t^{-2/3}$, in agreement with classical results of Tokunaga [185] and Kida [101]. In Figure 5.9, we plot the space-time portraits of the normalized
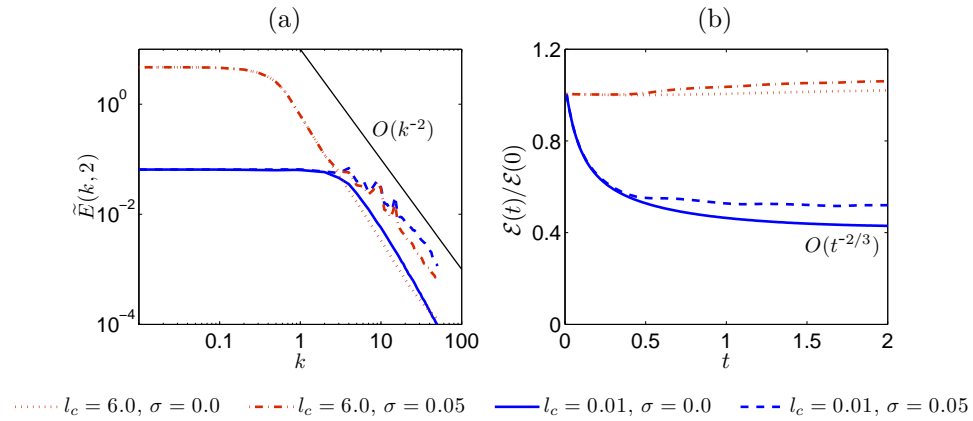
Figure 5.8: Stochastic Burgers turbulence simulations. Shown is the k^{-2} decay of the power spectral density in the inertial range (a). This property does not depend on the correlation length l_c of the initial condition, i.e., it is a universal property. On the contrary, the dynamics of the normalized turbulent energy per unit length (b) heavily depends on the specific choice of initial conditions. In particular, for rough initial conditions (i.e., those with small correlation length l_c) we observe a rapid decay of the turbulent energy due to shock clustering. After that, the train of triangular shocks settles down to a similarity state where the turbulent energy decays approximately as $t^{-2/3}$, in agreement with classical results of dimensional analysis. Random forcing terms of small amplitude σ inject additional energy into the system. As a consequence we observe a perturbation in the energy spectrum (a), and an increase in the turbulent energy per unit length (b).
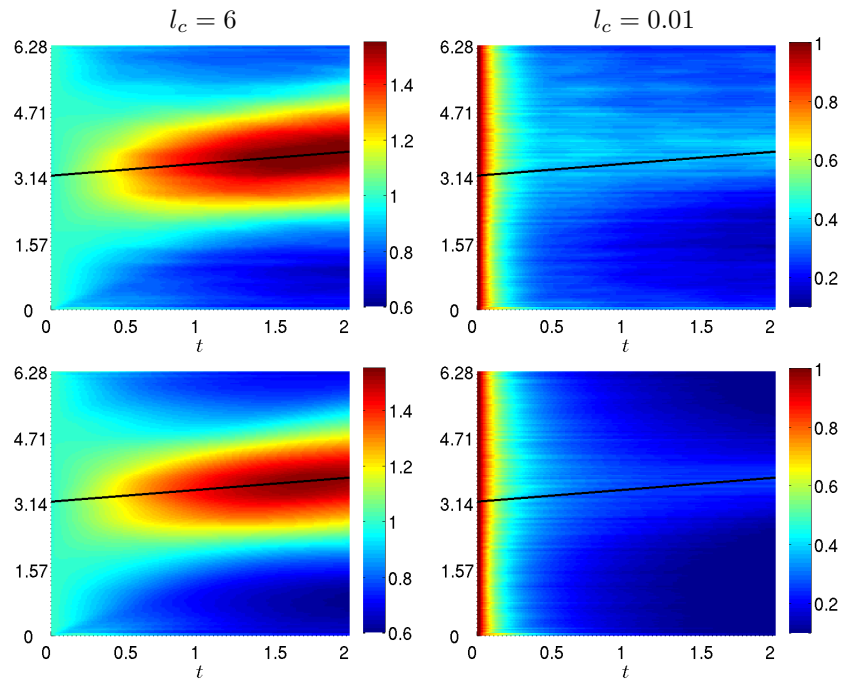
Figure 5.9: Space-time portraits of the normalized turbulent energy in Burgers turbulence. Specifically, we plot $\mathcal{E}(x,t)/\mathcal{E}(x,0)$ (5.1.45) for random initial conditions (5.1.40) with different correlation lengths l_c and random forcing terms (5.1.39) of different amplitudes σ. It is seen that the normalized turbulent energy is an indicator function of stochastic shock clustering for rough random initial conditions. In particular, the initial rapid decay of the turbulent energy observed for $l_c = 0.01$ corresponds to the transient dynamics in which the velocity field is regularized by shock clustering (see sample solutions in Figure 5.1) before settling down to the similarity state. The black line in each plot indicates the shock front associated with the $\sin(x)$ term in (5.1.40). Such contribution is responsible for the increase of the normalized turbulent energy, in particular for initial conditions with large correlation lengths.

turbulent energy $\widehat{E}(x,t)/\widehat{E}(x,0)$, where $\widehat{E}(x,t)$ is defined in Eq. (5.1.45). It is seen that the turbulent energy undergoes a rapid decay for initial conditions with short correlation length, i.e., for $l_c = 0.01$. Such rapid decay corresponds to the transient dynamics in which the velocity field is regularized by shock clustering (see sample solutions in Figure 5.1) before settling down to the similarity state. The black line in each plot indicates the shock front associated with the $\sin(x)$ term in (5.1.40). Such contribution is responsible for the increase of the normalized turbulent energy, in particular for initial conditions with large correlation lengths.

5.2   Conditional moment closure

In this section, we propose here a conditional moment closure to further reduce the dimensionality of a kinetic equation. Let us introduce the method with reference to a nonlinear dynamical system in the form

$$\frac{d\mathbf{x}(t)}{dt} = \mathbf{Q}(\mathbf{x}, \boldsymbol{\xi}, t), \qquad \mathbf{x}(0) = \boldsymbol{x}_0(\omega), \tag{5.2.1}$$

where $\mathbf{x}(t) \in \mathbb{R}^n$ is a multi-dimensional stochastic process, $\boldsymbol{\xi} \in \mathbb{R}^m$ is a vector of random variables, $\mathbf{Q} : \mathbb{R}^{n+m+1} \to \mathbb{R}^n$ is a Lipschitz continuous (deterministic) function, and $\mathbf{x}_0 \in \mathbb{R}^n$ is a random initial state. Upon definition of $\mathbf{y}(t) = (\mathbf{x}(t), \boldsymbol{\xi})$, we can rewrite (5.2.1) as

$$\frac{d\mathbf{y}(t)}{dt} = \mathbf{G}(\mathbf{y}, t), \qquad \mathbf{y}(0) = (\boldsymbol{x}_0(\omega), \boldsymbol{\xi}), \qquad \mathcal{G}(\mathbf{y}, t) = \begin{bmatrix} \mathbf{Q}(\mathbf{y}, t) \\ \mathbf{0} \end{bmatrix}. \tag{5.2.2}$$

Note that $\mathbf{y}(t) \in \mathbb{R}^N$ and $\mathcal{G} : \mathbb{R}^{N+1} \to \mathbb{R}^N$, where $N = n + m$. The joint PDF of $\mathbf{y}(t)$ evolves according to the Liouville equation

$$\frac{\partial p(\mathbf{z}, t)}{\partial t} + \nabla \cdot [\mathcal{G}(\mathbf{z}, t) p(\mathbf{z}, t)] = 0, \qquad \mathbf{z} \in \mathbb{R}^N, \tag{5.2.3}$$

whose solution can be computed numerically only for small N. This leads us to look for PDF equations involving only a reduced number of phase variables. For instance, the PDF of each component $y_i(t)$ satisfies[7]

$$\frac{\partial p_i(z_i, t)}{\partial t} = -\frac{\partial}{\partial z_i} \langle \dot{y}_i(t) \delta(z_i - y_i(t)) \rangle$$

$$= -\frac{\partial}{\partial z_i} \int [G_i(\mathbf{y}, t) p(\mathbf{y}, t)]_{y_i = z_i} \prod_{\substack{k=1 \\ k \neq i}}^{N} dy_k, \tag{5.2.4}$$

where $p(\mathbf{y}, t)$ is the full joint PDF of $\mathbf{y}(t)$. Similarly, the joint PDF of $y_i(t)$ and $y_j(t)$ $(i \neq j)$ satisfies

$$\frac{\partial p_{ij}(z_i, z_j, t)}{\partial t}$$
$$= -\frac{\partial}{\partial z_i} \langle \dot{y}_i(t) \delta(z_i - y_i(t)) \delta(z_j - y_j(t)) \rangle - \frac{\partial}{\partial z_j} \langle \dot{y}_j(t) \delta(z_i - y_i(t)) \delta(z_j - y_j(t)) \rangle$$
$$= -\frac{\partial}{\partial z_i} \int [G_i(\mathbf{y}, t) p(\mathbf{y}, t)]_{\substack{y_i = z_i \\ y_j = z_j}} \prod_{\substack{k=1 \\ k \neq i,j}}^{N} dy_k - \frac{\partial}{\partial z_j} \int [G_j(\mathbf{y}, t) p(\mathbf{y}, t)]_{\substack{y_i = z_i \\ y_j = z_j}} \prod_{\substack{k=1 \\ k \neq i,j}}^{N} dy_k. \tag{5.2.5}$$

Higher-order PDF equations can be derived similarly. At this point, we notice that the integrals in (5.2.4) and (5.2.5) can be written in terms of conditional averages

---

[7]Note that $p_i(z_i, t) = p(\xi_i)$ for all $n + 1 \leq i \leq n + m$, and for all $t \geq 0$.

[147, 209] of G_i, by using the well-known identities

$$\langle G_i(\mathbf{y},t)|y_i = z_i\rangle \, p_i(z_i,t) = \int [G_i(\mathbf{y},t)p(\mathbf{y},t)]_{y_i=z_i} \prod_{\substack{k=1 \\ k\neq i}}^{N} dy_k, \qquad (5.2.6)$$

$$\langle G_i(\mathbf{y},t)|y_i = z_i, y_j = z_j\rangle \, p_{ij}(z_i,z_j,t) = \int [G_i(\mathbf{y},t)p(\mathbf{y},t)]_{\substack{y_i=z_i \\ y_j=z_j}} \prod_{\substack{k=1 \\ k\neq i,j}}^{N} dy_k. \qquad (5.2.7)$$

Here $\langle G_i(\mathbf{y},t)|y_i = z_i\rangle$ is the conditional average of G_i given $y_i(t) = z_i$. Unfortunately, the computation of (5.2.6)-(5.2.7) requires the full joint PDF of $\mathbf{y}(t)$, which is available only if we solve the Liouville equation (5.2.3). As mentioned before, this is not feasible in practice even for a low number of variables. Therefore, we need to introduce approximations. The most common one is to assume that the joint PDF $p(\mathbf{z},t)$ can be written in terms of lower-order PDFs, e.g., as $p(\mathbf{z},t) = p(z_1,t)\cdots p(z_N,t)$. By using integration by parts, this assumption reduces the Liouville equation to a hierarchy of one-dimensional PDF equations (see, e.g., [195]).

Hereafter we follow a different approach based on conditional averages. To this end, let us consider a specific form of G_i that allows us to simplify all equations, i.e.,

$$G_i(\mathbf{y},t) = g_{ii}(y_i,t) + \sum_{\substack{k=1 \\ k\neq i}}^{N} g_{ik}(y_i,y_k,t).$$

The conditional average (5.2.6) can be now computed exactly by using the two-points PDFs $p(z_i,z_j,t)$ as

$$\langle G_i(\mathbf{y},t)|\, y_i = z_i\rangle \, p_i(z_i,t) = g_{ii}(z_i,t)p_i(z_i,t) + \sum_{\substack{k=1 \\ k\neq i}}^{N} \int g_{ik}(z_i,z_k,t)p_{ik}(z_i,z_k,t)dz_k.$$

On the other hand, the integral in (5.2.7) can be approximated as

$$
\int \left[G_i(\mathbf{y}, t) p(\mathbf{y}, t) \right]_{\substack{y_i = z_i \\ y_j = z_j}} \prod_{\substack{k=1 \\ k \neq i, j}}^{N} dy_k \simeq \left(g_{ii}(z_i, t) + g_{ij}(z_j, z_i, t) \right) p_{ij}(z_i, z_j, t) +
$$

$$
\left(\sum_{\substack{k=1 \\ k \neq i, j}}^{N} \int g_{ik}(z_i, z_k, t) p_{ik}(z_i, z_k) dz_k \right) p_j(z_j, t),
$$

$$(5.2.8)$$

where we discarded all contributions from the three-points PDFs and the two-points PDFs except the ones interacting with the i-th variable. A variance-based sensitivity analysis in terms of Sobol indices [167, 175, 192] can be performed to identify the system variables with strong correlations. This allows us to determine whether it is necessary to add the other two-points correlations or the three-points PDF equations for a certain triple $\{x_k(t), x_i(t), x_j(t)\}$.

5.2.1   CMC-PDF equation for dynamical systems

Kraichnan-Orszag Problem

Let us apply the conditional moment closure we described in the previous section to the Kraichnan-Orszag problem studied in [203]

$$
\begin{aligned}
\frac{dx_1}{dt} &= x_1 x_3, \\
\frac{dx_2}{dt} &= -x_2 x_3, \\
\frac{dx_3}{dt} &= -x_1^2 + x_2^2.
\end{aligned}
$$

In this case we have $n = 3$ phase variables and $m = 0$ parameters, i.e., a total number of $N = 3$ variables. The three-dimensional Liouville equation for the joint PDF of

$\{x_1(t), x_2(t), x_3(t)\}$, is

$$\frac{\partial p}{\partial t} + z_1 z_2 \frac{\partial p}{\partial z_1} + z_2 z_3 \frac{\partial p}{\partial z_2} + (z_2^2 - z_1^2)\frac{\partial p}{\partial z_3} = -(z_2 + z_3)p, \qquad (5.2.9)$$

where $p = p(z_1, z_2, z_3, t)$. On the other hand, by using the second-order conditional moment closure described in the previous section, we obtain the following hierarchy of PDF equations

$$\frac{\partial p_1(z_1, t)}{\partial t} = -\frac{\partial}{\partial z_1}\left[z_1 \langle x_3 \rangle_{3|1}\right], \qquad (5.2.10)$$

$$\frac{\partial p_2(z_2, t)}{\partial t} = -\frac{\partial}{\partial z_2}\left[-z_2 \langle x_3 \rangle_{3|2}\right], \qquad (5.2.11)$$

$$\frac{\partial p_3(z_3, t)}{\partial t} = -\frac{\partial}{\partial a_3}\left[\left(-\langle x_1^2 \rangle_{1|3} + \langle x_2^2 \rangle_{2|3}\right) p_3(z_3, t)\right], \qquad (5.2.12)$$

$$\frac{\partial p_{12}(z_1, z_2, t)}{\partial t} = -\frac{\partial}{\partial z_1}\left[z_1 \langle x_3 \rangle_{3|1} p_2(z_2, t)\right] + \frac{\partial}{\partial z_2}\left[z_2 \langle x_3 \rangle_{3|2} p_1(z_1, t)\right], \qquad (5.2.13)$$

$$\frac{\partial p_{13}(z_1, z_3, t)}{\partial t} = -\frac{\partial}{\partial z_1}\left[z_1 z_3 p_{13}(z_1, z_3, t)\right] + \frac{\partial}{\partial z_3}\left[z_1^2 p_{13}(z_1, z_3, t) - \langle x_2^2 \rangle_{2|3} p_1(z_1, t)\right],$$

$$(5.2.14)$$

$$\frac{\partial p_{23}(z_2, z_3, t)}{\partial t} = \frac{\partial}{\partial z_2}\left[z_2 z_3 p_{23}(z_2, z_3, t)\right] + \frac{\partial}{\partial z_3}\left[\langle x_1^2 \rangle_{1|3} p_2(z_2, t) - z_2^2 p_{23}(z_2, z_3, t)\right],$$

$$(5.2.15)$$

where

$$\langle f(\mathbf{x}) \rangle_{i|j} \doteq \int f(\mathbf{z}) p_{ij}(z_i, z_j, t) dz_i. \qquad (5.2.16)$$

We also emphasize that the PDF equation of a phase space function $h(x_1, x_2, x_3)$, can be easily derived based on the conditional moment closure. For example, the PDF equation of $h = x_1(t) + x_3(t)$ is

$$\frac{\partial p_h(z, t)}{\partial t} = -\frac{\partial}{\partial z}\left[\left(-z^2 + 3z\langle x_3 \rangle_{3|h} - 2\langle x_3^2 \rangle_{3|h} + \langle x_2^2 \rangle_{2|h}\right) p_h(z, t)\right].$$
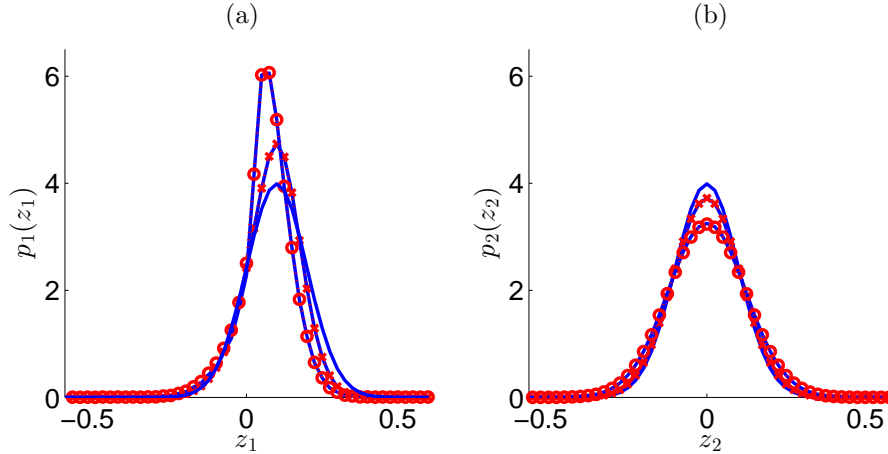
Figure 5.10: Kraichnan-Orszag problem: PDF of $x_1(t)$ (a) and $x_2(t)$ (b) at $t = 0$, $t = 4$ and $t = 8$. Blue lines: results from the full Liouville equation. Crosses and circles: results of the conditional moment closure (5.2.10)-(5.2.15) at $t = 4$ and $t = 8$, respectively.

Let us assume that the initial condition $\{x_1(0), x_2(0), x_3(0)\}$ is jointly Gaussian

$$p_0(z_1, z_2, z_3) = \frac{10^3}{(2\pi)^{3/2}} \exp\left[-50\left(z_1 - \frac{1}{10}\right)^2 - 50\left(z_2^2 + z_3^2\right) \right]. \tag{5.2.17}$$

Here, we assess the accuracy of the second-order conditional moment closure (5.2.10)-(5.2.15). We recall that such closure is obtained by truncating the hierarchy of conditional PDF equations to the two-points level. Each PDF equation is discretized by using a Fourier spectral collocation method with with $q_z = 50$ degrees of freedom in each variable. Time stepping is based on explicit forth-order Runge-Kutta scheme with $\triangle t = 10^{-3}$.

In Figure 5.10, we compare the PDF of $x_1(t)$ and $x_2(t)$ as computed by the full system and the two-points conditional moment closure. We observe that the two solutions are basically superimposed, suggesting that the effects of the three-points correlations are negligible. We also remark that if we are interested only in the PDF of one variable, then it is not necessary to solve the whole hierarchy of PDF equations in the conditional moment closure. For example, to obtain the PDF of $x_1(t)$, we can
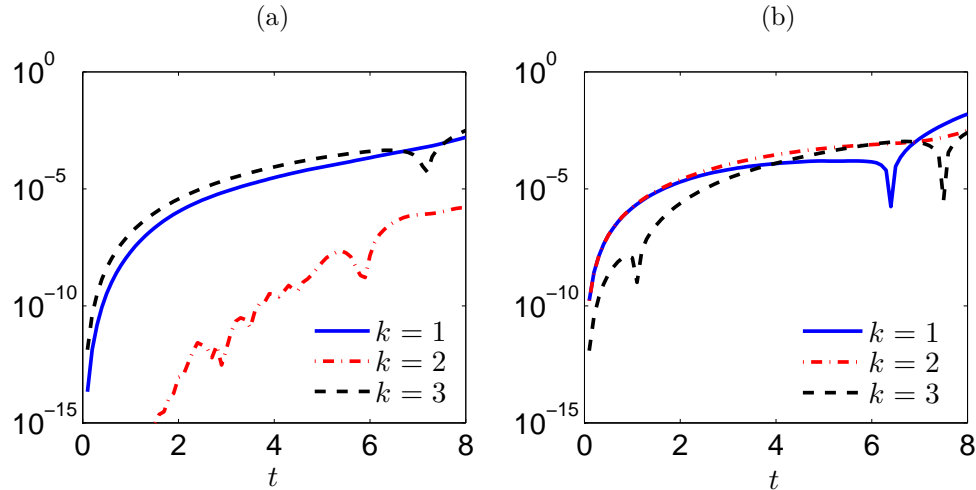
Figure 5.11: Kraichnan-Orszag problem: Absolute error in the mean (a) and in the standard deviation (b) of $x_k(t)$ ($k = 1, 2, 3$) computed by the second-order conditional moment closure (5.2.10)-(5.2.15).

just solve Eqs. (5.2.10), (5.2.15), and (5.2.15). In Figure 5.11, we plot the absolute error in the mean and the standard deviation of $\{x_1(t), x_2(t), x_3(t)\}$ as computed by the conditional moment closure. These errors arise because we are not including the three-points PDFs in the hierarchy of equations.

Lorenz-96 system

The Lorenz-96 system is a continuous in time and discrete in space model often used in atmospheric sciences to study fundamental issues related to forecasting and data assimilation [97, 116]. The basic equations are

$$\frac{dx_i}{dt} = (x_{i+1} - x_{i-2}) x_{i-1} - x_i + F, \qquad i = 1, ..., n. \tag{5.2.18}$$

Here we consider $n = 40$, $F = 1$, and assume that the initial state $\mathbf{x}(0) = [x_1(0), ..., x_{40}(0)]$ is jointly Gaussian with PDF

$$p_0(z_1, ..., z_{40}) = \left(\frac{25}{2\pi}\right)^{20} \prod_{i=1}^{40} \exp\left[-\frac{25}{2}\left(z_i - \frac{i}{40}\right)^2\right]. \tag{5.2.19}$$
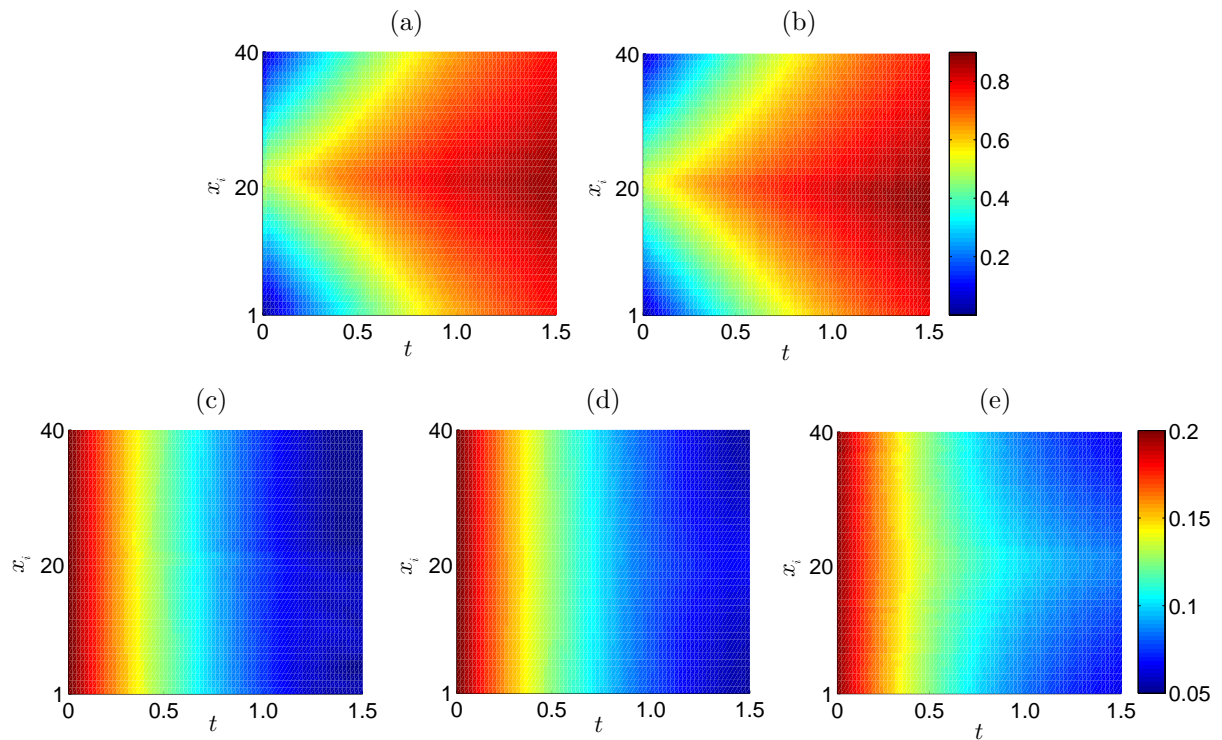
Figure 5.12: Lorenz-96 system: Mean (first row) and standard deviation (second row) of the solution computed by using the first-order conditional moment closure (a,c) and Monte-Carlo simulation (b,e). In (d) we compute the standard deviation by using the second-order conditional moment closure.
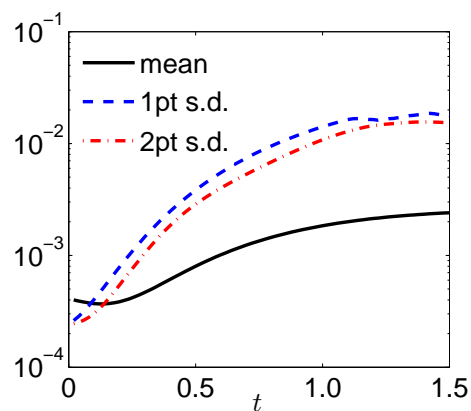
Figure 5.13: Lorenz-96 system: Absolute errors in the mean and in the standard deviation as computed by the first- and the second-order conditional moment closure (Eqs. (5.2.21) and (5.2.22), respectively). Errors are relative to MC results.

Thus, in this system we have $n = 40$ phase variables and $m = 0$ parameters, i.e., $N = n$. The kinetic equation governing the joint PDF of the phase variables $\mathbf{x}(t) = [x_1(t), ..., x_{40}(t)]$ is

$$\frac{\partial p(\mathbf{z}, t)}{\partial t} = -\sum_{i=1}^{40} \frac{\partial}{\partial z_i} \left[((z_{i+1} - z_{i-2})z_{i-1} - z_i + F) \, p(\mathbf{z}, t) \right], \quad \mathbf{z} \in \mathbb{R}^{40} \qquad (5.2.20)$$

and it cannot be obviously solved in a tensor product representation because of high-dimensionality and possible lack of regularity (for $F > 10$) related to the fractal structure of the attractor [97]. Thus, we are led to look for reduced-order PDF equations. Specifically, we consider here the first- and second-order conditional moment closures we discussed in section 5.2. The first one yields the approximated system

$$\frac{\partial p_i(z_i, t)}{\partial t} = -\frac{\partial}{\partial z_i} \left[(\langle x_{i+1} \rangle - \langle x_{i-2} \rangle) \langle x_{i-1} \rangle_{i-1|i} - (z_i - F)p_i(z_i, t) \right], \qquad (5.2.21)$$

where $\langle \ \rangle_{i|j}$ is defined in (5.2.16). In order to close such system within the level of one-point PDFs, $\langle x_{i-1} \rangle_{i-1|x_i}$ could be replaced, e.g., by $\langle x_{i-1} \rangle p(z_i, t)$. Similarly, the second-order conditional moment closure yields the hierarchy

$$\frac{\partial p_{i\,i+1}(z_i, z_{i+1}, t)}{\partial t} = -\frac{\partial}{\partial z_i} \left[z_{i+1} \left\langle x_{i-1} \right\rangle_{i-1|i} p_{i+1}(z_{i+1}, t) - \left\langle x_{i-2} \right\rangle \left\langle x_{i-1} \right\rangle_{i-1|i} p_{i+1}(z_{i+1}, t) \right.$$

$$- \left. (z_i - F) \, p_{i\,i+1}(z_i, z_{i+1}, t) \right] - \frac{\partial}{\partial z_{i+1}} \left[\left\langle x_{i+2} \right\rangle_{i+2|i+1} z_i p_i(z_i, t) - \left\langle x_{i-1} \right\rangle z_i p_{i\,i+1}(z_i, z_{i+1}, t) \right.$$

$$- \left. (z_{i+1} - F) \, p_{i\,i+1}(z_i, z_{i+1}, t) \right], \qquad (5.2.22)$$

where the quantity $\left\langle x_{i-1} \right\rangle z_i p_{i\,i+1}(z_i, z_{i+1}, t)$ can be substituted by $\left\langle x_{i-1} \right\rangle_{i-1|i} \left\langle x_i \right\rangle_{i|i+1}$. Each equation in (5.2.21)-(5.2.22) is discretized by using a Fourier spectral collocation method with $q_z = 50$ degrees of freedom in each variable, and fourth-order Runge-Kutta time integration with $\triangle t = 10^{-3}$.

In Figure 5.12, we plot the mean and the standard deviation of the solution to (5.2.18) computed by the first- and the second-order conditional moment closures (Eqs. (5.2.21) and (5.2.22), respectively), as well as with the Monte Carlo (MC) simulation - 50000 solution samples. It is seen that the mean of the conditional moment closure coincides with the one obtained from MC. However, the standard deviation is slightly different. This can be also seen in Figure 5.13, where we plot the absolute error (relative to MC) of the mean and standard deviation computed by the conditional moment closure. Note that adding the two-points PDFs to the hierarchy in this case improves the error in the standard deviation only by a small amount.

5.2.2 CMC-PDF equation for second-order PDEs

An interesting question arises whether it is possible to determine a closed PDF evolution equation of the solution to second order PDEs at a specific space-time location. Unfortunately, the answer is negative due to its nonlocal solutions in space and time. This nonlocal feature yields the impossibility to determine a point-wise equation for the probability density. Still, there has been extensive studies to tackle this problem by use of functional integral methods, in particular those ones involving the Hopf characteristic functional [91, 120, 143, 144]. These functional methods aim to cope with the global probabilistic structure of the solution and they have been employed to solve many fundamental problems in physics such as turbulence [124, 181]. However, functional differential equations involving the Hopf characteristic functional are unfortunately not amenable to numerical simulation. In addition, the amount of statistical information carried on by the Hopf characteristic functional is often far beyond the needs of practical uncertainty quantification, which usually reduces only to the computation of a few statistical moments of the solution at specific space-time locations.

Thus, the purpose of this section is to develop a computable algorithm to investigate the probability density of the stochastic solutions to higher-order PDEs. The algorithm relies on the semi-discrete form of PDEs that can be written in a form of multi-dimensional dynamical system that yields a Liouville type PDF equation. Afterwards, the conditional moment closure is employed to the corresponding multi-dimensional PDF system.

Advection-Diffusion equation

Let us consider an advection-diffusion equation as following.

$$\frac{\partial u}{\partial t} = \frac{\partial}{\partial x}\left(\nu(x,t;\omega)u\right) + \frac{\partial}{\partial x}\left(\mu(x,t;\omega)\frac{\partial u}{\partial x}\right), \qquad (5.2.23)$$

where $x \in [0, 2\pi]$, $t \geq 0$, $\nu(x,t;\omega)$ is the random advection coefficient, and $\mu(x,t;\omega) > 0$ is the random diffusivity. This equation is accompanied by a periodic boundary condition $u(0,t;\omega) = u(2\pi,t;\omega)$ and $u_x(0,t;\omega) = u_x(2\pi,t;\omega)$. We then discretize the solution in the physical space by using a set of orthogonal basis functions in $L^2([0,2\pi])$. Here, we consider the Fourier basis functions,

$$u(x,t;\omega) = \sum_k \hat{u}_k(t;\omega)e^{-ikx}. \qquad (5.2.24)$$

The semi-discretized system becomes,

$$\frac{\partial \hat{u}_k(t;\omega)}{\partial t} = -\sum_{n+m=k} i(n+m)\,\hat{\nu}_n(t;\omega)\,\hat{u}_m(t;\omega) - \sum_{n+m=k} m(n+m)\,\hat{\mu}_n(t;\omega)\,\hat{u}_m(t;\omega),$$

for each integer k. We assume that we have available a representation of the random coefficients in terms of random variables as $\nu(x,t;\omega) = \nu(x,t;\xi(\omega))$ and $\mu(x,t;\omega) = \mu(x,t;\gamma(\omega))$. Taking $p_{\hat{u}}$ as shorthand of $p_{\hat{u}}(a, b_\nu, b_\mu, t)$, this yields the joint REPDF

equation of the Fourier coefficients $\hat{u} = \{\hat{u}_k\}$,

$$\frac{\partial p_{\hat{u}}}{\partial t} = -\sum_k \frac{\partial}{\partial a_k} \left[\left(-\sum_{n+m=k} (n+m) \left(i\,\hat{\nu}_n(t;b_\nu) + m\,\hat{\mu}_n(t;b_\mu) \right) a_m \right) p_{\hat{u}} \right], \quad (5.2.25)$$

The dimensionality of the REPDF equation (5.2.25) depends on the truncation of the Fourier expansion (5.2.24). In other words, the dimensionality can be as high as the number of basis functions, which will be necessary when the solution in the physical space has low regularity. Thus, we employ the conditional moment closure approach developed in Section 5.2 to obtain a reduced-order PDF equation, approximating the system within lower order interactions.

The exact evolution equation of the one-point PDF of $\hat{u}_k$ can be written as follows

$$\frac{\partial p_{\hat{u}_k}}{\partial t} = -\frac{\partial}{\partial a_k} \int \left(-\sum_{n+m=k} (n+m) \left(i\,\hat{\nu}_n(t;b_\nu) + m\,\hat{\mu}_n(t;b_\mu) \right) a_m \right) p_{\hat{u}_{i^c}} \left(a_{i^c} | \hat{u}_k = a_k \right) da_{i^c},$$
$$(5.2.26)$$

where $i^c = [..., i-2, i-1, i+1, i+2, ...]$. While the exact one-point PDF equation (5.2.26) involves the marginalization with respect to the full joint PDF, we approximate the conditional expectation with lower order PDFs. The conditional moment closures by using the one- and two-point PDFs can be derived as follows:

$$\frac{\partial p_k}{\partial t} = -\frac{\partial}{\partial a_k} \left[-\sum_{n+m=k} \left((n+m) \left(i\,\hat{\nu}_n(t;b_\nu) + m\,\hat{\mu}_n(t;b_\mu) \right) \langle a_m \rangle \right) p_k \right], \quad (5.2.27)$$

$$\frac{\partial p_{kl}}{\partial t} = -\frac{\partial}{\partial a_k} \left[-\sum_{n+m=k} \left(\int k \left(i\,\hat{\nu}_n(t;b_\nu) + m\,\hat{\mu}_n(t;b_\mu) a_m p_{km} \right) da_m \right) p_l \right]$$
$$-\frac{\partial}{\partial a_l} \left[-\sum_{n+m=l} \left(\int l \left(i\,\hat{\nu}_n(t;b_\nu) + m\,\hat{\mu}_n(t;b_\mu) a_m p_{ml} \right) da_l \right) p_m \right], \quad (5.2.28)$$

In practice, we consider the solution in the following finite-order expansion by using

the trigonometric basis functions,

$$u(x, t; \omega) = \hat{\mathfrak{u}}_0(t; \omega) + \sum_{k=1}^{N} \left(\hat{\mathfrak{u}}_k(t; \omega) \sin(kx) + \hat{\mathfrak{u}}_{-k}(t; \omega) \cos(kx) \right). \qquad (5.2.29)$$

5.2.3 Stochastic simulation of second order PDEs

We first consider a time-dependent random coefficient for the diffusion term. In particular, $\mu(t; \omega)$ in Eq. (5.2.23) a log-normal random coefficient defined as $V(t; \omega) = \log(\mu(t; \omega))$, where $V(t; \omega)$ is exponentially correlated Gaussian process

$$\mathrm{Cov}[V(t; \omega)V(s; \omega)] = \frac{\sigma^2}{l_c} \exp\left[-\frac{|t - s|}{l_c} \right],$$

with $\langle V(t; \omega) \rangle = 0$ and $\sigma = 0.1$. The coefficient is represented in a series expansion by using KL expansion and we truncate the series to achieve 95% of the eigen-spectrum. When the random coefficient is independent to the physical variable, the semi-discretized system of each Fourier modes are independent. Therefore, with a sufficient regularity assumption for the PDF, we can truncate the conditional moment closure at the level of one-point PDFs. The first-order conditional moment closure becomes

$$\frac{\partial p_k}{\partial t} = -\frac{\partial}{\partial a_k} \left[-k^2 \mu(t, b_\mu) \, a_k \, p_k \right]. \qquad (5.2.30)$$

We remark that, in case of a constant coefficient μ the PDF solution of the one-point closure Eq. (5.2.30) coincides with the full exact solution. To clarify, assuming the random initial condition as $u(x, t_0; \omega) = \sum_k \sin(kx)\eta_k(\omega)$, the solution to Eq. (5.2.30) is $p_{\hat{\mathfrak{u}}_k}(t) = p_{\eta_k}(a_k e^{\mu k^2 t}) e^{\mu k^2 t}$. This solution is equivalent to the exact solution of the stochastic heat equation (5.2.23) written as an ensemble of the trajectory of the initial condition, i.e., $u(x, t; \omega) = \sum_k \eta_k(\omega) \sin(kx) e^{-\mu k^2 t}$.

Since each p_k is independent, we simply consider the initial condition $u(x, t_0; \omega) = \sin(x)\eta_\lambda(\omega)$ with Gaussian random variable $\eta_1(\omega) = N(1, 0.1)$. The solution with
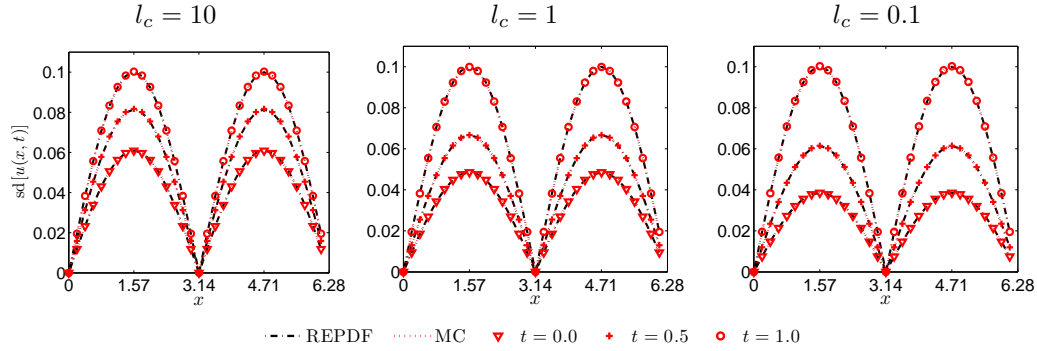
Figure 5.14: Standard deviation of the solution to the heat equation with time-correlated random coefficient with correlation length l_c upto time $t = 1$. The shown results are computed by the PDF, PCM, and MC approach, where we cannot visually distinguish the difference in the results.
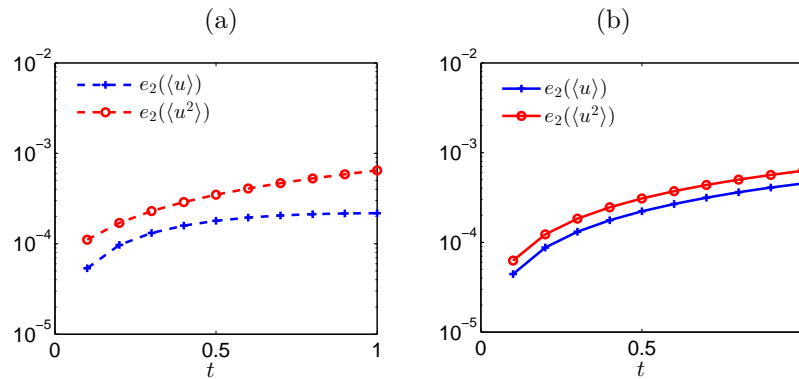
Figure 5.15: Relative L_2 error of the mean $e_2(\langle u \rangle)$ and standard deviation $e_2(\langle u^2 \rangle - \langle u \rangle^2)$ of the solution to the diffusion with $N = 1$ (a) and advection with $N = 3$ (b) equation with correlation length $l_c = 10$ up to time $t = 1$. We compute the reference solution by using 50,000 MC simulations.

$N = 1$ is computed for diffusive term with different correlation time $l_c = 10, 1, 0.1$, by using the forth-order Runge-Kutta method with step size $\triangle t = 10^{-3}$. Figure 5.14 shows the evolution of the standard deviation of the solution at time $t = 0, 0.5, 1$, computed by using the one-point conditional moment closure and the MC approach. The two lines cannot be visually distinguished. The relative L_2 error of the mean and standard deviation between the one-point closure and PCM solution is plotted in Figure 5.15(a). We observe reasonable accuracy considering the time step and the truncation of the computational domain.

In case of space dependent coefficients, interaction between the Fourier coeffi-
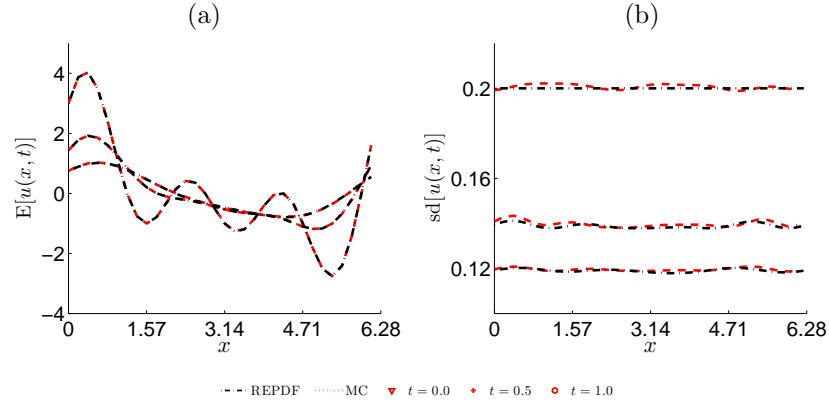
Figure 5.16: The evolution of the mean (a) and standard deviation (b) of the solution to the heat equation with space dependent random coefficient upto time $t = 1$. The shown results are computed by using the PDF approach (black-$\cdot$) and MC (red --).

cients occurs in the semi-discretized system. Hence, it becomes inevitable to include the higher-order joint PDFs. In our simulation, we compute the following two-point closure for the joint REPDF of the k-th and l-th coefficient

$$\frac{\partial p_{kl}}{\partial t} = -\frac{\partial}{\partial a_k}\mathbb{Q}(p_{kl}, k) - \frac{\partial}{\partial a_l}\mathbb{Q}(p_{kl}, l) \tag{5.2.31}$$

where

$$\mathbb{Q}(p_{ij}, i) \stackrel{\text{def}}{=} \begin{cases} -i^2\hat{\mu}_0 a_i p_{ij} + \sum_{n+m=i}\left(\frac{mi}{2}(-\hat{\mu}_n\langle a_{-m}|a_i\rangle - \hat{\mu}_{-n}\langle a_m|a_i\rangle)\right)p_j \\ \qquad + \sum_{n-m=|i|}\left(\frac{m(n-m)}{2}(\hat{\mu}_n\langle a_{-m}|a_i\rangle - \hat{\mu}_{-n}\langle a_m|a_i\rangle)\right)p_j, \quad i \geq 0. \\ -i^2\hat{\mu}_0 a_i p_{ij} + \sum_{n+m=|i|}\left(-\frac{mi}{2}(\hat{\mu}_n\langle a_m|a_i\rangle - \hat{\mu}_{-n}\langle a_{-m}|a_i\rangle)\right)p_j \\ \qquad + \sum_{n-m=|i|}\left(\frac{m(n-m)}{2}(\hat{\mu}_n\langle a_m|a_i\rangle + \hat{\mu}_{-n}\langle a_{-m}|a_i\rangle)\right)p_j, \quad i < 0. \end{cases} \tag{5.2.32}$$

Here, the excitation variables are omitted, and $\langle g(a_j)|a_i\rangle \stackrel{\text{def}}{=} \int g(a_j)p_{ij}da_j$. For the space dependent random coefficient, we consider $V(x;\omega) = \log(2\mu(x;\omega))$, where $V(x;\omega) = \sum_{k=1}^{2}\left(\sin(kx)\xi_k(\omega) + \cos(kx)\xi_{-k}(\omega)\right)$ and $\xi_k(\omega) \sim N(0, 1/3^2)$ for all k.

By taking the initial solution as

$$u(x, t_0; \omega) = \eta_0(\omega) + \sum_{k=1}^{3} \left(\sin(kx)\eta_k(\omega) + \cos(kx)\eta_{-k}(\omega) \right), \tag{5.2.33}$$

with independent Gaussian random variables $\eta_k(\omega) \sim N(1, 0.1)$ for $k \neq 0$ and $\eta_0(\omega) \sim N(0, 0.1)$, the initial PDF becomes $p_{kl}(a_k, a_l, t_0) = p_{\eta_k}(a_k)p_{\eta_l}(a_l)$. We take the resolution of the solution to be the same as the initial condition by using $N = 3$. Figure 5.16 compares the mean and standard deviation computed by using the conditional moment closure (5.2.34) and 50,000 MC simulations at time $t = 0, 0.1, ..., 1$. The relative L_2 error stays less than 10^{-3} and 10^{-2} in the first and second moment.

We then move on to the advection term, where the two-point conditional moment closures can be written as

$$\frac{\partial p_{kl}}{\partial t} = -\frac{\partial}{\partial a_k}\mathbb{P}(p_{kl}, k) - \frac{\partial}{\partial a_l}\mathbb{P}(p_{kl}, l) \tag{5.2.34}$$

where

$$\mathbb{P}(p_{ij}, i) \stackrel{\text{def}}{=} \begin{cases} -i\hat{\nu}_{-i}\langle a_0|a_i\rangle p_j - i\hat{\nu}_0\langle a_{-i}|a_i\rangle p_j + \sum_{n+m=i}\left(\frac{i}{2}(\hat{\nu}_n\langle a_m|a_i\rangle - \hat{\nu}_{-n}\langle a_{-m}|a_i\rangle)\right)p_j \\ \qquad + \sum_{n-m=|i|}\left(\frac{n-m}{2}(-\hat{\nu}_n\langle a_m|a_i\rangle - \hat{\nu}_{-n}\langle a_{-m}|a_i\rangle)\right)p_j, \quad i \geq 0. \\ -i\hat{\nu}_{-i}\langle a_0|a_i\rangle p_j - i\hat{\nu}_0\langle a_{-i}|a_i\rangle p_j + \sum_{n+m=|i|}\left(\frac{-i}{2}(\hat{\nu}_{-n}\langle a_m|a_i\rangle + \hat{\nu}_n\langle a_{-m}|a_i\rangle)\right)p_j \\ \qquad + \sum_{n-m=|i|}\left(\frac{n-m}{2}(-\hat{\nu}_{-n}\langle a_m|a_i\rangle + \hat{\nu}_n\langle a_{-m}|a_i\rangle)\right)p_j, \quad i < 0. \end{cases} \tag{5.2.35}$$

By considering the initial condition as in Eq. 5.2.33 with $N = 3$ and time dependent coefficients with correlation length $l_c = 10$, we again compute the solution by using seven terms in the Fourier series. Figure 5.17 plots the mean and standard deviation of the solution at time $t = 0, 0.5$ and 1 for the advection equation and the errors are plotted in Figure 5.15 (b). We observe that the error of this approach compared to the solution of the exact REPDF equation in section 4.3.1 stays in the same level for
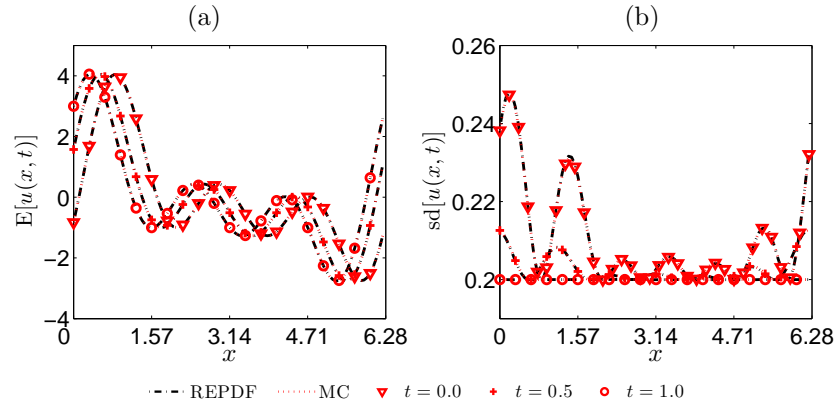
Figure 5.17: The evolution of the mean (a) and standard deviation (b) of the solution to the advection equation with time dependent random coefficient up to time $t = 1$ computed by using the PDF approach (black-·) and MC (red --).

the time dependent coefficient case. However, the error increases for space dependent coefficients that indicates the magnitude of the higher Fourier modes in the solution being nontrivial.

5.3   Summary

In this chapter, we presented two methodologies to derive reduced-order PDF equations for quantities of interest in nonlinear stochastic systems. The first idea by using MZ framework relies on defining suitable phase space functions and corresponding projection operators, yielding formally exact reduced-order PDF equations. The effective numerical simulation of such reduced order PDF equations relies on appropriate approximations. The schemes proposed so far are limited to identification of a small quantity that serves as a basis for perturbation expansion in terms of generalized operator cumulants. In spite of its restriction, we studied the statistical properties of random shock waves governed by the stochastic Burgers equation with this approach. We revisited this fundamental problem of classical fluid mechanics and provided new insights into the analysis of the underlying non-linear processes. Specifically, the reduced-order MZ-PDF equations are derived for the one- and the

two-point PDF of the velocity field in the inviscid limit. We also addressed question of how random shock waves in space-time manifest themselves in probability space and proved that information on shock dynamics and clustering is not encoded in the one-point PDF. However, by using the two-point PDF of the velocity field, whose exact dynamics is governed by a Mori-Zwanzig-type equation, we can compute important quantities, such as the turbulent energy, which is is ultimately related to shock dynamics and clustering.

An alternative approach based on a hierarchy of coupled PDF equations is presented, that is the conditional moment closures. This system resembles the BBGKY and the Lundgren-Monin-Novikov hierarchies, which approximates the system based on the level of interaction commonly truncated at low level. The main feature of this approach is that it allows us to reduce the high-dimensional kinetic equation into a sequence of low-dimensional problems. We studied the accuracy and the computational efficiently of first- and second- order truncations of the such hierarchy for non-linear dynamical systems including the Kraichnan-Orszag and the Lorenz-96 system. In particular, this approach is employed to compute the probability density evolution of advection-diffusion equation. By semi-discretization in the physical space, non-local character of the system is associated to the global basis and the interaction is approximated with the conditional moment closure.

Part II

Uncertainty propagation across heterogeneous domains

Chapter 6

Extension of Karhunen-Loève expansion

In this chapter, we present two extensions of the classical KL expansion to characterize the random fields focusing on the mutually correlated statistical structure. In section 6.1, we present two expansion methods to represent multi-correlated non-stationary stochastic processes. We call the first method as multiple uncorrelated KL (muKL) expansion based on the spectral decomposition of a suitable *assembled process*, and it yields series expansions in terms an identical set of *uncorrelated* random variables. The second approach, multiple correlated (mcKL) expansion method, relies on expansions in terms of *correlated* sets of random variables. The cross-covariance structure of the processes is imposed by setting the cross-correlation between such sets of random variables appropriately. Both methods are straightforward to use and can be readily employed in stochastic simulations based on Monte-Carlo, polynomial chaos [71, 213], or probabilistic collocation [61]. The effectiveness and the computational efficiently of both methods is discussed in section 6.2 with an application of muKL to a tumor growth model driven by two mutually correlated stochastic processes. In section 6.3, we introduce our second extension to obtain a

localized expansion of random processes and fields for the purpose of domain decomposition. This expansion preserves second-order global statistical properties, i.e., the two-point correlation function across different domains. The convergence result of the local expansion method is presented in section 6.3.2.

6.1   KL expansion for multi-correlated processes

Let us consider an ensemble of n zero-mean, square integrable random processes

$$\{f_1(t;\omega), \dots, f_n(t;\omega)\} \tag{6.1.1}$$

in a complete probability space $(\Omega, \mathcal{F}, P)$, where Ω denotes the sample space, $\mathcal{F}$ is a σ-field on Ω, and P is the applicable probability measure on $\mathcal{F}$. We assume that each process is defined in a bounded time interval $[0, T]$. The correlation structure between the processes $\{f_1(t;\omega), \dots, f_n(t;\omega)\}$ can be represented in terms of $n(n+1)/2$ covariance kernels C_{ij},

$$C_{ij}(s,t) \stackrel{\text{def}}{=} \mathbb{E}\left[f_i(t;\omega)f_j(s;\omega)\right] , \quad 1 \le i \le j \le n \,,$$

where $\mathbb{E}[\cdot]$ denotes the statistical expectation operator. The quantity $C_{ii}(s,t)$ is the auto-covariance of the process $f_i(t;\omega)$, which will be also denoted as $C_i(s,t)$, for notational convenience. If the processes $\{f_1(t;\omega), \dots, f_n(t;\omega)\}$ are mutually independent, then the classical KL expansion can be applied to each process, leading to multiple series which can be constructed separately [88, 141]. However, if the cross-covariances $C_{ij}(s,t)$ are not zero, then it is not straightforward to obtain consistent expansions for all random processes, reflecting both the autocorrelation as well as the cross covariance structure.

Hereafter we propose two different methods to overcome this problem. The first

relies on series expansions of all processes in terms of a single set of uncorrelated random variables (see also [156]). The second employs distinct but correlated sets of random variables for each process [202,211,218]. We will examine both stationary as well as non-stationary processes. In particular, we will consider Gaussian processes with exponential

$$C_i(s,t) = \frac{D_i}{\tau_i} \exp\left[-\frac{|t-s|}{\tau_i}\right] \tag{6.1.2}$$

and Gaussian

$$C_i(s,t) = \frac{D_i}{\tau_i} \exp\left[-6\frac{(t-s)^2}{\tau_i^2}\right] \tag{6.1.3}$$

covariances, where τ_i and D_i represent, respectively, the correlation length and the correlation amplitude of the process $f_i(t;\omega)$. We will also consider non-stationary covariances [43, 76], such as those associated with fractional Brownian motion

$$C_i(s,t) = \frac{D_i}{2}\left(|s|^{2H_i} + |t|^{2H_i} - |s-t|^{2H_i}\right) , \tag{6.1.4}$$

where $0 < H_i < 1$ is the Hurst parameter, and Brownian bridge

$$C_i(s,t) = D_i\left(\min(s,t) - st\right) \tag{6.1.5}$$

processes.

6.1.1 Multiple uncorrelated KL expansions (muKL)

In this method we look for a series expansion of each random process in (6.1.1) in terms of a single set of uncorrelated random variables. In order to construct such series, we first consider an *assembled process* $\tilde{f}(t;\omega)$ defined as

$$\tilde{f}(t;\omega) \overset{\text{def}}{=} f_i(t - T_{i-1};\omega) \qquad t \in \mathcal{I}_i , \tag{6.1.6}$$

where $T_i = iT$, $\mathcal{I}_1 = [0, T_1]$ and $\mathcal{I}_i = (T_{i-1}, T_i]$ $(1 \leq i \leq n)$. In other words, the restriction of the assembled process $\tilde{f}(t; \omega)$ to the time interval $\mathcal{I}_i$ coincides with the process $f_i(t; \omega)$. Note that here we assumed that all processes in (6.1.1) are defined on the same time interval $[0, T]$, although this requirement can be easily relaxed. Obviously, $\tilde{f}(t; \omega)$ is still a second-order process satisfying

$$\mathbb{E}\left[\tilde{f}(t; \omega)\right] = 0, \qquad \mathbb{E}\left[\tilde{f}(t; \omega)\tilde{f}(s; \omega)\right] = \widetilde{C}(s, t), \tag{6.1.7}$$

where the assembled covariance function $\widetilde{C}(s, t)$ is defined as

$$\widetilde{C}(s, t) \stackrel{\text{def}}{=} C_{ij}(s - T_{i-1}, t - T_{j-1}) \qquad s \in \mathcal{I}_i, \quad t \in \mathcal{I}_j. \tag{6.1.8}$$

At this point, we look for a KL-type expansion of the assembled process (6.1.6) in the form

$$\tilde{f}(t; \omega) = \sum_{k=1}^{\infty} \sqrt{\lambda_k} \tilde{f}_k(t)\xi_k(\omega), \tag{6.1.9}$$

where $\xi_k(\omega)$ are *uncorrelated* random variables

$$\xi_k(\omega) \stackrel{\text{def}}{=} \frac{1}{\sqrt{\lambda_k}} \int_0^{T_n} \tilde{f}(t; \omega)\tilde{f}_k(t)dt, \tag{6.1.10}$$

while λ_k and $\tilde{f}_k(t)$ are, respectively, eigenvalues and eigenfunctions of a symmetric compact integral operator [99, 160] with kernel (6.1.8), i.e., they are solutions to the homogeneous Fredholm integral equation of the second kind

$$\int_0^{T_n} \widetilde{C}(s, t)\tilde{f}(s)ds = \lambda\tilde{f}(t). \tag{6.1.11}$$

However, our assembled covariance $\widetilde{C}(s, t)$ could not be positive semi-definite, even when all the covariances are positive semi-definite. This might lead to negative eigenvalues. For practical applications it is desirable to have a non-negative operator.

In a discrete setting this yields the following positivity condition for the assembled discretized covariance $\widetilde{C}(t_i, t_j)$

$$\sum_{j=1}^{m}\sum_{i=1}^{m}\widetilde{C}(t_i, t_j)x_i x_j \geq 0, \tag{6.1.12}$$

for any finite time sequence $\{t_1, ..., t_m\}$ and real numbers $\{x_1, ..., x_m\}$. In other words, the $m \times m$ matrix

$$\widetilde{C} = \begin{bmatrix} \widetilde{C}(t_1, t_1) & \widetilde{C}(t_1, t_2) & \cdots & \widetilde{C}(t_1, t_m) \\ \widetilde{C}(t_2, t_1) & \widetilde{C}(t_2, t_2) & \cdots & \widetilde{C}(t_2, t_m) \\ \vdots & \vdots & \ddots & \vdots \\ \widetilde{C}(t_m, t_1) & \widetilde{C}(t_m, t_2) & \cdots & \widetilde{C}(t_m, t_m) \end{bmatrix} \tag{6.1.13}$$

should be positive semi-definite for any set of m distinct time instants in $[0, T]$. As we will see in section 6.1.1, the positivity requirement introduces several constraints, e.g., in the cross-correlation lengths. Once we have available the eigen-pair $\{\lambda_k, \tilde{f}_k(t)\}$ $(k = 1, 2, ...)$, ordered according to the magnitude of the eigenvalues λ_k, then we represent each eigenfunction $\tilde{f}_k(t)$ in terms of n *sub-components* $\phi_k^{(i)}(t)$ $(i = 1, ..., n)$ defined as

$$\phi_k^{(i)}(t) \overset{\text{def}}{=} \tilde{f}_k(t + T_{i-1})\mathcal{I}_{[0,T]}(t), \tag{6.1.14}$$

where $\mathcal{I}_{[0,T]}$ is the indicator function on the set $[0, T]$. In this way, the i-th random process $f_i(t; \omega)$ is expanded as

$$f_i(t; \omega) = \sum_{k=1}^{\infty} \sqrt{\lambda_k}\phi_k^{(i)}(t)\xi_k(\omega). \tag{6.1.15}$$

Note that λ_k and $\xi_k(\omega)$ appearing this equation are the same as those appearing in the assembled process (6.1.9). For each specific index i, the set of sub-components

$\{\phi_k^{(i)}(t)\}$ ($k = 1, 2, ..$) is not orthogonal[1] nor normalized in $t \in [0, T]$. However, $\phi_k^{(i)}(t)$ can be easily normalized within the time interval $[0, T]$. This leads the following series

$$f_i(t; \omega) = \sum_{k=1}^{\infty} \sqrt{\hat{\lambda}_k^{(i)}} \hat{\phi}_k^{(i)}(t) \xi_k(\omega), \qquad (6.1.16)$$

where $\hat{\phi}_k^{(i)}(t) \overset{\text{def}}{=} \phi_k^{(i)}(t)/\|\phi_k^{(i)}(t)\|_2$ and $\hat{\lambda}_k^{(i)} \overset{\text{def}}{=} \lambda_k \|\phi_k^{(i)}(t)\|_2^2$. We remark that each random process in (6.1.15) or (6.1.16) is represented in terms of the same set of random variables ξ_i. Therefore the muKL method cannot be used to represent heterogeneous sets of processes, i.e., processes with different types of random variables in the series expansion.

Next, we study the convergence properties of truncated muKL expansions. To this end, let us first define the truncated assembled process

$$S_M(t; \omega) \overset{\text{def}}{=} \sum_{k=1}^{M} \sqrt{\lambda_k} \tilde{f}_k(t) \xi_k(\omega), \qquad (6.1.17)$$

and the corresponding mean-squared error as

$$\varepsilon_M^2 \overset{\text{def}}{=} \int_0^{T_n} \mathbb{E}\left[\left(\tilde{f}(t; \omega) - S_M(t; \omega)\right)^2\right] dt. \qquad (6.1.18)$$

By using the fact that ξ_k are uncorrelated and that $\tilde{f}_k$ are orthonormal, we immediately obtain

$$\varepsilon_M^2 = \sum_{k=M+1}^{\infty} \lambda_k, \qquad (6.1.19)$$

i.e., the truncation error of the series (6.1.9) decreases with respect to the decay rate of the eigenvalues. The quantity ε_M^2 provides also an upper bound for the truncation

---

[1]The spectral theorem [99] guarantees that the solutions to Eq. (6.1.11) are orthonormal in $L_2([0, T_n])$. This does not obviously imply that their sub-components are orthogonal as well.

error of the muKL expansion (6.1.15). In fact, we have

$$\int_0^T \mathbb{E}\left[\left(f_i(t) - \sum_{k=1}^M \sqrt{\lambda_k}\phi_k^{(i)}(t)\xi_k\right)^2\right] dt = \int_{T_{i-1}}^{T_i} \mathbb{E}\left[\left(\tilde{f}(t) - S_M(t;\omega)\right)^2\right] dt \leq \varepsilon_M^2.$$
(6.1.20)

In addition, the errors of the cross-covariances C_{ij} are bounded by the error of the assembled covariance $\widetilde{C}(t,s)$ in Eq. (6.1.8). In fact, by the Mercer's theorem [160], the quantity

$$\varepsilon_M^{\widetilde{C}} \stackrel{\text{def}}{=} \frac{1}{\|\widetilde{C}(s,t)\|_1} \int_0^{T_n}\int_0^{T_n} \left|\widetilde{C}(s,t) - \sum_{k=1}^M \lambda_k \tilde{f}_k(s)\tilde{f}_k(t)\right| dtds$$
(6.1.21)

goes to zero uniformly in M, and this implies that

$$\frac{1}{\|\widetilde{C}(s,t)\|_1} \int_0^{T_n}\int_0^{T_n} \left|C_{ij}(s,t) - \sum_{k=1}^M \lambda_k \phi_k^{(i)}(s)\phi_k^{(j)}(t)\right| dtds$$
(6.1.22)

is bounded by $\varepsilon_M^{\widetilde{C}}$. Similar results hold for the covariances $C_i(s,t)$. The proper choice of M in (6.1.17) can be done, e.g., by imposing a certain threshold for the errors ε_M or $\varepsilon_M^{\widetilde{C}}$. Based on Eq. (6.1.19), this is equivalent to set a threshold for the relative cumulative spectrum, e.g.,

$$\sum_{k=1}^M \lambda_k \geq 0.95 \sum_{k=1}^\infty \lambda_k .$$
(6.1.23)

Positivity constraints for exponential covariances

We have seen in the previous section that the assembled covariance kernel (6.1.8) is, in general, not positive semi-definite. This could yield negative eigenvalues in the expansion of the assembled process and, consequently, in the expansions of all processes. In practical applications it is convenient to have positive eigenvalues. This requirement induces a positivity constraint in the integral operator at the left hand side of (6.1.11). In order to understand the implications of such constraint, let us

consider a simple prototype problem involving two random processes, $f_1(t; \omega)$ and $f_2(t; \omega)$, with exponential covariances and cross-covariance as in Eq. (6.1.2). We choose two time instants $(s_1, s_2) \in [0, T]^2$, such that $t_1 = s_1$ and $t_2 = s_2 + T$. This yields the following assembled covariance kernel

$$
\widetilde{C} = \begin{bmatrix} \dfrac{1}{\tau_1} & \dfrac{1}{\tau_{12}} \exp\left[-\dfrac{|s_1 - s_2|}{\tau_{12}} \right] \\[2em] \dfrac{1}{\tau_{12}} \exp\left[-\dfrac{|s_1 - s_2|}{\tau_{12}} \right] & \dfrac{1}{\tau_2} \end{bmatrix} ,
$$

which must be positive semi-definite for all s_1 and s_2. An equivalent statement for a matrix to be positive semi-definite is that all the eigenvalues are non-negative and a necessary condition is that the determinant is non-negative. In our case, this yields

$$
\det\left[\widetilde{C} \right] = \frac{1}{\tau_1 \tau_2} - \frac{1}{\tau_{12}^2} \exp\left[-2\frac{|s_1 - s_2|}{\tau_{12}} \right] \geq 0 , \tag{6.1.24}
$$

which is verified for all s_1 and s_2 provided $\tau_1 \tau_2 \leq \tau_{12}^2$. This result can be extended to n exponentially correlated random processes by choosing $t_1 \in [T_{i-1}, T_i]$ and $t_2 \in [T_{j-1}, T_j]$, where $i < j$. By using similar arguments we obtain that the assembled covariance kernel is non-negative if the correlation lengths satisfy

$$
\tau_i \tau_j \leq \tau_{ij}^2 . \tag{6.1.25}
$$

This positivity condition holds also for processes with Gaussian covariances in the form (6.1.3). In summary, the set of correlation lengths $\{\tau_{ij}\}$ for which the muKL method is applicable is *bounded*. The exact range will be determined numerically in section 6.2. Constraints of type Eq. (6.1.25) arise as a consequence of the assumption that each process f_i is a linear combination of an identical set of random variables. In order to see this, let us revisit the example above and assume that each process has the same correlation length, i.e., $\tau_i = \tau_j$. In this case the positivity condition of the

assembled covariance is satisfied by the requirement $\tau_i = \tau_j \leq \tau_{ij}$. Thus, the cross-correlation length between two processes must be larger than the correlation length of each process. In other words, expanding different random processes relatively to the same set of random variables (as done in muKL) makes sense if the processes are "enough correlated" to each other.

6.1.2 Multiple correlated KL expansion (mcKL)

Differently from the muKL technique introduced so far, where only one set of uncorrelated random variables was used to represent the whole set of stochastic processes (6.1.1), the mcKL expansion method employs different sets of mutually correlated random variables. Let

$$f_i(t;\omega) = \sum_{k=1}^{\infty} \sqrt{\gamma_k^i} \psi_k^i(t) \eta_k^i(\omega) \tag{6.1.26}$$

be the standard KL expansion of $f_i(t;\omega)$. For a fixed index i, $\{\gamma_k^i, \psi_k^i(t)\}$ are eigenpairs of the auto-covariance $C_i(s,t)$, while $\{\eta_k^i(\omega)\}$ is a set of zero-mean uncorrelated random variables with unit variance. Upon definition of

$$K_{km}^{ij} \stackrel{\text{def}}{=} \mathbb{E}\left[\eta_k^i \eta_m^j\right], \tag{6.1.27}$$

we obtain from Eq. (6.1.26) the cross-covariances

$$C_{ij}(s,t) = \mathbb{E}\left[f_i(s;\omega)f_j(t;\omega)\right] = \sum_{k,m=1}^{\infty} K_{km}^{ij} \sqrt{\gamma_k^i \gamma_m^j} \psi_k^i(s) \psi_m^j(t). \tag{6.1.28}$$

The correlation constants K_{km}^{ij} in Eq. (6.1.27) can be determined by projecting the kernels $C_{ij}(s,t)$ onto the eigenfunction set of each random process. This yields (see also [225])

$$K_{km}^{ij} = \frac{1}{\sqrt{\gamma_k^i \gamma_m^j}} \int_0^T \int_0^T C_{ij}(s,t) \psi_k^i(s) \psi_m^j(t) ds dt. \tag{6.1.29}$$

Let K be the block matrix

$$K \stackrel{\text{def}}{=} \begin{bmatrix} I & K^{12} & \cdots & K^{1n} \\ K^{21} & I & \cdots & K^{2n} \\ \vdots & \vdots & \ddots & \vdots \\ K^{n1} & K^{n2} & \cdots & I \end{bmatrix}, \tag{6.1.30}$$

where I is the identity matrix and K^{ij} is the matrix defined in Eq. (6.1.29). Note that, in general, K is symmetric but not necessarily positive definite. We will revisit this issue in section 6.2.2.

The next question is how to obtain the random variables $\{\eta_k^i(\omega)\}$ in Eq. (6.1.26) from K_{km}^{ij}. To this end, let

$$\eta \stackrel{\text{def}}{=} \begin{bmatrix} \{\eta_k^1(\omega)\} \\ \{\eta_k^2(\omega)\} \\ \vdots \\ \{\eta_k^n(\omega)\} \end{bmatrix} \tag{6.1.31}$$

be a correlated random vector collecting all random variables $\{\eta_k^i(\omega)\}$ in which the processes (6.1.26) are expanded. In order to generate realizations η we assume that K is positive definite and perform a Cholesky decomposition in the form $K = RR^T$. Then we transform the random variables as $\widetilde{\eta} = R^{-1}\eta$. This yields $\mathbb{E}\left[\widetilde{\eta}\widetilde{\eta}^T\right] = I$, i.e., the random vector $\widetilde{\eta}$ has uncorrelated components. Thus, in order to represent our processes we can first consider a set of uncorrelated random variables $\widetilde{\eta}$ and then transform them into the specified correlated set η by simply applying R to $\widetilde{\eta}$[2]. The eigenfunctions $\psi_k^i(t)$ in (6.1.26) can be transformed as well by applying R to the

---

[2]We recall that correlated non-normal random variables can be also transformed into a set of uncorrelated normal random variables by using Nataf transformation [107]. This technique first transforms each non-normal random variable into a normal random variable by using the inverse cumulative distribution function, and then apply the Cholesky decomposition to the correlation matrix to convert them into uncorrelated variables.

muKL	mcKL
1. Assemble the random processes $\{f_1, ..., f_n\}$ and the covariance function as in Eqs. (6.1.6)-(6.1.8)	1. Apply KL expansion to each process as in Eq. (6.1.26)
2. Apply KL expansion to the assembled process (6.1.9)	2. Compute the correlation coefficients that yield the proper correlation structure (6.1.29)
3. Determine the basis function of each process and represent it as in Eqs. (6.1.14)-(6.1.15)	3. Represent each process as in (6.1.26), where η_j^k are determined by a singular value decomposition of (6.1.30)

Table 6.1: Summary of the algorithms for muKL and mcKL expansions.

right. In fact, if we denote by $\Psi(t)$ the vector collecting the eigenfunctions of all the auto-covariances, then we have $\widetilde{\Psi}(t) = \Psi(t)R$. The series expansions (6.1.26) obtained in this way satisfy the correlation structure (6.1.28). Similar expansions have been obtained by [202], by directly imposing the correlation constants rather than considering their expression in terms of cross-covariance kernels. The truncation error of the mcKL series can be defined as the summation of the error in each covariance kernel

$$\varepsilon_{M_{ij}}^{C_{ij}} \stackrel{\text{def}}{=} \frac{1}{\|C_{ij}(s,t)\|_1} \int_0^T \int_0^T \left| C_{ij}(s,t) - \sum_{k=1}^{M_i} \sum_{m=1}^{M_j} K_{km}^{ij} \sqrt{\gamma_k^i \gamma_m^j} \psi_k^i(s) \psi_m^j(t) \right| ds dt \,.$$
(6.1.32)

Analytical results for exponentially correlated processes

The eigenvalues and eigenfunctions of integral operators in the form (6.1.11) with exponential covariances (6.1.2) admit an analytical expression [71,89]. In particular, let $c_i = 1/\tau_i$, where τ_i is the correlation length of the process $f_i(t; \omega)$. Then γ_k^i and $\psi_k^i(t)$ in Eq. (6.1.26) are given by

$$\gamma_k^i = \frac{2c_i}{w_{ik}^2 + c_i^2}$$
(6.1.33)

$$\psi_k^i(t) = \frac{1}{A_{ik}} \left(\frac{w_{ik}}{c_i} \cos(w_{ik}t) + \sin(w_{ik}t) \right) ,$$
(6.1.34)

where w_{ik} ($k = 1, 2, ...$) are solutions to the transcendental equation $(w_{ik}^2 - c_i^2) \tan(w_{ik}T) - 2c_i w_{ik} = 0$ and

$$A_{ik} = \left[\frac{1}{2} \left(1 + \frac{w_{ik}^2}{c_i^2} \right) T + \left(\frac{w_{ik}^2}{c_i^2} - 1 \right) \frac{\sin(2w_{ik}T)}{4w_{ik}} + \frac{1}{2c_i}(1 - \cos(2w_{ik}T)) \right]^{1/2} .$$

A substitution of Eqs. (6.1.33)-(6.1.34) into Eq. (6.1.29) yields the following analytical expression for the cross-covariances

$$K_{km}^{ij} = B_{km}^{ij0} \left[B_{km}^{ij1} + B_{km}^{ij2} \cos(w_{ik}T) + B_{km}^{ij3} \sin(w_{ik}T) \right]$$
$$\times \left[B_{km}^{ij4} + B_{km}^{ij5} \cos(w_{jm}T) + B_{km}^{ij6} \sin(w_{jm}T) \right],$$

where

$$B_{km}^{ij0} = \frac{c_{ij}^2 e^{-T/c_{ij}}}{A_{ik} A_{jm} c_i c_j \left(1 + c_{ij}^2 w_{ik}^2 \right) \left(1 + c_{ij}^2 w_{jm}^2 \right)}, \quad c_{ij} = \frac{1}{\tau_{ij}},$$

$$B_{km}^{ij1} = (1 + c_i c_{ij}) e^{T/c_{ij}} w_{ik}, \quad B_{km}^{ij2} = - (1 + c_i c_{ij}) w_{ik},$$

$$B_{km}^{ij3} = -c_i + c_{ij} w_{ik}^2, \quad B_{km}^{ij4} = (-1 + c_j c_{ij}) w_{jm},$$

$$B_{km}^{ij5} = (1 - c_j c_{ij}) e^{T/c_{ij}} w_{jm}, \quad B_{km}^{ij6} = \left(c_j + c_{ij} w_{jm}^2 \right) e^{T/c_{ij}} .$$

Similar analytical results can be obtained for regularized exponential covariances [176]. Clearly, the availability of analytical results for the KL decomposition of each process f_i, significantly reduces the computational cost of the mcKL method.

6.2 Numerical simulation of multiple correlated processes

In this section we compare the proposed methods, i.e., muKL and mcKL, in terms of accuracy and computational cost. To this end, we consider multi-correlated random
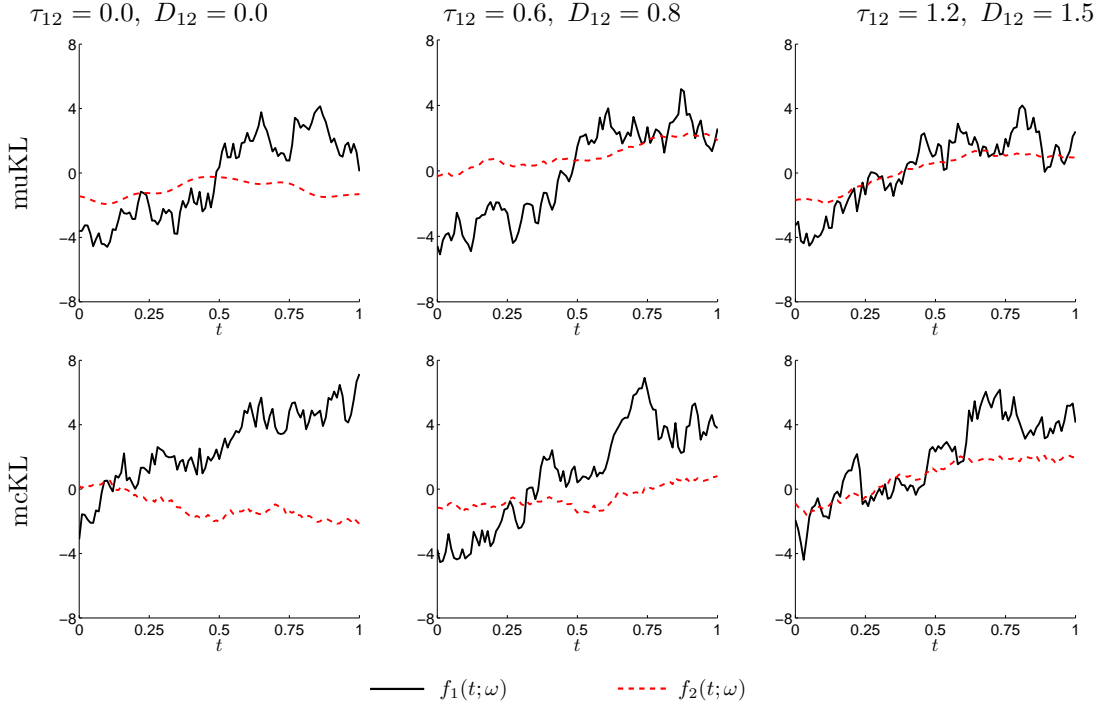
Figure 6.1: Sample paths of two exponentially correlated random processes $f_1(t;\omega)$ and $f_2(t;\omega)$ generated by using muKL (first row) and mcKL (second row). Shown are results for $D_1 = D_2 = 1$, $\tau_1 = 0.2$, $\tau_2 = 1$ and different cross-covariance lengths τ_{12} and amplitudes D_{12}. It is seen that the sample paths of $f_2(t;\omega)$ tend to follow those of $f_1(t;\omega)$ when τ_{12} and D_{12} increase.

processes with both stationary and non-stationary covariances (6.1.2)-(6.1.5) in the time interval $[0, 1]$. Unless otherwise stated, we set $D_i = 1$, for all i. We first consider two exponentially correlated processes, $f_1(t;\omega)$ and $f_2(t;\omega)$. Several realizations (sample paths) of these processes are shown in Figure 6.1 for $\tau_1 = 0.2$, $\tau_2 = 1$ and different cross-correlation lengths and amplitudes D_{12}. The truncation dimension in the muKL and mcKL series expansions (see Eqs. (6.1.22)-(6.1.32)) is set to $M = 50$ and $M_1 = M_2 = 25$, respectively. It is seen that, as we increase the cross-correlation length and amplitude the samples of f_1 and f_2 are more and more correlated, i.e., they tend to follow the same trend.
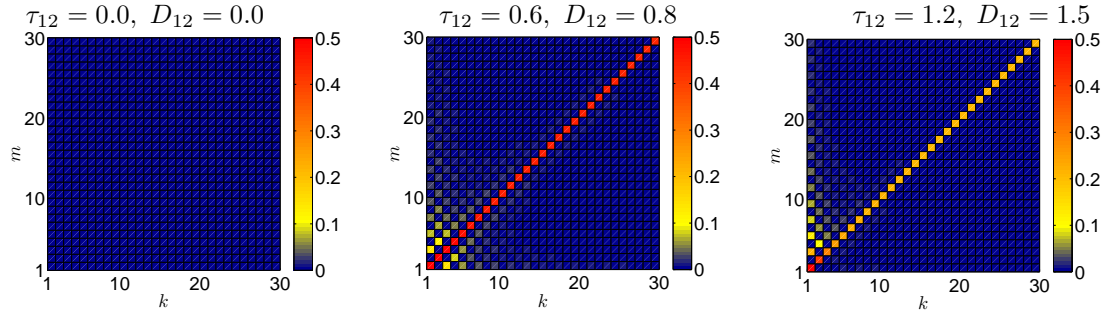
Figure 6.2: Absolute value of the cross correlation coefficients K_{km}^{12} defined in Eq. (6.1.29). We see that for non-zero cross-correlation lengths τ_{12} several coefficients are activated.

Imposing a cross-covariance between f_1 and f_2 results in different effects in muKL and mcKL expansions. In particular, in the muKL framework the cross covariance structure affects the basis functions $\phi_k^{(i)}$ in Eq. (6.1.14). On the other hand, in the mcKL framework the cross-covariance affects the correlation coefficients (6.1.29). Specifically, if the cross-correlation length is non-zero we see that several cross-correlation coefficients are activated (see Figure 6.2).

Next, we compare muKL and mcKL methods in terms of accuracy. To this end we consider two correlated random processes with Gaussian covariances and cross-covariance. First of all, we examine the L_2 errors (6.1.21) and (6.1.32) as a function of the number of expansion terms M, and verify convergence of both muKL and mcKL expansions. This is done in Figure 6.3 where we show the error of the assembled covariance kernel for different values of τ_1, fixed $\tau_2 = \tau_{12} = 2$, and $M_1 = M_2 = M/2$. It is seen that the error depends significantly τ_1. In particular, the convergence of the series becomes slower as τ_1 decreases. Despite the smaller error in the first few dimensions of mcKL expansion, the convergence rate of the muKL expansion is faster than the mcKL expansion and the overall error is lower as well. The plateau observed in error plot of the mcKL method for large M is due to the correlation coefficients K_{ij}^{12}, which remain of order 10^{-10} for large k.
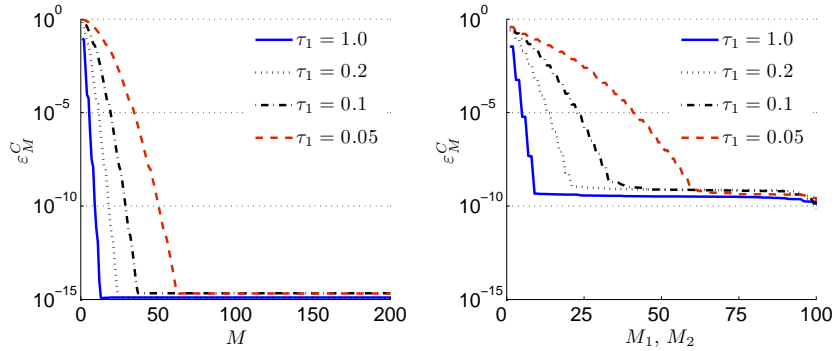
Figure 6.3: L_2 error in the assembled Gaussian covariance $\widetilde{C}$ by using muKL (left) and mcKL (right) expansions. Shown are results for different correlation lengths τ_1 and fixed $\tau_2 = \tau_{12} = 2$. Smaller correlation lengths require more random variables for a prescribed level of accuracy in both methods. However, muKL shows faster convergence and smaller errors than mcKL.

τ	1.0	0.2	0.1	0.05	0.02
M (muKL)	2	5	7	13	31
(M_1, M_2) (mcKL)	(2, 1)	(3, 2)	(6, 3)	(11, 6)	(25, 13)

Table 6.2: Number of random variables to achieve a truncation error smaller than 3%. The correlation lengths of the processes f_1 and f_2 are set as $\tau_1 = \tau$, $\tau_2 = 2\tau$, $\tau_{12} = 2\tau$. We see that the muKL expansion requires less random variables than the mcKL expansion, in particular for small τ.
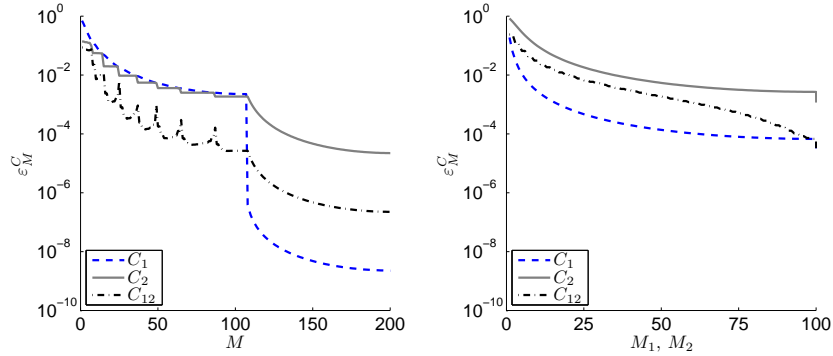
Figure 6.4: L_2 errors in representing exponential covariances C_1, C_2, and C_{12} by using muKL (left) and mcKL (right). Here we set $\tau_1 = 1$, $\tau_2 = 0.1$, $\tau_{12} = 1$. Note that the error of C_{12} decreases monotonically in mcKL but not in muKL. The overall error is lower in muKL expansion.

In Table 6.2 we summarize the number of random variables in muKL and mcKL expansions that yield 97% of the total energy of the processes, i.e., M is the truncation dimension defined by the condition $\varepsilon_M^{\widetilde{C}} < 0.03$. As expected, muKL achieves the same level of accuracy by using less random variables than mcKL (see also Figure 6.3). This is particularly true for *weakly correlated* processes, i.e. processes with small correlation length.

Next, we examine the error of exponentially correlated processes. This is done in Figure 6.4, for the case $\tau_1 = 1$, $\tau_2 = 0.1$, $\tau_{12} = 1$. Note that the error decays slower compared to the Gaussian case. This is due to the fact that the exponential kernel is less smooth than the Gaussian one [170]. Figure 6.4 also emphasizes different aspects in the decay of the covariance errors obtained by muKL and mcKL. In fact, the error in the cross covariance $\varepsilon_M^{C_{12}}$ decreases monotonically in mcKL, but not in muKL. Nevertheless, the total error turns out to be smaller by using muKL. We also apply muKL and mcKL methods to random processes with non-stationary covariance functions. In particular, we consider fractional Brownian motion (FBM) and Brownian bridge (BB) processes (see Eqs. (6.1.4)-(6.1.5)). In Figure 6.5 we show the *assembled covariances* for the specific cases we consider here, i.e., FBM and FBM/BB. The truncation dimensions for muKL and mcKL expansions are set

to $M = 48$ and $M_1 = 36$, $M_2 = 12$ in FBM, and to $M = 54$ and $M_1 = 34$, $M_2 = 20$ in FBM/BB. With these parameters the absolute error in the representation of the covariances in less than 10^{-2} (see Figure 6.6). Note that that in both muKL and mcKL methods, the maximum error occurs at the locations where the covariance function is less smooth. In particular, the mcKL expansion exhibits larger absolute and L_2 errors in the cross-covariance function, which is consistent with previous results.
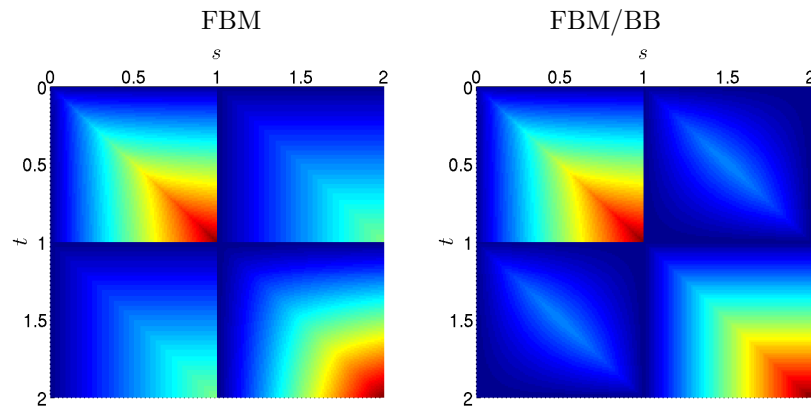
Figure 6.5: Left: Assembled covariance function of two fractional Brownian motion (FBM) processes with Hurst indexes $H_1 = 0.4$ and $H_2 = 0.7$. The cross covariance is also of FBM-type with $H_{12} = 0.5$ Right: Assembled covariance of two FBM processes ($H_1 = 0.4$, $H_2 = 0.5$) with Brownian bridge (BB) cross-covariance. In both cases the correlation amplitudes are set to $D_1 = 1$, $D_2 = 1$ and $D_{12} = 0.5$.

6.2.1 Computational cost

The muKL method requires solving an eigenproblem of size nN, where N denotes the number instants discretizing the time interval $[0, T]$. Thus, the computational cost of muKL is $O(n^3 N^3)$. On the other hand, the mcKL expansion involves n eigen-decompositions of size N, i.e., $O(nN^3)$. In addition, the projection of the eigenfunctions has to to be computed. The computational cost of this operation is affected by the truncation dimensions M_1 and M_2 of the expansions and n, i.e., we obtain $O(M_i M_j n^2 N^2)$. In Figure 6.7 we compare the computation time (in seconds)
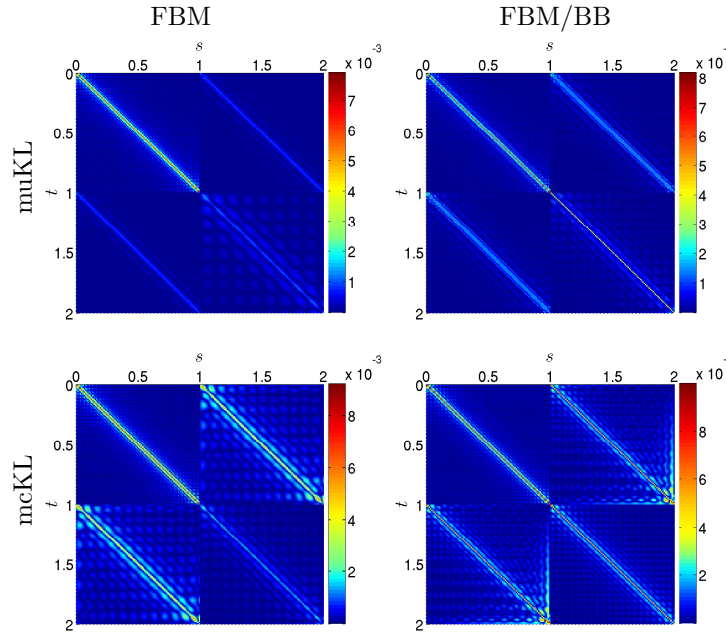
Figure 6.6: Absolute errors of muKL (first row) mcKL (second row) in representing the assembled covariance functions shown in Figure 6.5.

required by muKL and mcKL to decompose n Gaussian correlated random processes with $\tau_i = 0.2$ and $\tau_{ij} = 1.0$. The expansions are are truncated at $M = 18n$ (muKL) and $M_i = 18$ $(i = 1, ..., n)$ (mcKL).

6.2.2 Constraints for positive-definiteness

Both muKL and mcKL have to satisfy a positive-definiteness constraint. In fact, the assembled covariance function (6.1.8) in muKL and the correlation matrix (6.1.30) of the random variables in mcKL have to be positive-definite. In Figure 6.8 we show the eigenvalues λ_k of the assembled exponential covariance kernel (6.1.13) and the minimum eigenvalue for different choices of the cross-correlation length τ_{12} and fixed $\tau_1 = \tau_2 = 0.1$. The existence of negative eigenvalues clearly indicates that the assembled covariance function is not always positive-definite. The minimum eigenvalue becomes negative when the cross-correlation length is small compared to the auto-correlation lengths of both processes. In the present example, this happens
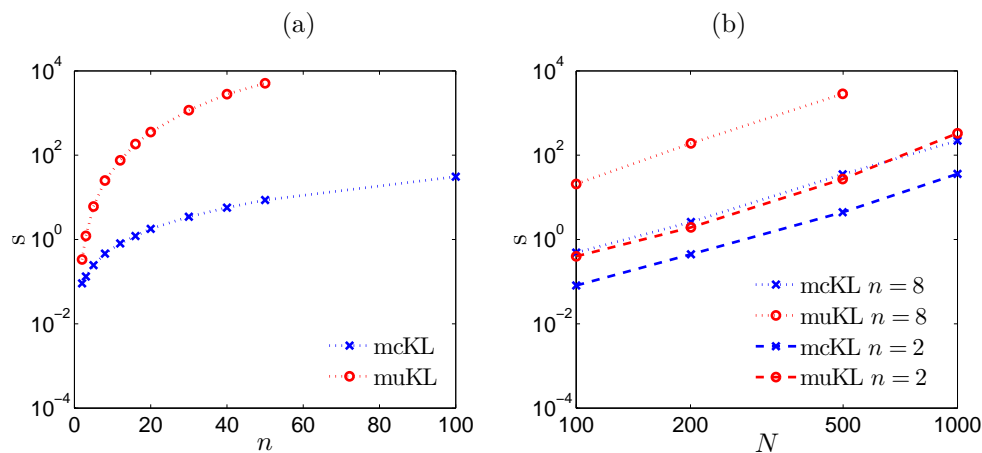
Figure 6.7: (a) Computation time (in seconds) versus the number of random processes n; (b) Computation time (in seconds) versus the number of degrees of freedom N in time domain (number of equally spaced points within $[0, 1]$). The mcKL expansion is scalable and it requires less operations than the muKL.
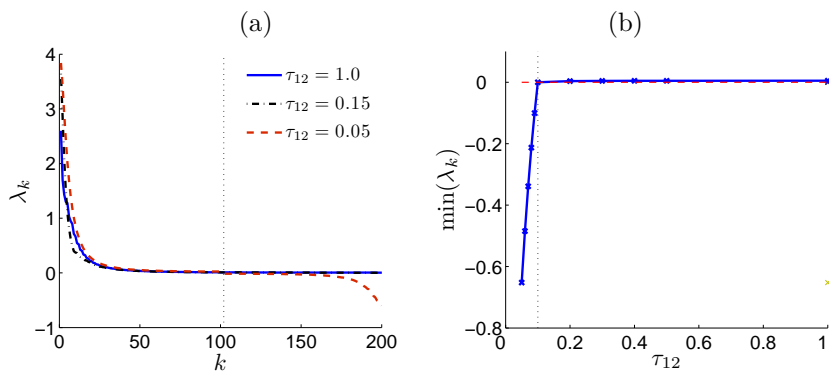
Figure 6.8: (a) Eigenvalues λ_k of the assembled covariance kernel in muKL. (b) Smallest eigenvalue as a function of the cross-correlation lengths τ_{12}. Here we set $\tau_1 = \tau_2 = 0.1$. Note that all eigenvalues are positive for $\tau_{12} \geq 0.1$.

when $\tau_{12} \leq 0.1$, which coincides exactly with the theoretical condition we obtained in Eq. (6.1.25). In Figure 6.9, we plot the the set of correlation lengths τ_2 and τ_{12}
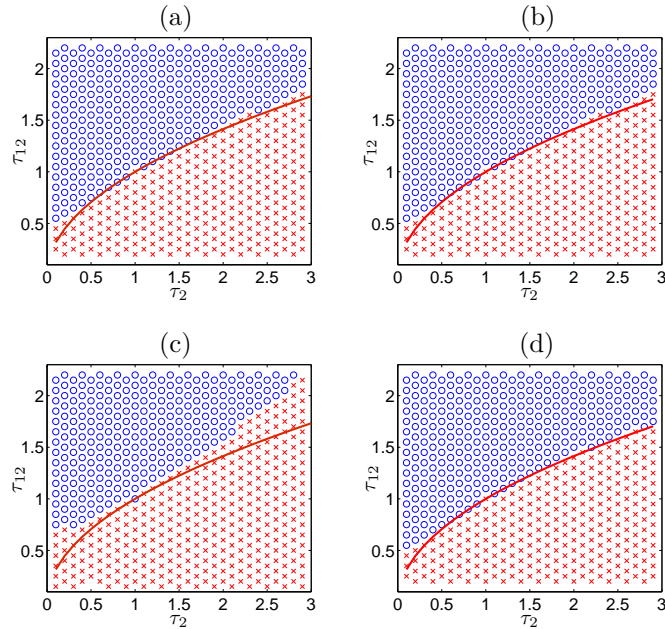
Figure 6.9: Set of correlation lengths τ_2 and τ_{12} satisfying the positive-definiteness condition (blue circles) for $\tau_1 = 1$. We consider exponential covariance kernels in (a) and (b) and Gaussian covariance kernels in (c) and (d). In (a) and (c) we employ muKL while in (b) and (d) mcKL. The red line denotes the theoretical constraint in Eq. (6.1.25) of the muKL expansion. We notice that not only muKL, but also mcKL satisfies a similar constraint.

satisfying the positive-definiteness condition for exponential and Gaussian covariance kernels with $\tau_1 = 1$. Note that the analytical condition we obtained in Eq. (6.1.25) is in agreement with the numerical results and it provides a lower bound for τ_{12}, given τ_2. We also study the positive-definiteness constraint for *three* random processes. This is done in Figure 6.10 where we plot the level sets of the cross-correlation lengths τ_{13} and τ_{23} for which the minimum eigenvalue of the assembled correlation is negative. Specifically we set $\tau_1 = 1$, $\tau_2 = 2$ and $\tau_{12} = 5$ and consider different values of τ_3. It is seen that the conditions in Eq. (6.1.25) still represent lower bounds for the cross-correlation lengths.
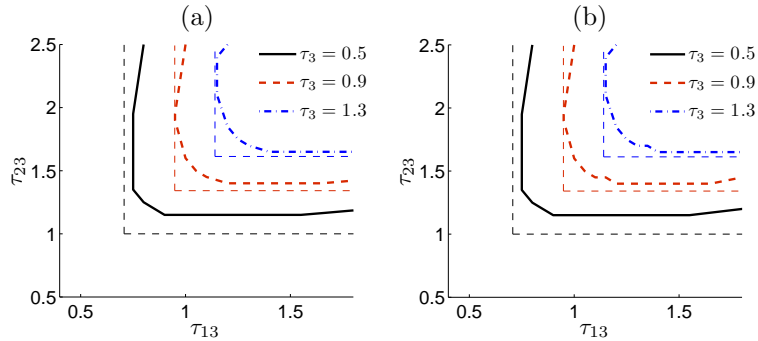
Figure 6.10: Three Gaussian random processes. Level sets of the cross-correlation lengths τ_{13} and τ_{23} for which the minimum eigenvalue of the assembled covariance is zero. In particular, we set $\tau_1 = 1$, $\tau_2 = 2$ and $\tau_{12} = 5$ and consider different τ_3. Shown are results of muKL (a) and mcKL (b). The thin dashed lines are the analytical constraints in Eq. (6.1.25).

6.2.3 Comparison with moPPCA

In the multiple version of the probabilistic principal component analysis (moP-PCA) [183] we look for a representation of multiple random processes in terms of a linear combinations of random variables. Therefore this method shares similar characteristics with the proposed mcKL. However, differently from mcKL, moPPCA assumes that all the random variables representing the processes are independent, while mcKL expansion drops such assumption to impose cross-correlation. Therefore we expect that moPPCA cannot properly represent cross-correlated processes. In order to show this we consider two exponentially correlated random processes $f_1(t;\omega)$ and $f_2(t;\omega)$ having correlation lengths $\tau_1 = 0.2$, $\tau_2 = 1.0$, and τ_{12} equal to 0 and 1.5 as in Figure 6.1. In Figure 6.11 we compare the basis functions of $f_1(t;\omega)$ as computed by mcKL and moPPCA. Note that the results of two methods coincide when f_1 and f_2 are uncorrelated ($\tau_{12} = 0$). Also, the eigenfunctions computed by moPPCA are insensitive to changes in τ_{12}. This suggests that moPPCA cannot represent cross-correlated random processes.
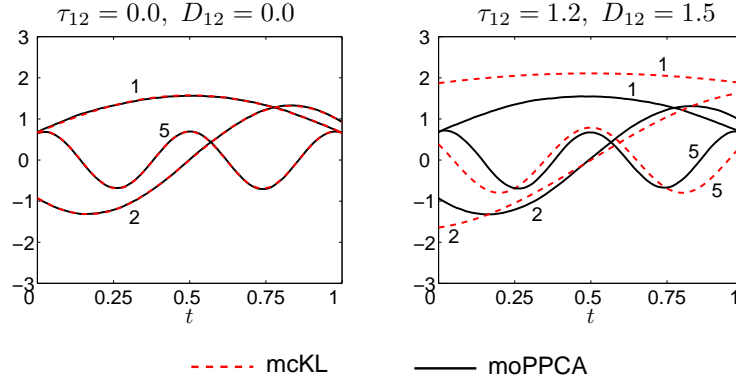
Figure 6.11: Basis functions $\psi_1^1(t)$, $\psi_2^1(t)$ and $\psi_5^1(t)$ (denoted as 1, 2 and 5 for notational convenience) as computed by mcKL and moPPCA. Note the results of two methods coincide when f_1 and f_2 are uncorrelated ($\tau_{12} = 0$). Also, the eigenfunctions computed by moPPCA are insensitive to changes in τ_{12}. This suggests that moPPCA cannot represent cross-correlated random processes.

6.2.4 Application to a tumor cell growth model

Many recent studies aim at developing simple models of complex systems based on empirical or historical data [159, 219, 222]. This is the case, for example, of biological models described in terms of stochastic differential equations [58, 224]. The muKL and mcKL methods can be applied in these contexts to find an appropriate representation of the random input processes, provided we have available their correlation structure, e.g., from empirical data. Let us illustrate the procedure with specific reference to the tumor growth model recently studied by [224]. The governing equation is

$$\begin{cases} \dot{x}(t;\omega) = G(x) + g(x)f_1(t;\omega) + f_2(t;\omega) \\ x(0;\omega) = x_0(\omega) \end{cases} \tag{6.2.1}$$

where $x(t;\omega)$ denotes the tumor cell population at time t,

$$G(x) \overset{\text{def}}{=} x(1 - \theta x) - \beta \frac{x}{x+1}, \qquad g(x) \overset{\text{def}}{=} -\frac{x}{x+1}, \tag{6.2.2}$$

β is the immune rate, and θ is related to the rate of growth of cytotoxic cells. The random process $f_1(t;\omega)$ represents the strength of the treatment (i.e., the dosage

of the medicine in chemotherapy or the intensity of the ray in radiotherapy) while the process $f_2(t;\omega)$ is related to other factors, such as drugs and radiotherapy, that restrain the number of tumor cells. The parameters β, θ and the covariance structure of the random processes f_1 and f_2 are usually estimated by using empirical data. In the present chapter, we assume that $f_1(t;\omega)$ and $f_2(t;\omega)$ are cross-correlated Gaussian processes with zero mean and Gaussian correlation functions given in Eq. (6.1.3). We also set $\beta = 2.26$ and $\theta = 0.1$. The initial condition $x_0(\omega)$ for the tumor density is assumed to be a standard Gaussian variable with mean $\langle x_0(\omega) \rangle = 7.266$ and unit variance. Such mean value corresponds to the state of stable tumor in the absence of random noise [224]. We represent the random forcing processes f_1 and f_2 by using both the muKL or mcKL methods. This allows us to solve the stochastic ODE (6.2.1) with a high-order probabilistic collocation method [212]. We also employ sparse collocation of level three [135] when the number of random variables in the forcing terms exceeds four. In Figure 6.12 we show the mean and the standard deviation of the tumor population $x(t;\omega)$ obtained by using mcKL expansions of random forcing processes with different cross-covariance structure. The dimension of each random process is at most 12 in all cases. When we set $D_{12} = 0.3$, the mean population decays slower with smaller variance for smaller values of τ_{12}. On the other hand, if we set $\tau_{12} = 1$ and change D_{12}, a similar phenomenon happens for larger values of D_{12}. The mean population decays much faster with increasing variance when D_{12} is negative. Similar results are obtained by using mcKL expansion. We conclude that the solution of the tumor cell growth model is significantly affected by the cross-covariance structure of the random input processes f_1 and f_2. Therefore it is of fundamental importance to have available techniques, such as those developed in the present chapter, capable of representing effectively the correlation structure of multiple random processes.
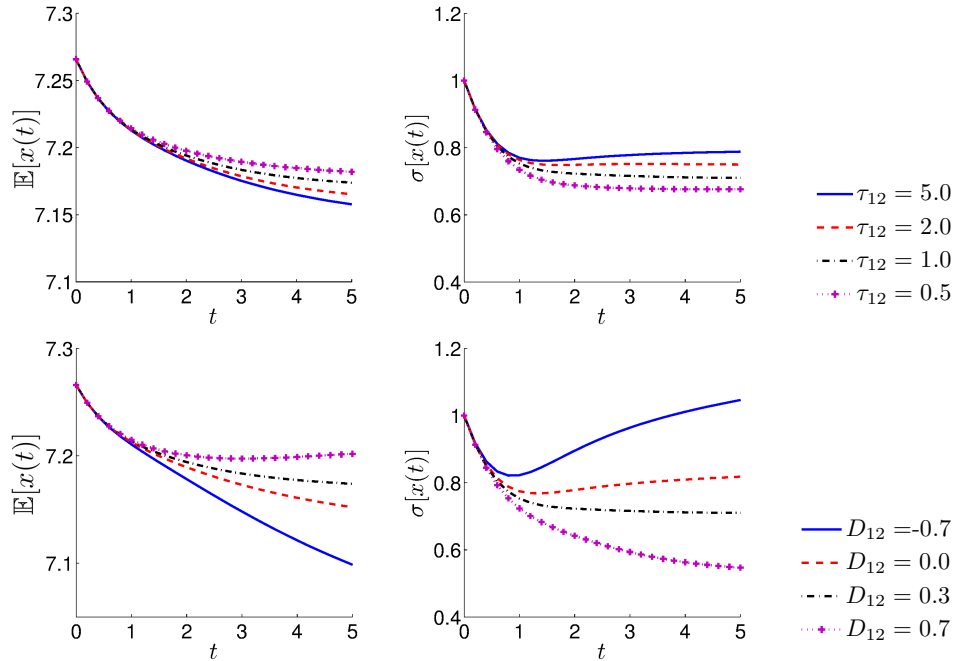
Figure 6.12: Mean (left column) and standard deviation (right column) of the tumor population. The covariance kernels of the random processes f_1 and f_2 are assumed to be Gaussian with parameters $\tau_1 = \tau_2 = 0.5$, $D_1 = D_2 = 0.1$, $D_{12} = 0.3$ (first row) and $\tau_1 = \tau_2 = 0.5$, $\tau_{12} = 1$, $D_1 = D_2 = 0.1$ (second row). Note that the statistical properties of tumor population are significantly affected by the cross-covariance structure of the noise.

6.3 Embedding Random Processes by KL expansion

Embedding a random process or a random field over a domain decomposition relies on representing it locally. This has advantages in terms of dimensionality if the process has a finite correlation length, as the local representation usually involves a reduced number of random variables (see figure 6.13 and Table 7.3). Consequently, the global stochastic problem can be, in principle, reduced to a sequence of local problems of smaller stochastic dimension. A major challenge when embedding globally defined processes and fields in a set of subdomains is related to the preservation of global statistical properties. Indeed, we cannot expect that, in general, the two- or three-point correlation functions are preserved across different subdomains. This is a
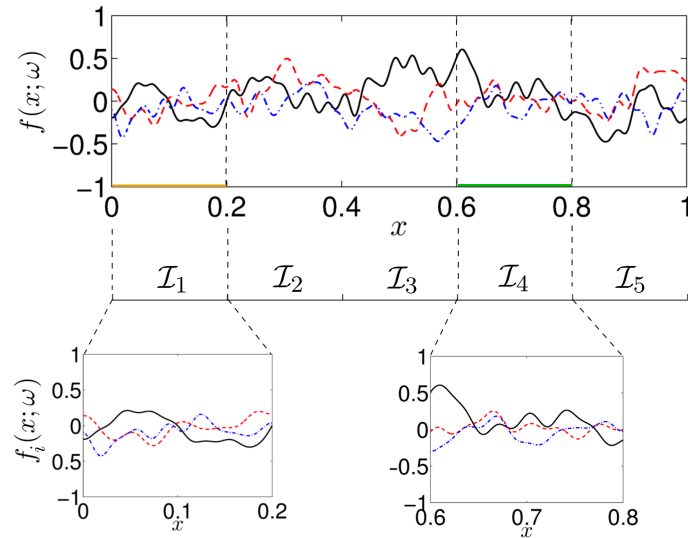
Figure 6.13: Embedding a stochastic process with finite correlation length into a non-overlapping covering of $[0, 1]$: the restriction of the process to each subdomain $\mathcal{I}_i$ can be represented in terms of a *small number* of random variables.

serious issue, since such multi-point statistics are key elements of the stochastic solution. In other words, if domain decomposition is not done appropriately in terms of local expansions and stochastic interface conditions, we may introduce a systematic error in the solution to the SPDE Eq. (7.0.1).

6.3.1 Local KL expansions

Let us consider a random function $f(x; \omega)$, $x \in \mathcal{D}$ with given mean and covariance function

$$\langle f(x; \omega) \rangle = \bar{f}(x), \qquad \text{Cov}\{f(x; \omega)f(y; \omega)\} = C(x, y). \tag{6.3.1}$$

Given a domain decomposition of $\mathcal{D}$ in terms of P overlapping subdomains $\{\mathcal{D}_1, ..., \mathcal{D}_P\}$, we would like to represent $f(x; \omega)$ locally in each subdomain $\mathcal{D}_i$, in such a way that the two-point statistical properties are preserved, even when computed across different subdomains. In particular, let us assume that the correlation length of $f(x; \omega)$ is relatively short, compared to the characteristic length of $\mathcal{D}$. Then, it is
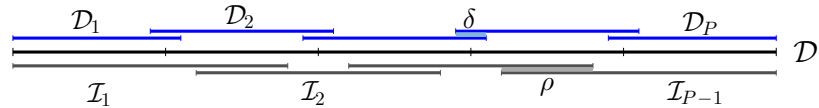
Figure 6.14: One-dimensional domain decomposition with overlapping subdomains. Shown are the subdomains $\{\mathcal{D}_i\}$ used to compute the solution to (7.0.1) and the subdomains $\{\mathcal{I}_i\}$ used to represent the external random forcing f.

reasonable to assume that the restriction of $f(x;\omega)$ to $\mathcal{D}_i$ is statistically correlated only with the restriction of $f(x;\omega)$ to the neighboring subdomains, say $\mathcal{D}_{i-1}$ and $\mathcal{D}_{i+1}$ in a one-dimensional setting. This allows us to to represent $f(x;\omega)$ in $\mathcal{D}_i$ by using a set of random variables that are shared only among adjacent sub-domains.

In order to do so, we introduce a new set of sub-domains $\{\mathcal{I}_1, ..., \mathcal{I}_{P'}\}$ to propagate the correlation structure of $f(x;\omega)$ across different $\mathcal{D}_i$. For instance, if $\mathcal{D}_i$ and $\mathcal{D}_{i+1}$ are adjacent, and the correlation length of f is smaller than both $|\mathcal{D}_i|$ and $|\mathcal{D}_{i+1}|$, then we could define the sub-domain $\mathcal{I}_i \subset \mathcal{D}_i \cup \mathcal{D}_{i+1}$. In this way, the restriction of the random process f to $\mathcal{I}_i$ allows to propagate the correlation structure of f from one domain to the other. It is important to remark that the random process $f(x;\omega)$ is first represented locally on the new decomposition $\{\mathcal{I}_1, ..., \mathcal{I}_{P'}\}$, then, later redistributed on $\{\mathcal{D}_1, ..., \mathcal{D}_P\}$ to obtain the solution to the stochastic problem. In general, $\{\mathcal{I}_i\}$ is different from $\{\mathcal{D}_i\}$, unless the local processes on each $\mathcal{D}_i$ are statistically independent, in which case we can take $\mathcal{I}_i = \mathcal{D}_i$. In general, however, when solving (7.0.1) we allow for a *multi-level* domain decomposition. The procedure is illustrated in Figure 6.14 for two-levels. The overlap between the subdomains $\{\mathcal{I}_1, ..., \mathcal{I}_{P'}\}$, i.e.,

$$\rho \stackrel{\text{def}}{=} \min_i |\mathcal{I}_{i-1} \cap \mathcal{I}_i|$$

should be chosen to be larger than the correlation length of $f(x;\omega)$. This yields better accuracy when representing $f(x;\omega)$ (see appendix for the error analysis). In the presence of multi-correlated random processes we can use our recently devel-
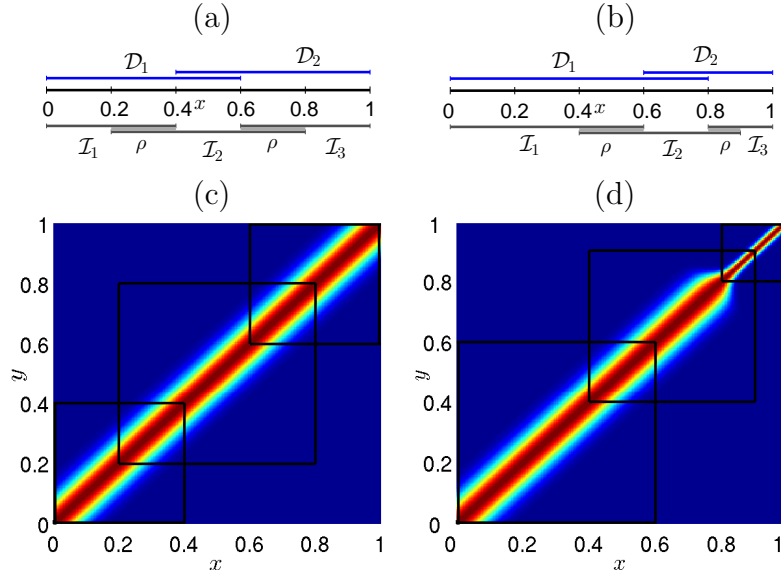
Figure 6.15: One-dimensional domain decomposition of $[0,1]$ into two overlapping domains $\{\mathcal{D}_1, \mathcal{D}_2\}$ and three expansion intervals $\{\mathcal{I}_1, \mathcal{I}_2, \mathcal{I}_3\}$ (figures (a) and (b)). In figures (c) and (d) we show how $\{\mathcal{I}_1, \mathcal{I}_2, \mathcal{I}_3\}$ partition the domain of a Gaussian covariance function with constant correlation length $l_c = 0.08$ (figure (c)) and variable correlation length (figure (d)) ranging from 0.08 to 0.02. The overlap ρ between different $\mathcal{I}_i$ is chosen to be larger that the correlation length l_c.

oped theory [35], and define a domain decomposition for each random process. At this point, it is convenient to define an index set L_i characterizing the relationship between the coverings $\{\mathcal{I}_i\}$ and $\{\mathcal{D}_i\}$

$$L_i \stackrel{\text{def}}{=} \{1 \leq j \leq P' : \mathcal{D}_i \cap \mathcal{I}_j \neq \emptyset\}, \quad 1 \leq i \leq P.$$

In particular, when we compute in the domain $\mathcal{D}_i$, the set L_i identifies the subdomains $\mathcal{I}_j$ which we should consider for the representation of the external random noise $f(x;\omega)$. For instance, $L_1 = \{1,2\}$ and $L_2 = \{2,3\}$ in Figure 6.15.

A One-Dimensional Example

With reference to Figure 6.14, let us consider two overlapping coverings of $\mathcal{D}$, $\{\mathcal{I}_1, ..., \mathcal{I}_{n-1}\}$ and $\{\mathcal{D}_1, ..., \mathcal{D}_n\}$ in which $\mathcal{D}_i$ and $\mathcal{D}_{i+1}$ share the same local representation of $f(x;\omega)$ in $\mathcal{I}_i$. We first compute the K-L expansion of $f(x;\omega)$ on the
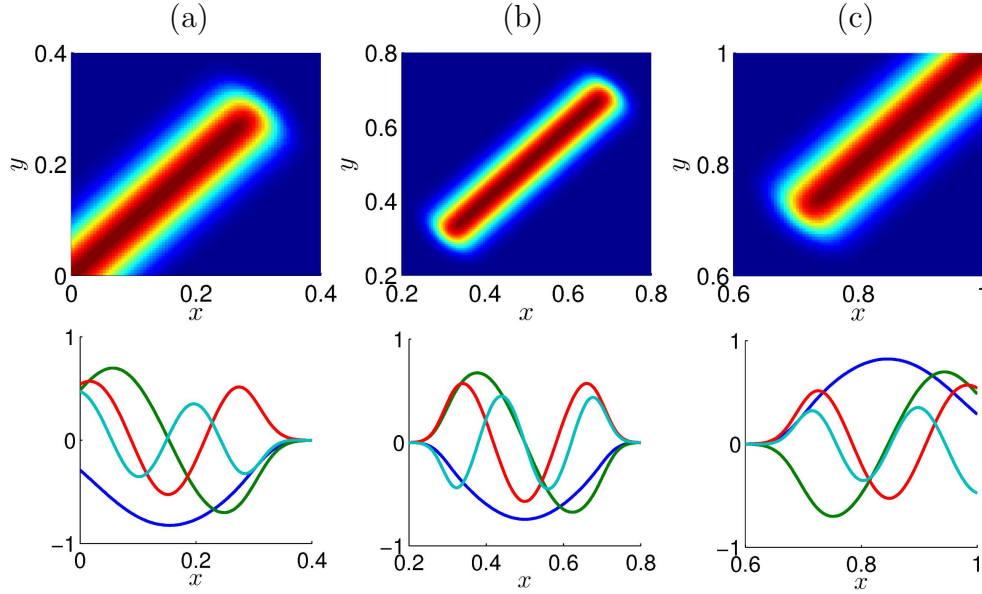
Figure 6.16: Filtered local covariance functions (6.3.3) over three expansion intervals $\{\mathcal{I}_1, \mathcal{I}_2, \mathcal{I}_3\}$ as in Figure 6.15(c) and corresponding first four K-L eigenfunctions.

i-th subdomain $\mathcal{I}_i$. To this end, we simply restrict (6.3.1) to $\mathcal{I}_i$ and solve the well-known K-L eigenvalue problem [35, 190, 191] locally. In order to ensure that the local expansions preserve global statistical properties on the overlapping region, the local covariance function $C_i(x, y)$ on $\mathcal{I}_i$ is smoothly filtered to zero on $(\mathcal{I}_i \cap \mathcal{I}_{i+1})^2$. In order words, we define a filter $\mathcal{F}_i$ such that

$$\mathcal{F}_i[C_i(x,y)] = \begin{cases} C_i(x,y), & (x,y) \notin (\mathcal{I}_i \cap \mathcal{I}_{i+1})^2, \\ C_i(x,y)\mathfrak{f}(x,y), & (x,y) \in (\mathcal{I}_i \cap \mathcal{I}_{i+1})^2, \end{cases} \tag{6.3.2}$$

where $\mathfrak{f}(x, y)$ is a smooth function (e.g., a Gaussian or an arctan function) that decays to zero toward the boundary of $\mathcal{I}_i$. This allows us to define the following filtered local covariances

$$\begin{cases} C_1(x,y) = \mathcal{F}_1\left[C(x,y)\right], & x,y \in \mathcal{I}_1, \\ C_i(x,y) = \mathcal{F}_i\left[C(x,y) - C_{i-1}(x,y)\right], & x,y \in \mathcal{I}_i, \quad (i = 2, ..., P-2) \\ C_{P-1}(x,y) = C(x,y) - C_{P-2}(x,y), & x,y \in \mathcal{I}_{P-1}, \end{cases} \tag{6.3.3}$$

As an example, in Figure 6.16 we show the arctan filter applied to a Gaussian covariance function whose domain has been decomposed into three subdomains as in Figure 6.15. More generally, we have

$$C(x,y) = \sum_{i=1}^{P-1} C_i(x,y)\mathbf{1}_{\mathcal{I}_i \times \mathcal{I}_i}, \qquad (x,y) \in \mathcal{D} \times \mathcal{D}. \qquad (6.3.4)$$

Now, the local K-L expansion of $f(x;\omega)$ on $\mathcal{I}_i$ can be computed by using the local covariance function $C_i(x,y)$ as

$$f_i(x;\omega) = \sum_{k=1}^{\infty} \sqrt{\lambda_{k,i}} e_{k,i}(x) \xi_{k,i}(\omega), \quad x \in \mathcal{I}_i, \qquad (6.3.5)$$

where $\lambda_{k,i}$ and $e_{k,i}(x)$ are eigenvalues and (normalized) eigenfunctions of the integral equation

$$\int_{\mathcal{I}_i} C_i(x,\,y) e_{k,i}(x) dx = \lambda_{k,i} e_{k,i}(y).$$

The (uncorrelated) random variables $\xi_{k,i}(\omega)$ can be obtained through projection as

$$\xi_{k,i}(\omega) = \frac{1}{\sqrt{\lambda_{k,i}}} \int_{\mathcal{I}_i} f_i(x;\omega) e_{k,i}(x) dx,$$

Finally, the approximation of the random function $f(x;\omega)$, can be written as a summation of truncated local K-L expansion as

$$f_M(x;\omega) \stackrel{\text{def}}{=} \sum_{i=1}^{P-1} \left(\sum_{k=1}^{M_i} \sqrt{\lambda_{k,i}} e_{k,i}(x) \mathbf{1}_{\mathcal{I}_i} \xi_{k,i}(\omega) \right), \quad x \in \mathcal{D}, \qquad (6.3.6)$$

where M_i is chosen to achieve a prescribed level of accuracy. Thanks to the finite correlation length of $f(x;\omega)$, the number of random variables M_i to represent the process within each subdomain $\mathcal{I}_i$ can be very small (depending on the size of $\mathcal{I}_i$). By using the decomposition (6.3.6), we have that the solution to the stochastic problem (7.0.1) in 1D depends on $(M_{i-1} + M_i)$ random variables on each subdomain $\mathcal{D}_i$. Also,
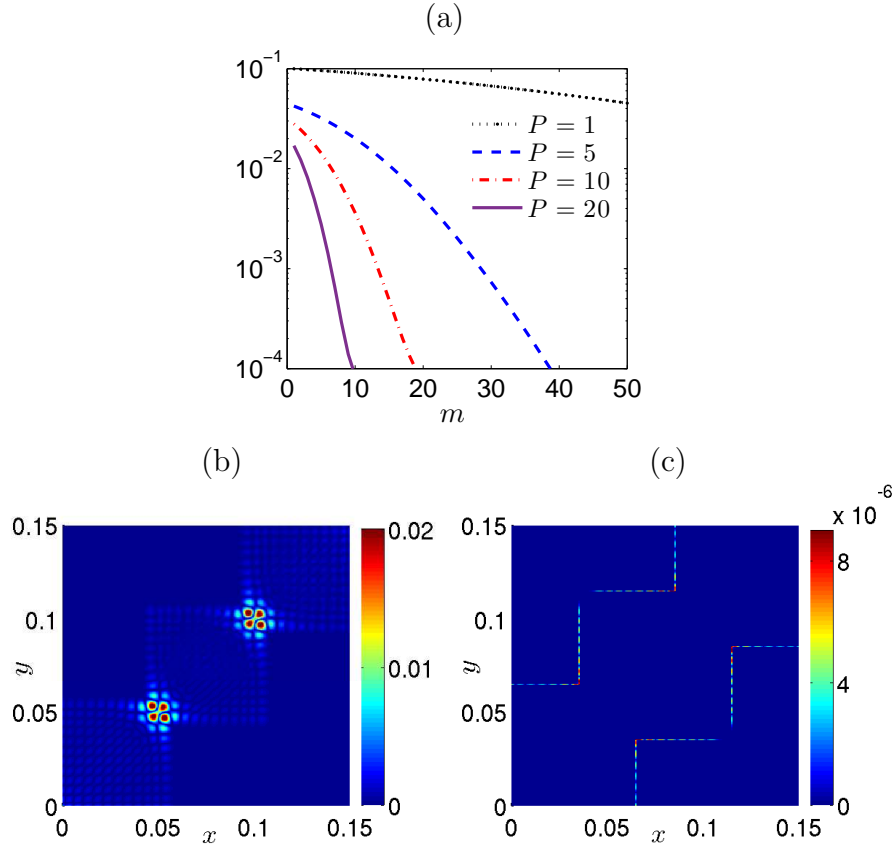
Figure 6.17: L_2 error of the Gaussian covariance with $l_c = 0.008$ by using the decomposed K-L expansion on $\mathcal{I}_i$ with respect to the number of expansion terms k, where P is the number of sub-domains (a). For the case of $P = 20$, the absolute error from the truncation at $k = 10$ on $\cup_i(\mathcal{I}_i \times \mathcal{I}_i)$ (b) and the absolute error on $\cap_i(\mathcal{I}_i \times \mathcal{I}_i)^c$ (c) illustrates ε_i and ε_C, respectively.

$\mathcal{D}_i$ shares M_{i-1} and M_i random variables with its adjacent domains $\mathcal{D}_{i-1}$ and $\mathcal{D}_{i+1}$, respectively.

6.3.2 Convergence Analysis and numerical results

In this section we prove that the local expansion method introduced in section 6.3, preserves the two-point correlation function of the field across different subdomains. To this end, let us compute the error in representing the global covariance function

in terms of local expansions, i.e.,

$$\left\| C(x,y) - \sum_{i=1}^{P-1} C_i(x,y) \mathbf{1}^{(x,y)}_{\mathcal{I}_i \times \mathcal{I}_i} \right\| = \left\| C(x,y) \mathbf{1}^{(x,y)}_{\cap_i (\mathcal{I}_i \times \mathcal{I}_i)^c} \right\| \leq O(\varepsilon_C). \tag{6.3.7}$$

Here ε_C is an upper bound for $C(x,y)$ which depends on the length of the subdomains and the overlapping region. The convergence of the local K-L expansion is given by the usual K-L theorem, provided that the filtered covariance function $C_i(x,y)$ is smooth and positive semi-definite. In fact, the usual L_2 error is obtained as

$$\varepsilon_i^2 \stackrel{\text{def}}{=} \int_{\mathcal{I}_i} \left\langle \left(f_i(x;\omega) - \sum_{k=1}^{M_i} \sqrt{\lambda_{k,i}} e_{k,i}(x) \xi_{k,i}(\omega) \right)^2 \right\rangle dx = \sum_{M_i+1}^{\infty} \lambda_{k,i}, \tag{6.3.8}$$

so that each series can be truncated according to the error of the local eigenspectrum. An upper bound for the error in the covariance function is obtained as

$$
\begin{aligned}
\| C(x,y) - \langle f_M(x;\omega) f_M(y;\omega) \rangle \| &\leq \left\| C(x,y) - \sum_{i=1}^{P-1} C_i(x,y) \mathbf{1}^{(x,y)}_{\mathcal{I}_i \times \mathcal{I}_i} \right\| \\
&+ \left\| \sum_{i=1}^{P-1} C_i(x,y) \mathbf{1}^{(x,y)}_{\mathcal{I}_i \times \mathcal{I}_i} - \left(\sum_{i=1}^{P-1} \sum_{k=1}^{M_i} \lambda_{k,i} e_{k,i}(x) e_{k,i}(y) \mathbf{1}^{(x,y)}_{\mathcal{I}_i \times \mathcal{I}_i} \right) \right\| \\
&\leq \left\| C(x,y) \mathbf{1}^{(x,y)}_{\cap_i (\mathcal{I}_i \times \mathcal{I}_i)^c} \right\| + \left\| \sum_{i=1}^{P-1} \left(C_i(x,y) - \sum_{k=1}^{M_i} \lambda_{k,i} e_{k,i}(x) e_{k,i}(y) \right) \mathbf{1}^{(x,y)}_{\mathcal{I}_i \times \mathcal{I}_i} \right\| \\
&\leq O(\varepsilon_C) + \sum_{i=1}^{P-1} O(\varepsilon_i).
\end{aligned}
$$

The first part is due to domain decomposition while the second part is due to the truncation of the local expansions. If $\mathcal{D}$ is bounded and $C_i(x,y)$ are positive semi-definite, both ε_C and ε_i go to zero. This is proved numerically in Figure 6.17(a), where we plot the the error in the covariance function as the number of subdomains P increases. In this particular example, the covariance function of $f(x;\omega)$ is chosen to be Gaussian with correlation length $l_c = 0.008$. Compared to the global K-L expansion ($P = 1$), the decomposed K-L expansion converges much faster in each

subdomain as we increase P. This is due to the fact that the relative correlation length of the process is much larger when we "zoom-in" with domain decomposition (see Figure 6.13). This implies that the local K-L expansion requires a smaller number of random variables to achieve the same level of accuracy, making the algorithm suitable for parallel implementation. However, if we keep increasing the number of subdomains, $\cup_i(\mathcal{I}_i \times \mathcal{I}_i)$ will not be sufficient to cover the whole domain and ε_C will increase. The absolute errors arising from the truncation and the restricted covariance function are plotted in Figure 6.17(b,c) for $P = 20$ and $\rho = 0.03$ by using $M = 10$ terms. We observe that ε_C is still small and it is dominated by the truncation error ε_i.

6.4   Summary

In this chapter, we proposed two different methods to represent multi-correlated non-stationary stochastic processes. The first method (muKL) is based on the spectral decomposition of a suitable *assembled process* and yields series expansions in terms an identical set of *uncorrelated* random variables. A similar strategy has been proposed in the context of functional principal component analysis by [156]. The second method (mcKL) relies on expansions in terms of *correlated* sets of random variables reflecting the cross-covariance structure of the processes. In some sense, muKL can be regarded as a combination of KL expansion and orthogonal polynomial methods [225]. A similar idea was developed independently by [202], but the method is restricted to the case where the auto-covariances are identical. We demonstrated the effectiveness and the computational efficiency of the proposed algorithms through numerical examples involving Gaussian processes with exponential and Gaussian covariances as well as fractional Brownian motion and Brownian bridge processes. We found that muKL usually provides better accuracy and convergence rates but it

is computationally more expensive than mcKL. The latter approach yields scalable algorithms and it can be applied to cases where the sets of random variables in each process are different. We used muKL and mcKL approaches to model and simulate cross-correlated random processes in a stochastic tumor model and found that the response of the system is significantly affected by the cross-correlation structure of the noise. More general applications to systems driven by multiple correlated processes such those arising in the the stochastic modeling of materials and devices can be readily done.

The effectiveness and the computational efficiently of both methods is discussed in section 6.2 with an application of muKL to a tumor growth model driven by two mutually correlated stochastic processes.

Chapter 7

Stochastic domain decomposition

In this chapter, we propose two different stochastic decomposition methods, based on conditional moment (section 7.1.1) and PDE-constrained (section 7.1.2) interfacing conditions. In section 7.2, we apply the proposed algorithms to a wide range of stochastic problems. Specifically, we consider stochastic elliptic problems (section 7.2.1), stochastic advection of scalar fields (section 7.2.2) and nonlinear advection-reaction problems (section 7.2.3). In addition, the interface methods are employed to couple distinct PDF models in section 7.3. This PDF decomposition method is applied to the advection-reaction problem (section 7.3.2).

To this end, we first recall the classical procedure of domain decomposition based on deterministic Schwarz algorithm and subsequently propose stochastic extensions where uncertainty is involved. We consider a nonlinear stochastic PDE system in the form,

$$
\begin{cases}
N(x, t, u(x, t; \omega); \omega) = f(x, t; \omega) & x \in \mathcal{D}, \\
B(u(x, t; \omega)) = g(x, t; \omega) & x \in \partial\mathcal{D},
\end{cases}
\tag{7.0.1}
$$

where $\mathcal{D} \subseteq \mathbb{R}^d$ is a bounded spatial domain with boundary $\partial\mathcal{D}$, N is a nonlinear operator, B is a boundary operator, and ω denotes an element of the sample space Ω. We assume that the initial/boundary value problem (7.0.1) is well posed for

Diffusion	$N(x,t,u;\omega) = \nabla a(x;\omega) \cdot \nabla u + a(x;\omega)\nabla^2 u$
Advection	$N(x,t,u;\omega) = \dfrac{\partial u}{\partial t} + V(x;\omega)\nabla u$
Advection-Reaction	$N(x,t,u;\omega) = \dfrac{\partial u}{\partial t} + V(x)\nabla u - k(x;\omega)(1-u^2)$

Table 7.1: Examples of nonlinear operators N appearing in Eq. (7.0.1). These equations are studied numerically in section 7.2 by using the new stochastic domain decomposition algorithms proposed in section 7.1.1 and section 7.1.2.

every realization of the random forcing term, random boundary and random initial condition. Examples of N are given in table 7.1 The domain $\mathcal{D}$ is decomposed into an a set of P *overlapping domains* $\{\mathcal{D}_1, ..., \mathcal{D}_P\}$ such that

$$\overline{\mathcal{D}} = \bigcup_{i=1}^{P} \overline{\mathcal{D}}_i. \tag{7.0.2}$$

where the overline denotes the closure set, i.e., $\overline{\mathcal{D}} = \mathcal{D} \cup \partial\mathcal{D}$. Let Γ_i be the boundary of $\mathcal{D}_i$ lying in the interior of $\mathcal{D}$, and let $\mathcal{N}_i$ be the index set of the neighboring domains, i.e.,

$$\Gamma_i \overset{\text{def}}{=} \partial\mathcal{D}_i \setminus \partial\mathcal{D}, \qquad \mathcal{N}_i \overset{\text{def}}{=} \{1 \leq j \leq P \,|\, \mathcal{D}_j \cap \mathcal{D}_i \neq \emptyset\}.$$

For example, in one-dimensional spatial domains we have $\mathcal{N}_1 = \{2\}$, $\mathcal{N}_i = \{i-1, i+1\}$ $(1 < i < P)$, and $\mathcal{N}_P = \{P - 1\}$. In this chapter we assume that $\{\mathcal{D}_i\}_{i=1}^{P}$ is an *overlapping covering* of $\mathcal{D}$, so that we can impose Dirichlet boundary condition when performing Schwarz iterations. More general boundary conditions of Robin-type can be implemented as well, e.g., in the context of optimized Schwarz algorithms (see section 7.1).

A classical domain decomposition method for the SPDE (7.0.1) is summarized

begin

    $n = 1$;

    initialize $\{u_i^0\}_{i=1}^P$ at random;

    while $\left\| u^{n-1} - u^n \right\|_{x \in \mathcal{D}} > \varepsilon$ *or* $\left\| u_i^n - u_j^n|_{j \in \mathcal{N}_i} \right\|_{x \in \Gamma_i} > \varepsilon$ **do**

        for $1 \leq i \leq P$ **do**

          solve

$$
\begin{aligned}
N_i(x, t, u_i^n(x, t; \omega); \omega) &= f_i(x, t; \omega), & x \in \mathcal{D}_i, \\
B(u_i^n(x, t; \omega)) &= g(x, t; \omega), & x \in \partial \mathcal{D}_i \setminus \Gamma_i, \quad (7.0.3) \\
B(u_i^n(x, t; \omega)) &= \widetilde{g}(x, t; \omega), & x \in \Gamma_i,
\end{aligned}
$$

        end

        $n = n + 1$;

    end

end

Algorithm 2: Domain decomposition with overlapping domains.

in Algorithm 2. At the n-th iteration, the algorithm consists of P substeps in which we solve the restricted PDE system on $\mathcal{D}_i$ $(i = 1, ..., P)$, where N_i and f_i are the restrictions of N and f on $\mathcal{D}_i$. The *artificial boundary condition* $\widetilde{g}$ on Γ_i is taken from the solution among the neighboring domains $\{\mathcal{D}_j\}_{j \in \mathcal{N}_i}$ at previous iteration, that is, $\{ u_j^m|_{\Gamma_i} : j \in \mathcal{N}_i, m = n - 1 \text{ or } n\}$. Within each iteration, the local system must be solved in a predetermined sequence $\{j_k\}_{k=1}^P$, and if $u_j^n|_{\Gamma_i}$ is not available for $\widetilde{g}$, we use $u_j^{n-1}|_{\Gamma_i}$ from the previous iteration. This completes the description of the domain decomposition algorithm in the spatial domain. But how do we solve the stochastic problem in the decomposed domain $\{\mathcal{D}_1, ..., \mathcal{D}_P\}$? The first step is to represent the stochastic solution to (7.0.1) or (7.0.3) appropriately. This is a crucial step in stochastic domain decomposition, as local stochastic expansions usually do not preserve global multi-point statistical properties (see section 6.3). If we follow a naive approach, we can simply discretize (7.0.1), e.g., in terms of probabilistic collocation [60, 61, 130], polynomial chaos [204, 213], or reduced basis methods [54], and then apply the domain decomposition algorithm 2, say to each sample of (7.0.1). Although this might have advantages in parallel computations [53],

it does not overcome the dimensionality problem of the random space. Indeed, a global stochastic approach applied to (7.0.1) does not exploit the low-dimensional stochastic structure of the local solution within each subdomain $\mathcal{D}_i$. Such low-dimensional structure is a consequence of the finite correlation lengths of the solution field.

Thus, our goal is to develop new SDD algorithms that exploit the advantages of both domain decomposition in spatial domain as well as low-dimensional stochastic structures of the solution within each subdomain. These methods are based on a local representation of the stochastic solution, which is chosen to preserve multipoint statistical properties across different domains.

7.1 Interfacing Subdomains

The choice of the interface condition between different subdomains is an *open question* in stochastic domain decomposition methods. No rigorous theory has yet been developed for interfaces defined in terms of *functionals* of a stochastic field, e.g., mean, variance or multi-point correlations, although this is of fundamental importance when we are interested in propagating uncertainty across different subdomains efficiently. Indeed, interfacing the whole stochastic field, e.g., through Monte Carlo or sparse collocation approaches [53, 54] is prohibitively expensive, since the interface operator (e.g., Schwarz iterations) has to be applied to each sample. On the other hand, if we interface only *low-dimensional functionals* of the stochastic solution, e.g., few statistical moments, then we obtain a tremendous reduction in computational cost at the expense of an accuracy loss. In this section we propose two new SDD algorithms that exploit this basic idea, i.e., interfacing only low-dimensional functionals of the solution in different subdomains. Specifically, the first algorithm uses an interface condition between subdomains defined in terms of a set of *conditional*

moments (section 7.1.1) . The second algorithm, on the other hand, simultaneously interfaces multiple functionals of the stochastic solution, such as the first few statistical moments, by using PDE-*constrained optimization* (section 7.1.2). The accuracy of both methods is assessed section 7.2.

7.1.1 Conditional Moment Interface Method

Our first algorithm is based on interfacing moments or cumulants of the stochastic solution across different subdomains by using Schwarz methods. These are well-established for deterministic problems and convergence results can be found in several books [98, 154, 173, 187], and reviews [215, 216]. For example, it has been found that the convergence rate of the classical Schwarz method is rather slow and very much dependent on the extent of the overlap between different subdomains. To overcome these drawbacks, new classes of Schwarz methods were proposed in recent years, e.g., optimized Schwarz methods. These new algorithms are based on a more effective transmission of information at interfaces between subdomains. For instance, Robin-Robin conditions [69] and conditions expressed in terms on *non-local* operators [42, 66, 67, 79] can yield convergence without overlap.

In the conditional moment interface method, we set the interface condition between different subdomain by using conditional statistical moments, which can be easily computed by using the random variables representing the K-L expansion in the overlapping region. We denote such random variables as $\boldsymbol{\xi}_i = (\xi_{i,1}, \cdots, \xi_{i,M_i})$ and the aforementioned conditional average as

$$\langle u(x; \boldsymbol{\xi}_j, \boldsymbol{\xi}_i) | \boldsymbol{\xi}_i \rangle \overset{\text{def}}{=} \int_{\Xi_j} u(x; \boldsymbol{a}_j, \boldsymbol{a}_i) p_{\boldsymbol{\xi}_j | \boldsymbol{\xi}_i}(\boldsymbol{a}_j | \boldsymbol{a}_i) d\boldsymbol{a}_j,$$

where $p_{\boldsymbol{\xi}_j | \boldsymbol{\xi}_i}(\boldsymbol{a}_j | \boldsymbol{a}_i)$ is the probability density of $\boldsymbol{\xi}_j$ given $\boldsymbol{\xi}_i$ The boundary condition

in Eq. (7.0.3) that preserves the k-th conditional moment can be expressed as

$$\left\langle u_i^n(x;\omega)^k \big| \boldsymbol{\xi}_j \right\rangle = \left\langle \widetilde{g}(x;\omega)^k \big| \boldsymbol{\xi}_j \right\rangle, \qquad x \in \Gamma_i, \quad j = i-1 \text{ or } i. \tag{7.1.1}$$

Clearly, the stochastic solution satisfying such boundary condition is not unique. One simple idea is to impose the same conditional mean for fixed $\boldsymbol{\xi}_i$ over all collocation points of $\boldsymbol{\xi}_{i+1}$, i.e.,

$$\widetilde{g}(x;\cdot,\boldsymbol{\xi}_i) = \left\langle u_{i+1}^{n-1}(x;\boldsymbol{\xi}_i,\boldsymbol{\xi}_{i+1}) \big| \boldsymbol{\xi}_i \right\rangle. \tag{7.1.2}$$

Although this scheme satisfies Eq. (7.1.1) for $k = 1$, we found out that it dissipates excessively the variance at the boundary. Thus, we propose hereafter several corrections in order to mitigate this effect and achieve better accuracy for higher-order moments.

To this end, we first introduce the *mean-shifted boundary condition*, which basically sets the mean of the solution at the subdomain boundaries to be coincident with the mean computed from the adjacent subdomain. The following boundary condition is then imposed

$$\widetilde{g}_i^n[1](x;\boldsymbol{\xi}_{i-1},\boldsymbol{\xi}_i) \overset{\text{def}}{=} u_i^{n-1}(x;\boldsymbol{\xi}_{i-1},\boldsymbol{\xi}_i) - \left\langle u_i^{n-1}(x;\boldsymbol{\xi}_{i-1},\boldsymbol{\xi}_i) \big| \boldsymbol{\xi}_i \right\rangle$$
$$+ \left\langle u_{i+1}^{n-1}(x;\boldsymbol{\xi}_i,\boldsymbol{\xi}_{i+1}) \big| \boldsymbol{\xi}_i \right\rangle. \tag{7.1.3}$$

Note that (7.3.3) satisfies Eq. (7.1.1) for $k = 1$, and at the same time it does not affect the variance of the solution within the subdomain. This overcomes the variance dissipation arising from the simpler boundary condition (7.1.2). A further improvement of the interface condition can be obtained by using second-order statistical properties. We shall call it *variance scaling boundary condition*, and it relies

in setting

$$\widetilde{g}_i^n[2](x;\boldsymbol{\xi}_{i-1},\boldsymbol{\xi}_i) \overset{\text{def}}{=} \left(u_i^{n-1}(x;\boldsymbol{\xi}_{i-1},\boldsymbol{\xi}_i) - \left\langle u_i^{n-1}(x;\boldsymbol{\xi}_{i-1},\boldsymbol{\xi}_i)\big|\boldsymbol{\xi}_i\right\rangle\right)\frac{\sigma_{i+1}^{n-1}}{\sigma_i^{n-1}}$$
$$+ \left\langle u_{i+1}^{n-1}(x;\boldsymbol{\xi}_i,\boldsymbol{\xi}_{i+1})\big|\boldsymbol{\xi}_i\right\rangle, \qquad (7.1.4)$$

where σ_i^{n-1} and σ_{i+1}^{n-1} are standard deviations defined as

$$\sigma_i^n(x;\boldsymbol{\xi}_{i-1},\boldsymbol{\xi}_i|\boldsymbol{\xi}_i) \overset{\text{def}}{=} \left[\langle u_i^n(x;\boldsymbol{\xi}_{i-1},\boldsymbol{\xi}_i)|\boldsymbol{\xi}_i)^2\rangle - \langle u_i^n(x;\boldsymbol{\xi}_{i-1},\boldsymbol{\xi}_i)|\boldsymbol{\xi}_i)\rangle^2\right]^{1/2}.$$

Note that this condition satisfies Eq. (7.1.1) for both $k = 1$ and 2, but it may lead to unstable Schwarz iterations due to the division by σ_i^n. To avoid such instabilities, we combine (7.3.3) and (7.3.4) into one Algorithm. This yields the conditional moment interface method whose steps are summarized in Algorithm 3 for two domains $\mathcal{D}_1$ and $\mathcal{D}_2$. In such algorithm $\widetilde{g}_r^n[1](x;\omega) = \widetilde{g}_1^n[1](x;\boldsymbol{\xi}_1,\boldsymbol{\xi}_2)$, $\widetilde{g}_r^n[2](x;\omega) = \widetilde{g}_1^n[2](x;\boldsymbol{\xi}_1,\boldsymbol{\xi}_2)$, and the left-end boundary conditions for $\mathcal{D}_2$ are

$$\widetilde{g}_l^n[1](x;\omega) \overset{\text{def}}{=} u_2^{n-1}(x;\boldsymbol{\xi}_2,\boldsymbol{\xi}_3) - \left\langle u_2^{n-1}(x;\boldsymbol{\xi}_2,\boldsymbol{\xi}_3)\big|\boldsymbol{\xi}_2\right\rangle + \left\langle u_1^n(x;\boldsymbol{\xi}_1,\boldsymbol{\xi}_2)|\boldsymbol{\xi}_2\right\rangle,$$
$$\widetilde{g}_l^n[2](x;\omega) \overset{\text{def}}{=} \left(u_2^{n-1}(x;\boldsymbol{\xi}_2,\boldsymbol{\xi}_3) - \left\langle u_2^{n-1}(x;\boldsymbol{\xi}_2,\boldsymbol{\xi}_3)\big|\boldsymbol{\xi}_2\right\rangle\right)\frac{\sigma_2^{n-1}}{\sigma_1^n} + \left\langle u_1^n(x;\boldsymbol{\xi}_1,\boldsymbol{\xi}_2)|\boldsymbol{\xi}_2\right\rangle.$$

We start the iterative sequence by using the mean boundary condition (7.3.3), and iterate until a prescribed tolerance ϵ in achieved on the residual

$$\|u^{n^*}(x;\omega) - u^{n^*-1}(x;\omega)\|/\|u^{n^*-1}(x;\omega)\| < \epsilon$$

We call n^* the transition iteration, ϵ the transition threshold, and denote the computed boundary condition as $\widetilde{g}_i^{n^*}[1](x;\boldsymbol{\xi}_{i-1},\boldsymbol{\xi}_i)$. After the transition iteration, we

begin

    $n = 1$;

    initialize $\{u_i^0\}_{i=1}^2$ at random;

    while $\|u^{n-1} - u^n\|_{x \in \mathcal{D}} > \varepsilon$ *or* $\|u_1^n - u_2^n\|_{x \in \mathcal{D}_1 \cap \mathcal{D}_2} > \bar{\varepsilon}$ **do**

        solve

$$
\begin{aligned}
N_1(x, t, u_1^n(x,t;\omega); \omega) &= f_1(x,t;\omega), & x \in \mathcal{D}_1; \\
B(u_1^n(x,t;\omega)) &= g(x,t;\omega), & x \in \partial\mathcal{D}_1 \setminus \Gamma_1;
\end{aligned}
$$

$$
\begin{aligned}
N_2(x, t, u_2^n(x,t;\omega); \omega) &= f_2(x,t;\omega), & x \in \mathcal{D}_2; \\
B(u_2^n(x,t;\omega)) &= g(x,t;\omega), & x \in \partial\mathcal{D}_2 \setminus \Gamma_2;
\end{aligned}
$$

        if $\|u^{n-1} - u^n\|_{x \in \mathcal{D}} > \epsilon$ **then**

            $B(u_1^n(x,t;\omega)) = \widetilde{g}_r^n[1](x,t;\omega), \quad x \in \Gamma_1$

            $B(u_2^n(x,t;\omega)) = \widetilde{g}_l^n[1](x,t;\omega), \quad x \in \Gamma_2$

            $n^* = n$

        else

            $B(u_1^n(x,t;\omega)) = w\widetilde{g}_r^{n*}[1](x,t;\omega) + (1-w)\widetilde{g}_r^n[2](x,t;\omega), \quad x \in \Gamma_1$

            $B(u_2^n(x,t;\omega)) = w\widetilde{g}_l^{n*}[1](x,t;\omega) + (1-w)\widetilde{g}_l^n[2](x,t;\omega), \quad x \in \Gamma_2$

        end

        $n = n + 1$;

    end

end

Algorithm 3: Conditional moment interface method.

switch the boundary condition to the following weighted one

$$u_i^n(x; \boldsymbol{\xi}_{i-1}, \boldsymbol{\xi}_i) = w\widetilde{g}_i^{n^*}[1](x; \boldsymbol{\xi}_{i-1}, \boldsymbol{\xi}_i) + (1 - w)\widetilde{g}_i^n[2](x; \boldsymbol{\xi}_{i-1}, \boldsymbol{\xi}_i), \qquad (7.1.5)$$

where $w \in [0, 1]$, is the weight between the converged solution from the mean shifting boundary condition and the new solution from variance scaling. Note that the condition (7.1.5) is equivalent to the mean shifting condition (7.3.3) in the limit $w \to 1$.

7.1.2 PDE-Constrained Interface Method

An alternative method to preserve statistical properties of the solution across different domains relies on optimization. In practice, we minimize suitable (nonlinear) functionals measuring the error of the random solution at the boundary of different overlapping domains. In each subdomain $\mathcal{D}_i$ we solve local problem (7.0.3), while the boundary conditions $\tilde{\boldsymbol{g}} = (\tilde{g}_1, \tilde{g}_2, \cdots, \tilde{g}_n)$ are stochastic and usually unknown. By using a PDE-constrained optimization method, we can set an interface condition between different subdomain that preserves continuity of the first k statistical moments or cumulants. To this end, we first define the object function

$$\mathcal{J}(\tilde{\boldsymbol{g}}) = \sum_{i=1}^{n-1}\sum_{r=1}^{R} \|\mu_r(u_i(x, t; \tilde{g}_i)\mathbf{1}_{\mathcal{D}_i \cap \mathcal{D}_{i+1}}) - \mu_r(u_{i+1}(x, t; \tilde{g}_{i+1})\mathbf{1}_{\mathcal{D}_i \cap \mathcal{D}_{i+1}})\|_2, \qquad (7.1.6)$$

where $\|\cdot\|_2$ is the L^2 norm on physical space, and μ_r is defined as

$$\mu_r(u) = \begin{cases} \langle u \rangle, & r = 1, \\ \langle (u - \langle u \rangle)^r \rangle, & r > 1. \end{cases} \qquad (7.1.7)$$

Then we solve the PDE-constrained optimization problem

$$\min_{\tilde{\boldsymbol{g}}} \mathcal{J}(\tilde{\boldsymbol{g}}) \qquad \text{s.t.} \qquad \text{Eq. (7.0.3) holds.} \qquad (7.1.8)$$

Note that in each subdomain $\mathcal{D}_i$ the solution u_i is determined by $f_i, \tilde{g}_i$ and N_i. Therefore, given f_i and N_i, the solver in each D_i is a mapping $F_i : \tilde{g}_i \mapsto u_i$. Since $\tilde{g}_i$ is a random variable, we can represent it in a gPC expansion and identify its coefficients or identify the value of $\tilde{g}_i$ at specific collocation points. More specifically, if $\tilde{g}$ is represented by the gPC expansion

$$\tilde{g}_i = \sum_m^{M_i} c_{im} \psi_{im}(x),$$

then Eq.(7.1.6) can be rewritten as

$$\mathcal{J}(\boldsymbol{c}_1, \boldsymbol{c}_2, \cdots, \boldsymbol{c}_n) = \sum_{i=1}^{n-1} \sum_{r=1}^{R} \|\mu_r(u_i(x, t; \boldsymbol{c}_i) \mathbf{1}_{\mathcal{D}_i \cap \mathcal{D}_{i+1}}) - \mu_r(u_{i+1}(x, t; \boldsymbol{c}_{i+1}) \mathbf{1}_{\mathcal{D}_i \cap \mathcal{D}_{i+1}})\|_2,$$
$$(7.1.9)$$

where $\boldsymbol{c}_i = (c_{i,1}, c_{i,2}, \cdots, c_{i,M_i})$. Note that here we build a mapping in each subdomain as $F^\dagger : \boldsymbol{c}_i \mapsto u_i$. Similarly, if we track the value of $\tilde{g}_i$ at collocation points $\boldsymbol{s}_i = (s_{i,1}, s_{i,2}, \cdots, s_{i,Z_i})$, we can find a mapping from the samples of $\tilde{g}_i$ to the moments of u_i, i.e., $F^* : \boldsymbol{s}_i \mapsto \mu_r(u_i)$. This allows us to minimize $\mathcal{J}$ with respect to $\boldsymbol{s}$:

$$\mathcal{J}(\boldsymbol{s}_1, \boldsymbol{s}_2, \cdots, \boldsymbol{s}_n) = \sum_{i=1}^{n-1} \sum_{r=1}^{R} \|\mu_r(u_i(x, t; \boldsymbol{s}_i) \mathbf{1}_{\mathcal{D}_i \cap \mathcal{D}_{i+1}}) - \mu_r(u_{i+1}(x, t; \boldsymbol{s}_{i+1}) \mathbf{1}_{\mathcal{D}_i \cap \mathcal{D}_{i+1}})\|_2,$$
$$(7.1.10)$$

The object function can also take the weighted form

$$\mathcal{J}(\tilde{\boldsymbol{g}}) = \sum_{i=1}^{n-1} \sum_{r=1}^{R} w_r \|\mu_r(u_i(x, t; \tilde{g}_i) \mathbf{1}_{\mathcal{D}_i \cap \mathcal{D}_{i+1}}) - \mu_r(u_{i+1}(x, t; \tilde{g}_{i+1}) \mathbf{1}_{\mathcal{D}_i \cap \mathcal{D}_{i+1}})\|_2, \quad (7.1.11)$$

to account for possible different magnitudes in the statistical moments or cumulants.

The SPDE-constrained optimization algorithm is summarized in Algorithm 4.

begin
    1. Initialize $\boldsymbol{c}_i$ with the results of deterministic problem. ;
    2. Prepare SPDE solver in each subdomain $\mathcal{D}_i$, i.e., set the mapping $F^{\dagger} : \boldsymbol{c}_i \mapsto u_i$. ;
    3. Set object function $\mathcal{J}(\boldsymbol{c}_1, \boldsymbol{c}_2, \cdots, \boldsymbol{c}_n)$ in 7.1.2 and choose appropriate weights w_r defining the weighted norm, if necessary. ;
    4. Solve the optimization problem $\min \mathcal{J}(\boldsymbol{c}_1, \boldsymbol{c}_2, \cdots, \boldsymbol{c}_n)$ with constraint Eq. (7.0.3).
end

Algorithm 4: PDE-constrained interface method.

7.2 Numerical Results

In this section we apply the stochastic domain decomposition algorithms proposed in section 7.1.1 and section 7.1.2 to different stochastic problems. Specifically, we consider elliptic problems with random diffusion coefficients, advection problems for scalar fields with random advection velocity, and nonlinear advection-reaction problems with random reaction rate (see Table 7.1).

7.2.1 Stochastic Elliptic Problem

Let us consider the stochastic elliptic problem

$$-\frac{d}{dx}\left(a(x;\omega)\frac{du(x;\omega)}{dx}\right) = \sin(2\pi x) \qquad u(0;\omega) = u(1;\omega) = 0 \qquad x \in [0,1],$$
$$(7.2.1)$$

where the diffusion coefficient $a(x;\omega)$ is assumed to be a random process satisfying

$$\langle a(x;\omega)\rangle = 1, \qquad \text{Cov}\{a(x;\omega), a(y;\omega)\} = \sigma_a^2 \exp\left[-\frac{|x-y|^2}{l_c^2}\right]. \qquad (7.2.2)$$

In particular, we study constant as well as variable correlation lengths l_c, as in Figure 6.15(c,d). The stochastic problem (7.2.1) has been extensively studied in the past by using different methods, e.g., stochastic collocation or Wick-Malliavin approximations [6, 200]. Recently, Elman *et al.* [53, 54] proposed a domain decomposition method in spatial domain and reduced basis collocation in stochastic space to solve (7.2.1). Such approach was shown to be effective, but it does not exploit the relation between the correlation length of the random diffusivity and the domain decomposition. Hereafter we follow our new approach that has such property, and demonstrate its effectiveness. To this end, we consider the following overlapping covering of the spatial domain $[0, 1]$ in terms of two subdomains $\{\mathcal{D}_1, \mathcal{D}_2\}$. By using our local K-L expansion method (section 6.3), we embed the random function $a(x; \omega)$ into the set of subdomains $\mathcal{I}_i$ shown in Figure 6.15(a,b). This yields a set of sub-processes in the form (6.3.5), which allows us to construct *local* reduced-order stochastic representations of $a(x; \omega)$ preserving second-order statistical properties (see section 6.3.2). Specifically, we assume that the random variables $\boldsymbol{\xi}_i(\omega)$ are uniform in $[-1, 1]$ on each $\mathcal{I}_i$, and that $\sigma_a = 0.2$ in (7.2.2). The solution on $\mathcal{D}_i$ can be written as $u^i(x; \omega) = u^i(x; \boldsymbol{\xi}_i(\omega), \boldsymbol{\xi}_{i+1}(\omega))$; $\boldsymbol{\xi}_2(\omega)$ are the random variables shared between the sub-domains. The spatial domain $\mathcal{D}$ is discretized by using 10 spectral elements of order 10, and we consider a probabilistic collocation method (tensor product or sparse grid) for the random space.

In Figure 7.1 we compare the first four moments computed by the global K-L and the decomposed K-L expansion for random diffusion coefficients $a(x; \omega)$ with variable correlation length. The domain decomposed solution is computed by using the SDD algorithm with mean boundary condition (SDD-M) - Eq. (7.3.3). We have found that although we are interfacing the subdomain $\mathcal{D}_1$ and $\mathcal{D}_2$ only through the mean field, the decomposed solution basically coincides with the global one just after few iterations. Specifically, the result of Figure 7.1 are obtained at the fourth iteration.
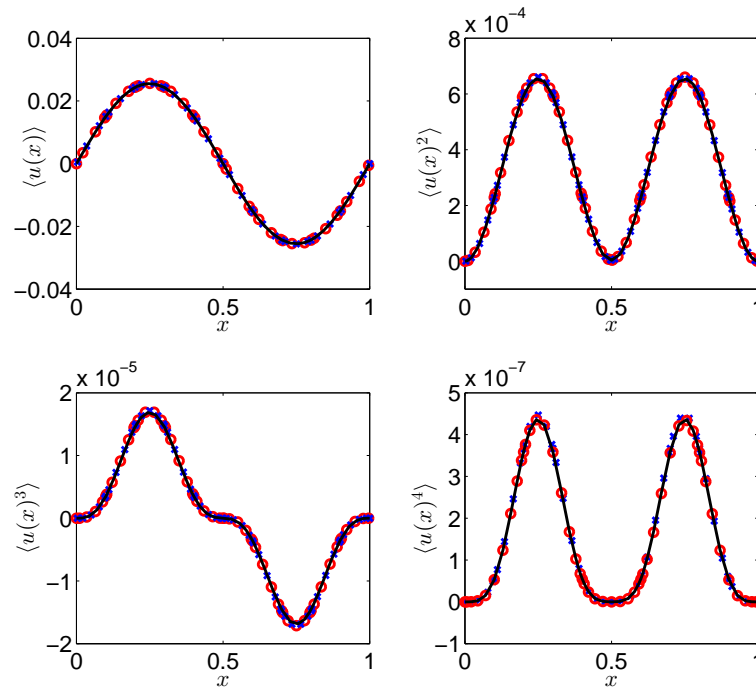
Figure 7.1: Stochastic elliptic problem. Statistical moments of the solution corresponding to random diffusion coefficients with variable correlation length. Reference solution (black line); Results from the conditional moment (SDD-M) interface method (red circles) and the PDE-constrained interface method (blue x). It is seen that the solution computed by the proposed domain decomposition methods is accurate.
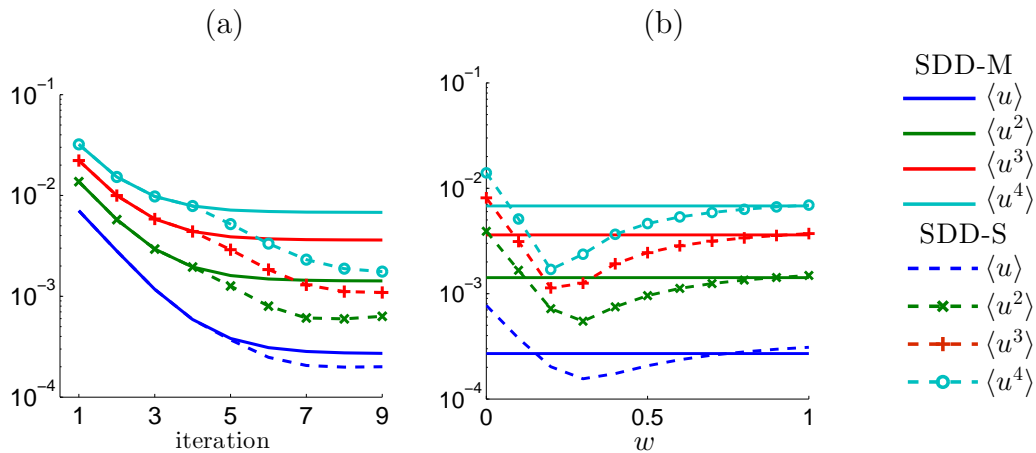
Figure 7.2: Stochastic elliptic problem. (a) Relative L_2 error in the first four moments as computed by the conditional mean (SDD-M) and conditional standard deviation (SDD-S) algorithms with $w = 0.2$ and $\epsilon = 10^{-3}$. (b) Relative error versus the weight w for fixed $\epsilon = 10^{-4}$. It is seen that the SDD-S algorithm improves the accuracy of higher-order statistical moments in the range $0.2 \leq w \leq 0.5$.
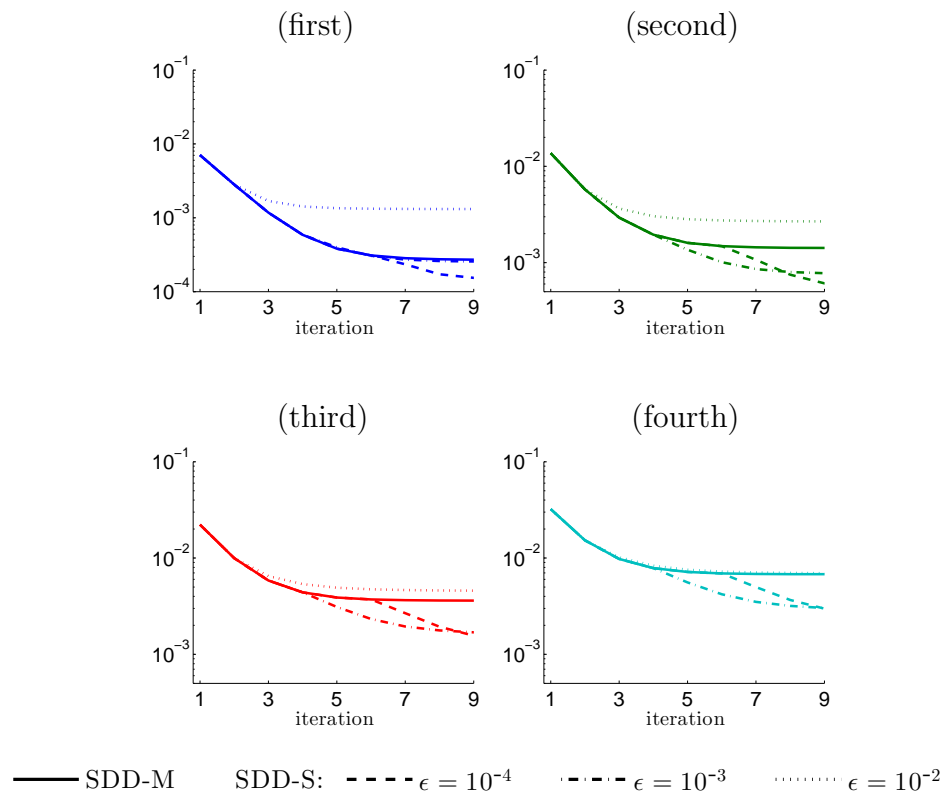
Figure 7.3: Stochastic elliptic problem. Relative L_2 error in the first four moments (a-d) for different transition thresholds ϵ. The threshold determines the accuracy and number of iteration for convergence, hence, it must be selected by taking into account the target error level.

error in $\langle u^k \rangle$	$k = 1$	$k = 2$	$k = 3$	$k = 4$
Decomposed K-L	9.1666e-05	1.5549e-04	1.8446e-04	1.8044e-04
Conditional moment method	2.9514e-04	1.0076e-03	1.7654e-03	2.8584e-03
PDE-constrained method	7.4173e-04	2.9523e-03	4.7312e-03	7.7749e-03

Table 7.2: Stochastic elliptic problem. Relative L_2 errors in the first four statistical moments and the standard deviation of the solution computed by using the conditional moment and the PDE-constrained interface methods. The decomposed K-L method provides the lower bound for relative error that we can achieve in this case by using the domain decomposition algorithm.

Convergence of Schwarz iterations obtained by using the mean field interface method (SDD-M) - Eq. (7.3.3) - and the standard deviation interface method (SDD-S) - Eq. (7.1.5) - is shown in Figure 7.2(a), for $w = 0.2$ and $\epsilon = 10^{-3}$. It is seen that the L_2 error in the fourth moment, which is the largest one, becomes less than 1% after the third iteration. Also, the SDD-S method turns out to be more accurate that SDD-M, most likely because it takes advantage of higher-order statistical information. We have also performed convergence studies in terms of other parameters appearing in the conditional moment interface method, in particular the transition threshold ϵ and w. The results are summarized in Figure 7.2(b) and Figure 7.3. In particular, in Figure 7.2(b) we plot the L_2 error of the SDD solution versus w for fixed $\epsilon = 10^{-4}$. It is seen that there exist an optimal value of w lying near $w = 0.2$, which coincides with the magnitude of the noise σ_a. Thus, a good choice for w is the ratio between the mean $\langle a(x; \omega) \rangle$ and σ_a. Also, as we mentioned in section 7.1.1, in the limit $w \to 1$ the SDD-S method is equivalent to SDD-M (note that the error plots are superimposed for $w = 1$). The effects of the transition threshold on the convergence of Schwarz iterations is shown in Figure 7.3 for $\epsilon = 10^{-2}$, 10^{-3}, and 10^{-4}. We found that the solution computed with smaller ϵ is more accurate but it exhibits a slower convergence rate. Thus, ϵ determines both accuracy and convergence of the Schwarz

(a) (b)
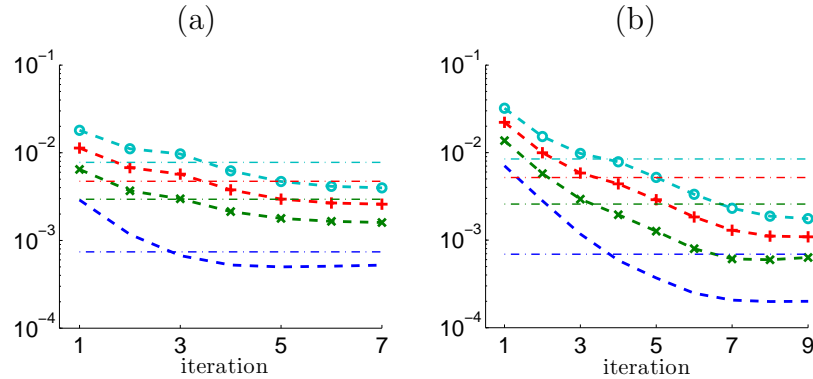
Figure 7.4: Stochastic elliptic problem. Comparison between the relative L_2 errors of the conditional moment interface method (–) and the PDE-constrained interface method (-) for constant $l_c = 0.08$ (a) and variable l_c (b). The conditional moment interface methods is more accurate than the PDE-constrained interface method, and it requires less computational time.

iterations. The errors using $\epsilon = 10^{-2}$ are the largest, but still bounded by 10^{-2}. In Table 7.2 and Figure 7.4 we compare the relative L_2 errors obtained by using the conditional moment and PDE-constrained interface methods. Specially, we consider the problem (7.2.1) with random diffusion coefficient of correlation length $l_c = 0.08$. In all cases, it is seen that the conditional moment interface method is more accurate than the PDE-constrained interface method, and it also has a lower computational cost (see section 7.4). In addition, the error in the standard deviation computed by the SDD-S method is $3.4992 \cdot 10^{-2}$, while in the PDE-constrained method we obtain $1.20202 \cdot 10^{-1}$.

Extension to Multiple Subdomains So far we solved the stochastic elliptic problem (7.2.1) in an overlapping covering with of $[0, 1]$ with only two subdomains $\mathcal{D}_1$ and $\mathcal{D}_2$. Now we consider the extension of the SDD algorithms to multiple subdomains $\{\mathcal{D}_1, ..., \mathcal{D}_P\}$ and $\{\mathcal{I}_1, ..., \mathcal{I}_{P+1}\}$, with $P = 5$, 10 or 20. In particular, we set

$$\mathcal{D}_i = [x_{i-1} - \delta', x_i + \delta'], \qquad \mathcal{I}_i = [x_{i-1} + \rho', x_{i+1} - \rho'], \qquad (7.2.3)$$

P	1	5	10	20
$\|\mathcal{I}_i\|$	1	0.2	0.1	0.05
M_i	119	23	12	6

Table 7.3: Stochastic elliptic problem. Length of $\mathcal{I}_i$ and number of random variables M_i in the local K-L expansion within each $\mathcal{I}_i$ as a function of the total number of subdomains P. Here M_i is determined by setting a threshold of 5% in the error of the second order moment computed by the truncated K-L series.

where $\{x_i\}_{i=0}^{P}$ are points in $[0, 1]$, while δ' and ρ' are positive numbers determining the overlapping region (See Figure 6.14). When $\{x_i\}_{i=0}^{P}$ are uniformly spaced, with spacing Δx (i.e., $x_i = i\Delta x$), then the overlapping region is $\delta = |\mathcal{D}_i \cap \mathcal{D}_{i+1}| = 2\delta'$ and $\rho = |\mathcal{I}_i \cap \mathcal{I}_{i+1}| = \Delta x - 2\rho'$. We recall that the length of the expansion intervals $2\Delta x$ and the overlapping length ρ should be selected by taking into account the correlation length of the diffusion coefficient, here set to $l_c = 0.008$. Thus, we choose δ' and ρ' in order to obtain $\rho = 0.04$, 0.04, and 0.03 for $P = 5$, 10, and 20, respectively. Thanks to the finite correlation length of the diffusion coefficient, we have the number of terms in the local K-L expansion decrease significantly when we increase the number of subdomains (see Table 7.3). This allows us to solve a sequence of local low-dimensional problems when performing Schwarz iterations. Convergence of the conditional moment interface algorithm is shown in Figure 7.5, where plot the relative L_2 error of the first- and fourth-order moment. Note that as we increase the number of subdomains P, the convergence rate deteriorates.

7.2.2 Stochastic Advection

Let us consider the time-dependent stochastic advection problem,

$$\frac{\partial u(x,t)}{\partial t} = -a(x;\omega)\frac{\partial u(x,t)}{\partial x}, \qquad x \in [0,1], \quad t \geq 0, \tag{7.2.4}$$
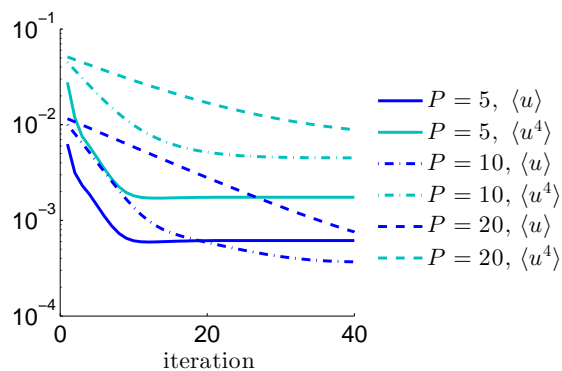
Figure 7.5: Stochastic elliptic problem. Relative L_2 error in the first- and fourth-order moment versus the iteration number in SDD-M method. Shown are results for different numbers of subdomains P.
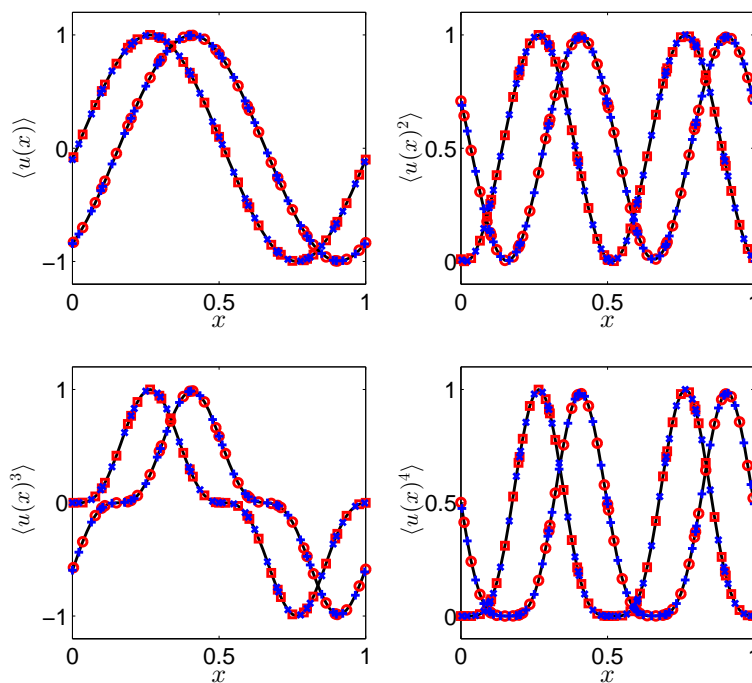
Figure 7.6: Stochastic advection problem. First four statistical moments of the solution The reference solution (black line) is compared with the SDD-S method (red line) and the PDE-constrained interface method (blue line) at two different times: $t = 0.1$ (red square, blue x) and $t = 1.0$ (red circle, blue +)
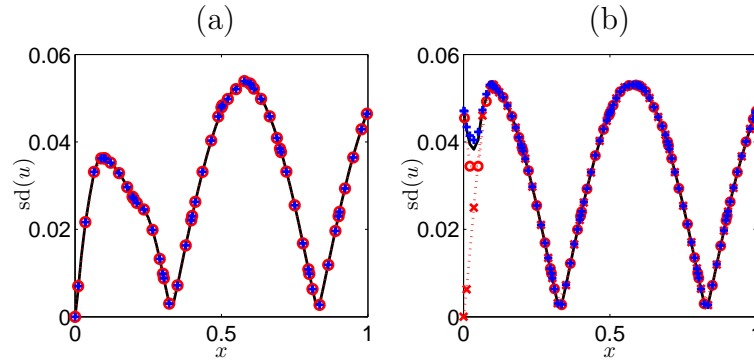
Figure 7.7: Stochastic advection problem. Standard deviation of the solution at $t = 0.5$. We show results obtained by using the conditional moment interface methods: SDD-M (red x), SDD-S (red o) and the PDE-constrained method (blue +). In particular, in (a) we study the case where the random advection velocity has variable correlation length ranging from from 0.05 to 0.2. The case with constant correlation length is shown in (b).

with initial condition $u(x, 0) = \sin(2\pi x)$. The mean velocity is set to $\langle a(x; \omega) \rangle = \pi/2$ and the covariance function is assumed to be as in Eq. (7.2.2) with $\sigma_a = \pi/10$. We consider both Gaussian covariances shown in Figure 6.15(c,d), i.e., with constant and variable correlation lengths, and represent $a(x; \omega)$ by using the expansion method discussed in section (6.3). Regarding the boundary conditions, we set periodic boundary conditions $u(0) = u(1)$ for the case of constant correlation length, and a Dirichlet condition $u(0) = \sin(-t)$ for variable correlation lengths. In Figure 7.6 we plot the first four moments of the solution to (7.2.4) as computed by the SDD-S and the PDE-constrained interface methods, for the case where the advection velocity has constant correlation length $l_c = 0.08$. Here we set $\epsilon = 10^{-2}$ and $w = 0.1$ in the SDD-S algorithm. It is seen that both methods yield accurate statistical moment up to $t = 1.0$ (see also Figure 7.8). In Figure 7.7 we study the standard deviation of the solution at $t = 0.5$, for advection velocities with variable and constant correlation lengths. In the latter case, Figure 7.7(b), we see that the SDD-S algorithm provides more accurate results than SDD-M, by preserving the periodicity of the standard deviation. This can be achieved because the SDD-S method interfaces subdomains
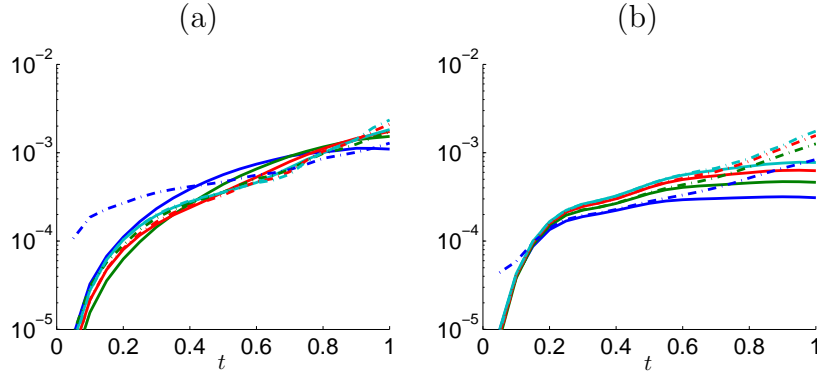
Figure 7.8: Stochastic advection problem. Relative L_2 errors in the first four statistical moments of the solution versus time. We show results computed by using the moment interface SDD-S ($-$) and the PDE-constrained ($-\cdot-$) methods for the cases of constant correlation length ($l_c = 0.08$) and periodic boundary conditions (a), and variable correlation length ranging from from 0.2 to 0.05 and Dirichlet boundary condition (b).

by using information from the standard deviation.

7.2.3 Stochastic Advection-Reaction

In this last example we consider the application of our stochastic domain decomposition methods to a nonlinear problem, i.e., an advection-reaction problem with nonlinear reaction term and stochastic reaction rate. In particular, we consider the following model problem

$$\frac{\partial u}{\partial t} = V(x)\frac{\partial u}{\partial x} + (k_0(x) + \sigma_k k_1(x;\omega)) R(u), \qquad (7.2.5)$$

where

$$V(x) = -\frac{1}{2}\left(1 + e^{(\sin(2\pi x)+\cos(2\pi x))/2} - \cos(2\pi x)\right),$$
$$k_0(x) = 1 - \frac{2}{5}\left(e^{-\sin(2\pi x)/2} + \cos(2\pi x)\right),$$

$\sigma_k = 0.2$, $R(u) = 1 - u^2$, with I.C. $u_0(x) = \sin(2\pi x)$ and periodic B.C.. This problem was proposed and studied in [195] by using Mori-Zwanzig projection operator meth-
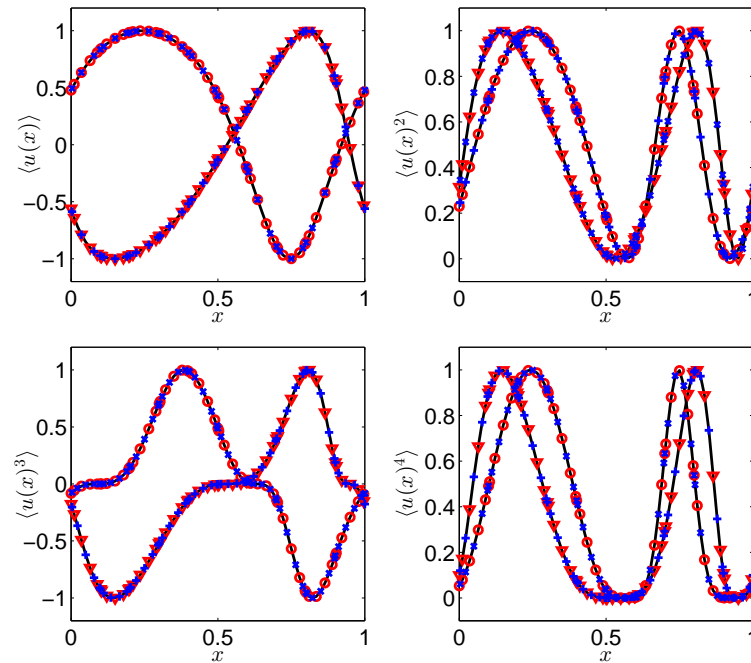
Figure 7.9: Stochastic advection-reaction problem. First four statistical moments of the solution to the advection reaction equation (7.2.5). The reference solution (black line) is compared with the SDD-M method (red line) and the PDE-constrained interface method (blue line) at two different times: $t = 0.5$ (red triangle, blue x) and $t = 1.0$ (red circle, blue +).
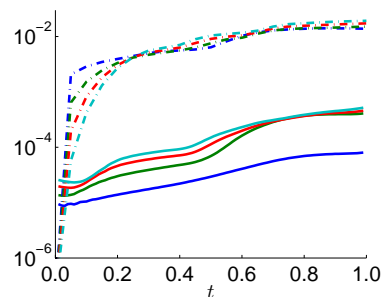
Figure 7.10: Stochastic advection-reaction problem. Relative L_2 errors in the first four statistical moments of the solution to the the stochastic advection reaction problem (7.2.5) versus time. We show results computed by using the moment interface SDD-M $(-)$ and the PDE-constrained $(- \cdot -)$ methods for the case of variable correlation length.

ods (see also [180, 197]). The perturbation in the reaction rate, $k_1(x; \omega)$ is modeled as Gaussian random field with Gaussian covariance function and correlation length varying from 0.2 to 0.05. The results of our simulations are shown in Figure 7.9 where we plot the first four moments of the stochastic solution at different times, as obtained by using the SDD-M and PDE-constrained interface method. The relative L_2 error of such moments is plotted in Figure 7.10 versus time. It is seen that both algorithms are accurate also for nonlinear problems.

7.3   Interface methods of PDF systems

In this section, we develop stochastic domain decomposition method to propagate uncertainty across heterogeneous PDF models. We employ similar methodologies presented in section 7.1 to the interface problem between distinct PDF systems.

Let us write the local PDF system on the i-th subdomain D_i as

$$
\begin{aligned}
\mathcal{L}_i(p_i(a, b_i, x; t), a, b_i, x; t) &= f_i(a, b_i, x; t), & x \in \mathcal{D}_i \\
B(p_i(x, a, b_i, t)) &= g(x, a, b_i, t)), & x \in \partial\mathcal{D}_i \cap \partial\mathcal{D} \qquad (7.3.1) \\
B(p_i(x, a, b_i, t)) &= \widetilde{g}_i(x, a, b, t), & x \in \Gamma_i,
\end{aligned}
$$

where x is the physical variable, $a \in \mathbb{R}^n$ is the response variable, $b^i \in \mathbb{R}^{m_i}$ are the excitation variables on D_i. The coupling problem between distinct PDF systems reduces to imposing an appropriate boundary condition $\widetilde{g}_i(x, a, b, t)$ on the subdomain boundary Γ_i.
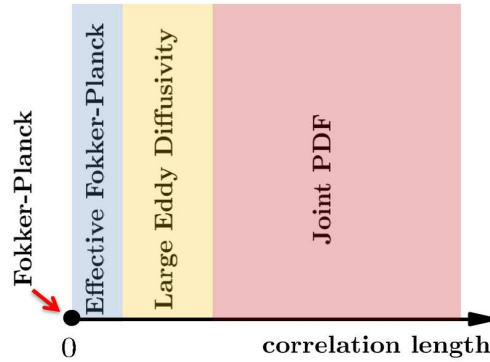
Figure 7.11: Range of PDF evolution equation according to the correlation length of the random excitation.

7.3.1 Schwarz algorithm between PDF models

We denote the marginalization of the variables b_i as

$$\langle p(x, a, b_i)\rangle_{b_i} \stackrel{\text{def}}{=} \int_{\Xi_i} p(x, a, b_i) db_i.$$

The boundary condition that impose continuity of the response PDF can be expressed as

$$\langle p(x, a, b_i)\rangle_{b_i} = \langle p(x, a, b_j)\rangle_{b_j}, \qquad j \in \mathcal{N}_i. \tag{7.3.2}$$

Clearly, the stochastic solution satisfying such boundary condition is not unique.

We first introduce the *mean-shifted boundary condition*, which sets the marginalized response PDF on the subdomain boundary to be coincident with the one computed from the adjacent subdomain. The boundary condition imposed on $x \in \Gamma_i \cup \mathcal{D}_j$ for $j \in \mathcal{N}_i$ is as follows.

$$\widetilde{g}_i^n[1](x, a, b_i) \stackrel{\text{def}}{=} p_i^n(x, a, b_i) - \langle p_i^n(x, a, b_i)\rangle_{b_i} + \langle p_j^n(x, a, b_j)\rangle_{b_j}. \tag{7.3.3}$$

Note that (7.3.3) satisfies Eq. (7.3.2), and at the same time, does not alter the variance of the PDF with respect to the b_i variables within $\mathcal{D}_i$. A further improvement of the interface condition can be obtained by using second-order statistical properties.

We shall call it *variance scaling boundary condition*, and it relies on setting

$$\widetilde{g}_i^n[2](x, a, b_i) \overset{\text{def}}{=} \left(p_i^n(x, a, b_i) - \langle p_i^n(x, a, b_i)\rangle_{b_i}\right) \frac{\sigma_{b_j}^n}{\sigma_{b_i}^n} + \langle p_j^n(x, a, b_j)\rangle_{b_j}, \qquad (7.3.4)$$

where $\sigma_{b_i}^n$ is a standard deviation defined as

$$\sigma_{b^i}^n(x, a) \overset{\text{def}}{=} \left[\langle p_i^n(x, a, b_i)^2\rangle_{b_i} - \langle p_i^n(x, a, b_i)\rangle_{b_i}^2\right]^{1/2}.$$

This condition guarantees continuity up to the second order statistics in the excitation dimension. However, it may lead to unstable Schwarz iterations due to the division by σ_i^n. To avoid such instabilities, we combine (7.3.3) and (7.3.4) into one Algorithm. This yields the conditional moment interface method whose steps are summarized in Algorithm 5, with a weight function $w(n) \in [0, 1]$. The two boundary conditions $\widetilde{g}_i^n[1]$ and $\widetilde{g}_i^n[2]$ are leveraged by decreasing $w(n)$ from $w(0) = 1$.

begin
    initialize $\{p_i^0\}_{i=1}^P$ at random;
    while $\left\|\langle p_i^n\rangle_{b_i} - \langle p_j^n\rangle_{b_j}|_{j\in\mathcal{N}_i}\right\|_{a\in\mathbb{R},x\in\Gamma_i} > \varepsilon$ **do**
        for $1 \le i \le P$ **do**
            solve

$$
\begin{aligned}
\mathcal{L}_i(p_i^n(x, a, b_i, t), a, b_i, x, t) &= f_i(x, a, b_i, t), & x \in \mathcal{D}_i,\\
B(p_i^n(x, a, b_i, t)) &= g(x, a, b_i, t)), & x \in \partial\mathcal{D}_i \setminus \Gamma_i,\\
B(p_i^n(x, a, b_i, t)) &= w(n)\widetilde{g}_i^{n-1}[1](x, a, b_j|_{j\in\mathcal{N}_i}, t) & (7.3.5)\\
&\quad + (1 - w(n))\widetilde{g}_i^{n-1}[2](x, a, b_j|_{j\in\mathcal{N}_i}, t), & x \in \Gamma_i,
\end{aligned}
$$

            $n = n + 1$;
        end
    end
end

Algorithm 5: Domain decomposition of distinct REPDF systems. The moment interface condition imposed on Γ_i couples the local excitation space on each subdomain. Here, the mean shifting and variance scaling condition is leveraged through the weight function $w(n)$, and iterated until the response PDF on the interface has converged.

7.3.2 Numerical simulation of advection-reaction equation

Reactive transport in a porous medium involving a heterogeneous reaction between dissolved species and solid is modeled by the stochastic advection-reaction equation. The evolution of the solute concentration $c(x, t)$ defined on $x \in \mathcal{D}$ is described as

$$\frac{\partial c}{\partial t} = -\nabla \cdot (vc) + \mathrm{Da} f_\kappa(c), \quad f_\kappa(c) = -\alpha \kappa (c^\alpha - 1), \qquad (7.3.6)$$

where α is the stoichiometric coefficient, Da is the Damköhler number, κ is the reaction rate constant, and v is the macroscopic flow velocity. Let us consider the random reaction rate to be exponentially correlated with correlation length ℓ with a positive constant mean K, i.e.,

$$\langle \kappa(x; \omega) \rangle = K, \quad \langle \kappa(x; \omega) \kappa(y; \omega) \rangle = \frac{\sigma_\kappa^2}{2\ell} e^{-|x-y|/\ell}. \qquad (7.3.7)$$

By using the K-L expansion, $\kappa(x; \omega)$ can be represented in a series expansion form based on uniform random variables as following,

$$\kappa(x; \omega) = K + \frac{\sqrt{3}\sigma_\kappa}{\sqrt{2\ell}} \sum_{j=1}^{N} \sqrt{\theta_j} \xi_j(\omega) \phi_j(x).$$

where $\xi_j(\omega)$ are zero-mean independent uniform random variables on $[-1, 1]$ and the quantities θ_j and $\phi_j(x)$ denote the eigenvalues and eigenfunctions computed by the K-L expansion.

The PDF of the solution $c(x, t)$ can be computed by the REPDF approach solving for

$$p_{c(x,t)\xi}^{(a,b)} = \langle \delta(a - c(x,t; \omega)) \prod_{j=1}^{N} \delta(b_j - \xi_j(\omega)) \rangle. \qquad (7.3.8)$$

Taking p_R as a shorthand for $p_{c(x,t)\xi}^{(a,b)}$, the evolution equation becomes

$$\frac{\partial p_R}{\partial t} = -v \cdot \nabla p_R + \frac{\partial}{\partial a} [a \nabla v \cdot p_R] - \text{Da} \alpha \frac{\partial}{\partial a} \left[(a^\alpha - 1) \left(K + \widetilde{\sigma}_\kappa \sum_{j=1}^{N} b_j \phi_j \right) p_R \right], \quad (7.3.9)$$

where $\widetilde{\sigma}_\kappa = \sqrt{3}\sigma_\kappa / \sqrt{2\ell}$. We take a homogeneous boundary condition in the response space a and Neunmann as $\partial p_R(x, a, b)/\partial x = 0$ at the left end of $\mathcal{D}$. Alternatively, either when the correlation length is small or large, the evolution of the response PDF can be approximated by the large-eddy diffusivity (LED) approach. The governing equation is as follows.

$$\frac{\partial p_L}{\partial t} = -\frac{\partial p_L}{\partial x} - \frac{(U_4 \partial p_L)}{\partial a} + \frac{\partial}{\partial a} \left(D_{44} \frac{\partial p_L}{\partial a} \right), \quad (7.3.10)$$

where p_L denotes $p_{c(x,t)}^{(a)}$, and U_4 and D_{44} are called the effective velocity and effective diffusion coefficients, respectively. The new coefficients are computed as

$$U_4(a, t) = \text{Da}(1 - a)K - \frac{\sigma_\kappa^2 \text{Da}^2(a - 1)}{2(\text{Da}\ell - 1)} \begin{cases} e^{(\text{Da}\ell - 1)t/\ell} - 1, & t \leq T(a) \\ e^{(\text{Da}\ell - 1)T/\ell} - 1, & t > T(a) \end{cases},$$

and

$$D_{44}(a, t) = \frac{\sigma_\kappa^2 Da^2(a - 1)^2}{2(2Da\ell - 1)} \begin{cases} e^{(2\text{Da}\ell - 1)t/\ell} - 1, & t \leq T(a) \\ e^{(2\text{Da}\ell - 1)T/\ell} - 1, & t > T(a) \end{cases},$$

with

$$T(a) \stackrel{\text{def}}{=} \frac{1}{\text{Da}} \ln \left(\frac{1}{1 - a} \right),$$

for the uniform reaction rate model. The boundary condition is imposed as in the REPDF equation.

We consider the system on the physical domain $\mathcal{D} = [0, 200]$ with reaction rate $K = 2$, and the parameters $Da = 0.5$, $\alpha = 1$, and $\sigma_\kappa = 2/3$. Figure 7.12 illustrates
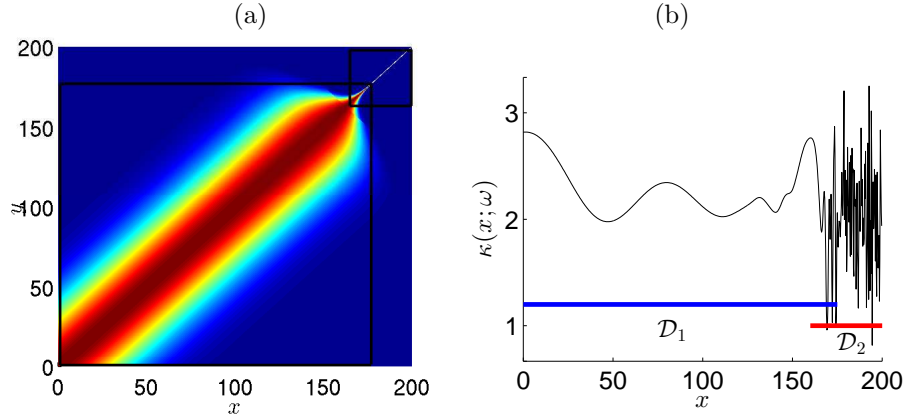
Figure 7.12: Gaussian correlated covariance function (a) where the correlation length varies from $l_c = 100$ to 0.1 and the corresponding sample functions (b). The sample function illustrates the contrast in the regularity, particularly low at the right end.

the covariance function of κ, where the correlation length varies from 100 to 0.1 towards the right. The global K-L expansion requires more than 200 random variables to attain 95% of the eigen-spectrum due to its weakly correlated region near $x = 200$. Thus, we decompose the domain into $\mathcal{D}_1 = [0, 175]$ and $D_2 = [160, 200]$ according to the strength of correlation, and compute the statistics of the solution by using the REPDF equation on $\mathcal{D}_1$ and the LED approximation on $\mathcal{D}_2$. The computational cost reduces substantially since the local K-L expansion of κ on $\mathcal{D}_1$ only requires four random variables to attain the same accuracy with the global representation. Similarly, we also test the case when the noise of the reaction rate is weakly correlated in the middle as in Figure 7.15. For time integration, we use the fourth-order Runge-Kutta method with time step $\triangle t = 10^{-3}$.

The interface condition coupling the REPDF and LED systems follows Eq. (7.3.5), but can be further reduced. This is because the LED system is a response PDF equation that stands without the excitation variables. Since the LED equation cannot provide any information about the statistics in the b dimension, the boundary condition on $\mathcal{D}_1$ simply reduces to the mean-shifted boundary condition in Eq.
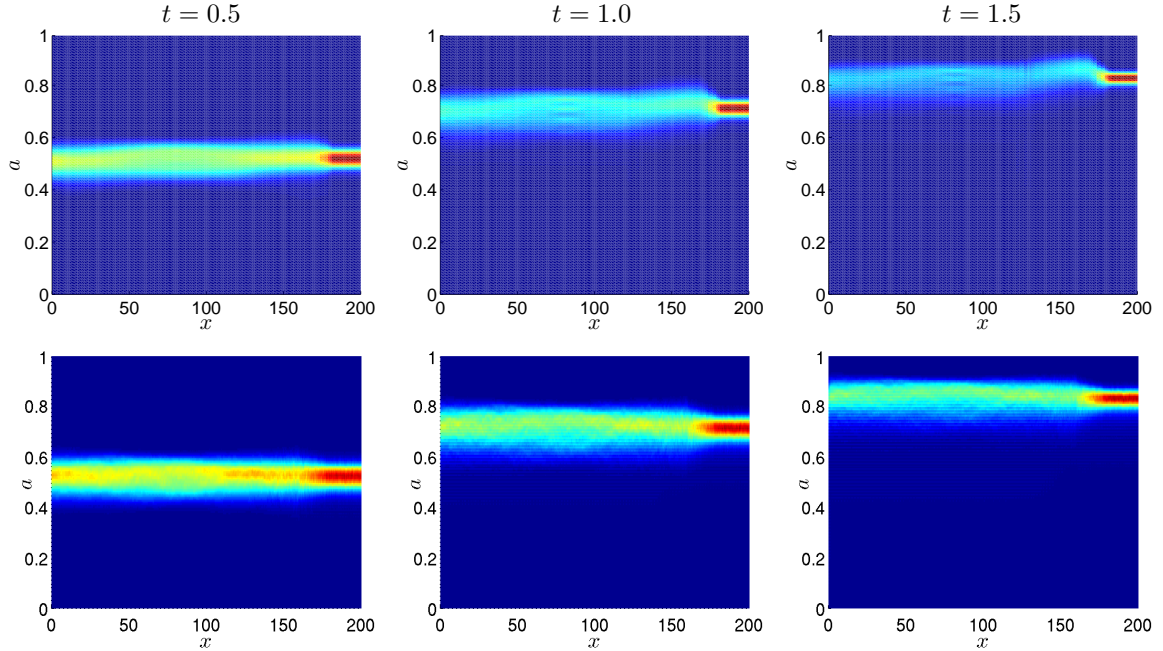
Figure 7.13: The response PDF solution computed by using combined REPDF-LED equation (top) and MC simulation with 2000 samples (bottom) at time $t = 0.5$, 1.0, and 1.5.

(7.3.3). The interface condition for each trajectory of b becomes

$$p_R(x, a, b) = p_R(x, a, b) - \int p_R(x, a, b)db + p_L(x, a), \quad x \in \Gamma_1. \qquad (7.3.11)$$

On the other hand, the boundary condition on $\mathcal{D}_2$ is further reduced which can be simply given by marginalizing the excitation dimensions of the REPDF. In short,

$$p_L(x, a) = \int p_R(x, a, b)db, \quad x \in \Gamma_2. \qquad (7.3.12)$$

Figure 7.13 compares the response PDF of the concentration $c(x, t)$ computed by the REPDF-LED approach and MC simulation. The MC solution is computed with 2000 samples estimated by the KDE method. We observe that the variance of the concentration strongly depends on the correlation of the random reaction coefficient, particularly, the variance decreases for smaller correlation length. The cross sections of the response PDF at $x = 80$ and $x = 180$, i.e., $p_{c(80,t)}(a)$ and $p_{c(180,t)}(a)$ are
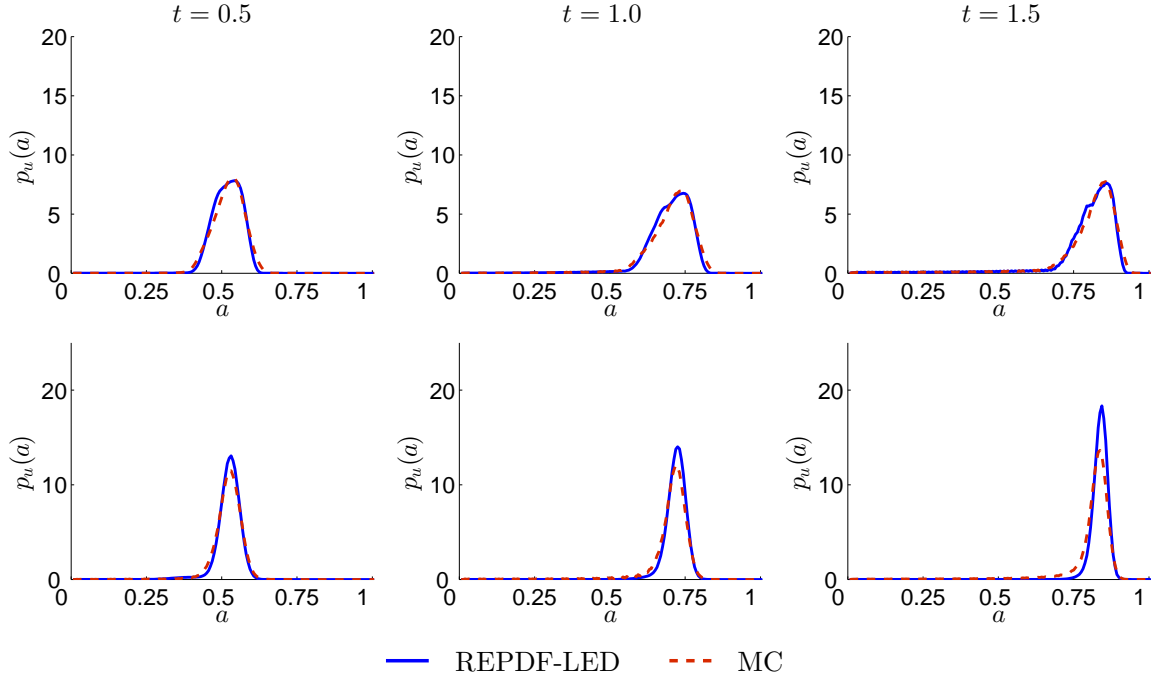
Figure 7.14: Comparison of the response PDF at $x = 80$ (top) and $x = 180$ (bottom) computed by the REPDF-LED approach and MC with 2000 samples.

shown in Figure 7.14. They correspond to the location computed by the REPDF and LED approach, respectively. Due to its approximative feature, the LED system induce larger error than the REPDF system. However, the computational cost of the combined REPDF-LED approach is far less than solving the global REPDF equation that lies in a 200 dimensional space. Assuming that we use PCM-ANOVA level 2 for the excitation space, the cost reduces to less than 1%. We also consider a covariance kernel as in Figure 7.15 where the noise becomes weakly correlated in the middle of the domain. In this case, the domain is decomposed into three subdomains $\{\mathcal{D}_i\}_{i=1}^3$, where $\mathcal{D}_2$ is computed by using the LED approximation. The PDF solutions at $x = 75$ and 125 are plotted in Figure 7.16 which is the PDF solution on the overlapping region, continuity imposed by (7.3.11) and (7.3.12). This example reveals similar accuracy and reduced computational cost as in the previous simulation.
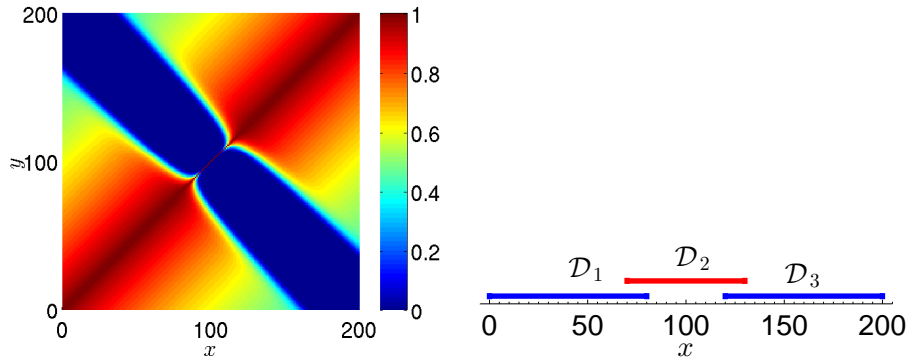
Figure 7.15: The Exponential covariance function of the random field $\kappa(x; \omega)$, where the correlation length reduces to $l_c = 0.2$ in the middle and $l_c = 200$ elsewhere. The domain is decomposed as $\mathcal{D}_1 = [0, 80]$, $\mathcal{D}_2 = [70, 130]$, and $\mathcal{D}_3 = [120, 200]$, where $\mathcal{D}_1$ and $\mathcal{D}_3$ are solved by the REPDF equation and $\mathcal{D}_2$ is solved by the LED equation.
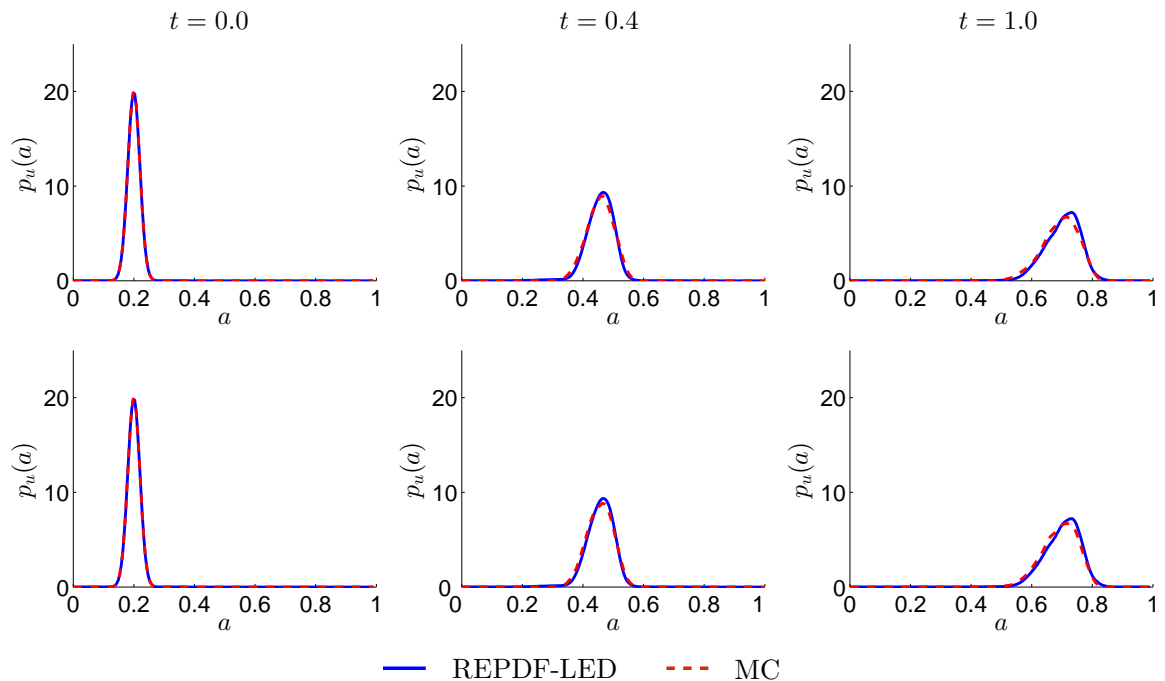
Figure 7.16: The REPDF-LED solution and the MC solution using 10000 samples at different location $x = 75$ (top) and $x = 125$ (bottom) on the overlapping region.

	Conditional moment method	PDE-constrained method
Computational Cost	$C_{det}\left(\frac{N}{P}\right) \cdot C(M) \cdot n_{itr} \cdot P$	$C_{det}\left(\frac{N}{P}\right) \cdot C_{opt}(M, P)$

Table 7.4: Comparison between the computational cost of the conditional moment and the PDE-constrained interface methods. Here C_{det} is the cost of the deterministic solver on a single subdomain, $C(M)$ is the number of (sparse grid) collocation points, n_{itr} is the Schwarz iteration number, and C_{opt} counts the number of deterministic solves in the PDE-constrained optimization. In our simulations, C_{opt} is of the same order of magnitude as $C(M)$.

7.4   Summary

In this chapter we proposed a new general framework for multi-scale propagation of uncertainty in heterogeneous stochastic systems and SPDEs based on domain decomposition methods. The key idea relies on new types of interface conditions combined with reduced-order local representations presented in section 6.3 and generalized Schwarz methods. We proposed two new algorithms for this purpose, based on conditional moments (section 7.1.1), and PDE-constrained optimization (section 7.1.2). In both cases, the interface conditions between different subdomains are defined by *low-dimensional functionals* of the stochastic solution (e.g., moments or cumulants). We emphasize that no rigorous theory has yet been developed for stochastic systems with interfaces defined in terms of *functionals* of the stochastic field. However, the numerical results we presented in section 7.2, demonstrate that the SDD methods we proposed here are relatively accurate and efficient for both linear and nonlinear problems. The computational cost of the proposed new algorithms is summarized in Table 7.4. The conditional moment interface method requires a deterministic solve at each Schwarz iteration within each subdomain. This has to be multiplied by the number of (sparse grid) collocation points we use to represent the random input process. On the other hand, the computational cost of PDE-constrained method is proportional to C_{opt} times the cost a deterministic solve, where C_{opt} in our ex-

amples is of the same order of magnitude as the number of gPC coefficients in the local polynomial chaos expansions. Furthermore, the conditional moment interface method can be easily parallelized and extended to stochastic systems with hybrid coupling, such as those arising in multi-physics and multi-scale problems. Finally, the conditional moment based interface method is applied to couple distinct REPDF systems, that is, to impose interface conditions between the local excitation space on each subdomains. In section 7.3.2, we apply this method to couple the REPDF system and the response PDF equation, namely, the LED approximation. It has been shown that by an appropriate choice of PDF equation according to the local stochasticity, this approach can significantly reduce the computational cost.

Chapter 8

Summary and future work

8.1 Summary

In this thesis, we have presented the joint response-excitation probability density approach for uncertainty quantification and multi-scale stochastic simulations.

The evolution equations of REPDF has been derived by using the functional integral method, which makes the REPDF evolution equations readily available for nonlinear dynamical systems and first-order PDEs. Various numerical methods for this system have been developed and they are illustrated in a diagram in Figure 1.2 according to the dimensionality of the stochastic system. The methods are classified with respect to the dimensionality of the response space and excitation space.

- For low-dimensional systems, we propose high-order spectral methods by using adaptive discontinuous Galerkin and probabilistic collocation method.

- When high-dimensionality occurs, we explore the use of algorithms involving the separated series expansion and ANOVA approximation.

- Alternatively for high-dimensions, we develop frameworks to obtain reduced-order PDF equations by using the Mori-Zwanzig formalism and BBGKY-type hierarchy.

205

The effectiveness of the response-excitation theory and the aforementioned numerical schemes is demonstrated in various stochastic systems including tumor cell model, chaotic nonlinear oscillators, random transport equation, and Burgers equation subject to shock waves, considering up to 40-dimensions in the response space (Lorenz-96 system) and 114-dimensions in the excitation space (Advection equation).

We also develop numerical algorithms for uncertainty propagation across decomposed domains and multi-scale systems. Extensions of KL expansion to multi-correlated random processes and locally distributed domains provide a framework to model multiple source of uncertainty in different scales. In addition, the interface methods based on the conditional moments and PDE-constrained optimization enable efficient stochastic domain decomposition methods that preserve the global statistics. Eventually, the interface schemes are recast in terms of coupling distinct PDF systems that significantly reduces the computational cost.

8.2 Future work

Although we have extended the probability density approach for stochastic simulations in various directions, several challenges remain. We list the possible improvements and future directions:

- *Advanced high-dimensional numerical technique* : Computational efficiency in extremely high-dimensional stochastic systems would always remain as a big challenge. Algorithms involving advanced anisotropic tensor decomposition can assist to overcome the curse of dimensionality. Possible extensions include Tucker Tensor decomposition [104], Hierarchical Tucker Tensor [72], and Tensor Train decomposition [139].

  Another issue that arises particularly in high-dimensional PDF systems is achieving conservative properties. In low dimensions, the idea of mass con-

servative schemes and positivity preserving schemes [87, 153] through numerical flux and limiters can be straightforwardly applied to the discontinuous Galerkin method. However, it is difficult to guarantee these properties in high-dimensional approximative algorithms including the proposed SSE and ANOVA method. Positivity can be achieved through separated series algorithms involving optimization with non-negativity constraints [104, 152]. Still, mass conservation would be an additional challenge and high-dimensional numerical schemes attaining appropriate features without abandoning computational efficiency is desirable.

- *Long-term integration and CDF evolution equation* : There are several issues arising in long-term PDF simulations. In addition to the numerical difficulties including stability, some variables can become more like a deterministic variable which yields the marginalized PDF function as a delta function. Also in systems that eventually become stable, the transition probability will evolve into an equilibrium distribution. Thus, detections of these phenomena and proper conversions between the full REPDF system and an appropriate reduced PDF system will extend the scope of the probability density approach.

An alternative approach to attain high-resolution in the probability space would be by considering the cumulative distribution function (CDF). It is defined as $F_X(x) \stackrel{\text{def}}{=} P_X(X \leq x)$, where P_X is the probability density measure of random variable X. By definition, the CDF is a monotonic increasing function with boundary condition zero and one on the left end and right end boundaries, respectively. Moreover, it possesses more regularity than the PDF which makes this approach numerically more attractive. For instance, the CDF of a random variable with the probability density prescribed as a delta function becomes a step function. While the CDF evolution has been employed to study the advection-reaction equation in [21, 206] for one-dimensions in the

physical space, in high-dimensions, an efficient numerical scheme that ensures monotonicity in every direction should be developed.

- *Goal oriented PDF evolution equation* : The proposed MZ-PDF approach is restricted to the case involving two assumptions. It requires scale separability in the operator and initial independence between the relevant and irrelevant variables. In fact, these assumptions cannot be satisfied when we consider the quantity of interest as a phase space function with the same order of magnitude. To overcome the scale separability, there are several methods using direct approximations to the memory term, exponential operators, and Krylov subspace type methods [30, 37, 40], and these approaches can be employed to generalize the MZ-PDF equation. In addition, the conditional moment closure can be adopted in the goal oriented framework and an appropriate sensitivity analysis will enhance its applicability.

- *Unified framework of stochastic methods from PDF systems to surrogate models* : Simulation methods of uncertainty quantification can be classified with respect to the response statistics, for instance, surrogate models that compute the central trend efficiently or extreme value models that capture large deviations and rare events. On top of that, the PDF approach provides the entire statistics of the solution, which makes it stand as the highest fidelity model. Apparently, the computational cost is in general more expensive than other methods. Thus, an appropriate interface method that couples distinctive stochastic models in space and time will enhance computational efficiency, while making the PDF solution available at certain location and time.

Extension of PDE-constrained method to couple different stochastic models is in progress by constructing an appropriate object function, involving arbitrary polynomial chaos expansion [138] or Kullback-Leibler divergence [105].

The time-steppers [3] can assist to adjoin distinct systems with time correlated noise in different scales. In addition, distribution free Skorokhod-Malliavin framework proposed by R. Mikulevicius and B. Rozovskii derives reduced-order stochastic differential equations with proper basis functions corresponding to the underlying distribution. Interface conditions within this approach managing the transition between distributions with completely distinct properties would be interesting problem.

- *Application to complex systems combined with high-performance computing* : This thesis work has been focused on generalizing the probabilistic models into a more complex setting involving various types of random excitation and multi-scale physics with mutual correlation. Therefore, these methods can be applied to investigate problems that the probabilistic models were over-simplified through strong assumptions such as Gaussian or Markovian. In addition, extensions of the methodologies to higher dimensions in the physical space and parallelization of these algorithms in both the physical space and the random space would be the next challenge.

Bibliography

[1] A. H. AL-MOHY AND N. J. HIGHAM, *Computing the action of the matrix exponential with an application to exponential integrators*, SIAM J. Sci. Comput., 33 (2011), pp. 488–511.

[2] A. AMMAR, B. MOKDAD, F. CHINESTA, AND R. KEUNINGS, *A new family of solvers for some classes of multidimensional partial differential equations encountered in kinetic theory modelling of complex fluids: Part II: Transient simulation using space-time separated representations*, Journal of Non-Newtonian Fluid Mechanics, 144 (2007), pp. 98–121.

[3] A. ARMAOU, C. I. SIETTOS, AND I. G. KEVREKIDIS, *Time-steppers and coarse control of distributed microscopic processes*, Int. J. Robust Nonlin., 14 (2004), pp. 89–111.

[4] U. ATXITIA, O. CHUBYKALO-FESENKO, R. W. CHANTRELL, U. NOWAK, AND A. REBEI, *Ultrafast spin dynamics: the effect of colored noise*, Phys. Rev. Lett., 102 (2009), p. 057203 (4pp).

[5] M. AVELLANEDA AND W. E, *Statistical properties of shocks in Burgers turbulence*, Commun. Math. Phys., 172 (1995), pp. 13–38.

[6] I. BABUSKA, F. NOBILE, AND R. TEMPONE, *A stochastic collocation method for elliptic partial differential equations with random input data*, SIAM J. Numer. Analysis, 45 (2007), pp. 1005–1034.

[7] V. BEATO, I. SENDIÑA-NADAL, I. GERDES, AND H. ENGEL, *Coherence resonance in a chemical excitable system driven by coloured noise*, Phil. Trans. R. Soc. A, 366 (2008), pp. 381–395.

[8] M. J. BERAN, *Statistical continuum theories*, New York: Interscience Publishers, 1968.

[9] G. BEYLKIN, J. GARCKE, AND M. J. MOHLENKAMP, *Multivariate regression and machine learning with sums of separable functions*, SIAM J. Sci. Comput., 31 (2009), pp. 1840–1857.

[10] G. BEYLKIN AND M. J. MOHLENKAMP, *Algorithms for numerical analysis in high dimensions*, SIAM J. Sci. Comput., 26 (2005), pp. 2133–2159.

[11] M. BIERI AND C. SCHWAB, *Sparse high order FEM for elliptic sPDEs*, ETH Seminar for Applied Mathematics, (2008).

[12] G. A. BIRD, *Molecular gas dynamics and direct numerical simulation of gas flows*, Clarendon Press, 1994.

[13] J. A. BLACKBURN, Z. YANG, S. VIK, H. J. T. SMITH, AND M. A. H. NERENBERG, *Experimental study of chaos in a driven pendulum*, Physica D, 26 (1987), pp. 385–395.

[14] S. BLANES, F. CASAS, J. A. OTEO, AND J. ROS, *The Magnus expansion and some of its applications*, Physics Reports, 470 (2009), pp. 151–238.

[15] D. BLÖMKER AND A. JENTZEN, *Galerkin approximations for the stochatic Burgers equation*, SIAM J. Numer. Anal., 51 (2013), pp. 694–715.

[16] G. N. BOCHKOV AND A. A. DUBKOV, *Concerning the correlation analysis of nonlinear stochastic functionals*, Radiophysics and Quantum Electronics, 17 (1974), pp. 288–292.

[17] G. N. BOCHKOV, A. A. DUBKOV, AND A. N. MALAKHOV, *Structure of the correlation dependence of nonlinear stochastic functionals*, Radiophysics and Quantum Electronics, 20 (1977), pp. 276–280.

[18] V. V. BOLOTIN, *Statistical methods in structural mechanics*, Holden-Day, San Francisco, 1969.

[19] C. BONATTO, J. A. C. GALLAS, AND Y. UEDA, *Chaotic phase similarities and recurrences in a damped-driven Duffing oscillator*, Phys. Rev. E, 77 (2008), pp. 026217(1–5).

[20] N. BOOIJ, R. C. RIS, AND L. H. HOLTHUIJSEN, *A third-generation wave model for coastal regions*, Journal of Geophysical Research, 104 (1999), p. 76497666.

[21] F. BOSO, S. V. BROYDA, AND D. M. TARTAKOVSKY, *Cumulative distribution function solutions of advection-reaction equations with uncertain parameters*, Proc. R. Soc. A, 470 (2014), p. 20140189.

[22] Z. I. BOTEV, J. F. GROTOWSKI, AND D. P. KROESE, *Kernel density estimation via diffusion*, Annals of Statistics, 38 (2010), pp. 2916–2957.

[23] H.-P. BREUER, B. KAPPLER, AND F. PETRUCCIONE, *The time-convolutionless projection operator technique in the quantum theory of dissipation and decoherence*, Annals of Physics, 291 (2001), pp. 36–70.

[24] J. M. BURGERS, *The Nonlinear Diffusion Equation*, Dordrecht: Reidel, 1974.

[25] Y. CAO, Z. CHEN, AND M. GUNZBUGER, *ANOVA expansions and efficient sampling methods for parameter dependent nonlinear PDEs*, Int. J. Numer. Anal. Model., 6 (2009), pp. 256–273.

[26] C. CERCIGNANI, *The Boltzmann equation and its applications*, Springer, 1988.

[27] C. CERCIGNANI, U. I. GERASIMENKO, AND D. Y. PETRINA, *Many particle dynamics and kinetic equations*, Kluwer Academic Publishers, first ed., 1997.

[28] S. Chaturvedi and F. Shibata, *Time-convolutionless projection operator formalism for elimination of fast variables. Applications to Brownian motion*, Z. Phys. B, 35 (1979), pp. 297–308.

[29] J.-B. Chen and J. Li, *A note on the principle of preservation of probability and probability density evolution equation*, Prob. Eng. Mech., 24 (2009), pp. 51–59.

[30] M. Chen, , X. Li, and C. Liu, *Computation of the memory functions in the generalized langevin models for collective dynamics of macromolecules*, J. Chemical Physics, 141 (2014), pp. 064112.1–12.

[31] Y. Cheng, I. M. Gamba, A. Majorana, and C.-W. Shu, *A brief survey of the discontinuous Galerkin method for the Boltzmann-Poisson equations*, SEMA J., 54 (2011), pp. 47–64.

[32] J. P. Chiles and P. Delfiner, *Geostatistics: Modeling Spatial uncertainty*, Wiley Series in Probability and statistics, 1999.

[33] F. Chinesta, A. Ammar, and E. Cueto, *Recent advances and new challenges in the use of the proper generalized decomposition for solving multidimensional models*, Arch. Comput. Methods. Appl. Mech. Engrg., 17 (2010), pp. 327–350.

[34] H. Cho, D. Venturi, and G. Karniadakis, *Adaptive discontinuous Galerkin method for response-excitation PDF equations*, SIAM J. Sci. Comput., 35 (2013), pp. B890–B911.

[35] H. Cho, D. Venturi, and G. E. Karniadakis, *Karhunen-loeve expansion for multi-correlated stochastic processes*, Prob. Eng. Mech., 34 (2013), pp. 157–167.

[36] ——, *Statistical analysis and simulation of random shocks in Burgers equation*, Proc. R. Soc. A, 260 (2014), pp. 20140080(1–21).

[37] A. J. Chorin, O. H. Hald, and R. Kupferman, *Optimal prediction and the Mori-Zwanzig representation of irreversible processes*, Proc. Natl. Acad. Sci. USA, 97 (2000), pp. 2968–2973.

[38] B. Cockburn, G. E. Karniadakis, and C.-W. Shu, *Discontinuous Galerkin methods*, Springer, 2000. vol. 11 of Lecture Notes in Computational Science and Engineering.

[39] B. Cockburn and C.-W. Shu, *Runge-Kutta discontinuous Galerkin methods for convection dominated problems*, J. Sci. Comput., 16 (2001), pp. 173–261.

[40] E. Darve, J. Solomon, and A. Kia, *Computing generalized Langevin equations and generalized Fokker-Planck equations*, Proc. Natl. Acad. Sci. USA, 106 (2009), pp. 10884–10889.

[41] H. Dekker, *Correlation time expansion for multidimensional weakly non-Markovian Gaussian processes*, Phys. Lett. A, 90 (1982), pp. 26–30.

[42] Q. Deng, *An analysis for a nonoverlapping domain decomposition iterative procedure*, SIAM J. Sci. Comput., 18 (1997), pp. 1517–1525.

[43] G. Deodatis, *Non-stationary stochastic vector processes: seismic ground motion applications*, Probabilistic Engineering Mechanics, 11 (1996), pp. 149–168.

[44] D. D'Humieres, M. R. Beasley, B. A. Huberman, and A. Libchaber, *Chaotic states and routes to chaos in the forced pendulum*, Phys. Rev. A, 26 (1982), pp. 3483–3496.

[45] G. Dimarco and L. Paresci, *Numerical methods for kinetic equations*, Acta Numerica, 23 (2014), pp. 369–520.

[46] M. D. Donsker, *On function space integrals*, in Proceedings of a Conference on the Theory and Applications of Analysis in Function Space, Dedham (MA), June 913, 1963, W. T. M. an I. Segal, ed., MIT Press, 1963, pp. 17–30.

[47] A. Doostan and G. Iaccarino, *A least-squares approximation of partial differential equations with high-dimensional random inputs*, J. Comp. Phys., 228 (2009), pp. 4332–4345.

[48] A. Doostan and H. Owhadi, *A non-adapted sparse approximation of PDEs with stochastic inputs*, J. Comput. Phys., 230 (2011), pp. 3015–3034.

[49] B. G. Dostupov and V. S. Pugachev, *The equation for the integral of a system of ordinary differential equations containing random parameters*, Automatika i Telemekhanica (in Russian), 18 (1957), pp. 620–630.

[50] M. I. Dykman, R. Mannella, P. V. E.McClintock, F. Moss, and S. M. Soskin, *Spectral density of fluctuations of a double-well Duffing oscillator driven by white noise*, Phys. Rev. A, 37 (1988), pp. 1303–1313.

[51] W. E and E. V. Eijnden, *Statistical theory for the stochastic Burgers equation in the inviscid limit*, Comm. Pure Appl. Math., 53 (2000), pp. 852–901.

[52] W. S. Edwards, L. S. Tuckerman, R. A. Friesner, and D. C. Sorensen, *Krylov methods for the incompressible Navier-Stokes equations*, J. Comput. Phys., 110 (1994), pp. 82–102.

[53] H. Elman, D. G. Furnival, and C. E. Powell, *H(div) preconditioning for a mixed finite element formulation of the diffusion problem with random data*, Mathematics of Computation, 79 (2010), pp. 733–760.

[54] H. Elman and Q. Liao, *Reduced basis collocation methods for partial differential equations with random coefficients*, SIAM/ASA J. Uncertainty Quantification, 1 (2013), pp. 192–217.

[55] K.-J. Engel and R. Nagel, *One-parameter semigroups for linear evolution equations*, Springer, 2000.

[56] S. Faetti, L. Fronzoni, P. Grigolini, and R. Mannella, *The projection operator approach to the Fokker-Planck equation. I. Colored Gaussian noise*, J. Stat. Phys., 52 (1988), pp. 951–978.

[57] S. Faetti and P. Grigolini, *Unitary point of view on the puzzling problem of nonlinear systems driven by colored noise*, Phys. Rev. A, 36 (1987), pp. 441–444.

[58] A. Fiasconaro, B. Spagnolo, A. Ochab-Marcinek, and E. Gudowska-Nowak, *Co-occurrence of resonant activation and noise-enhanced stability in a model of cancer growth in the presence of immune response*, Phys. Rev. E, 74 (2006), p. 041904 (10pp).

[59] F. Filbet and G. Russo, *High-order numerical methods for the space non-homogeneous Boltzmann equations*, J. Comput. Phys., 186 (2003), pp. 457–480.

[60] J. Foo and G. E. Karniadakis, *The multi-element probabilistic collocation method (ME-PCM): Error analysis and applications*, J. Comp. Phys., 227 (2008), pp. 9572–9595.

[61] ——, *Multi-element probabilistic collocation method in high dimensions*, J. Comput. Phys., 229 (2010), pp. 1536–1557.

[62] R. F. Fox, *Functional-calculus approach to stochastic differential equations*, Phys. Rev. A, 33 (1986), pp. 467–476.

[63] R. O. Fox, *Computational Models for Turbulent Reactive Flows*, Cambridge University Press, 2003.

[64] U. Frisch, *Turbulence: the legacy of A. N. Kolmogorov*, Cambridge University Press, 1995.

[65] K. Furutsu, *On the statistical theory of electromagnetic waves in fluctuating medium (i)*, J. Res. Natl. Bur. Stand. (Sect. D), 67 (1963), pp. 303–323.

[66] M. J. Gander, L. Halpern, and F. Nataf, *Optimal Schwarz waveform relaxation for the one dimensional wave equation*, SIAM J. Num. Anal., 41 (2003), pp. 1643–1681.

[67] M. J. Gander, F. Magoules, and F. Nataf, *Optimized Schwarz methods without overlap for the Helmholtz equation*, SIAM J. Sci. Comput., 24 (2002), pp. 38–60.

[68] Z. Gao and J. S. Hesthaven, *On ANOVA expansions and strategies for choosing the anchor point*, Applied Mathematics and Computation, 217 (2010), pp. 3274–3285.

[69] L. Gerardo-Giorda, F. Nobile, and C. Vergara, *Analysis and optimization of Robin-Robin partitioned procedures in fluid-structure interaction problems*, SIAM J. Num. Anal., 48 (2010), pp. 2091–2116.

[70] T. Gerstner and M. Griebel, *Dimension-adaptive tensor-product quadrature*, Computing, 71 (2003), pp. 65–87.

[71] R. G. Ghanem and P. D. Spanos, *Stochastic finite elements: A spectral approach*, Springer-Verlag, 1998.

[72] L. GIRALDI, A. NOUY, AND G. LEGRAIN, *Low-rank approximate inverse for preconditioning tensor-structured linear systems*, SIAM J. Sci. Comput., 36 (2014), pp. A1850–A1870.

[73] M. GITTERMAN, *The noisy oscillator: The first hundred years, from Einstein until now*, World Scientific Publishing Company, 2005.

[74] M. GRIEBEL, *Sparse grids and related approximation schemes for higher dimensional problems*, in Foundations of Computational Mathematics, Santander 2005, L. M. Pardo, A. Pinkus, E. Süli, and M. J. Todd, eds., no. 331, Cambridge University Press, 2006, pp. 106–161.

[75] P. GRIGOLINI, *The projection approach to the problem of colored noise*, Physics Letters, 119 (1981), pp. 183–210.

[76] M. GRIGORIU, *A class of models for non-stationary Gaussian processes*, Probabilistic Engineering Mechanics, 18 (2003), pp. 203–213.

[77] F. F. GRINSTEIN, L. G. MARGOLIN, AND W. J. RIDER, *Implicit Large Eddy Simulation : Computing Turbulent Fluid Dynamics*, Cambridge University Press, 2011.

[78] J. GUCKENHEIMER AND P. HOLMES, *Nonlinear oscillation dynamical systems and bifurcation of vector fields*, (1983). Vol. 42 of Applied Mathematical Sciences.

[79] T. HAGSTROM, R. P. TEWARSON, AND A. JAZCILEVICH, *Numerical experiments on a domain decomposition algorithm for nonlinear elliptic boundary value problems*, Appl. Math. Lett., 1 (1988), pp. 299–302.

[80] M. HAIRER AND J. VOSS, *Approximation to the stochastic Burgers equation*, J. Nonlinear Sci., 21 (2011), pp. 897–920.

[81] P. HÄNGGI, *Correlation functions and master equations of generalized (non-Markovian) Langevin equations*, Z. Physik B, 31 (1978), pp. 407–416.

[82] ——, *The functional derivative and its use in the description of noisy dynamical systems*, in Stochastic processes applied to physics, L. Pesquera and M. Rodriguez, eds., World Scientific, 1985, pp. 69–95.

[83] ——, *Colored noise in continuous dynamical system*, in Noise in nonlinear dynamical systems (Vol. 1), F. Moss and P. V. E. McClintock, eds., Cambridge Univ. Press, 1989, pp. 307–347.

[84] P. HÄNGGI AND P. JUNG, *Colored noise in dynamical systems*, in Advances in Chemical Physics: Volume 89, I. Prigogine and S. A. Rice, eds., Wiley-Interscience, 1995, pp. 239–326.

[85] J. S. HESTHAVEN, S. GOTTLIEB, AND D. GOTTLIEB, *Spectral methods for time-dependent problems*, Cambridge Univ. Press, 2007.

[86] I. HOSOKAWA AND K. YAMAMOTO, *Numerical study of the Burgers' model of turbulence based on the characteristic functional formalism*, Phys. Fluids, 13 (1970), pp. 1683–1692.

[87] X. Y. Hu, N. A. Adams, and C.-W. Shu, *Positivity-preserving method for high-order conservative schemes solving compressible euler equations*, J. Comput. Phys., 242 (2013), pp. 169–180.

[88] S. P. Huang, S. T. Quek, and K. K. Phoon, *Convergence study of the truncated KarhunenLoeve expansion for simulation of stochastic processes*, International Journal for Numerical Methods in Engineering, 52 (2001), pp. 1029–1043.

[89] M. Jardak, C.-H. Su, and G. E. Karniadakis, *Spectral polynomial chaos solutions of the stochastic advection equation*, J. Sci. Comput., 17 (2002), pp. 319–338.

[90] R. V. Jensen, *Functional integral approach to classical statistical dynamics*, J. Stat. Phys., 25 (1981), pp. 183–210.

[91] B. Jouvet and R. Phythian, *Quantum aspects of classical and statistical fields*, Phys. Rev. A, 19 (1979), pp. 1350–1355.

[92] P. Jung and P. Hänggi, *Dynamical systems: a unified colored-noise approximation*, Phys. Rev. A, 35 (1987), pp. 4464–4466.

[93] ——, *Optical instabilities: new theories for colored-noise-driven laser instabilities*, J. Opt. Soc. Am. B, 5 (1988), pp. 979–986.

[94] N. G. V. Kampen, *A cumulant expansion for stochastic linear differential equations. II*, Physica, 74 (1974), pp. 239–247.

[95] ——, *Stochastic processes in physics and chemistry*, North Holland, third ed., 2007.

[96] R. P. Kanwal, *Generalized functions: theory and technique*, Birkhäuser Boston, second ed., 1998.

[97] A. Karimi and M. R. Paul, *Extensive chaos in the Lorenz-96 model*, Chaos, 20 (2010), pp. 043105(1–11).

[98] G. E. Karniadakis and S. Sherwin, *Spectral/hp element methods for computational fluid dynamics*, Oxford University Press, 2005.

[99] T. Kato, *Perturbation theory for linear operators*, Springer-Verlag, fourth ed., 1995.

[100] A. I. Khuri, *Applications of Dirac's delta function in statistics*, Int. J. Math. Educ. Sci. Technol., 35 (2004), pp. 185–195.

[101] S. Kida, *Asymptotic properties of Burgers turbulence*, J. Fluid. Mech., 93 (1979), pp. 337–377.

[102] S. B. Kim, *hp-version discontinuous Galerkin methods for hyperbolic conservation laws*, Comput. Methods Appl. Mech. Engrg., 133 (1996), pp. 259–286.

[103] V. I. Klyatskin, *Dynamics of stochastic systems*, Elsevier Publishing Company, 2005.

[104] T. G. KOLDA AND B. W. BADER, *Tensor decompositions and applications*, SIAM Review, 51 (2008), pp. 455–500.

[105] S. KULLBACK, *Information Theory and Statistics*, John Wiley Sons, 1959.

[106] F. LANGOUCHE, D. ROEKAERTS, AND E. TIRAPEGUI, *Functional integral methods for stochastic fields*, Physica A: Statistical and Theoretical Physics, 95 (1979), pp. 252–274.

[107] R. LEBRUNA AND A. DUTFOYB, *Do Rosenblatt and Nataf isoprobabilistic transformations really differ?*, Probabilistic Engineering Mechanics, 24 (2009), pp. 577–584.

[108] G. LEONENKO AND T. PHILLIPS, *On the solution of the Fokker-Planck equation using a high-order reduced basis approximation*, Comput. Methods Appl. Mech. Engrg., 199 (2009), pp. 158–168.

[109] R. M. LEWIS AND R. H. KRAICHNAN, *A space-time functional formalism for turbulence*, Communications on Pure and Applied Mathematics, 15 (1962), pp. 397–411.

[110] G. LI, S.-W. WANG, H. RABITZ, S. WANG, AND P. JAFFÉ, *Global uncertainty assessments by high dimensional model representations (HDMR)*, Chemical Engineering Science, 57 (2002), pp. 4445–4460.

[111] J. LI AND J.-B. CHEN, *Stochastic dynamics of structures*, Wiley, 2009.

[112] G. LIN, A. M. TARTAKOVSKY, AND D. TARTAKOVSKY, *Uncertainty quantification via random domain decomposition and probabilistic collocation on sparse grids*, J. Comput. Phys., 299 (2010), p. 69957012.

[113] K. LINDENBERG AND B. J. WEST, *Finite correlation time effects in nonequilibrium phase transitions: I. dynamic equation and steady state properties*, Physica A: Statistical and Theoretical Physics, 119 (1983), pp. 485–503.

[114] K. LINDENBERG, B. J. WEST, AND J. MASOLIVER, *First passage time problems for non-Markovian processes*, in Noise in nonlinear dynamical systems (Vol. 1), F. Moss and P. V. E. McClintock, eds., Cambridge Univ. Press, 1989, pp. 110–158.

[115] W. Y. LIU, W. Q. ZHU, AND Z. L. HUANG, *Effect of bounded noise on chaotic motion of Duffing oscillator under parametric excitation*, Chaos, Solitons, Fractals, 12 (2001), p. 527537.

[116] E. N. LORENZ, *Predictability - A problem partly solved*, in ECMWF seminar on predictability: Volume 1, Reading, 1996, pp. 1–18.

[117] D. LUCOR, C. H. SU, AND G. E. KARNIADAKIS, *Generalized polynomial chaos and random oscillators*, Int. J. Numer. Meth. Engng., 60 (2004), pp. 571–596.

[118] A. N. MALAKHOV AND A. I. SAICHEV, *Kinetic equations in the theory of random waves*, Radiophysics and Quantum Electronics, 17 (1974), pp. 526–534.

[119] P. Markovich, C. Ringhofer, and C. Schmeiser, *Semiconductor equations*, Springer, 1989.

[120] P. C. Martin, E. D. Siggia, and H. A. Rose, *Statistical dynamics of classical systems*, Phys. Rev. A, 8 (1973), pp. 423–437.

[121] A. J. McCane, H. C. Luckock, and A. J. Bray, *Path integrals and non-Markov processes. 1. general formalism*, Phys. Rev. A, 41 (1990), pp. 644–656.

[122] G. Menon and R. Srinivasan, *Kinetic theory and Lax equations for shock clustering and Burgers turbulence*, J. Stat. Phys., 140 (2010), pp. 1195–1223.

[123] C. Moler and C. V. Loan, *Nineteen dubious ways to compute the exponential of a matrix, twenty-five years later*, SIAM review, 45 (2003), pp. 3–49.

[124] A. S. Monin and A. M. Yaglom, *Statistical Fluid Mechanics, Volume I: Mechanics of Turbulence*, Dover, 2007.

[125] ——, *Statistical Fluid Mechanics, Volume II: Mechanics of Turbulence*, Dover, 2007.

[126] D. Montgomery, *A BBGKY framework for fluid turbulence*, Phys. Fluids, 19 (1976), pp. 802–810.

[127] F. Moss and P. V. E. McClintock, eds., *Noise in nonlinear dynamical systems. Volume 1: theory of continuous Fokker-Planck systems*, Cambridge Univ. Press, 1995.

[128] ——, eds., *Noise in nonlinear dynamical systems. Volume 2: theory of noise induced processes in special applications*, Cambridge Univ. Press, 1995.

[129] M. Muradoglu, P. Jenny, S. B. Pope, and D. A. Caughey, *A consistent hybrid finite-volume/particle method for the PDF equations of turbulent reactive flows*, J. Comput. Phys., 154 (1999), pp. 342–371.

[130] F. Nobile, R. Tempone, and C. Webster, *A sparse grid stochastic collocation method for partial differential equations with random input data*, SIAM J. Numer. Analysis, 46 (2008), pp. 2309–2345.

[131] A. Nouy, *A priori model reduction through proper generalized decomposition for solving time-dependent partial differential equations*, Comput. Methods Appl. Mech. Eng., 199 (2010), pp. 1603–1626.

[132] ——, *A priori model reduction through proper generalized decomposition for solving time-dependent partial differential equations*, Comput. Methods Appl. Mech. Engrg., 199 (2010), pp. 1603–1626.

[133] ——, *Proper generalized decompositions and separated representations for the numerical solution of high dimensional stochastic problems*, Arch. Comput. Methods Appl. Mech. Eng., 17 (2010), p. 403434.

[134] A. Nouy and O. P. L. Maître, *Generalized spectral decomposition for stochastic nonlinear problems*, J. Comput. Phys., 228 (2009), pp. 202–235.

[135] E. Novak and K. Ritter, *Simple cubature formulas with high polynomial exactness*, Constructive Approximation, 15 (1999), pp. 499–522.

[136] E. A. Novikov, *Functionals and the random-force method in turbulence*, Sov. Phys. JETP, 20 (1965), pp. 1290–1294.

[137] D. Nozaki, D. J. Mar, P. Grigg, and J. J. Collins, *Effects of colored noise on stochastic resonance in sensory neurons*, Phys. Rev. Lett., 82 (1999), pp. 2402–2405.

[138] S. Oladyshkin and W. Nowak, *Data-driven uncertainty quantification using the arbitrary polynomial chaos expansion*, Reliability Engineering & System Safety, 106 (2012), pp. 179–190.

[139] I. V. Oseledets, *Tensor-train decomposition*, SIAM J. Sci. Comput., 33 (2011), pp. 2295–2317.

[140] C. Pantano and B. Shotorban, *Least-squares dynamic approximation method for evolution of uncertainty in initial conditions of dynamical systems*, Phys. Rev. E, 76 (2007), pp. 066705.1–13.

[141] A. Papoulis, *Probability, random variables and stochastic processes*, McGraw-Hill, third ed., 1991.

[142] L. Pesquera, M. A. Rodriguez, and E. Santos, *Path integrals for non-Markovian processes*, Physics Letters, 94 (1983), pp. 287–289.

[143] R. Phythian, *The operator formalism of classical statistical dynamics*, J. Phys A: Math. Gen., 8 (1975), pp. 1423–1432.

[144] ——, *The functional formalism of classical statistical dynamics*, J. Phys A: Math. Gen., 10 (1977), pp. 777–788.

[145] A. D. Polyanin, V. F. Zaitsev, and A. Moussiaux, *Handbook of first-order partial differential equations*, CRC Press, 2001.

[146] S. B. Pope, *A Monte Carlo method for the PDF equations of turbulent reactive flow*, Combust. Sci. Technol., 25 (1981), pp. 159–174.

[147] ——, *Lagrangian PDF methods for turbulent flows*, Annu. Rev. Fluid Mech., 26 (1994), pp. 23–63.

[148] ——, *Simple models of turbulent flows*, Phys. Fluids, 23 (2011), pp. 011301(1–20).

[149] G. D. Prato, A. Debussche, and R. Temam, *Stochastic Burgers equation*, Nonlinear Differ. Equ. Appl., 1 (1994), pp. 389–402.

[150] G. D. Prato and J. Zabczyk, *Stochastic equations in infinite dimensions*, Cambridge Univ. Press, 1992.

[151] W. H. Press, S. A. Teukolsky, W. T. Vetterling, and B. P. Flannery, *Numerical Recipes: The Art of Scientific Computing*, Cambridge University Press, 2007.

[152] L. Qi, C. Xu, and Y. Xu, *Nonnegative tensor factorization, completely positive tensors, and a hierarchical elimination algorithm*, SIAM. J. Matrix Anal. and Appl., 35 (2014), p. 12271241.

[153] J.-M. Qiu and C.-W. Shu, *Positivity preserving semi-lagrangian discontinuous galerkin formulation: theoretical analysis and application to the vlasov-poisson system*, J. Comput. Phys., 230 (2011), pp. 8386–8409.

[154] A. Quarteroni and A. Valli, *Domain decomposition methods for partial differential equations*, Oxford, 1999.

[155] H. Rabitz, O. F. Alics, J. Shorter, and K. Shim, *Efficient input-output model representations*, Computer Physics Communications, 117 (1999), pp. 11–20.

[156] J. Ramsay and B. W. Silverman, *Functional Data Analysis (Springer Series in Statistics)*, Springer, second ed., 2005.

[157] J.-F. Remacle, J. E. Flaherty, and M. S. Shephard, *An adaptive discontinuous Galerkin technique with an orthogonal basis applied to compressible flow problems*, SIAM Rev., 45 (2003), pp. 53–72.

[158] H.-K. Rhee, R. Aris, and N. R. Amundson, *First-order partial differential equations, volume 1: Theory and applications of single equations*, Dover, 2001.

[159] J. A. Rice and B. W. Silverman, *Estimating the mean and covariance structure nonparametrically when the data are curves*, Journal of the Royal Statistical Society Series B, 53 (1991), pp. 233–243.

[160] F. Riesz and B. Sz-Nagy, *Functional Analysis*, Dover, 1953.

[161] H. Risken, *The Fokker-Planck equation: Methods of solution and applications*, Springer-Verlag, second ed., 1989. Mathematics in science and engineering, vol. 60.

[162] S. Rjasanow and W. Wagner, *Stochastic numerics for the Boltzmann equation*, Springer, 2004.

[163] P. L. Roe, *Approximate Riemann solvers, parameter vectors and difference schemes*, J. Comput. Phys., 43 (1981), pp. 357–372.

[164] G. Rosen, *Dynamics of probability distributions over classical fields*, International Journal of Theoretical Physics, 4 (1971), pp. 189–195.

[165] Y. Saad, *Analysis of some Krylov subspace approximations to the matrix exponential operator*, SIAM J. Numer. Anal., 29 (1992), pp. 209–228.

[166] S. Sadooghi-Alvandi, A. Nematollahi, and R. Habibi, *On the distribution of the sum of independent uniform random variables*, Statistical Papers, 50 (2002), pp. 171–175.

[167] A. Saltelli, K. Chan, and M. Scott, *Sensitivity Analysis*, John Wiley, 2000.

[168] T. Sapsis and G. Athanassoulis, *New partial differential equations governing the response-excitation joint probability distributions of nonlinear systems under general stochastic excitation*, Prob. Eng. Mech., 23 (2008), pp. 289–306.

[169] A. Sarkar, N. Benabbou, and R. Ghanem, *Domain decomposition of stochastic PDEs: theoretical formulations*, Int. J. Numer. Meth. Engng., 77 (2009), pp. 689–701.

[170] C. Schwab and R. A. Todor, *Karhunen-Loeve approximation of random fields by generalized fast multipole methods*, Journal of Computational Physics, 217 (2006), pp. 100–122.

[171] M. F. Shlesinger and T. Swean, *Stochastically excited nonlinear ocean structures*, World Scientific, 1998.

[172] Y. G. Sinai, *Statistics of shocks in solutions of inviscid Burgers equation*, Commun. Math. Phys., 148 (1992), pp. 601–621.

[173] B. Smith, P. Bjørstad, and W. Gropp, *Domain decomposition: parallel multilevel methods for elliptic partial differential equations*, Cambridge University Press, 1996.

[174] K. Sobczyk, *Stochastic differential equations: with applications to physics and engineering*, Springer, 2001.

[175] I. M. Sobol, *Global sensitivity indices for nonlinear mathematical models and their monte carlo estimates*, Math. Comput. Simul., 55 (2001), pp. 271–280.

[176] P. Spanos, M. Beer, and J. Red-Horse, *KarhunenLoeve expansion of stochastic processes with a modified exponential covariance kernel*, Journal of Engineering Mechanics, 133 (2007), pp. 773–779.

[177] R. Srinivasan, *An invariant in shock clustering and burgers turbulence*, Nonlinearity, 25 (2012), pp. 781–789.

[178] R. L. Stratonovich, *Topics in the theory of random noise: Vols. 1 and 2*, Gordon and Breach, 1967.

[179] ——, *Some Markov methods in the theory of stochastic processes in nonlinear dynamical systems*, in Noise in nonlinear dynamical systems (Vol. 1), F. Moss and P. V. E. McClintock, eds., Cambridge Univ. Press, 1989, pp. 16–68.

[180] D. M. Tartakovsky and S. Broyda, *PDF equations for advective-reactive transport in heterogeneous porous media with uncertain properties*, Journal of Contaminant Hydrology, 120-121 (2011), p. 129140.

[181] H. Tennekes and J. L. Lumley, *A first course in turbulence*, MIT Press, 1972.

[182] M. Thalhammer, *High-order exponential operator splitting methods for time-dependent Schrödinger equations*, SIAM J. Numer. Anal., 46 (2008), pp. 2022–2038.

[183] M. E. TIPPING AND C. M. BISHOP, *Mixtures of probabilistic principal component analysis*, Neural Computation, 11 (1999), pp. 443–482.

[184] M. TOKMAN AND J. LOFFELD, *Efficient design of exponential-Krylov integrators for large scale computing*, Procedia Comput. Sci., 1 (2010), pp. 229–237.

[185] H. TOKUNAGA, *A numerical study of the Burgers turbulence at extremely large Reynolds numbers*, J. Phys. Soc. Jpn., 52 (1983), pp. 827–833.

[186] E. F. TORO AND V. A. TITAREV, *Solution of the generalized Riemann problem for advection-reaction equations*, Proc. R. Soc. Lond. A, 458 (2002), pp. 271–281.

[187] A. TOSELLI AND O. WIDLUND, *Domain Decomposition Methods - Algorithms and Theory*, Springer Series in Computational Mathematics, 2004.

[188] L. VALINO, *A field Monte Carlo formulation for calculating the probability density function of a single scalar in a turbulent flow*, Flow, Turbul. Combust., 60 (1998), pp. 157–172.

[189] T. G. VENKATESH AND L. M. PATNAIK, *Effective Fokker-Planck equation: Path-integral formalism*, Phys. Rev. E, 48 (1993), pp. 2402–2412.

[190] D. VENTURI, *On proper orthogonal decomposition of randomly perturbed fields with applications to flow past a cylinder and natural convection over a horizontal plate*, J. Fluid Mech., 559 (2006), pp. 215–254.

[191] ——, *A fully symmetric nonlinear biorthogonal decomposition theory for random fields*, Physica D, 240 (2011), pp. 415–425.

[192] D. VENTURI, M. CHOI, AND G. E. KARNIADAKIS, *Supercritical quasi-conduction states in stochastic Rayleigh-Bénard convection*, Int. J. Heat and Mass Transfer, 55 (2012), pp. 3732–3743.

[193] D. VENTURI AND G. E. KARNIADAKIS, *Differential constraints for the probability density function of stochastic solutions to the wave equation*, International Journal for Uncertainty Quantication, 2 (2012), pp. 131–150.

[194] ——, *New evolution equations for the joint response-excitation probability density function of stochastic solutions to first-order nonlinear PDEs*, J. Comput. Phys., 231 (2012), pp. 7450–7474.

[195] ——, *Convolutionless Nakajima-Zwanzig equations for stochastic analysis in nonlinear dynamical systems*, Proc. R. Soc. A, 470 (2014), pp. 1–20.

[196] D. VENTURI, T. P. SAPSIS, H. CHO, AND G. E. KARNIADAKIS, *A computable evolution equation for the probability density function of stochastic dynamical systems*, Proc. Roy. Soc. A, 468 (2012), pp. 759–783.

[197] D. VENTURI, D. M. TARTAKOVSKY, A. M. TARTAKOVSKY, AND G. E. KARNIADAKIS, *Exact PDF equations and closure approximations for advective-reactive transport*, J. Comput. Phys., 243 (2013), pp. 323–343.

[198] D. Venturi, X. Wan, and G. E. Karniadakis, *Stochastic low-dimensional modelling of a random laminar wake past a circular cylinder*, J. Fluid Mech., 606 (2008), pp. 339–367.

[199] ———, *Stochastic bifurcation analysis of Rayleigh-Bénard convection*, J. Fluid. Mech., 650 (2010), pp. 391–413.

[200] D. Venturi, X. Wan, R. Mikulevicious, B. L. Rozovsky, and G. E. Karniadakis, *Wick-Malliavin approximation to nonlinear stochastic partial differential equations: analysis and simulations*, Proc. R. Soc. A, 469 (2013), pp. 1–20.

[201] C. Villani, *A review of mathematical topics in collisional kinetic theory*, in Handbook of mathematical fluid mechanics, S. Friedlander and D. Serre, eds., vol. 1, North-Holland, 2002, pp. 71–305.

[202] M. Vovrechovský, *Simulation of simply cross correlated random fields by series expansion methods*, Structural Safety, 30 (2008), pp. 337–363.

[203] X. Wan and G. E. Karniadakis, *An adaptive multi-element generalized polynomial chaos method for stochastic differential equations*, J. Comput. Phys., 209 (2005), pp. 617–642.

[204] ———, *Multi-element generalized polynomial chaos for arbitrary probability measures*, SIAM J. Sci. Comput., 28 (2006), pp. 901–928.

[205] C.-J. Wang, *Effects of colored noise on stochastic resonance in a tumor cell growth system*, Phys. Scr., 80 (2009), p. 065004 (5pp).

[206] P. Wang, D. M. Tartakovsky, J. K. D. Jarman, and A. M. Tartakovsky, *CDF solutions of Buckley-Leverett equation with uncertain parameters*, Multiscale Model. Simul., 11 (2013), pp. 118–133.

[207] G. B. Whitham, *Linear and nonlinear waves*, Wiley, New York, 1974.

[208] N. Wiener, *The homogeneous chaos*, American Journal of Mathematics, 60 (1938), pp. 897–936.

[209] M. Wilczek, A. Daitche, and R. Friedrich, *On the velocity distribution in homogeneous isotropic turbulence: correlations and deviations from Gaussianity*, J. Fluid Mech., 676 (2011), pp. 191–217.

[210] H. S. Wio, P. Colet, M. San Miguel, L. Pesquera, and M. A. Rodríguez, *Path-integral formulation for stochastic processes driven by colored noise*, Phys. Rev. A, 40 (1989), pp. 7312–7324.

[211] L. E. Wittig and A. K. Sinha, *Simulation of multicorrelated random processes using the FFT algorithm*, Journal of the Acoustical Society of America, 58 (1975), pp. 630–634.

[212] D. Xiu and J. Hesthaven, *High-order collocation methods for differential equations with random inputs*, SIAM J. Sci. Comput., 27 (2005), pp. 1118–1139.

[213] D. XIU AND G. E. KARNIADAKIS, *The Wiener–Askey polynomial chaos for stochastic differential equations*, SIAM J. Sci. Comput., 24 (2002), pp. 619–644.

[214] ———, *Modeling uncertainty in flow simulations via generalized polynomial chaos*, J. Comp. Phys., 187 (2003), pp. 137–167.

[215] J. XU, *Iterative methods by space decomposition and subspace correction*, SIAM Review, 34 (1992), pp. 581–613.

[216] J. XU AND J. ZOU, *Some nonoverlapping domain decomposition methods*, SIAM Review, 40 (1998), pp. 857–914.

[217] Y. XU, R. GU, H. ZHANG, W. XU, AND J. DUAN, *Stochastic bifurcations in a bistable Duffing-Van der Pol oscillator with colored noise*, Phys. Rev. E, 83 (2011).

[218] F. YAMAZAKI AND M. SHINOZUKA, *Simulation of stochastic fields by statistical preconditioning*, Journal of Engineering Mechanics, 116 (1990), pp. 268–287.

[219] W. YANG, H. MULLER, AND U. STADTMULLER, *Functional singular component analysis*, Journal of the Royal Statistical Society Series B, 73 (2011), pp. 303–324.

[220] X. YANG, M. CHOI, AND G. E. KARNIADAKIS, *Adaptive ANOVA decomposition of stochastic incompressible and compressible fluid flows*, J. Comput. Phys., 231 (2012), pp. 1587–1614.

[221] Y. YANG AND C.-W. SHU, *Discontinuous Galerkin method for hyperbolic equations involving δ-singularities: negative-order norm error estimate and applications*, Numerische Mathematik, 124 (2013), pp. 753–781.

[222] F. YAO, H. MULLER, AND J.-L. WANG, *Functional data analysis for sparse longitudinal data*, Journal of the American Statistical Association, 100 (2005), pp. 577–590.

[223] C. ZENG AND H. WANG, *Colored noise enhanced stability in a tumor cell growth system under immune response*, J. Stat. Phys., 141 (2010), pp. 889–908.

[224] ———, *Colored noise enhanced stability in a tumor cell growth system under immune response*, Journal of Statistical Physics, 141 (2010), pp. 889–908.

[225] H. ZHANG, W. XU, AND Y. XU, *The study on a stochastic system with non-Gaussian noise and Gaussian colored noise*, Physica A: Statistical Mechanics and its Applications, 388 (2009), pp. 781–788.

[226] Z. ZHANG, M. CHOI, AND G. E. KARNIADAKIS, *Anchor points matter in ANOVA decomposition*, Proceedings of ICOSAHOM'09, Springer, eds. E. Ronquist and J. Hesthaven, (2010).

[227] ———, *Error estimates for the ANOVA method with polynomial chaos interpolation: Tensor product functions*, SIAM J. Sci. Comp., 34 (2012), pp. 1165–1186.

[228] S. Zhong and H. Xin, *Effects of colored noise on internal stochastic resonance in a chemical model system*, Chem. Phys. Lett., 333 (2001), pp. 133–138.

[229] X. Zhou, *Cooperative atomic scattering of light from a laser with a colored noise spectrum*, Phys. Rev. A, 80 (2009), p. 023818 (6pp).

[230] R. Zwanzig, *Memory effects in irreversible thermodynamics*, Phys. Rev., 124 (1961), pp. 983–992.